Netrin-1 isoforms and macrophage phenotype: role in the pathophysiology of atherosclerosis

Claro, Vasco

Awarding institution:
King's College London

Netrin-1 isoforms and macrophage phenotype: role in the pathophysiology of atherosclerosis

A thesis submitted for the degree of
Doctor of Philosophy
King's College London

Vasco Andre Marques Claro

School of Cardiovascular & Metabolic Medicine and Sciences,

British Heart Foundation Centre of Research Excellence,

King's College London

Abstract

Atherosclerosis is a chronic inflammatory disease and is the main cause of ischaemic heart disease, stroke, and other cardiovascular diseases. The development of atherosclerotic plaques incidence has been increasing significantly during the last few decades and is due to different factors, such as the increased consumption of high fat food, smoking and increased incidence of diabetes mellitus. This is currently a major burden on health systems, which require new therapeutic targets to address this challenge.

The involvement of netrin-1 in inflammation and atherosclerosis has been studied during the last two decades. Different groups have established that netrin-1 plays a prominent role in these contexts and has different effects depending on where it is produced, and which cells are targeted by it. While endothelial-derived netrin-1 secreted into the circulation gives rise to a protective effect against atherosclerosis, macrophage-derived netrin-1 within the plaque has a pro-atherogenic effect, promoting the trapping and survivability of foam cells.

More recently, a truncated isoform of netrin-1 was found in the nuclei of different types of cancer cells. This form of netrin-1 has also been studied in endothelial cells, but so far, no relationship between the expression of truncated netrin-1 and macrophages has been established. The link between cytokine stimulation, macrophage phenotype and netrin-1 isoforms has until now been unclear. The work described in this thesis looked at the expression and function of netrin-1 on monocytes and different macrophage phenotypes.

Gene expression analysis revealed that macrophages express both full-length and truncated netrin-1. Classical activated is the macrophage phenotype that presents higher expression of netrin-1, and the expression of both isoforms is at least partially dependent on NF-κB activation pathway.

Netrin-1 inhibits monocyte migration by inhibiting chemokines' chemoattractant effect. CCL2 and netrin-1 individually showed an attractant effect towards THP-1-derived macrophages, but the signals were inhibited when the two were combined. The apoptotic agent selected to study netrin-1 anti-apoptotic effect was not UNC5b-dependent and, therefore, limited our ability to acquire relevant data regarding this process.

Administration of exogenous netrin-1 to mice, increasing its systemic levels, showed an acute and chronic protective effect against inflammation. Mice treated with netrin-1 showed less macrophages within the tissue after the induction of local inflammation. Furthermore, increasing the netrin-1 systemic levels of mice prevented the enlargement of the aortic sinus and development of plaque after feeding them 60% HFD over a 6-week period.

This thesis provides relevant insights into the role of macrophage phenotypes in the expression of netrin-1 isoforms within atherosclerotic plaques, and how netrin-1 affects these immune cells. The findings highlight the significance of netrin-1 as a potential therapeutic target for treating not only cardiovascular disease but also other inflammatory conditions. Therefore, this research sheds light on the promising future of netrin-1 as a treatment option for a range of diseases.

Acknowledgements

The work I performed in this thesis would not have been possible without the help and support from my colleagues, friends, and family. First and foremost, I would like to thank my supervisor Professor Albert Ferro for accepting going through this journey with me, for his help and support and for always having a positive and encouraging attitude, even when the work did not go well. I would also like to thank the Vascular Biology & Inflammation division for the support, friendship and care that were always present during difficult times, such as the COVID-19 pandemic. A special thank you to Professor Sue Brain for including me in her group activities, Doctor Yanira Vasquez for her help in the intravital microscopy, Doctor Fulye Argunhan for teaching me how to perform surgery in mice and Doctor Fan Yang for the companionship while writing up together late evenings and weekends.

My thanks also go to the British Heart Foundation for their generous funding, without which this research would not have been possible.

Finally, I would like to express my gratitude to my family, especially James and my parents, who always made sure I was on the right track and have provided me with unwavering love and support during my research.

Abbreviations

ABCA1	ATP-binding cassette transporter A1
ACTA2	Smooth muscle alpha-actin 2
ADORA2B	A2B adenosine receptor
acLDL	Acetylated low-density lipoprotein
ApoE	Apolipoprotein E
AUC	Area under the curve
BMDM	Bone marrow-derived macrophages
BMP	Bone morphogenic protein
BSA	Bovine serum albumin
CC3	Cleaved caspase-3
CCLx	C-C motif ligand x
CI	Cell index
CDx	Cluster of differentiation x
CP	Crossing point
CS1	Connecting segment-1
COX-2	Cyclooxygenase-2
C_t	Cycle threshold
CVD	Cardiovascular disease
CXCL-x	C-X-C motif ligand x
DAMP	Damage-associated molecular pattern
DAPI	4',6-Diamidino-2-Phenylindole, Dilactate
DCC	Deleted in colorectal cancer
DNA	Deoxyribonucleic acid
DSCAM	Down syndrome cell adhesion molecule
eGFP	Enhanced green fluorescent protein
E	Amplification factor
EDTA	Ethylene-diamine-tetra-acetic acid
EGF	Epidermal growth factor
eNOS	Endothelial nitric oxide synthetase
EPC	Endothelial progenitor cell
FnIII	Fibronectin type III
FBS	Foetal bovine serum

g	G-force
GM-CSF	Granulocyte-macrophage colony-stimulating factor
h	Hour
HFD	High-fat diet
HDL	High-density lipoprotein
HPR	Horseradish peroxidase
HPRT-1	Hypoxanthine phosphoribosyl transferase 1
HUVEC	Human umbilical vein endothelial cell
ICAM-1	Intercellular adhesion molecule 1
IFN-γ	Interferon γ
IL-x	Interleukin x
IP	Immunoprecipitation
LDL	Low-density lipoprotein
LDLR	Low-density lipoprotein receptor
LPS	Lipopolysaccharide
M0	Unstimulated macrophages
M1	Classical activated macrophages
M2	Alternative activated macrophages
MCP-1	Monocyte chemoattractant protein-1
M-CSF	Macrophage colony-stimulating factor
min	Minute
moLDL	Minimally oxidised low-density lipoprotein
mRNA	Messenger ribonucleic acid
NF-κB	Nuclear factor κB
nLDL	Native low-density lipoprotein
NO	Nitric oxide
NOX1	NADPH oxidase 1
oxLDL	Oxidised low-density lipoprotein
PAMP	Pathogen-associated molecular pattern
PAGE	Polyacrylamide gel electrophoresis
PBMC	Peripheral blood mononuclear cells
PBS	Phosphate buffer saline
PFA	Paraformaldehyde
PGE2	Prostaglandin E2

PEM	Peritoneal macrophages
PMA	Phorbol 12-myristate 13-acetate
PPAR	Peroxisome proliferation-activated receptor
PRR	Pattern recognition receptors
R	Relative expression ratio
R^2	Coefficient of determination
RNA	Ribonucleic acid
ROS	Reactive oxygen species
Runx2	Runt-related transcription factor-2
qPCR	Quantitative polymerase chain reaction
SD	Standard deviation
SDS	Sodium dodecyl sulphate
siRNA	Small interfering RNA
SPMs	Specialised pro-resolving mediators
SR-A	Scavenger receptor A
TBE	Tris/Borate/EDTA buffer
TBS	Tris-buffered saline
TBS-T	Tris-buffered saline plus TWEEN 20 detergent
TEB	Terminal end buds
TGF-β	Transforming growth factor β
TLR	Toll-like receptor
TNF-α	Tumour necrosis factor α
TSP-1	Thrombospondin-1
UNC5	Uncoordinated 5
VC	Vascular calcification
VCAM-1	Vascular cell adhesion molecule 1
VEGF	Vascular endothelial growth factor
VSMC	Vascular smooth muscle cell
WT	Wild-type

Table of Contents

Chapter Two: Materials & Methods

List of Figures

List of Tables

Chapter One

Introduction

1.1. Atherosclerosis

Atherosclerosis is an inflammatory disease that is characterised by the accumulation of fatty and fibrous material withing the arterial wall, as well as cells. This inflammatory process is the main cause of a range of cardiovascular diseases (CVD), such as stroke, ischaemic heart disease and peripheral arterial disease, which together account for the majority of deaths worldwide. 1.68 million people died of diseases of the heart and circulatory system in the European Union in 2018 and 168,000 in the United Kingdom in 2020, which is the equivalent to 37.1% and 24% of all deaths, respectively. Currently, there are 7.6 million people living with this type of disease in the UK alone, and this has a £9 billion cost for the NHS, annually. The total cost of CVD to the UK economy is estimated to be £19 billion each year, due to premature death, disability and related costs.[1,2]

There are several risk factors that will promote the development of atherosclerosis. Some of the most relevant ones are hypertension, smoking, obesity, diabetes mellitus and hypercholesteremia. Hypertension leads to an increased permeability of the endothelium due to haemodynamic pressure, which damages the arterial wall and facilitates the accumulation of cholesterol particles.[3]

Smoking also plays a very important role in the development of this inflammatory disease. However, it is very difficult to understand the full range of the effects of smoking due to the enormous number of different substances that cigarette smoke contains. It has been stated that smoking promotes hypertension, since it promotes the release of catecholamines, as well as platelet aggregability. Moreover, smoking upregulates the expression of pro-inflammatory cytokines, such as C-reactive protein, TNF-α and IL-6. It also induces the

expression of soluble ICAM-1, VCAM-1 and E-selection which will increase the leukocyte-endothelium interactions and leukocyte recruitment to the inflammation site.[4,5]

Similarly to smoking, it is not possible to emphasise one single mechanism that links obesity and atherosclerosis. Lovren and colleagues gathered information that identified some important features related to obesity that play a role in atherosclerosis. Increased levels of free lipids circulating in the bloodstream are found in obesity. Adipokine imbalance, where the balance between pro- and anti-inflammatory adipokines is skewed towards the progression of inflammation is another feature found in obesity during endothelial dysfunction. The downregulation of adiponectin (the most common anti-inflammatory adipokine) leads to insulin resistance, as does upregulation of pro-inflammatory cytokines such as TNF-α, IL-1 and IL-6. Endothelial dysfunction is also found in obesity, in both animal and human models. Decreased expression of endothelial nitric oxide synthetase (eNOS) and increased expression of the vasoconstrictor peptide ET-1 are two of the characteristics observed in obese subjects.[6]

1.1.1. Low-density lipoprotein accumulation

Atherosclerosis is an inflammatory process triggered by progressive lipid accumulation and retention in the arterial wall. High plasma concentrations of cholesterol, particularly in the form of low-density lipoproteins (LDL), are considered one of the main risk factors in the development of this chronic inflammatory disease.[7] Due to the local turbulence of blood flow observed in segments of arteries, such as branching points and bends, the integrity and function of the endothelium becomes compromised. This area is especially prone to the development of atherosclerotic lesions (Figure 1.1).[8]

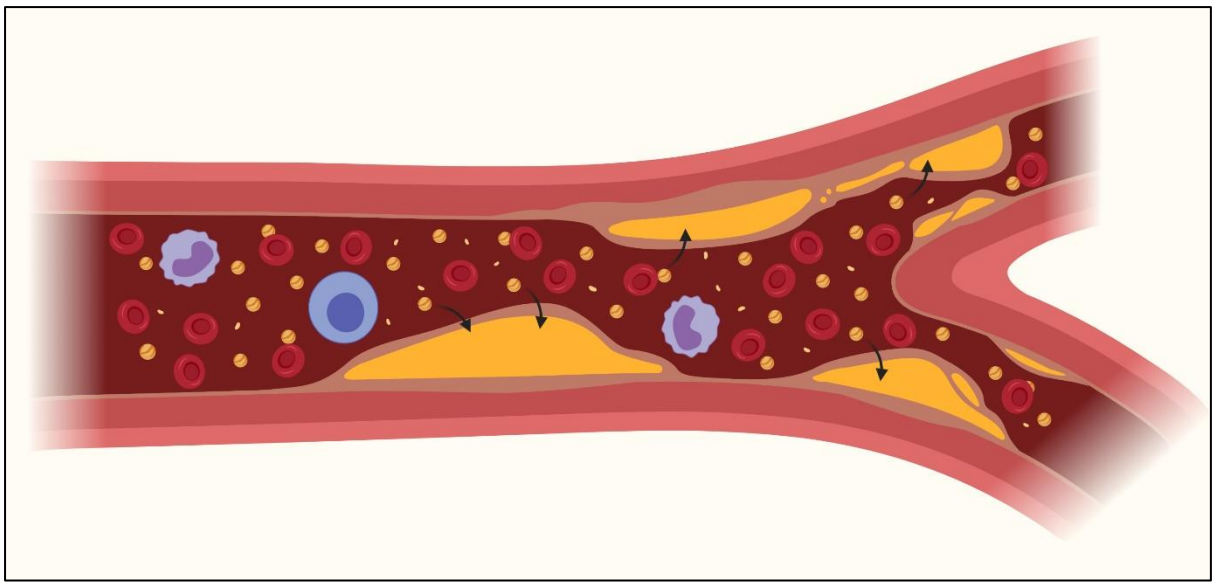

Figure 1.1 - Representation of LDL accumulation in the arterial wall of an arterial branching point. Figure created using *BioRender*.

1.1.2. LDL oxidation and cholesterol esters

LDL is a vehicle for transport of cholesterol in the circulation. Each LDL particle is formed by a surface of phospholipids and apolipoproteins and a core which contains cholesterol, cholesterol esters and trilglycerides.[9] LDL diffuses freely between endothelial junctions and attaches to the arterial wall through interactions of its membrane constituent apolipoprotein E and the matrix proteoglycans.[10]

As the LDL accumulates in the arterial wall, a long chain of enzymatic and chemical reactions is triggered. Both enzymatic and non-enzymatic mechanisms are found in this oxidation process. On the one hand, cyclooxygenases, lipoxygenases and cytochrome p450 are the main enzymes that enable oxidation of the LDL, and on the other hand, free radicals mediate non-enzymatic oxidation processes.[11,12]

This oxidative reaction not only changes the biological function of the phospholipids present in the LDL membrane, but also generates degradation products which propagate the effects

of oxidative stress. Oxidised lipids and degradation products can interact with most of the cell types present in the atherosclerotic plaque, but it is their interaction with leukocytes that majorly contributes to the development of inflammation and cardiovascular disease. These products interact with other proteins modifying them and forming oxidation-specific epitopes, which are recognised by the immune system[12] and will be described below.

Cholesterol esters are another form of lipid found in the plaque. These can be hydrolysed to unesterified cholesterol (free cholesterol) and then transported out of the lysosomes. In macrophages, the free cholesterol can be re-esterified to fatty acids and stored as cholesterol esters in the cytoplasm.[13,14]

1.1.3. Endothelial response to oxLDL

Oxidation specific markers present in oxidised LDL (oxLDL), also known as oxidation-specific epitopes, are recognised by the endothelium and trigger pro-inflammatory pathways in overlying endothelial cells. OxLDL has been shown to activate endothelial cells' β1 integrins, promoting their interaction with an alternative splice of fibronectin - connecting segment-1 (CS1) present as soluble form in the plasma. This works as a ligand for integrin α4β1, an adhesion molecule present in the cellular membrane of monocytes.[15] A P-selectin-dependent mechanism has also been described in endothelial cells due to oxLDL activation. When human aortic endothelial cells were treated with oxLDL, P-selectin upregulation was demonstrated. Moreover, translocation of intracellular P-selectin organised in Weibel-Palade bodies to the cell surface was observed.[16] P-selectin promotes the adhesion of monocytes and neutrophils.[17] Dever and colleagues showed that upregulation of P-selectin led to increased leukocyte adhesion through binding to its ligand CD162 in a concentration-

dependent manner in murine aortic segments.[18] Furthermore, Furnkranz *et al* demonstrated that blockade of this adhesion molecule led to abrogated leukocyte adhesion and rolling ability in murine carotid arteries.[19]

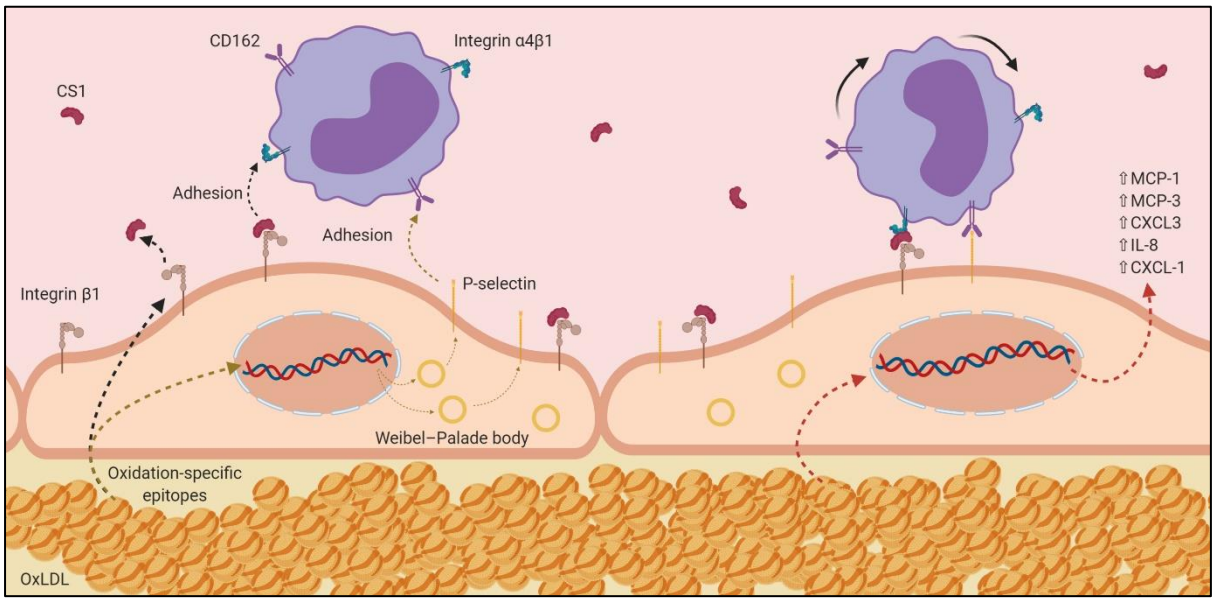

Figure 1.2 - Endothelial response to oxLDL and early recruitment of leukocytes. The oxLDL accumulated in the arterial wall induce the expression of chemokines and adhesion molecules by the endothelial cells. Figure created using *BioRender*.

There is a vast range of proinflammatory chemokines which become upregulated in the endothelial cells when stimulated by oxLDL. Monocyte-targeted specific chemokines, such as MCP-1, MCP-3 or CXCL-3, are highly expressed in these conditions. Similarly, there is evidence that other types of leukocytes are targeted, with an upregulation of cytokines such as IL-8 or CXCL-1.[20] All these endothelial-derived stimuli contribute to the initiation and development of the inflammatory response observed in atherosclerosis (Figure 1.2).

1.1.4. Leukocyte recruitment

After the initial endothelial response, which promotes recruitment of leukocytes to the site, oxLDL interacts with the immune cells that accumulate in the sub-intimal layer. Berliner *et al* showed that in the early stages, mild oxidation of LDL only induced the recruitment of monocytes, but not neutrophils.[21] OxLDL mimics damage-associated molecular patterns (DAMP) which are recognized by toll-like receptors and scavenger receptors present in the macrophages accumulated on site. This initiates different pathways which lead to cell activation, co-stimulation of other immune cells and production of reactive oxygen species (ROS), nitrogen species and pro-inflammatory eicosanoids and cytokines, such as prostaglandin E, leukotriene B4, IL-1β, TNF-α and IL-6.[22] A positive feed-back loop starts, leading to a self-perpetuating inflammatory process, which is less dependent on oxLDL, and enhances further recruitment of leukocytes to the plaque. Chemokines, produced by the activated endothelium target mostly circulating monocytes and T-cells, attracting them to the inflammation site.

1.1.5. Macrophage phenotypes in the atherosclerotic plaque

The progression of the inflammatory process in atherosclerosis involves different cell types, including endothelial cells, lymphocytes, monocytes, macrophages and vascular smooth muscle cells (VSMC).[23]

Different macrophage phenotypes can be found within the atherosclerotic plaque. A simplified way of looking at these phenotypes show M1 (classical activated macrophages) and M2 (alternative activated macrophages) as extreme polarizations of a spectrum. However, techniques such as single-cell RNA sequencing or next-generation microRNA

sequencing provide a much more accurate picture of how vast the range of macrophages subtypes can be.[24,25] These cells can switch between pro-inflammatory and anti-inflammatory phenotypes depending on the cytokines expressed and the environment around them.[26]

A diverse range of macrophage subtypes are present in atherosclerotic lesions in early as well as advanced lesions.[27] The atherosclerotic plaque composition affects the plasticity of the macrophages present within, and at the same time, the macrophage subtypes affect the composition of the plaque, resulting in a constant loop of responses. The traditional classification of M1/M2 macrophages, which is an approach skewed towards the cell phenotypes found *in vitro*, will be described. Furthermore, newly identified macrophage subtypes will also be presented, revealing a more realistic classification to what is found *in vivo*.

Classical activated macrophages

Classical activated macrophages, often simply called M1 macrophages, were the first phenotype characterised as pro-inflammatory. High expression of pro-inflammatory cytokines, such as TNF-α, IL-1β, IL-12 and IL-18, is found in these cells. M1 macrophages differentiation/activation is usually induced by T helper 1 cell (T_H1) cytokines or through recognition of Pathogen-Associated Molecular Patterns (PAMP), such as lipopolysaccharide (LPS), through Pattern Recognition Receptors (PRR).[28] As part of the innate immune response, M1 macrophages are activated in order to remove pathogens using ROS and phagocytosis. This response is not specific to pathogens and induces tissue damage when activated.[29]

During the early stages of plaque progression, cholesterol crystals that accumulate within the arterial wall are phagocytosed by macrophages and act as an M1-polarising stimulus. The uptake and accumulation of cholesterol crystals induces inflammation through activation of the nucleotide-binding oligomerization domain-like receptor family pyrin domain containing 3 (NLRP3) inflammasome and upregulation of inflammasome-related genes.[30,31]

M1 macrophages are enriched in progressing atherosclerotic plaques. After obtaining samples using carotid endarterectomy and comparing patients with symptomatic and asymptomatic carotid disease, Cho *et al* found that M1 macrophages were present in higher amounts within the plaques in patients which suffered from acute ischemic attack (symptomatic).[32] Stoger *et al* arrived at the same conclusions as the previous study and went further, demonstrating that not only is there an increased number of M1 macrophages in vulnerable plaques, but these also accumulate particularly in the 'shoulders' of the plaques, which are more vulnerable areas and are susceptible to rupture.[33,34]

The formation of necrotic cores in advanced plaques is usually instigated by an early phase of calcification, named microcalcification. Studies suggest that this process is predominately initiated by M1 macrophages, rather than M2 macrophages, which promote macrocalcification.[35]

The balance between progression and regression of the atherosclerotic plaque influences the phenotype of the accumulated macrophages. Specific signals can promote reversible conversion of classical and alternative activated macrophages, depending on the microenvironment, due to the high plasticity of these cells. Studies by Gong *et al* and Rahman *et al* suggest that polarization from M1 to M2 macrophages promotes atherosclerosis stabilization.[36,37] For instance, Baitsch and colleagues showed that

apolipoprotein E, which is a major component of high-density lipoproteins (HDL) and plays a key role in the prevention of atherosclerosis, promotes macrophage phenotype conversion from M1 to M2.[38]

Alternative activated macrophages

M2 macrophages regulate inflammation and counterbalance the M1 macrophage response.[29] In the plaque, this macrophage phenotype is generated in the presence of specialised pro-resolving mediators (SPMs), such as nitric oxide, resolvins, IL-10 and annexin-derived peptides.[39] These macrophages are characterised by an upregulation in the expression of arginase 1, CD163 and mannose receptor.

M2 macrophages are more abundant in regressing plaques, where they promote repair and stability. The development of atherosclerosis results from an imbalance of the pro-inflammatory and pro-resolving response. Pro-resolving mediators block influx and promote egress of leukocytes from the inflammatory site.[40] In active plaques, alternative activated macrophages can be found mainly in stable regions of the lesion, where the cap is thicker and less prone to rupture.[32,41] Cardilo-Reis *et al* found that treating *LDLR*$^{-/-}$ mice exogenously with M2 macrophages increased the collagen content within the plaque, as well as reducing the recruitment of monocytes to the area.[42] Calkin *et al* showed that inducing M2-polarization through activation of the nuclear transcription factor peroxisome proliferation-activated receptor (PPAR) led to decreased development of atherosclerosis in the *ApoE*$^{-/-}$ mouse model.[43] Babaev and colleagues obtained similar results using a different approach. Polarising the M2 phenotype through generation of macrophage deficiency of Akt2 (a serine/threonine protein kinase B) led to a reduction of both early and advanced atherosclerotic lesions in *LDLR*$^{-/-}$ mice.[44] Interestingly, when plaques from patients with

atherosclerosis were analysed, M2 macrophages were the predominant phenotype present in asymptomatic disease.[32]

Mox and M4 Macrophages

A different macrophage phenotype, named Mox macrophages, was described by Kadl *et al*. This subset of macrophages was generated after exposure to oxidised phospholipids and microscopic analysis showed morphological differences in the cytoskeleton organisation. Migration in Mox macrophages was impaired when compared with M1 and M2 phenotypes, as well as phagocytic ability. Furthermore, genome analysis revealed that Mox macrophages have a gene expression pattern very different from the conventional M1 and M2 subtypes. Kadl and colleagues also reported that the levels of Mox macrophages in the atherosclerotic plaque are high, within the ranges observed for M1 and M2 phenotypes.[45]

Macrophages stimulated by platelet factor 4 (CXCL4) induce another macrophage phenotype designated M4. This subtype shares more morphological characteristics with M1 and M2 than Mox but has a suppressed ability to phagocytose. The M4 transcriptome is distinct from M1 and M2, however it shares some similarities with them. Gleissner and colleagues showed that similarly to M1 and M2 phenotypes, M4 macrophages present an upregulation of some cytokines, chemokines and membrane markers such as CCL18, IL-6 and CD86. Interestingly, their data suggests that CXCL4-stimulated macrophages express lower levels of scavenger receptors, which are associated with the uptake of acetylated LDL (acLDL) and oxLDL. Experiments performed by this group show a lower intracellular lipid content in M4 macrophages when compared with M0.[46]

Foam cells

Foam cells mainly originate from macrophages and VSMC. The ratio between VSMC- and macrophage-derived foam cells varies and has been described to be as high as 40:60 in advanced lesions.[47] The formation of foam cells does not depend exclusively on the uptake abilities of each cell type, but also on the cell's ability to release excess cholesterol from the cytoplasm. ATP-binding cassette transporter A1 (ABCA1) mediates the active transport phospholipids and cholesterol by flipping the lipids from the inner to the outer membrane leaflet. Lipid-poor HDL interacts with the lipid domains generated by the ABCA1 and removes it, clearing the excess of cholesterol in the foam cells.[48]

The main cellular source of foam cell formation are macrophages, which are recruited in a monocyte form, by the activated endothelium.[49] Macrophages migrate to the atherosclerotic plaque and remove lipids and lipoproteins at different stages of oxidation, which accumulate between the endothelium and the intima layer. Different researchers have worked towards characterising macrophage-derived foam cells, but this has proven to be a difficult task. Bisgaard and colleagues looked at two different types of macrophages, bone marrow-derived (BMDM) and peritoneal (PEM) and could not get conclusive data regarding the cell features of cholesterol-loaded cells. Although the generation of foam cells from BMDM and PEM was similar, the effect of oxLDL on mRNA expression was remarkably different. Significant downregulation of genes found in one type of macrophage, such as *SREBP2* and *MSR1*, was not observed in the other. Moreover, the foam cells found in the atherosclerotic plaque express a combination of both M1 and M2 markers, without a clear association with either phenotype.[27]

Native LDL uptake - Macropinocytosis

Two of the mechanisms for the uptake of native LDL (nLDL) by the macrophages are fluid-phase macropinocytosis and micropinocytosis, where the lipid particles are brought inside the cell through small vesicles, which stay in suspension in the cytoplasm.[50] Fluid-phase pinocytosis is an endocytosis mechanism independent of any receptors and contributes to the generation of foam cells. This process is stimulated by cytokines and growth factors and requires actin remodelling, which produces vesicles of heterogenous size, being preceded by membrane ruffling. The cellular membrane folds and fuses with the vesicle membrane, creating fluid-filled vacuoles that detach from the cellular membrane into the cytoplasm.[51] Although the initiation of these processes is poorly understood, some researchers have studied possible candidates that play a role in this signalling cascade.

Scányi and colleagues showed that the matrix glycoprotein thrombospondin-1 (TSP1) stimulates the macrophage NADPH oxidase 1 (NOX1) signalling pathway, leading to membrane ruffle formation and fluid-phase macropinocytosis.[52] NOX proteins are a family of membrane-associated enzymes which catalyse the reduction of oxygen into superoxide or hydrogen peroxide, using NADPH as source of electrons. This is an important source of ROS in different environments, such as vasculature and the immune system, functioning as an essential process in the respiratory burst that occurs in macrophages.[53] This group showed that treatment of human and murine macrophages with TSP1 induced membrane ruffle-mediated macropinocytosis of nLDL and that NOX1 and CD47 are essential for TSP1-induced macropinocytosis. Using THP-1 macrophages, it was shown that there is 4-fold increase in the uptake of nLDL when macrophages were treated with TSP-1 when compared with vehicle. Interestingly, no difference in expression of LDL receptor (LDLR) was observed,

suggesting that the mechanism described above is receptor independent. Furthermore, evidence has shown that Nox1 and CD47 are essential for TSP-1 induced macropinocytosis. Through the NOX1 signalling pathway, TSP-1 increased the intracellular levels of superoxide in macrophages, and this plays a role in the uptake of non-oxidized nLDL. In fact, NOX inhibition in BMDM led to a significant suppression of TSP1-induced macropinocytosis. Using scanning electron microscopy (SEM), Scányi and colleagues were able to verify that TSP1 did not induce membrane ruffle formation in $Nox1^{y/-}$ macrophages, contrary to what was verified in a wild-type model, corroborating therefore the role of this signalling pathway in the initiation of fluid-phase macropinocytosis.[52] Finally, work performed by the same group showed that CD47 mediates TSP1-induced activation of NOX1.[54] Treating macrophages with a CD47 blocking antibody abolished the expression of NOX1-derived superoxide. Images collected using SEM show that the membrane ruffling and subsequent macropinocytosis observed on the surface of wild-type macrophages did not happen in $CD47^{-/-}$ macrophages (Figure 1.3).[52]

Minimally oxLDL uptake – TLR4-induced macropinocytosis

The toll-like receptor-4 (TLR4) has also been associated with fluid-phase uptake of lipoproteins by macrophages. TLR4 is a type of receptor that recognizes PAMPs, which plays a role in the development of different pathologies, such as chronic inflammatory diseases, including atherosclerosis.[55] Choi *et al* showed that TLR4 participates in the uptake of minimally oxidised LDL (moLDL) by macrophages through macropinocytosis and in the generation of foam cells[56]. MoLDL is not modified enough to bind to scavenger receptors as much as oxLDL, but it binds to CD14, which is associated with TLR4 and its adaptor protein

MD-2. The binding of this moLDL to CD14 triggers the expression of pro-inflammatory cytokines and induces a robust and fast cellular spreading through an increase of actin polymerization on macrophages.[55] Experiments conducted by Choi and colleagues showed that moLDL promotes macropinocytosis of lipoproteins to a higher extent than nLDL or oxLDL. In fact, treating macrophages with moLDL promotes the uptake of nLDL and oxLDL in a scavenger receptor-independent manner. TLR4-knock-out macrophages show a 60% lower uptake of moLDL. Moreover, treatment of macrophages with the TLR4-ligand LPS led to increased uptake of nLDL and oxLDL, supporting the hypothesis that this receptor plays a relevant role in the enhanced uptake of lipoproteins in a scavenger receptor-independent manner. The mechanism by which moLDL induces these effects is dependent on TLR4 and the recruitment of spleen tyrosine kinase (Syk), which binds to the C-terminal domain of the receptor. This research group found that both TLR4 and Syk were required for moLDL activation of the exchanging factor Vav1, small GTPase Ras and kinases Raf, MEK1 and ERK1/2. ERK1/2 phosphorylated palaxin and activated GTPases Rac, Cdc42 and Rho. It is suggested that moLDL induces macropinocytosis through cytoskeletal rearrangements (Figure 1.3).[56]

OxLDL uptake – CD36

In advanced lesions, oxLDL is the main type of lipoprotein that is taken up, through scavenger receptors. Although there is a range of scavenger receptors that are expressed in the cell membrane of macrophages, SR-A and CD36 are the most relevant ones in this process, being responsible for the uptake of up to 90% of the total oxLDL leading to lipid-laden macrophages.[57] Febbraio *et al* showed that knocking-out the CD36 receptor nullified

atherosclerotic lesion development in *ApoE*$^{-/-}$ mice, after both a high fat diet and normal chow. The binding of oxLDL and acLDL to macrophages was 87% and 64% less in CD36$^{-/-}$ *ApoE*$^{-/-}$ when compared with *ApoE*$^{-/-}$ mice, respectively.[58]

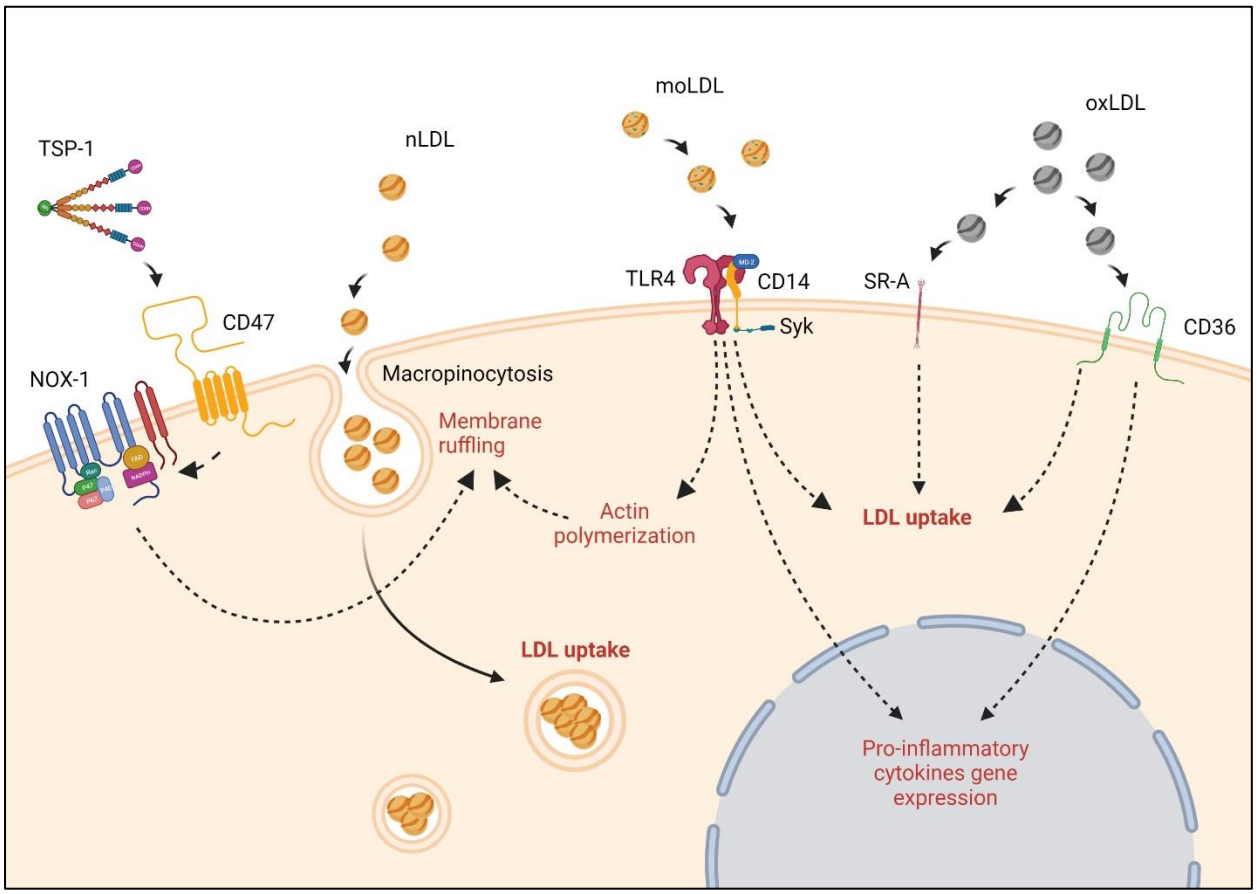

Figure 1.3 - Mechanisms for the uptake of forms of LDL by macrophages. Representation of the mechanisms that induce uptake of nLDL via macropinocytosis, the uptake of moLDL via CD14 and oxLDL via CD36 and SR-A. Figure created using *BioRender*.

Different pro-inflammatory pathways derived from the interaction between oxLDL and CD36 receptor have been identified in the last few decades. Janabi and colleagues' data suggests that the expression of TNF-α and IL-1β is upregulated in PBMC-derived macrophages when compared with macrophages isolated from CD36-deficient patients. Moreover, they showed that while oxLDL significantly enhanced NF-κB activity in nuclear extracts of control samples,

no significant activation was observed in the CD36-deficient patient group.[59] Sheedy *et al* not only showed concordant data to the previous study, but also that the uptake of oxLDL generates NLRP3-activating crystals, which depends on priming by CD36.[60] NLRP3 is an inflammasome that leads to caspase 1-dependent expression of pro-inflammatory cytokines, such as IL-1β (Figure 1.3).[61]

Newly identified macrophage subtypes in atherosclerosis

Single-cell RNA sequencing (scRNAseq) analysis of macrophages obtained *in vivo* show a more diverse range of subsets than initially anticipated. Cochain and colleagues identified three macrophage subtypes using scRNAseq in aortas from *Ldlr*$^{-/-}$ mice that suffered from atherosclerosis. These were inflammatory, resident-like and Trem2^{hi} macrophages and their proportions in the aorta were 47%, 34.4% and 18.6%, respectively. Interestingly, data acquired by the same group, from aortas from *Apoe*$^{-/-}$ mice revealed macrophage populations with similar characteristics and proportions, when compared with *Ldlr*$^{-/-}$ mice.[62]

In atherosclerosis, pro-inflammatory macrophages not only present an increase in the expression of M1-associated genes (*Il1b, Tnf, Ccr1* and *Trem1*), but there is an upregulation of atherosclerosis specific genes, such as *Egr1, Nlrp3* and *Phlda1*.[25,63] This population expressed genes mainly related with NF-κB, TNF, TLR and IL-17 signalling pathways, as well as cytokine-cytokine receptor interactions.[64] The pro-inflammatory macrophages accumulate mainly at the sites of the atherosclerotic lesion and promote plaque progression by activating interleukin family members and promoting monocyte recruitment through increased expression of the Nlrp3 domain.[65] Interestingly, *Mrc1,* which encodes CD206 and has been traditionally defined as an M2 marker was also found in a substantial proportion of

inflammatory macrophages, indicating that there is an overlap in the gene expression pattern between populations.[62]

Gene expression of human carotid plaques also presented cluster of macrophages with pro-inflammatory profiles. Upregulation in genes involved in the inflammatory response such as *CYBA, LIZ*, *JUNB* and *NFKBIA*. An upregulation in the metalloprotease inhibitor *TIMP1* was also found in one of the clusters of pro-inflammatory macrophages.[66]

The resident-like macrophages play roles in immunity, homeostasis, and repair after injury. These macrophages express lymphatic vessel endothelial hyaluronan receptor 1 (Lyve1).[65] The genes expressed by this subtype were previously associated with aortic resident macrophages and genes associated with M2-like macrophages, such as *Mrc1* and *Folr2*.[62,64] However, genes associated with inflammatory activation such as *Pf4* and *Txnip* are also expression by Res-like macrophages. This subtype is found in healthy arteries, as well as arteries undergoing atherosclerosis.[62] Furthermore, Lin and colleagues provided evidence that Res-like macrophages can proliferate, with a stem cell-like signature, derived from $CX3CR1^{+}$ precursors.[67]

$Trem2^{hi}$ macrophages present high expressions of *Trem2*, as well as a variety of other genes such as enconding osteopontin *Spp1* or cathepsins *Ctsd*, *Ctsb* and *Ctsz*. This subtype of macrophages is not present in healthy mice. Interestingly, this set of macrophages showed susceptibility to functions that were not found in the other two types, such as organic substance and cellular catabolic processes, lipid metabolic processes, regulation of cholesterol efflux and oxidative stress. Although $Trem2^{hi}$ macrophages show the expression of different markers, no clear pattern associated with the traditional M1/M2 phenotypes was observed.[62] This cell subtype, which presents the classical foam cell-like phenotype, showed

no contribution in the generation of a pro-inflammatory microenvironment, showing no production of inflammatory cytokines or chemokines.[68] Mechanistic studies showed that downregulation in the expression of Trem2 resulted in reduced endocytosis and lipid metabolism genes. This led to an increase in the inflammatory process and progression of atherosclerosis. In contrast, increased expression of Trem2 promoted the clearing of lipid debris and necrotic cells by macrophages and inhibited inflammation.[69]

Kim and colleagues showed that there is a distinct difference in the gene expression profiles of foamy and non-foamy cells. These differences were related with cholesterol and fatty acid transport, cholesterol uptake and inflammatory response. While inflammatory genes such as *Tlr2, Tnf* and *I1b* were upregulates in non-foamy cells, efferocytosis and resolving related genes including *Cd36* and *Mertk* were only elevated in foamy cells.[64] Moreover, the expression of metalloproteins *Mmp12* and *Mmp14* were only increased in foamy Trem2^{hi} macrophages.[70] Similarly, single-cell RNA and single-cell ATAC sequencing of human carotid plaques revealed the presence of a non-inflammatory subtype of macrophages that expressed foam cell markers such as *ABCA1, ABCG1, MMP9* and *OLR1*.[71]

Smaller clusters of macrophages have been identified in atherosclerosis by different groups. van Kuijk *et al* and Fidler *et al*, identified cavity macrophages in the plaque, in mice.[72,73] This cell subtype is characterised by the expression of *Cd226, Itgx, Ccr2* and *Retnla*.[74] Li and colleagues identified a macrophage subset that overexpressed NECTIN2 in advanced atherosclerotic lesions. These macrophages were located in the fibrous cap of the atheroma. These findings were observed in both mouse and human plaques.[75]

Macrophage subtype	Species/model	Marker genes	Reference
Inflammatory	Murine – *LDLR$^{-/-}$, ApoE$^{-/-}$*	*Il1b, Tnf, Ccr1, Trem1, Egr1, Nlrp3, Phlda1, Tlr2, Ccl3-5, Mrc1*	Cochain *et al*[62] Zernecke *et al*[25] Kim *et al*[64]
	Human	*NFKBIA, JUNB, CYBA, LYZ, TIMP1*	Fernandez *et al*[66]
Resident-like	Murine – *LDLR$^{-/-}$, ApoE$^{-/-}$*	*Mrc1, Lyve1, Lyve6, Pf4, Txnip*	Cochain *et al*[62] Kim *et al*[64] Lin *et al*[67]
	Human	*MRC1, CD163*	Fernandez *et al*[66]
Trem2^{hi}	Murine – *LDLR$^{-/-}$, ApoE$^{-/-}$, PHD2cko*	*Trem2, Spp1, Lgals3, Cd9, Fabp5*	Cochain *et al*[62] Kim *et al*[64] Park *et al*[70] van Kuijk *et al*[73]
	Human	*TREM2, CD63*	Do *et al*[76] Fernandez *et al*[66]
Foamy	Murine – *LDLR$^{-/-}$, ApoE$^{-/-}$*	*Cd36, Mertk, Fabp4*	Kim *et al*[64]
	Human	*ABCG1, ABCA1, MMP9, OLR1*	Depuydt *et al*[71]
Cavity	Murine – *Jak2VF Gsdmd$^{-/-}$, PHD2cko*	*Retnla, Lyz1, Fn1*	Fidler *et al*[72] van Kuijk *et al*[73]
Nectin2^{hi}	Murine – ApoE$^{-/-}$	*Nectin2^{+}*	Li *et al*[75]
	Human	*NECTIN2^{+}*	

Table 1. 1. – Newly identified macrophage subtypes in atherosclerosis. Identification of macrophage subtypes using single-cell RNA sequencing analysis in mice and humans.

1.1.6. Fibrous cap and vascular smooth muscle cell migration

VSMC are a major component of the arterial wall and are responsible for regulating blood pressure through their contractile properties.[77] As atherosclerotic inflammation develops, VSMC are also recruited to the plaque. Different VSMC phenotypes can found in different areas of the plaque. Smooth muscle alpha actin 2 (ACTA2) is one of the proteins responsible for the contractability of the VSMC that is expressed in the media layer of healthy vessels

but it can be downregulated upon the development of atherosclerosis.[78] In fact, there is evidence that while ACTA2^{+} VSMC are found predominantly in the fibrous cap, ACTA2^{-} are more prevalent in the plaque core.[79] VSMC, together with extracellular matrix molecules, create a fibrous cap which will cover lesions in an attempt to stabilize them.[80,81] The plaque stability depends on the composition and thickness of the fibrous cap.[82] VSMC are the primary source of collagen within the cap, which provides mechanical resistance to rupture.[83] In the presence of cholesterol products, VSMC can transform into a foam-like cell and contribute to the plaque cellular burden.[47] As the inflammation progresses, necrotic cores start forming within the atherosclerotic plaque.

1.1.7. Necrotic cores and cap rupture

The persistent inflammatory response observed inside the plaque leads to cell apoptosis and, due to an impaired phagocytic system, an accumulation of debris and apoptotic cells generates an necrotic core.[39] Macrophages remove apoptotic cells and cellular debris through a process called efferocytosis, in an attempt to avoid the formation of plaques. This is a protective process that removes lipid overloaded cells. In advanced plaques, the elevated number of apoptotic cells affects macrophages phagocytic capacity and efficiency and therefore a deficient efferocytosis.[84] This promotes the release of pro-inflammatory mediators, further aggravating the chronic inflammation associated with atherosclerosis. Studies suggest that the inability to remove apoptotic VSMC significantly contributes to the development of the necrotic core since this cell type corresponds to an average of 70% of its cellular content.[85,86] Plaques with larger necrotic cores and a thinner fibrous cap are

particularly prone to rupture and exposure of thrombogenic contents to circulating cellular and non-cellular blood elements, causing thrombosis.[87]

Another factor that plays a role in the progression of atherosclerotic plaques and cap vulnerability is vascular calcification (VC).[88] Micro- and macrocalcifications occur at different stages of atheroma development. Microcalcification is more commonly found in the early stages of plaque progression and is associated with active inflammation. Both VSMC and macrophages produce matrix vesicles, which surround the lipid pools of the plaques and serve as initiation products for mineral crystal formation. Cytokines present in that microenvironment, such as TNF-α, promote an upregulation of the calcification regulators Runt-related transcription factor-2 (Runx2) and bone morphogenic protein (BMP). These two regulators activate osteogenic differentiation (VSMC differentiate into osteoblast-like cells) and mineralization of the extracellular matrix. Having multiple microcalcifications, located in proximity to each other, considerably increases the vulnerability of the cap and can lead to its rupture.[89,90]

Macrocalcification, on the other hand, provides stability to the plaque.[91] In a multinational clinical study, researchers found that although calcified plaques are a marker of risk and disease progression, higher percentages of calcification per plaque volume are associated with plaque stability and reduced risk of lesion rupture and of cardiovascular events.[92]

Unstable plaques are particularly prone to structural defects, such as thinning of the fibrous cap. This usually happens because there has been a gradual loss of VSMC and therefore less production of collagen, or an increased infiltration of macrophages, which produce proteolytic enzymes (such as metalloproteinases) and degrade the collagen-rich cap matrix. A range of triggers, such as physical activity, may lead to the rupture of a thin cap and

exposure of the plaque contents to the bloodstream. The magnitude of the thrombogenic response after rupture is extremely variable, since there are different factors that will affect this process: systemic thrombotic propensity; thrombogenicity of the exposed plaque material; and local flow disturbances.[93–95]

1.2. The netrin family of proteins

Netrins are a family of laminin-like proteins, first described in the early 1990s as axonal guidance cues during embryonic development. In humans, four different netrins have been described (netrin-1, -3, -4 and -5), presenting a secondary structure which is highly conserved between species. Netrin-1 to -4 are composed of one N-terminal domain VI, a positively charged C-terminal domain and three laminin V-type epidermal growth factor (EGF) domains with the same characteristic number and spacing of Cys residues as observed in laminins.[96,97] Unlike the structures of netrin-1, -3, and -4, full length netrin-5 comprises three V-type EGF and the C-terminal domains but lacks the N-terminal laminin VI domain.[98] While netrin-1 and 3 present similar V- and VI-type domains to those observed in laminin-γ1, netrin-4 amino-terminal domains are most similar to the amino terminus of the laminin-β1 chain1 (Figure 1.4).[99,100] The C-terminal domain is the part which varies the greatest between species. The C-terminal sequences are rich in basic amino acids, which are binding sites for membrane glucolipids and proteoglycans, thereby allowing interaction with cell surface components and the extracellular matrix.[97]

Most of the members of the netrin family are secreted proteins and they are bifunctional, acting as both short- and long-range signals.[101] They bind to different receptors due to the different homologies between them.

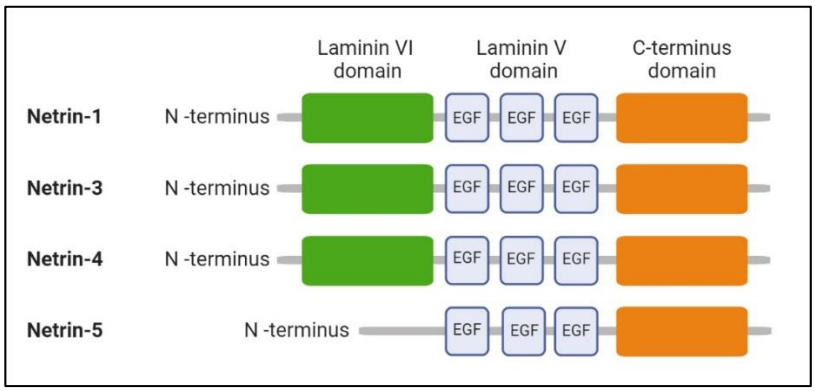

Figure 1.4 - Schematic structure of the netrin family members. Figure reprinted from *Claro and Ferro* (2020).[102]

Although netrins were first defined due to their role in the development of the central nervous system, more recently other physiological and pathological roles have been ascribed to these proteins. There is evidence that netrins play important roles in different types of cancer and in the morphogenesis of various tissues.[103] Nonetheless, the only netrin that has been described in the cardiovascular system to date is netrin-1.

1.3. Netrin-1

Netrin-1 is the most extensively studied of all the netrins. In humans, it is encoded by the gene *NTN1* in chromosome 17 and encodes a highly conserved 604 amino acid protein (Figure 1.5). It is expressed by different types of cells and can be found in most tissues. Relative quantification of mRNA shows high expression of netrin-1 in brain, heart, kidney and lungs, and low expression in the liver, intestine and spleen.[104] Netrin-1 possesses two

receptor-binding sites in the two ends of an elongated flower-shaped structure, which interact with two different receptor molecules.[105]

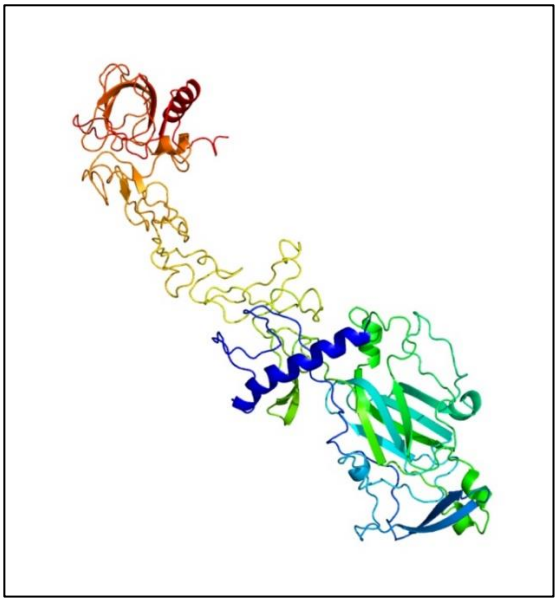

Figure 1.5 - Predicted unbound netrin-1 tertiary structure generated by Phyre2 software, using the human netrin-1 UniProt sequence. The structure is flower-shaped. The N- terminus is located on the bottom right hand-side of the structure (dark blue). There are three V-type epidermal growth factor domains (green and yellow motifs) and the C-terminus at the top (red motif). Figure reprinted from *Claro and Ferro* (2020).[102]

The functions of netrin-1 were initially identified as mediation of axonal orientation, axonal outgrowth and neuronal migration.[106] The ability of netrin-1 to repel neuronal cells makes it a potential candidate for the regulation of inflammatory cell migration. Netrin-1 has been identified as having roles in angiogenesis[107], tumorigenesis[108], organogenesis[109] and inflammation, suggesting that it regulates cell migration in a broad context, as described below.

1.3.1. Netrin-1 in angiogenesis

Netrin-1 has been reported as an angiogenic agent in both physiological and pathological contexts, acting either as a promoter or as an inhibitor of angiogenesis. It is well established that netrin-1 participates in both angiogenesis and morphogenesis of the vasculature during foetal life, as well as in adult homeostasis. Similar to what is observed in axon formation, the specific effects of netrin-1 depend on which receptors it binds to. Park *et al* showed that netrin-1 not only promotes angiogenesis itself, but also enhances the angiogenic activity of vascular endothelial growth factor (VEGF) both *in vitro* and *in vivo.*[107] Pro-angiogenic effects were also observed in pathological angiogenesis, where it promoted the creation of new vessels in conditions such as cancer. Shimizu *et al* and Akino *et al* respectively showed that netrin-1 promotes the creation of new vessels in glioblastoma and paediatric medulloblastoma, leading to a more aggressive pathology.[110,111]

1.3.2. Netrin-1 in apoptosis

Apoptosis is another physiological process in which netrin-1 plays a role. Its ability to inhibit apoptosis is related to binding to its specific receptors, which trigger apoptosis in the absence of the ligand. Therefore, netrin-1 inhibits apoptosis and promotes survivability. Castets and colleagues showed that netrin-1 blocks endothelial cell apoptosis in a zebrafish model. This inhibition was shown to be related to the interaction between netrin-1 and its receptor UNC5b.[112] Llambi *et al* identified similar results in embryonic kidney cells after transient transfection to express UNC5H2, where treating the cells with netrin-1 drastically reduced UNC5H2-induced cell death.[113]

The interaction of netrin-1 with its receptor DCC has also been reported to be important in the pathogenesis of Parkinson's disease. Neuronal loss and motor defects were observed in netrin-1-depleted mice. Furthermore, conditional knockout of netrin-1 caused apoptosis of dopaminergic neurons. Netrin-1 expression on both gene and protein levels were progressively reduced in adult substantia nigra, in an age-dependent manner.[114,115]

The interaction between netrin-1 and its receptors and the pathways triggered will be described in more detail in section 1.5.

1.3.3. Netrin-1 in cancer

Netrin-1 has also been classified as an oncogene due to its various roles in tumorigenesis, including inhibition of macrophage recruitment, promotion of cell survival, stimulation of invasiveness and of pathological angiogenesis. Several groups have shown that netrin-1 is upregulated in glioblastoma, medulloblastoma and other malignancies, and its overexpression leads to a poorer prognosis.[110,111] Li *et al* reported that netrin-1 abrogated the tumour-suppressive effects of SOX6. The study showed that netrin-1 was highly expressed in malignant ovarian tumour cells but not on normal epithelial cells. While SOX6 inhibited the growth and invasiveness of the cells, netrin-1 suppressed this protective effect.[116] Another group studied serum netrin-1 as a biomarker for colorectal cancer and found that patients that suffered from this malignancy presented significantly higher expression of serum netrin-1 than did controls.[117] Upregulation of netrin-1 was also found in metastatic renal carcinoma. Frees and colleagues showed, using qPCR and microarrays, that netrin-1 is highly upregulated in this type of malignancy. However, in their experiments, this upregulation did not enhance migration or cell viability.[118]

As mentioned previously, high expression of netrin-1 leads to enhanced vascularisation and inhibition of apoptosis, promoting a more aggressive pathology and a poorer prognosis for cancer patients.

1.3.4. Netrin-1 in organogenesis

In addition to apoptosis and angiogenesis, the role of netrin-1 and its receptors in organogenesis has been studied in terms of its regulation of migration, differentiation, and branching morphogenesis. The importance of this molecule in the development of tissues, such as lungs, pancreas or mammary glands, has been revealed in the last couple of decades.[109,119,120] Srinivasan and colleagues reported that loss of either netrin-1 or its receptor DCC leads to abnormal terminal end buds (TEB), which are part of the mammary glands and that adding back netrin-1 restores the normal TEB topology.[109] Dalvin *et al* showed that netrin-1 controls epithelial-mesenchymal interaction, which is a key process in lung organogenesis. [119] Furthermore, De Breuck *et al* demonstrated that netrin-1 is involved in pancreatic morphogenesis and tissue remodelling *in vivo.*[120] Opitz and colleagues studied the importance of *ntn1a*, which is a paralogous homolog of the human *NTN1*, in thyroid and cardiovascular development and showed that knockout of this protein led to morphological defects in zebrafish embryos. They highlighted that *ntn1a*-deficient embryos exhibited abnormal thyroid morphology and defective morphogenesis of the aortic arch, ranging from hypoplasia to severe underdevelopment of the entire aortic arch system.[121] Together, this data shows that netrin-1 and its receptors play an important role in the morphogenesis of branched tissues.

1.3.5. Netrin-1 in inflammation

As mentioned above, there is evidence that netrin-1 mediates inflammation due to its effect on immune cells, having a role in their recruitment and motility, as well as in their stimulation and production of cytokines. Nonetheless, it is controversial whether a high expression of netrin-1 is beneficial or detrimental. Some studies show that netrin-1 has a protective effect in pathological models. *In vivo* work performed by Mirakaj *et al* showed that expression of netrin-1 was repressed in acute inflammation in lung injury and peritonitis. Moreover, this group showed that treatment with exogenous netrin-1 dampened the inflammation and reduced tissue damage.[122,123] Chen and colleagues found that netrin-1 and T_{reg} cells were significantly downregulated in lung ischemia-reperfusion injury. Treating mice with netrin-1 led to decreased lung tissue necrosis and an increase in the T_{reg} cell type population, reducing injury.[124]

In accordance with the above, Grenz *et al* demonstrated that acute kidney injury was aggravated in a mouse model with partial netrin-1 deficiency, and treatment with exogenous netrin-1 attenuated the effects observed, reducing tissue injury.[125] Work performed by Wang *et al* showed that transgenic mice that overexpressed netrin-1 were resistant to ischemia-reperfusion-induced renal dysfunction and presented reduced oxidative stress, pro-inflammatory cytokine expression and tubular epithelial cell apoptosis.[126] Additionally, overexpression of netrin-1 induced M2 phenotype polarisation through the PPAR pathway.[127]

Similarly to what was observed in the renal system, reports show that netrin-1 plays a cardioprotective role after ischemia-reperfusion injury. Treating mice with netrin-1 during the reperfusion period led to a significantly smaller size of injury.[128] Zhang *et al* reported that netrin-1 stimulates the production of nitric oxide (NO) and this mediates the cardioprotective

effects observed. Netrin-1 inhibited expression of inflammatory cytokines, leukocyte infiltration, oxidative stress and apoptosis in cardiac cells and promoted the generation of M2 macrophages.[129,130]

Aherne and colleagues studied the potential role of netrin-1 in inflammatory bowel disease and found that deficiency in the expression of this protein led to an increase in the severity of the disease. The numbers of neutrophils found in netrin-1-deficient mice were greater than in the wild-type, as were the expression of IL-1β and TNF-α. Treatment with netrin-1 limited leukocyte infiltration within the intestinal lamina propria and attenuated the severity of the disease.[131,132]

In contrast, Mediero *et al* have proposed a pro-inflammatory role for netrin-1, which is required for the development of particle-induced osteolysis, hypothesising that it leads to the recruitment, retention and enhancement of osteoclast differentiation and activity.[133] Van Gils and colleagues have provided evidence that netrin-1 promotes atherosclerosis due to its effect on inhibiting the emigration of macrophages and increasing recruitment of smooth muscle cells to the plaque.[134] Ramkhelawon *et al* showed that adipose tissue produces high amounts of netrin-1, promoting macrophage retention, chronic inflammation and insulin resistance.[135] The pro- and anti-inflammatory effects of netrin-1 therefore appear to vary depending on the specific microenvironment and system.

1.4. Netrin-1 truncated isoform

In the last decade, a number of studies have shown the existence of two isoforms of netrin-1, which may help to explain some of the apparently conflicting effects reported for this protein.[108,136,137] Delloye-Bourgeois *et al* first described a new netrin-1 isoform which is

truncated and abundantly expressed in a neuroblastoma cell line model.[108] This isoform is produced by an alternative promoter, localised in intron I of the netrin-1 DNA sequence, which is NF-κB dependent and its primary sequence consists of 420 amino acids (Figure 1.6).[108,138] The research group reported that the C-terminus of netrin-1 mediates its nucleolar localisation and the N-terminus prevents it, the latter instead promoting its secretion from the cell. As a result, the truncated netrin-1, which lacks part of the N-terminal domain, stays localised within the nuclei.[108] Truncated netrin-1 has been shown to be expressed in a range of types of cancer, and high expression of this isoform appears to associate with poorer patient prognosis.[108,137] This truncated isoform affects nucleolar function; for instance, in cancer cells, overexpression of this isoform promotes ribosome synthesis, tumour growth and cell proliferation.[108]

Passacquale *et al* showed that endothelial cells also express the truncated isoform of netrin-1. TNF-α treatment disturbs the balance of expression between the two isoforms, promoting upregulation of the truncated one and downregulation of the secreted (full-length) isoform. They also demonstrated that the two isoforms are regulated differently in endothelial cells. As previously described by Delloye-Bourgeois *et al* in neuroblastoma cells, the truncated isoform promoter was found to be NF-κB dependent, so that treating endothelial cells with an NF-κB inhibitor supressed TNF-α-induced expression of the truncated isoform, both at the transcriptional and protein levels. They also showed that the induction of secreted full-length netrin-1 is NF-κB-independent, but on the other hand is dependent on histone H3 acetylation, which in turn could be induced by aspirin treatment of endothelial cells.[136]

The effects of the nucleolar isoform in other cell types, such as leukocytes, has not been determined as yet. Further work is required to clarify whether this isoform is expressed in

inflammatory conditions such as atherosclerosis, and what its contribution to the modulation of such inflammatory pathologies might be.

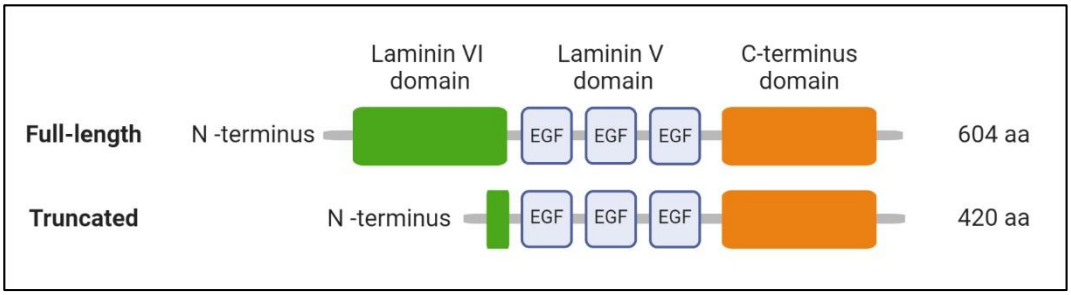

Figure 1.6 - Schematic structure of netrin-1 isoforms. The initial portion of the Laminin VI-like domain is absent in the truncated isoform. Figure reprinted from *Claro and Ferro* (2020).[102]

1.5. Netrin-1 receptors

The function of netrin-1 in regulating neuronal navigation has been associated with two main types of receptors, termed dependence receptors: DCC (Deleted in Colorectal Cancer) and its orthologue neogenin, and UNC5 (UNCoordinated protein 5) receptors (UNC5a-d) (Figure 1.7). These are receptors that play a dual role, triggering different cellular responses in the presence or absence of ligand. On the one hand cell proliferation, migration and survival are promoted in the presence of netrin-1 whilst, on the other hand, apoptosis is induced in the absence of the ligand. Moreover, relative expression levels of both families of receptors will mediate the attraction or repulsion effects observed in neuronal development, which will be further explored below.[113,139]

Different signalling pathways have been proposed for these receptors and receptor complexes. In the development of the central nervous system, netrin-1 exerts a bifunctional effect, depending on which combination of receptors it binds to. Netrin-1 can promote

attraction if it binds to a DCC-DCC complex, leading to the activation of several cascades of events which promote directional axonal outgrowth. The opposite effect, namely repulsion, occurs when netrin-1 binds exclusively to an UNC5 receptor or UNC5 and DCC simultaneously, promoting short- and long-range repulsion respectively.[139,140]

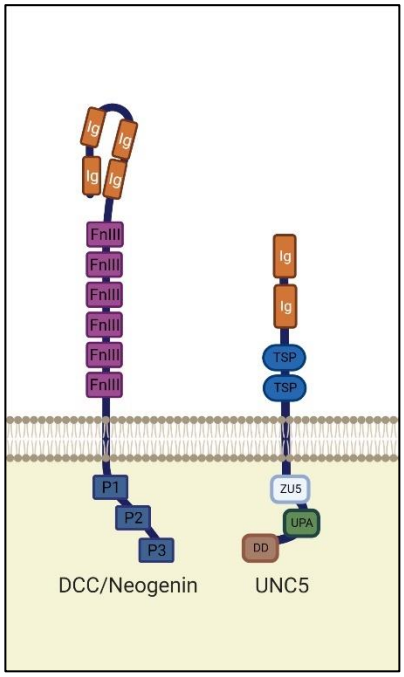

Figure 1.7 - Netrin-1 dependence receptors. Receptors subunits representation. Figure reprinted from *Claro and Ferro* (2020).[102]

1.5.1. Uncoordinated 5 family

UNC5 receptors are single-pass transmembrane receptors with an extracellular region consisting of two Ig-like motifs, followed by two TSP modules.[141] On the cytosolic side, UNC5 receptors have a long tail which consists of a ZU5 domain, a DCC-binding motif (UPA) and a death domain (DD).[142] Both Ig-like domains may be responsible for the primary binding of netrins and it is suggested that the second motif (Ig2) contributes more to the binding than Ig1 (Figure 1.7).[143]

Cleavage of UNC5 by caspase-3 induces cell apoptosis, through its intracellular death domain. However, mutation of the caspase-3 cleavage site of UNC5 does not inhibit apoptosis; at the same time, deletion of the myristoylation signal peptide, which is localized in the C-terminus of the receptor, prevents the triggering of apoptosis.[144]

So far, four different homologues of UNC5 have been found, UNC5a-d. UNC5a is mainly expressed in the ventral spinal cord; UNC5b is predominantly expressed in brain, lung, immune tissues and haematopoietic cells; UNC5c is found in migrating neural crest cells, kidney and cartilage and UNC5d is found in inner ear, brain and glands.[104]

1.5.2. UNC5b

Netrin-1 has been shown to play a key role in modulating the migration of leukocytes through its UNC5b receptor.[104] Although the precise signalling pathway is not yet understood, there is strong evidence that this event is an important modulator in the recruitment of leukocytes and inflammation. Ly and colleagues showed that in monocytes, UNC5b is responsible for the inhibition of fMLP chemotactic effect in the presence of netrin-1, in a dose-dependent manner. Moreover, netrin-1 significantly inhibited granulocyte migration towards IL-8, and lymphocyte migration towards stromal cell-derived factor 1α, through interaction with this receptor. Using an *in vivo* model, they showed that intraperitoneal injection of fMLP or IL-8 caused a rapid recruitment of leukocytes, predominately granulocytes to the peritoneum, but combining either treatment with netrin-1 led to a reduction in 45% and 48% in the cell recruitment, respectively.[104]

Tadagavadi *et al* reported that the receptor UNC5b is responsible for improved renal function after ischemia-reperfusion injury. Mice treated with netrin-1 showed lower levels of serum

creatinine and therefore improved renal function. However, when the animals were pre-treated with an UNC5b blocking antibody, netrin-1-mediated improvement was attenuated. Using the same model, the expression of different cytokines and chemokines were measured. Netrin-1 administration promoted a downregulation of IL-1β, IL-6, TNF-α and MCP-1, but mice pre-treated with UNC5b blocking antibodies exhibited a significant reduction in netrin-1-mediated cytokine downregulation.[145]

1.5.3. Deleted in Colon Carcinoma/Neogenin

DCC and neogenin are receptor homologues which share nearly half of their amino acid identity and display the same secondary structure.[146] They are single-pass transmembrane receptors with an extensive extracellular region, which comprises four immunoglobulin (Ig)-like domains in a horseshoe configuration[147], followed by six fibronectin type III domains (FnIII). The intracellular portion of the receptor contains three conserved motifs, which are responsible for signalling (P1, P2 and P3).[148] Biochemical studies suggest that FnIII4, FnIII5 and FnIII6 are the DCC domains responsible for the binding of netrins (Figure 1.7).[143,149]

DCC was originally characterised as a suppressor of colorectal cancer when a pronounced reduction of its expression was observed in several colorectal carcinoma cell lines, due to a deletion in chromosome 18q21.[150] Many studies have established the importance of DCC/neogenin and netrin-1 in different pathologies. For example, Reyes-Mugica *et al* and Koren *et al* showed that loss of DCC expression is associated with poor prognosis in patients with glioma and breast cancer respectively.[151,152] In a cardiac ischemia-reperfusion model, treating $DCC^{+/+}$ mice with netrin-1 led to a 45% decrease in the size of the lesion when compared with the control group. This effect was attenuated in $DCC^{+/-}$ mice after treatment,

where the protective effect of netrin-1 led to a decrease of the lesion size of only 15%.[128] Furthermore, a different group showed that the netrin-1 cardioprotective effect relies on NO expression, which is a product DCC-dependent activation of ERK1/2 and eNOS. The expression of NO in $DCC^{+/-}$ models was substantially lower after ischemia-reperfusion than in the wild-type model.[130]

In the immune system, the DCC/neogenin receptor family mediates a pro-migration response to netrin-1. Boneschansker *et al* reported that netrin-1 plays an important role, inducing migration of lymphocytes via its receptor neogenin. Netrin-1 is an inducer of $CD4^+$ T cells, and its interactions with neogenin augmented the migration of these leukocytes in an *in vitro* model. The same group also reported that neogenin-expressing T cells are recruited in pro-inflammatory environments where netrin-1 is expressed. Using a humanized severe combined immunodeficient mouse model engrafted with human skin, injection of netrin-1 intradermally into the skin graft, led to an increase in T cell infiltration compared to vehicle injection. After histological analysis of the grafts, it was determined that the infiltration was associated with neogenin-expressing $CD3^+$ T cells.[153]

Apoptosis and cell survival have also been identified as downstream effects dependent on netrin-1 and its receptors. Mehlen *et al* showed that, in the absence of netrin-1, DCC induces apoptosis. Moreover, this receptor is a caspase substrate which loses its pro-apoptotic effect if there is a mutation at the site where caspase-3 cleaves DCC.[154]

1.5.4. Other netrin-1 receptors

CD146, an adhesion molecule expressed by endothelial cells, mostly in the vasculature, has also been described as a netrin-1 receptor. The molecular mechanisms associated with this

receptor are angiogenesis, vessel permeability and leukocyte transendothelial migration.[155] CD146 has been described as a pro-angiogenic mediator, counterbalancing the UNC5b anti-angiogenic signal. Jiang *et al* reported that CD146 also plays a role in apoptosis in endothelial progenitor cells (EPC), under hypoxic conditions. Netrin-1 was upregulated in EPC and plays a protective role when the cells are under hypoxic stress, promoting survivability. Transfecting EPC with CD146-siRNA led to inhibition of the netrin-1-dependent survivability signal, under hypoxia.[156]

A2B adenosine receptor (ADORA2B) has also been identified as a netrin-1 receptor in dextran sulphate sodium-induced colitis. ADORA2B-deficient mice experienced the same extent of inflammation after treatment with netrin-1 that netrin-1-deficient mice suffered, indicating that this was the key receptor in mediating netrin-1 effect.[131,132] Furthermore, the same receptor has been shown to affect netrin-1-dependent transepithelial migration of neutrophils. Using an ADORA2B antagonist, Rosenberger and colleagues showed that the upregulation of cAMP needed for the neutrophils to migrate only happened when the antagonist was not present.[157]

Down syndrome cell adhesion molecule (DSCAM) has more recently been proposed as a novel receptor for netrin-1. Its collaboration with DCC has been shown to be essential for commissural axons to grow towards and across the midline.[158] There is no evidence to date that this receptor plays a role in cardiovascular disease.

1.6. Netrin-1 in atherosclerosis

Atherosclerosis is a chronic inflammatory disease that progresses over many years and often is only detected when the patient develops symptoms such as myocardial ischaemia. It is triggered by lipid retention in the arterial walls, predominantly in certain segments of arteries, such as branching points and bends which are especially prone to atherosclerotic plaque development because of local disturbance of endothelial function, due in turn to local turbulence of blood flow.[8] Monocytes are recruited to the arterial wall in areas of developing atherosclerotic plaque, where they differentiate into macrophages. These macrophages take up cholesterol from the sub-intimal layer and transform into foam cells, losing their ability to egress to the lymphatic system, ultimately contributing to the development of necrotic plaque core and thinning of the fibrous cap. The plaque thereby becomes more vulnerable to erosion or rupture, with resultant superadded arterial thrombosis giving rise to cardiovascular events such as myocardial infarction or stroke.[23]

The reported effects of netrin-1 in atherosclerosis have been conflicting, having been shown to play both pro- and anti-inflammatory roles in the development of the disease. This conflicting evidence may be explained by the temporal and spatial expression of netrin-1: endothelial-derived netrin-1 has been reported as playing a protective role, whilst netrin-1 secreted within the atherosclerotic plaque by macrophages appears to exert a pro-atherogenic effect. These are described in detail below.

1.6.1. Endothelial-derived netrin-1 (systemic)

Endothelial cells secrete full length netrin-1, leading to a reduction of monocyte chemotaxis

into the arterial wall, as first demonstrated by Passacquale *et al*, in *ApoE*$^{-/-}$ mice. They found that UNC5b blockade inhibited the effects of netrin-1 with a consequent increase in accumulation of monocytes in the brachiocephalic artery.[136] Furthermore, Lin *et al* and Bruikman *et al* showed that netrin-1 reduces the expression of adhesion molecules induced by the pro-inflammatory cytokine TNF-α. In an *in vitro* model of human aortic endothelial cells stimulated with TNF-α, a significant reduction in the expression of VCAM-1, ICAM-1 and E-selectin was observed when cells were co-treated with netrin-1, and high concentrations of netrin-1 completely abolished the expression of these adhesion molecules.[159] Significant downregulation of ICAM-1, IL-6 and MCP-1 has also been observed in endothelial cells from patients with underlying atherosclerosis, this effect being abolished by UNC5b blockade (Figure 1.8A).[160] Furthermore, Lin *et al* also showed that netrin-1 supresses endothelial-derived cytokine production induced by TNF-α in a concentration-dependent manner. They demonstrated that netrin-1 selectively suppresses TLR4 and inhibits the NF-κB pathway by suppressing TNF-α-induced IKK and IκBα activation in the cytoplasm. They also showed that netrin-1 affects the nuclear NF-κB subunit p65 by reducing its accumulation in the nuclei. While stimulation with TNF-α led to an approximately 3.4-fold increase of p65 in the nuclei compared with basal levels, treatment with 200 and 400 ng/ml netrin-1 reduced its nuclear accumulation by 25% and 50%, respectively. Moreover, netrin-1 suppressed NF-κB promoter activation in endothelial cells after TNF-α stimulation: TNF-α increased the promoter activity 70-fold, and this was supressed by 30% and 60% after treatment with 200 and 400 ng/ml netrin-1, respectively.[159]

From a different perspective, Passacquale *et al* showed that pro-inflammatory stimuli cause downregulation of endothelial-derived netrin-1 expression.[136] Thus, it would be expected that the protective effect of netrin-1 will decrease as the atherosclerotic process proceeds,

thereby further accelerating its progression. Indeed, Bruikman and colleagues showed that netrin-1 plasma levels are inversely correlated with arterial wall inflammation as well as total plaque volume. Additionally, patients with calcified atherosclerotic lesions presented lower levels of netrin-1 in their plasma.[160] Fiorelli and colleagues obtained concordant results, where cohorts of patients were studied and compared depending on the severity of their diseases. Patients that suffered myocardial infarction presented lower levels of systemic netrin-1 than patients with stable angina, whilst the control group had the highest level of all.[161]

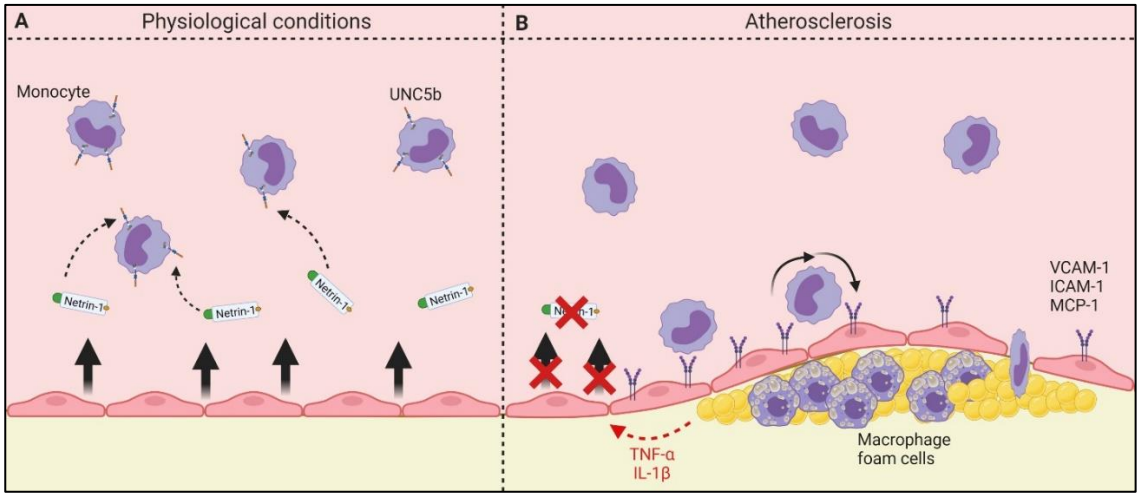

Figure 1.8 - Overview of netrin-1 effects in the context of normal physiology and atherosclerosis. (A) Chemorepulsive effect of endothelial-derived netrin-1 on monocytes. (B) During atherosclerosis, pro-inflammatory cytokines expressed by the foam cells induce the expression of adhesion molecules on endothelial cells and downregulate the secretion of endothelial-derived netrin-1. Figure reprinted from *Claro and Ferro* (2020).[102]

Studies in a family that have a mutation in netrin-1 revealed exacerbated anti-inflammatory effects on endothelial cells, and stronger chemorepulsion against macrophages, when compared with non-mutant netrin-1. Individuals with this mutation developed atherosclerosis in earlier stages of life and in one case, myocardial infarction at 30 years of age. This individual did not present classical risk factors for cardiovascular disease.[162]

1.6.2. Macrophage-derived netrin-1

Macrophages can also express netrin-1.[104,134,135,163] Nonetheless, what effects macrophage-derived netrin-1 may exert on the ability of macrophages to migrate in response to chemokines or on modulation of their phenotype remains entirely unclear. Tadagavadi *et al* and Komatsuzaki *et al* reported, using immunohistochemistry and quantitative RT-PCR, that only UNC5b is expressed in monocytes, granulocytes and lymphocytes.[104,145] We will therefore concentrate on the possible effects of netrin-1 on macrophages on the basis that it interacts with UNC5b only.

Ly *et al* showed that, in infection and pro-inflammatory models, the levels of netrin-1 decrease and the recruitment of leukocytes to the site is promoted. They hypothesised that netrin-1 is an immunomodulator, which keeps leukocyte influx in check, preventing aberrant tissue destruction. This inhibitory effect on migration was verified *in vitro* and *in vivo* in response to a range of chemoattractive stimuli, whilst not affecting other functions, for example the production of superoxide.[104] Moreover, Taylor *et al* demonstrated that netrin-1 is also capable of inhibiting macrophage chemotaxis to non-chemokine attractants.[163] This group showed that the chemotaxis generated by the complement component C5a can be partially inhibited by netrin-1, through UNC5b.

In contrast, other researchers describe netrin-1 as a pro-inflammatory mediator. Van Gils and colleagues showed that netrin-1 can promote atherosclerosis, inhibiting the migration of foam cells to the lymph nodes, becoming trapped in the atherosclerotic plaque and thereby contributing to its development and instability. In accordance with what was reported in cancer cell models, they also reported that netrin-1 promotes cell survival in the

atherosclerotic plaque. Deficiency of netrin-1 in the macrophages reduced atherosclerosis and allowed egress of foam cells to the lymphatic system.[134]

Similarly, Ramkhelawon *et al* showed that netrin-1 promotes the retention of macrophages in adipose tissue, enhancing metabolic dysfunction and chronic inflammation. In an experiment where mutant mice, whose macrophages do not express netrin-1, and wild-type mice were fed a high fat diet, they found that recruitment of macrophages to the adipose tissue was initially similar in both groups. However, on the 14th day, the retention of macrophages was significantly lower in the mutant mice compared with the wild-types, consistent with the hypothesis that netrin-1 traps macrophages in the site and promotes chronic inflammation. Furthermore, adipose tissue macrophages isolated from the mutant mice exhibited lower mRNA expression of pro-inflammatory markers and cytokines as well as a higher expression of M2 macrophage markers, compared with the wild-type.[135]

Cardiovascular disease has been revealed to be positively associated with intracellular levels of netrin-1 in macrophages. Patients with coronary artery disease presented higher expression of netrin-1 by macrophages than healthy patients. The increased expression was more significant in patients that suffered a myocardial infarction than patients with stable angina.[161]

Regarding macrophage phenotypes, Ranganathan *et al* and Mao *et al* showed the opposite to what was observed in the Ramkhelawon *et al* study. In their experiments, they found that higher expression of netrin-1 is protective, enhancing the shifting of macrophage phenotype towards M2, with concomitant upregulation of anti-inflammatory markers such as IL-4 and IL-13 and downregulation of IL-6 and COX-2.[127,129] Both groups showed that netrin-1 activates anti-inflammatory pathways that are known to regulate macrophage polarization,

such as PPAR. PPAR mediate a variety of inflammatory mechanisms, which include repressing the activities of pro-inflammatory transcription factors such as NF-κB or STATs.[164] Netrin-1 led to a decrease in M1 polarization and cytokine production induced by interferon-γ (IFN-γ) and suppressed ischaemia-reperfusion injury, effects which were inhibited by PPAR antagonists.[127] Further work by Ranganathan *et al* suggests that netrin-1 regulates inflammation and cell migration through suppression of NF-κB, leading to downregulation of COX-2-mediated PGE2 and thromboxane A2 production, both *in vitro* and *in vivo.*[165]

Schlegel *et al* studied the role of netrin-1 in macrophages, in the context of advanced and complex atherosclerotic plaque. Using genetically modified mice, they showed that targeting netrin-1 and silencing its expression in monocytes and macrophages led to regression of the plaque. This was achieved by reducing the cellular burden through decreasing proliferation, survivability and retention. Silencing macrophage-derived netrin-1 also led to an upregulation of pro-resolution cytokines such as transforming growth factor-β (TGF-β) and IL-10. Also, there was a significant increase in M2 macrophage markers after silencing netrin-1, as well as a 2-fold increase in apoptotic cell markers, when compared with the control samples.[166]

The current data suggest that the immunomodulatory effects of netrin-1 depend on which cell type expresses it and in which environment. Macrophage-derived netrin-1 in the plaque may be detrimental because it stops macrophage egress to lymph nodes, whereas endothelial-derived (systemic) netrin-1 may be essential to suppress levels of inflammation.

1.6.3. Role of netrin-1 in murine models of atherosclerosis

Genetically modified murine models have been created to study the effects of netrin-1 in different physiological and pathological processes (Table 1.2). One of the first models was developed by Serafini and colleagues to study the development of the nervous system. *Ntn1* $^{\beta geo/\beta geo}$ model was generated using the embryonic stem cell line ST629, containing an insertion of the secretory gene trap vector pGT1.8TM within an intron of the netrin-1 gene.[167]

Generation of a netrin-1 knockout mouse model was achieved by crossing *Ntn1*$^{fl/fl}$ heterozygote mice. The *Ntn1*$^{fl/fl}$ were generated by introducing two unidirectional *loxP* sites flanking the first coding exon of the *netrin-1* gene and then crossing them with a *CMVcre* line. The loss in netrin-1 led to embryonic lethality and only *Ntn1*$^{fl/fl}$ pups were born.[168] This was a more severe model than the *Ntn1*$^{\beta geo/\beta geo}$ mutant studied by Serafini and colleagues which still showed severe neural-development deficiencies at foetal development stage.[167]

van Gils et al crossed the *Ntn1*$^{fl/fl}$ mouse model mentioned above and backcrossed eight generations onto a C57BL/6 background. *Ntn1*$^{fl/fl}$ were paired to generate *Ntn1*$^{-/-}$ embryos. At day 14 of the foetal development, bone marrow was transplanted into irradiated *Ldlr*$^{-/-}$ mice, to generate *Ldlr*$^{-/-}$ mice which monocytes/macrophages did not express netrin-1. This model was used to study the role of netrin-1 in atherosclerosis.[134]

Schlegel and colleagues also developed a mouse model which allowed temporally silencing of netrin-1 expression in monocytes and macrophages (*Ntn1*$^{fl/fl}$*Cx3cr1*$^{\text{Cre-ERT2+}}$) by treating the mouse with tamoxifen. This model was created by crossing *Ntn1*$^{fl/fl}$ with C57BL6 *Cx3cr1*$^{CreERT2+/-}$.[166]

An inducible model for netrin-1 expression (*CAG-CreERT2*$^{+/-}$*;Rosa26-LSL-Ntn1*$^{+/+}$) has also been created by Jasmin *et al* by crossing a tamoxifen-dependent *Cre* recombinase allele (*CAG-*

CreERT2$^{+/+}$) with a transgenic mouse containing the human netrin-1 cDNA preceded by a lox-stop-lox inserted in a *Rosa26* locus.[115]

Mouse model	Features	Model	Reference
Ntn1$^{\beta geo/\beta geo}$	Mutation leads to a generalised reduction in the expression of netrin-1.	CNS development	Serafini *et al*[167]
Ntn1$^{fl/fl}$	Mice express less netrin-1 than wild-type littermates.	CNS development Atherosclerosis Kidney Injury	Bin *et al*[168] van Gils *et al*[134] Grenz *et al*[169]
Ntn1$^{-/-}$	Complete loss of netrin-1 – mutation leads to embryonic lethality.	Parkinson's CNS development Atherosclerosis	Jasmin *et al*[115] Bin *et al*[168] van Gils *et al*[134]
Ldlr$^{-/-}$→ *Ntn1*$^{-/-}$	Depletion of the expression of netrin-1 by monocytes and macrophages.	Atherosclerosis	van Gils *et al*[134]
Ntn1$^{fl/fl}$*Cx3cr1*$^{Cre-ERT2+}$	Treatment with tamoxifen resulted in Cre-mediated deletion of *Ntn1* in the monocyte/macrophage lineage.	Atherosclerosis	Schlegel et al [166]
CAG-CreERT2$^{+/-}$*; Rosa26-LSL-Ntn1*$^{+/+}$	Treatment with tamoxifen induces Cre-mediated netrin-1 overexpression.	Parkinson's	Jasmin *et al*[115]

Table 1. 2 – Genetically modified murine models used to study the role of netrin-1 in different physiological and pathological processes. Conditional and tissue specific knockout and knockin models.

The two murine models that are more commonly used to study the role of netrin-1 in atherosclerosis is *Ldlr* $^{-/-}$ and *Apoe*$^{-/-}$. These do not involve mutations in the expression or function of netrin-1 but are generally accepted in the scientific community as standard for the studying of vascular inflammatory diseases. The model developed by Schlegel and colleagues brought important insight for the role of netrin-1 in atherosclerosis. A summary of the main findings relating netrin-1 in atherosclerosis were described in table 1.3.

Atherosclerosis murine model	Findings on the role of netrin-1	Reference
Ldlr$^{-/-}$	Macrophages within the atherosclerotic plaque express netrin-1 and this leads to inhibition of their migration. Targeted deletion of macrophage-derived netrin-1 led to a lower degree of atherosclerosis development and promoted the emigration of macrophages from the plaque.	van Gils *et al*[134]
	Hypoxia induces the expression of netrin-1 and its receptor UNC5b in atherosclerotic plaque by promoting macrophage survivability and inhibiting their egress to the lymph nodes.	Ramkhelawon *et al*[170]
	Proatherogenic chemokines downregulate the expression of endothelial-derived netrin-1 and reduce its monocyte-adhesion inhibitory effect.	van Gils *et al*[171]
Apoe$^{-/-}$	Aspirin enhances the expression of systemic netrin-1 in ApoE$^{-/-}$ mice fed with HFD. The modulation of the systemic netrin-1 leads to a reduction in monocyte trafficking within the atherosclerotic plaque.	Passacquale *et al*[136]
Ntn1$^{fl/fl}$*Cx3cr1*$^{Cre-ERT2+}$	Silencing macrophage-derived netrin-1 led to a reduction in the plaque burden and complexity found in the aorta. An upregulation in the gene expression related to migration and phagocytosis pathways was observed. These plaques also showed higher amount of pro-resolving cytokines then the wild-type model.	Schlegel *et al*[166]

Table 1. 3 – Murine models used to study the role of netrin-1 in atherosclerosis.

1.7. Hypotheses and aims

In the light of the above literature and based on previous findings by different groups we hypothesise that the expression of netrin-1 by macrophages varies depending on cytokine stimulation and phenotype. Moreover, this variation may affect the migration and apoptosis of this type of leukocyte. We also hypothesise that increasing the levels of systemic netrin-1 exogenously will have a protective effect against inflammation and atherosclerotic plaque formation, *in vivo*.

The aims of this thesis were as follows:

- Chapter three: To determine how the expression of netrin-1 isoforms vary depending on macrophage phenotype and cytokine stimulation.
- Chapter four: To investigate the effect of full-length netrin-1 in the apoptosis and migration of macrophages.
- Chapter five: To understand the acute and chronical effects of netrin-1 on recruitment of monocytes to the site of inflammation and development of atherosclerotic plaque.

Chapter Two

Materials & Methods

2.1. Materials

Cell culture	Company	Product Code
12,000 Daltons dialysis sacks	Sigma-Aldrich	D6191-25EA
2-Mercaptoethanol	ThermoFisher Scientific	31350010
3,000 NMWL Amicon Ultra filtres	Merck	UFC200324
Bay 11-7085	Sigma-Aldrich	B5681
Bovine Serum Albumin (BSA)	Sigma-Aldrich	A2153
CD14 magnetic MicroBeads	Miltenyi Biotec	130-050-201
Ethylenediaminetetraacetic acid (EDTA)	Cambridge Biosciences	60-00030-10
Foetal Bovine Serum (FBS)	Gibco	F7524
Glucose Solution	ThermoFisher Scientific	A2494001
Histopaque 1077	Sigma-Aldrich	10771
Human Acetylated LDL	Generon	770201-7
Human granulocyte-macrophage colony-stimulating factor (hGM-CSF)	Peprotech	300-03
Human macrophage colony-stimulating factor (hM-CSF)	Peprotech	300-25
Human plasma - nLDL	Lee Biosolutions	360-10
Interferon- γ (IFN-γ)	Sigma-Aldrich	SRP3058
Interleukine-4 (IL-4)	ThermoFisher Scientific	PHC0044
JSH 23	Abcam	ab144824
Lipopolysaccharide (LPS)	Sigma-Aldrich	L2630
LS separation column	Miltenyi Biotec	130-042-401
Penincillin/Streptomycin	Gibco	15140-122
Phorbol 12-myristate 13-acetate (PMA)	Sigma-Aldrich	P1585
Phosphate buffer saline (PBS)	ThermoFisher Scientific	14080055
Phosphate buffer saline [-Ca^{2+}/-Mg^{2+}] ($PBS^{-/-}$)	ThermoFisher Scientific	70013032
Pre-separation filters	Miltenyi Biotec	130-041-407
RPMI 1640	Sigma-Aldrich	R8758
Sodium Pyruvate	ThermoFisher Scientific	11360070
THP-1 cell line	Sigma-Aldrich	88081201
THP-1 cell line	ATCC	TIB-202
Trypan blue 0.4%	ThermoFisher Scientific	15250061

Molecular Biology	Company	Product Code
30% Acrylamide: 0.8% Bis-Acryl-amide Stock Solution	Geneflow Ltd	A2-0074
Agarose	Sigma-Aldrich	A9539-500G
Amersham™ Hyperfilm™ ECL	Fisher Scientific	10607665
Bovine anti-chicken IgY Microbeads	ThermoFisher Scientific	SA1-9588

Cell Lysis buffer (10x)	Cell Signalling	9803S
cOmplete Mini A protease cocktail	Roche	11836170001
DC protein assay	BioRad	5000 113/114
DNA LoBind tubes 1.5mL PCR clean	Eppendorf	30108051
Ethidium Bromide solution	Sigma-Aldrich	E1510
High-capacity RNA-to-cDNA Kit	appliedbiosystems	4387406
Immobilon™-P transfer membrane	Millipore	IPVH00010
Methanol	Sigma-Aldrich	34860-2.5L-R
MicroAmp Fast 96-well reaction plate	appliedbiosystems	4346907
Monarch Total RNA Miniprep Kit	New England BioLabs	T2010S
Pierce™ ECL Western Blotting Substrate	ThermoFisher Scientific	32106
Pierce™ IP Lysis buffer	ThermoFisher Scientific	87787
PowerUp SYBR Green Master Mix	appliedbiosystems	A25742
Precision plus Protein Dual colour Standards	BioRad	1610374
Restore™ Western Blot Stripping Buffer	ThermoFisher Scientific	21059
Tween 20	VWR Chemicals	437082Q
UltraPure™ 10x TBE buffer	Invitrogen	15581-044
Ultrapure Dnase/Rnase-free water	ThermoFisher Scientific	10977035

Antibodies (in vitro)	Company	Product Code
Sheep anti-human/Mouse/Rat netrin-1	R&D Systems	AF6419
Rabbit anti-sheep HRP	ThermoFisher Scientific	31480
Chicken anti-human netrin[#]	Abcam	ab39370
Goat anti-chicken HRP	Abcam	ab6877
Mouse anti-human HPRT-1	BioRad	VMA00483
Goat anti-mouse HRP	EMD Millipore	401215
Rabbit anti-human/mouse/rat/monkey cleaved caspase-3	Cell Signalling Technology	9661S
Goat anti-rabbit HPR	EMD Millipore	401315
Goat anti-rabbit AF488	ThermoFisher Scientific	A-11008

Imaging (in vitro)	Company	Product Code
4',6-Diamidino-2-Phenylindole, Dilactate (DAPI)	BioLegend	422801
4% paraformaldehyde (PFA)	Biotium	22023-20ML
Dibutylphthalate Polystyrene Xylene (DPX)	Sigma-Aldrich	06522
Eosin Y Solution	Sigma-Aldrich	HT110216
Harris Hematoxylin Solution	Sigma-Aldrich	HHS32
Oil Red O	Sigma-Aldrich	O0625
ProLong™ Gold Antifade Mountant with DAPI	ThermoFisher Scientific	P36935
Propan-2-ol	Sigma-Aldrich	109827
Triton™ X-100	Sigma-Aldrich	X100

Apoptosis and Migration	Company	Product Code
96-Well Optical-Bottom Black Plate	ThermoFisher Scientific	10281092
CIM-plate	Agilent Technologies	5665817001
E-plate	Agilent Technologies	5469830001
Human MCP-1	Peprotech	300-04
Recombinant human netrin-1	R&D Systems	6419-N1-025
Triptolide	Cayman	11973

In vivo	Company	Product Code
Isoflurane	Abbott Laboratories	
Meloxicam	Boehringer Ingelheim	
Mini-Osmotic Pump 2006	Azlet	10104856
Mouse/human anti-CD11b AF488 (rat)	BioLegend	101217
Mouse Netrin-1 ELISA	Invitrogen	EM56RB
Recombinant mouse netrin-1	R&D Systems	1109-N1-025
REDExtract-N-Amp™ Tissue PCR Kit	Merck	XNAT-100RXN
Urethane	Sigma-Aldrich	94300

Table 2. 1- List of reagents, product codes and manufacturers.

All experiments described in this thesis were optimised and performed by me, unless stated otherwise in each section description. I was also responsible for the optimisation and experiment design using the xCELLigence system. Even though this piece of equipment was used in an external institution, the researchers there use it for a different purpose and for that reason do not have the expertise to advise on adhesion and migration assays.

2.2. Tissue culture

2.2.1. THP-1 immortalised cell line

THP-1 monocytes were grown in RPMI 1640 supplemented with 10% FBS, glucose, sodium pyruvate and 2-mercaptoethanol and 100 U/mL Penicillin and Streptomycin (Appendix A) in T75 flasks. The flasks were incubated in a vertical position, at 37°C, 5% CO_2. The cell density was kept between 200,000 – 1,000,000 cells/mL.

Once the suspension reached the number of cells desired, 1.2 million cells were seeded per well of a 6-well plate and differentiated into macrophages by incubation with 100 ng/mL phorbol 12-myristate 13-acetate (PMA) for 24 to 48 h. During differentiation, the macrophages attached to the bottom of the well. The cells were then washed with PBS and incubated with PMA-free medium for 48 h. Afterwards, cells were stimulated for 24 - 48 h with 50 ng/mL IFN-γ and 10 ng/mL LPS to induce differentiation into classical activated macrophages. For alternative-activated macrophages, cultures were stimulated with 20 ng/mL IL-4 for 24 - 48 h (Figure 2.1A).

2.2.2. Primary PBMC cells

Isolation of PBMC from human whole blood

Cones of concentrated human blood (25 mL) were supplied by the NHS Blood and Transplant service. The complete isolation was performed at room temperature.

Blood was diluted 1:1 in 25mL RPMI medium. 15 mL Histopaque 1077 was transferred to a 50 mL falcon tube and the diluted blood was added on top gently, without mixing. The tube

was centrifuged at 400 x *g* for 30 min. The PBMC interphase layer was collected with sterile Pasteur pipettes, transferred to a new 50 mL tube and filled with isolation buffer ($PBS^{-/-}$ supplemented with 2 mM EDTA). The cells were pelleted at 300 x *g* for 10 min. The supernatant was removed, and fresh isolation buffer was added to the pellet. The cells were resuspended, and spun for 15 min at 200 x *g*. The pellet was resuspended in 20 mL isolation buffer.

Magnetic labelling and separation

Cells were counted and the appropriate number of cells, depending on the number of plates needed (9 million cells per plate), were spun at 300 x *g*. The cells were resuspended in an appropriate volume of MACS buffer ($PBS^{-/-}$ supplemented with 2 mM EDTA and 0.5% BSA) and labelled with CD14 magnetic MicroBeads, according to the manufacturer's instructions. MACS buffer was added to the labelled cells, and they were centrifuged at 300 x *g*, for 10 min. The supernatant was removed and up to 10^8 cells were resuspended in 500 μL of MACS buffer.

An LS column was placed in a MidiMACS™ Separator, together with a pre-separation filter. The column and filter were rinsed three times with 1 mL MACS buffer and the cell suspension was then added slowly. The run-through (unlabelled cells) was discarded. The column was washed three times with 3 mL MACS buffer. After that, the column was removed from the magnetic separator and placed in the collection tube. 5 mL MACS buffer was added to the column and immediately flushed by a plunger into the tube. Cells were counted and spun for 10 min, at 300 x *g*. The cells were resuspended in 2 mL RPMI 1640 per well (for 6-well plate),

supplemented with 2% FBS and antibiotics and seeded in 6-well plates at a density of 1.5 x 10^6 cells per well, for 1 h.

Culture of primary cells

After the initial incubation, where cells were allowed to attach to the bottom of the plate, the media was removed and fresh RPMI1640 supplemented with 10% FBS and either 20 ng/mL hGM-CSF or 25 ng/mL hM-CSF was added to each well. Media was changed twice, on day 3 and on day 6, with a mix of fresh and old media (1:1). On day 7, hGM-CSF stimulated cells were either left to incubate with no further additions (control) or were stimulated for 48 h, with 50 ng/mL IFN-γ and 20 ng/mL LPS to generate M1 macrophages. Similarly, hM-CSF stimulated cells were either incubated without further additions or were stimulated with 20 ng/mL IL-4 for 48 h, to generate M2 macrophages (Figure 2.1B).

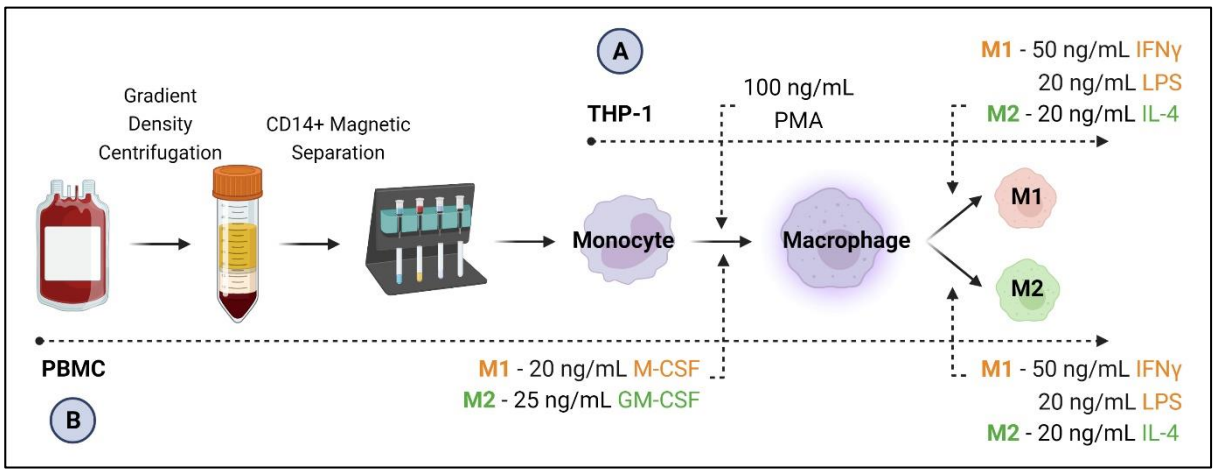

Figure 2.1 – Schematic representation of macrophage cell cultures. (A) Culture, differentiation and stimulation of THP-1 cells; (B) cell isolation, culture, differentiation and stimulation of human PBMC-derived macrophages.

2.2.3. Cell counting

A sample of the cell suspension was taken from the culture flask or tube and mixed 1:1 with Trypan blue 0.4%. 10 μL of the stained cells were transferred to a haemocytometer with a coverslip and counted. The four corner quadrants were counted (Q1-4, figure 2.2). Only cells located inside, and on the top and left limits of the grid, were counted. Cells positioned in the right and lower limits were ignored.

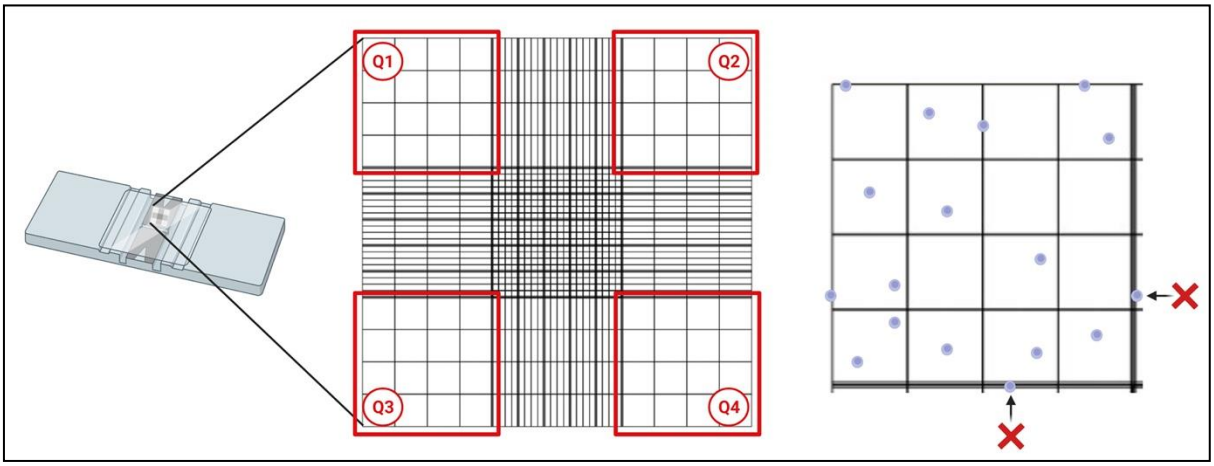

Figure 2.2 – Representation of a haemocytometer. Q1-4 are the selected areas to count cells. Only cells inside the grid or touching the top and left limits were considered.

Cell density was then determined using the equation:

$$Cell\ density\ (cells/mL) = \frac{Total\ number\ of\ cells\ \times Dilution\ factor \times 10{,}000}{Number\ of\ quadrants}$$

2.2.4. NF-κB inhibition

Two different NF-κB inhibitors were used in the cell cultures to study whether the activation of this nuclear transcription factor is involved in the expression of netrin-1 isoforms. Bay 11-7082 is an IκB kinase inhibitor. The phosphorylation and degradation of IκBα (IκBα maintains

NF-κB inactive) leads to dissociation from the nuclear localisation signals (p50/p65) and their migration to the nucleus. By inhibiting IκB kinase, Bay 11-7082 promotes the accumulation of IκBα in the cytoplasm (Figure 2.3). This inhibitor was added to the cell cultures at a concentration of 5 μM[134,136,172], 2 h prior to inflammatory stimulation.

JSH 23 inhibits p50/p65 nuclear translocation, leading to the accumulation of its active form in the cytoplasm, instead of the nucleus. This inhibitor was added to the cell cultures at a concentration of 50 μM[173,174], 2 h prior to inflammatory stimulation.

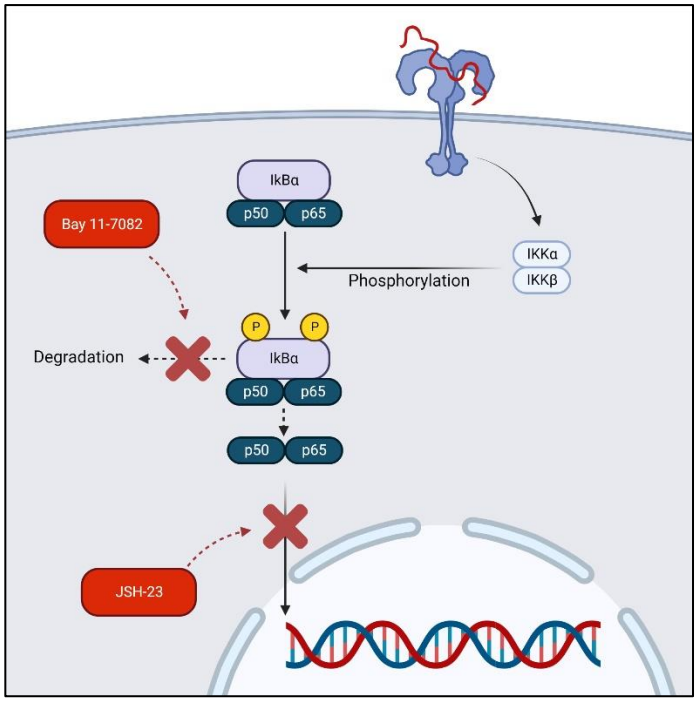

Figure 2.3 – Molecular mechanisms for Bay 11-7082 and JSH 23. Schematic representation of the molecular targets for the two NF-κB activation pathway inhibitors. Bay11-7082 is a IκB kinase inhibitor. JSH 23 is a nuclear translocation inhibitor.

2.2.5. Foam cell culture

Foam cells were generated by exposing macrophages to 50 μg/mL acLDL for 48 h. Two different sources of acLDL were used in our experiments, one commercially available and

one acetylated in house. If further inflammatory stimulation was desired, the cytokines were added to the culture in the last 24 h of the generation of foam cells.

2.2.6. Acetylation of native LDL

Chemical reaction

nLDL isolated from human plasma was commercially obtained. The LDL manipulation was performed in ice. nLDL was diluted in PBS to a final concentration of 4 mg/mL protein. 1 mL saturated sodium acetate per 10 mg of protein was added and the solution was mixed gently. 2.5 μL of acetic anhydride were added per mg of protein, divided in five doses. Each dose was added to the solution 15 min apart, while under gentle agitation, at 4°C.

Dialysis and LDL purification

The acetylation process was stopped through dialysis. AcLDL solution was transferred into 12,000 Daltons dialysis sacks and placed into 5 L PBS supplemented with 2 mM EDTA overnight at 4°C.

Excess of buffer was removed using 3,000 NMWL Amicon® Ultra filters and spun at 3,500 x *g* for 1 h at 4°C. AcLDL final concentration was determined using the DC protein assay as described below.

Protein measurement assay

Protein concentration was measured using the DC protein assay. Each sample was analysed in duplicate. Standard samples were prepared using a range of 0-2 mg/mL BSA. 5 μL of the sample or standard were loaded into each well of a 96-well plate as shown in Figure 2.4.

<table>
<tr><th></th><th>1</th><th>2</th><th>3</th><th>4</th><th>5</th><th>6</th><th>…</th></tr>
<tr><td>A</td><td colspan="2">2 mg/mL BSA</td><td colspan="2">0 mg/mL BSA</td><td colspan="3" rowspan="8">Samples (Duplicate)</td></tr>
<tr><td>B</td><td colspan="2">1 mg/mL BSA</td><td colspan="2">Buffer background</td></tr>
<tr><td>C</td><td colspan="2">0.5 mg/mL BSA</td><td colspan="2" rowspan="6">Samples (Duplicate)</td></tr>
<tr><td>D</td><td colspan="2">0.25 mg/mL BSA</td></tr>
<tr><td>E</td><td colspan="2">0.125 mg/mL BSA</td></tr>
<tr><td>F</td><td colspan="2">0.0625 mg/mL BSA</td></tr>
<tr><td>G</td><td colspan="2">0.0313 mg/mL BSA</td></tr>
<tr><td>H</td><td colspan="2">0.016 mg/mL BSA</td></tr>
</table>

Figure 2.4 – Example of plate setup for the DC Protein assay. Eight different standards (0.016 – 2 mg/mL BSA) were used in series of dilutions. Every standard and sample were analysed in duplicates.

Using a multichannel pipette, 25 μL DC Protein Assay Reagent A (1-5% sodium hydroxide; <1% sodium tartrate; <0.1% copper sulphate) were added to each well. Subsequently, 200 μL of DC Protein Assay Reagent B (lithium sulphate; tungstic acid; sodium salt hydrochloric acid; phosphoric acid) were added to each well. The plate was left in the dark for 10 min for colour development and then loaded into a plate reader, where the absorbance was measured at 700 nm.

The standard samples were used to draw a standard curve (Figure 2.5) and the concentrations of the samples were determined by plotting the absorbance values in the standard curve.

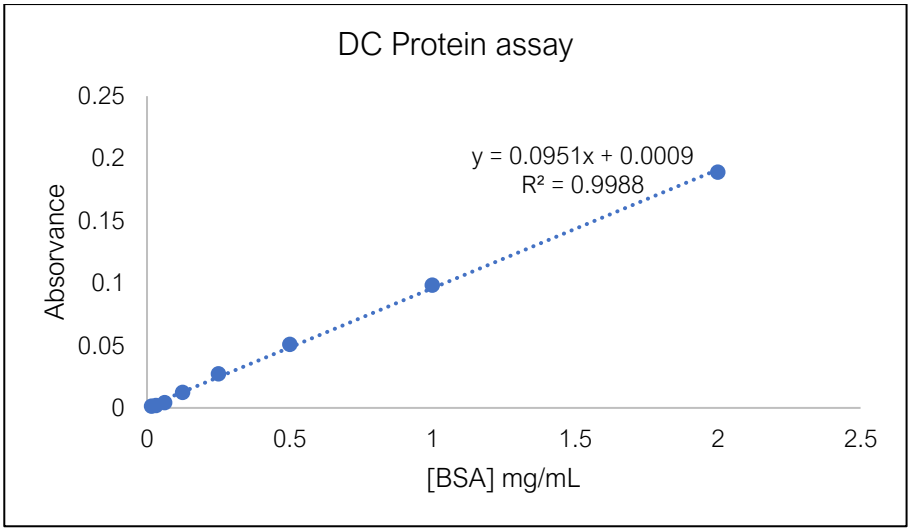

Figure 2.5 – Example of standard curve for the DC Protein assay. Eight different BSA concentrations were used to determine the fitted regression line equation, and the variation of the standards was determined by the coefficient of determination (R^2).

2.2.7. Oil Red O staining – confirmation of foam cell formation

Oil Red O stock solution was prepared by reconstituting Oil Red O powder in 100% propan-2-ol at a concentration of 3 mg/mL. Prior to staining, Oil Red O working solution was prepared by mixing three parts of stock solution and two parts of double-distilled water (ddH_20) and filtered using Whatman No. 1 filter paper. This solution was used within 2 h of preparation.

Cells were washed twice using PBS buffer and fixed with 4% paraformaldehyde (PFA) for 30 min. The cells were then washed twice with ddH_20 and permeabilised with 60% propan-2-ol for 5 min. The 60% propan-2-ol was discarded and the cells were covered with Oil Red O working solution for 20 min. The cells were washed three times with ddH_20 and counterstained with Harris Hematoxylin Solution for 1 min. The cells were washed three-time with ddH_20 and mounted for microscopy.

2.3. Protein analysis

2.3.1. Protein isolation

The cell isolation was performed in ice. The media in the well was removed and the cells were washed with ice cold PBS. Cell Lysis Buffer was freshly prepared in ice prior to cell lysis. cOmplete ™, Mini, EDTA-free Protease Inhibitor Cocktail was included in the lysis buffer following the manufacturer's instructions. 200 μL lysis buffer was added to each well of a 6-well plate and the bases gently scraped. The samples were pipetted into Eppendorf tubes and vortexed. After keeping them on ice for 15 min, the tubes were sonicated twice using a sonic probe and kept in ice for further 15 min. Then, the samples were centrifuged at 15,000 x *g* for 15 min. The supernatant was transferred into a new tube and stored at -20°C.

2.3.2. Protein transfer

20 μg protein suspension were mixed with the same volume of 2x Laemmli buffer, transferred to a Protein LoBind tube and boiled at 95°C for 5 min. The sample was separated by SDS-PAGE using a vertical, 1.5 mm thick, 10% acrylamide gel (Appendix B). Resolving separating gel was added between two glass plates, then covered with a thin layer of methanol to remove any bubbles and allowed to polymerise at room temperature. The methanol was removed and stacking gel (4% acrylamide gel – Appendix B) was added on the separating gel before being allowed to polymerise with a comb inserted between the glass plates, to create the wells for the samples. After that, the comb was removed, the gel was inserted in the running module and moved to the gel box. The box was filled in with tank buffer (Appendix

B) and the samples were loaded, together with a molecular weight reference ladder, in the wells and were subjected to electrophoresis for 1 h at 120V.

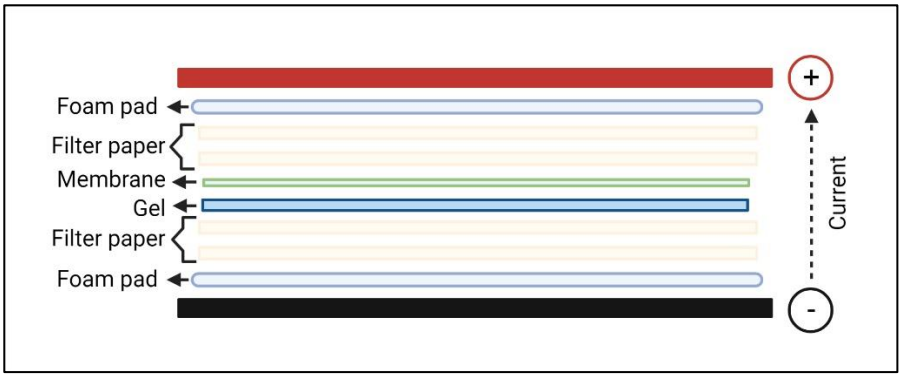

Figure 2.6 – 'Sandwich' for wet western blot transfer. The SDS-PAGE gel is in contact with the transfer membrane and the proteins are transferred in the cathode direction. Four filter paper sheets and two foam pads are also included.

The proteins were then transferred to an Immonilon™-P transfer membrane (polyvinylidene fluoride). The hydrophobic membrane was activated in methanol for 1 min and allowed to equilibrate in transfer buffer (Appendix B). The gel containing the proteins was transferred into an assembly tray, together with the transfer membrane and assembled in a sandwich, as shown in figure 2.6. The proteins were transferred for 1 h at 110V. Following transfer, the membrane was blocked in 5% BSA in Tris-buffered saline pH 7.4 containing 0.1% Tween-20 (TBS-T – Appendix B) for 1 h at room temperature.

2.3.3. Western blot

The membrane was incubated in TBS-T, containing 5% BSA, and primary antibody (Table 2.2) overnight at 4°C, on an orbital shaker. The membrane was washed in TBS-T three times for 10 min at room temperature on an orbital shaker. The membrane was then incubated in

TBS-T, containing 5% BSA, and secondary antibody for 2 h at room temperature. After three new washes with TBS-T, the membrane was exposed to Pierce ECL Western reagent according to the manufacturer's instructions. Signal was recorded using Amersham Hyperfilm ECL in the dark, for different lengths of time (between 60 s and 5 min) and developed using Konica Minolta SRX-101A tabletop processor. Subsequently, membranes were stripped using Stripping Buffer and re-incubated with different antibodies for housekeeping protein detection. Densitometric analysis of the radiographs was conducted with FIJI ImageJ (SciJava) and protein loading was normalized to *HPRT-1*.

Target	Primary antibody	*Supplier*	Conc	Secondary antibody	*Supplier*	Conc
Netrin-1 (1)	Polyclonal sheep	Thermo Fisher	1 ng/mL	Rabbit anti-sheep	Thermo Fisher	80 ng/mL
Netrin-1 (2)	Polyclonal chicken	Abcam	10 ng/mL	Goat anti-chicken	Abcam	400 ng/mL
HPRT-1	Monoclonal mouse	BioRad	50 ng/mL	Goat anti-mouse	EMD Millipore	200 ng/mL
Cleaved caspase-3	Polyclonal rabbit	Cell Signalling	1:1,000*	Goat anti-rabbit	EMD Millipore	500 ng/mL

Table 2.2 – List of antibodies. Primary and corresponding secondary antibodies trialled and used in western blotting, reactivities and dilution factors. **The manufacturer does not provide information regarding the antibody's initial concentration.*

2.3.4. Immunoprecipitation

THP-1 cells were differentiated in 6-well plates. 200 μL Pierce IP Lysis buffer was added to each well and mixed. The lysed cells suspensions were spun at 1200 x *g* and 4°C for 30 min. The supernatant was transferred to a new Eppendorf tube together with 10 μL of bovine anti-chicken IgY and was left in an orbital shaker for 45 min at 4°C. In a separate tube, 10 μL of

chicken anti-netrin-1 antibody was mixed with 100 μL microbeads and was left together with the samples in the orbital shaker. The samples were spun at 8,000 x *g* and 4°C for 3 min. 100 μL supernatant was transferred to a new tube, together with 25 μL antibody/beads mix. The mix was left in the orbital shaker overnight at 4°C.

On the following day, the samples were spun for 1 min at 5,000 x *g* and 4°C. The supernatant was removed and 200 μL fresh IP lysis buffer was added to the pellet. The pellet was resuspended using a vortex and spun for one min at 5,000 x *g* and 4°C. This step was repeated until four washes were completed. After the last wash, the pellet was resuspended in 50 μL Laemmli buffer and boiled at 95°C for 5 min. The samples were spun for 5 min at 10,000 x *g* and the supernatant was loaded in a 10% SDS-PAGE gel for western blot, as described in section 2.3.2.

2.4. DNA/RNA analysis

2.4.1. DNA sequence

Exon 1	5' UTR	actcccagcgcgagtggcggcggcggcggagccttcgggggcgagcgcgcgtgtgtgtgagt gcgcgccggccagc
Exon 2	5' UTR	gcgccttctgcggcaggcggacagatcctcggcgcggcagggccggggcaagctggacgca gcyy
	Starting codon – Full-length isoform	ATGCGGCCTTCGGCAAGGACGTGCGCGTGTCCAGCACCTGCGGCC GGCCCCCGGCGCGCTACTGCGTGGTGAGCGAGCGCGGCGAGGAG CGGCTGCGCTCGTGCCACCTCTGCAACGCGTCCGACCCCAAGAAG GCGCACCCGCCCGCCTTCCTCACCGACCTCAACAACCCGCACAAC CTGACGTGCTGGCAGTCCGAGAACTACCTGCAGTTCCCGCACAACG TCACGCTCACACTGTCCCTCGGCAAGAAGTTCGAAGTGACCTACGTG AGCCTGCAGTTCTGCTCGCCGCGGCCCGAGTCCATGGCCATCTACA AGTCCATGGACTACGGGCGCACGTGGGTGCCCTTCCAGTTCTACTC CACGCAGTGCCGCAAG

	Starting codon – Truncated isoform	**ATG**TACAACCGGCCGCACCGCGCGCCCATCACCAAGCAGAACGAG CAGGAGGCCGTGTGCACCGACTCGCACACCGACATGCGCCCGCTC TCGGGCGGCCTCATCGCCTTCAGCACGCTGGACGGGCGGCCCTCG GCGCACGACTTCGACAACTCGCCCGTGCTGCAGGACTGGGTCACG GCCACAGACATCCGCGTGGCCTTCAGCCGCCTGCACACGTTCGGC GACGAGAACGAGGACGACTCGGAGCTGGCGCGCGACTCGTACTTCT ACGCGGTGTCCGACCTGCAGGTGGGCGGCCGGTGCAAGTGCAACG GCCACGCGGCCCGCTGCGTGCGCGACCGCGACGACAGCCTGGTGT GCGACTGCAGGCACAACACGGCCGGCCCGGAGTGCGACCGCTGCA AGCCCTTCCACTACGACCGGCCCTGGCAGCGCGCCACAGCCCGCG AAGCCAACGAGTGCGTGG
Exon 3		CCTGTAACTGCAACCTGCATGCCCGGCGCTGCCGCTTCAACATGGA GCTCTACAAGCTTTCGGGGCGCAAGAGCGGAGGTGTCTGCCTCAAC TGTCGCCACAACACCGCCGGCCGCCACTGCCATTACTGCAAGGAGG GCTACTACCGCGACATGGGCAAGCCCATCACCCACCGGAAGGCCT GCAAAG…

Table 2.3 – Netrin-1 DNA sequence. Identification of the full-length and truncated isoforms starting codons. The sequence is continuous throughout the rows. The two 'ATG' that start the full-length and the truncated isoforms were identified in underlined bold.

Table 2.3 shows the three first exons of netrin-1 DNA. Starting codons for both full-length and truncated netrin-1 are shown in bold in different rows in exon 2. The full DNA sequence is included in appendix C.

2.4.2. mRNA extraction and reverse transcription

Cells were lysed, and mRNA was collected using Monarch Total RNA Miniprep Kit following the instructions of the manufacturer. During mRNA extraction, extra steps were taken including DNase digestion. The quality and quantity of purified mRNA was assessed using Nanodrop. Samples with absorbance ratios 280/260 and 230/260 nm lower than 2.00 were rejected and were not used for qPCR. mRNA samples were kept at -80°C until used. These samples were then used to produce cDNA (500 ng mRNA used per reaction) using High-

capacity RNA-to-cDNA kit according to manufacturer's instructions. cDNA was then diluted in 1:20 using Ultrapure DNase/RNase-free water and kept at -20 °C until used.

2.4.3. Quantitative Real-Time Polymerase chain reaction (qPCR)

Gene		Primer sequence	Notes
HPRT-1 [175]	Forward	GCGTCGTGATTAGTGATG	Housekeeping Gene
	Reverse	GTCCATGAGGAATAAACACC	
IL-1β [176]	Forward	GGGCCTCAAGGAAAAGAATC	M1 Macrophage Marker
	Reverse	TTCTGCTTGAGAGGTGCTGA	
IL-6 [177]	Forward	AGCCACTCACCTCTTCAGAAC	M1 Macrophage Marker
	Reverse	GCCTCTTTGCTGCTTTCACAC	
CD206 [176]	Forward	CGAGGAAGAGGTTCGGTTCACC	M2 Macrophage Marker
	Reverse	GCAATCCCGGTTCTCATGGC	
Ntn1 Total [108]	Forward	ACTATGCCGTCCAGATCCAC	
	Reverse	TCTTGAGGGGCTTGATTTTG	
Ntn1 Full-length [108]	Forward	CCCGGACTTTGTCAATGC	
	Reverse	TTGCAGAGGTGGCACGAG	
Ntn1 Total (2)	Forward	GAGTGCGTGGCCTGTAAC	Rejected
	Reverse	CAGACACCTCCGCTCTTG	
Ntn1 Full-length (2)	Forward	GCGCGTGTGTGTGAGTGC	Rejected
	Reverse	GCATCATGCTGCGTCCAG	

Table 2.4 – Primer sequences used in the qPCR reactions. Forward and reverse sequences for netrin-1, housekeeping gene *HPRT-1* and inflammatory markers. Two sets of primers targeting *NTN1* (2) were designed in-house but rejected after trial.

A total 5 µL cDNA was used in each reaction, together with 0.5 µM forward and reverse primers of interest (Table 2.3) and 10 µL SyBR Green Master mix in each well of a 96-Micro Amp Fast well reaction plate. The plate was loaded in the thermocycler, and the cycles were set as shown figure 2.7A.

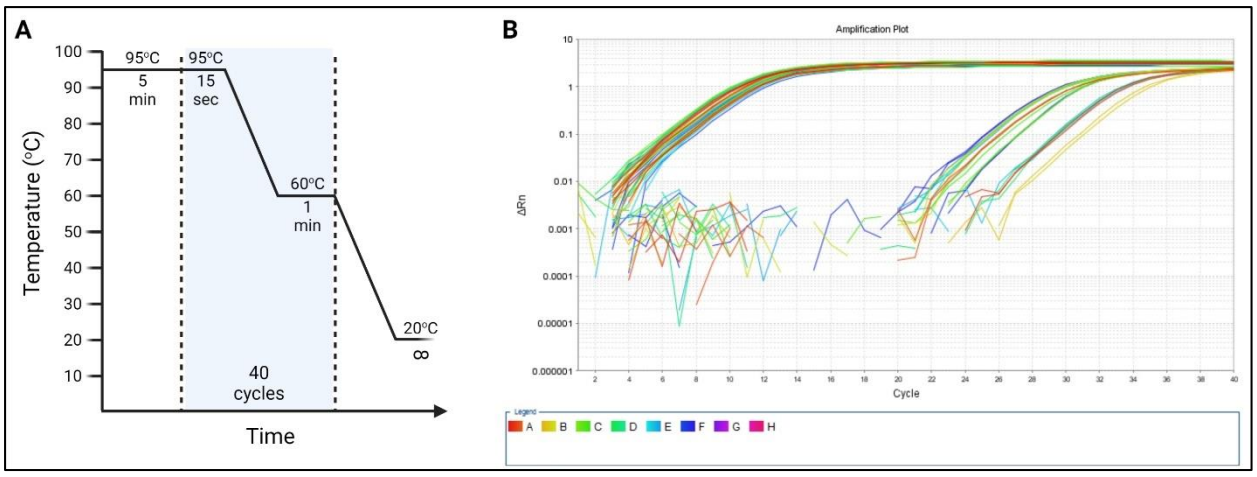

Figure 2.7 – Quantitative PCR. (A) Thermocycler program for qPCR using SyBR Green method. (B) Example of the results acquired after the 40 cycles were completed in the thermocycler. ΔRn is the ratio of fluorescence minus the baseline Rn value. The software determined the C_t value for each well.

For netrin-1 sets of primers, the fold expression was calculated using the threshold cycle (C_t) values generated by the thermocycler (Figure 2.7B) and the Pfaffl equation, which is described in detail below. For inflammatory markers, the delta-delta C_t equation was used instead.

2.4.4. Melting Curves

Melting curves were generated to verify whether more than one product was being generated in each well after the qPCR was completed. The products from both sets of primers targeting netrin-1 were analysed using electrophoresis, as described in section 2.7.2, to verify whether only one band was visible in the gel and therefore confirm that the primer pairs do not bind to the cDNA sequence in multiple places (Figure 2.8A). The melting curves were generated by gradually increasing the temperature of the products after the qPCR was completed. This increase in temperature leads to the dissociation of the double strands and increase in the absorbance. This data was presented in a graph (Figure 2.8B),

where a peak was present. If more than one peak was shown in the graph, this indicated that more than one product was amplified in the reaction.

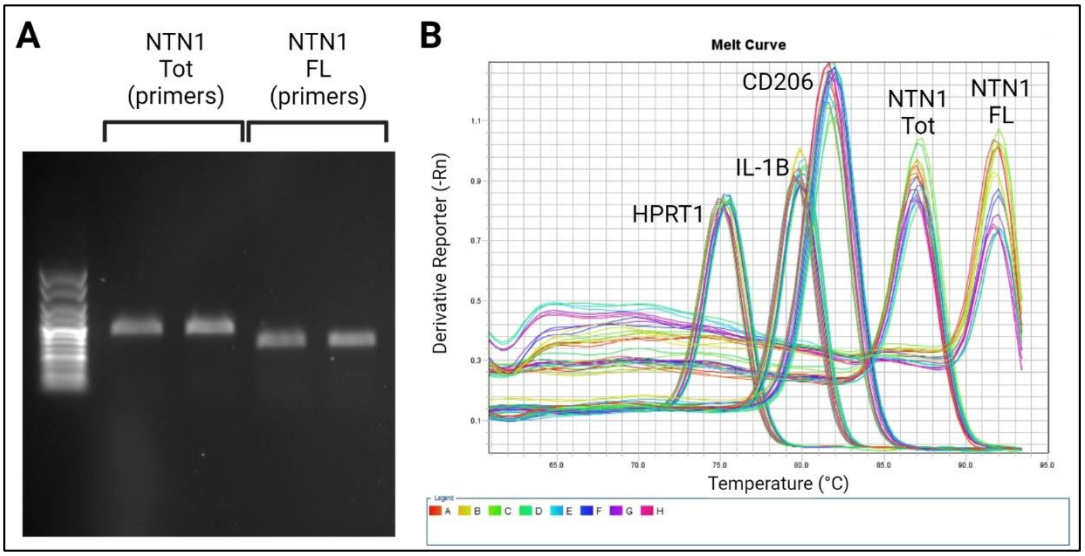

Figure 2.8 – Confirmation of the products generated in the qPCR. (A) *NTN1* Tot and *NTN1* FL products were run in a 1.8% agarose gel. Two different samples were tested for each set of primers. Only one product was detected in each sample. (B) Melting Curves for the different sets of primers used in the qPCR experiments.

2.4.5. Primer efficiencies

The efficiency of *NTN1* FL, *NTN1* Tot and *HPRT-1* primer sets was determined so that direct comparison between the relative quantities of the different products was possible. To achieve more reliable results, different types of samples were used in these experiments (THP-1 cell line and primary cells, M0 and M1 phenotypes) in series of dilutions of 1:5.

300 µg cDNA was diluted in serial dilutions of 1:5. Each dilution was prepared in triplicate in a 96-well plate, as described in section 2.4.3. The obtained C_t values were plotted in a graph together with the quantity of cDNA used (Figure 3.10 – chapter 3). A linear regression model was generated, and the amplification factor (E) was calculated using the slope of the curve:

$$E = 10^{\frac{-1}{slope}}$$

2.4.6. Mathematical models for relative quantification in qPCR

Two different mathematical models were used to analyse the qPCR results. The Pfaffl equation allows a direct comparison between the products obtained using different sets of primers since this equation considers the different primers' efficiencies. The expression of inflammatory markers was analysed individually and did not require the comparison between different targets; therefore, the delta-delta C_t equation was used instead. Both methods measure relative gene expression and rely on C_t values, which are the cycles in which fluorescence reaches the threshold value and are measured by the thermocycler. Reference genes can be used to correct for any pipetting errors or variation in the cycling process.

Pfaffl equation

The relative expression ratio (R) of a target gene is calculated considering the crossing point (CP) acquired through thermocycler software and the efficiencies of the treated sample versus a control in comparison to a reference gene using the following equation:

$$R = \frac{(E_{target})^{\Delta CP_{target}(control-treated)}}{(E_{reference})^{\Delta CP_{ref}(control-treated)}}$$

E_{target} is the RT-PCR efficiency of the set of primers of interest in the experiment; $E_{reference}$ is the RT-PCR efficiency of the set of primers of our reference gene - *HPRT-1*; ΔCP_{target} is the CP deviation of control minus the treated sample of the gene of interest; ΔCP_{ref} is the CP deviation of control minus the treated sample of the reference gene[178].

Delta-delta C_t equation

The most common method for relative quantification of gene expression in qPCR is the delta-delta C_t method. Similar to the Pfaffl method, it determines the change in gene expression relative to a housekeeping gene. This method considers that the primer efficiency is 100% and the amplification factor is 2; so that the product doubles after each cycle.

$$R = 2^{-\Delta\Delta Ct}$$

$$\Delta\Delta Ct = \Delta Ct(treated\ sample) - \Delta Ct(control\ sample)$$

$$\Delta Ct = Ct(target\ gene) - Ct(reference\ gene)$$

Control and treated samples are the groups of samples used in the experiment. Target and reference genes are the targets for which the set of primers were designed[179].

2.5. Migration assay – xCELLigence RTCA DP

The migration study was performed in the Cell & Tissue Therapy Laboratory, at Royal Free Hospital, University College London. The xCELLigence Real-Time Cell Analysis DP analyser

was kindly made available by Professor Mark Lowdell. Details about the technique are included in section 4.4.

2.5.1. E-plate

The xCELLigence RTCA DP system was calibrated using resistor plates following the manufacturer's instructions. Each well of the E-plate contained 50 μL RPMI 1640 + 10% FBS. A background sweep was run to validate each plate. Then, the plate was left in the incubator to calibrate to experimental conditions for 30 min.

Stimulated cells were detached from T75 flasks using 2 mM EDTA in RPMI 1640 + 2% FBS and after 15 min incubation the cells were gently scraped. The cells were spun at 300 x *g* for 5 min and resuspended in fresh RPMI 1640 + 2% FBS. Different cell densities (10,000 – 80,000 cells in a total of 100 μL per well) were pipetted into each well of the E-plate (in quadruplicates) and ran for 21 h (Figure 2.9). These measurements show how firmly the cells attached to the well and which number of cells presented best cell index (CI). This preliminary experiment was designed to determine the best number of cells to be used in the CIM-plates.

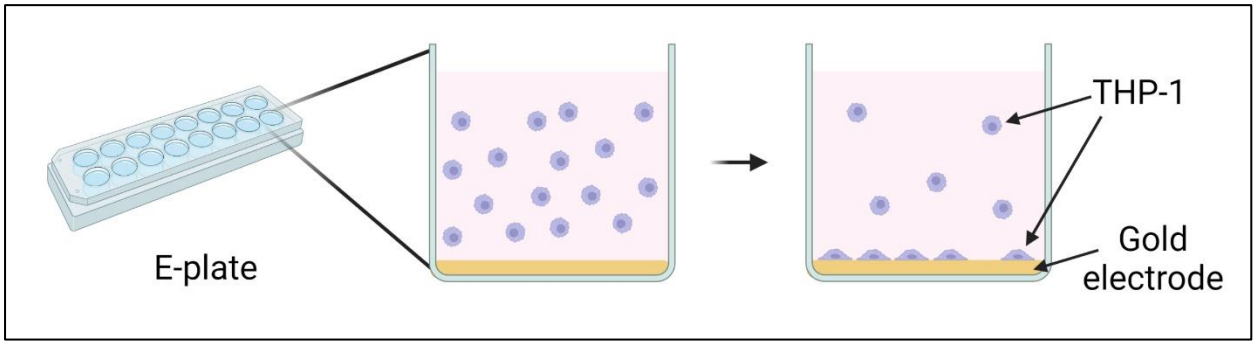

Figure 2.9 – E-plates functionality in the xCELLigence RTCA DP system. Impedance increased when cells attach to the gold electrode, increasing the CI value.

2.5.2. CIM-plate

The xCELLigence system was calibrated using resistor plates following the manufacturer's instructions. The bottom chamber of the CIM-plate was filled with 160 μL RPMI 1640 + 2% FBS with or without cytokines/chemokines as described in table 2.5.

Conditions/treatments	Cell phenotypes
No chemokines	THP-1 macrophage – M0
CCL2 (100 ng/mL)	THP-1 macrophage – M1
Netrin-1 (300 ng/mL)	THP-1 macrophage – M2
CCL2 (100 ng/mL) + netrin-1 (300 ng/mL)	THP-1 macrophage – Foam cell

Table 2.5 – List of conditions and cell phenotypes tested using the xCELLigence system. All conditions and treatments were tested in each macrophage phenotype.

The top chamber was assembled on the bottom chamber and kept in the incubator for 30 min to allow the formation of the gradient. Stimulated cells were then detached from T75 flasks using 2 mM EDTA solution in 10 mL RPMI 1640 media for 15 min and gently scraped. The cells were spun at 300 x *g* for 5 min and transferred as described for E-plates. 80,000 cells were seeded in each well.

The plate was inserted in the xCELLigence system, and the run was started with sweeps happening every 5 min for 21h. Using this type of plate, the measurements show how many cells migrate from the top to the bottom chamber over time and remain attached to the electrode, located in the bottom side of the membrane that separates the chambers (Figure 2.10).

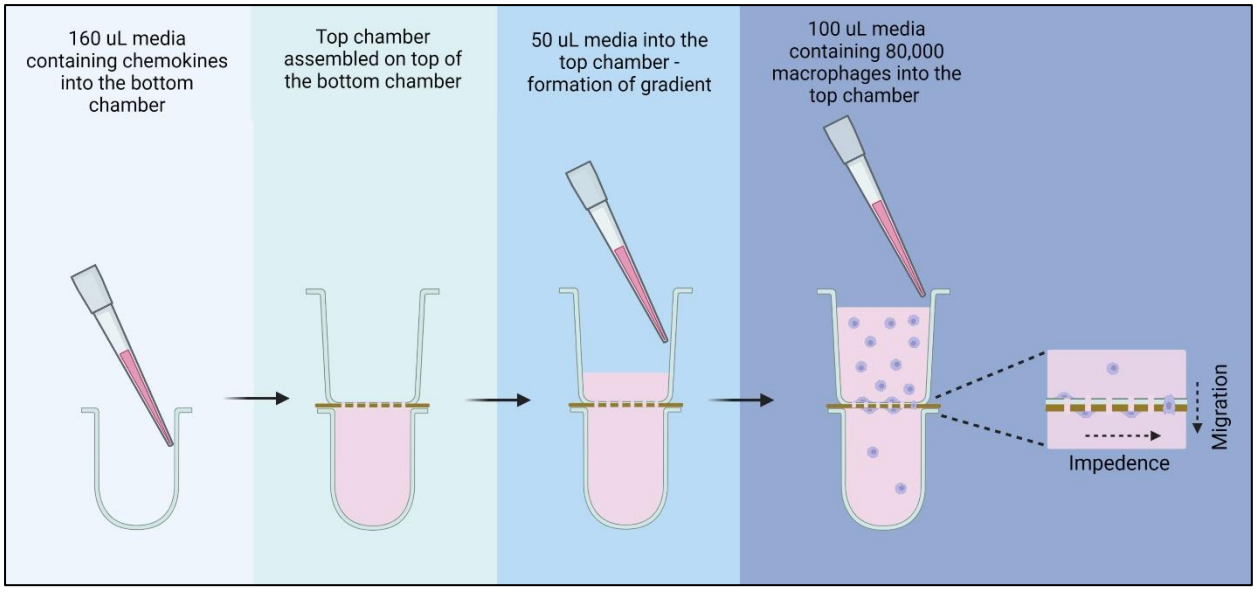

Figure 2.10 - Representation of the assembly and functionality of a CIM-plates in the xCELLiegence RTCA DP system. The bottom chamber contains media with or without chemokines. Impedance increased when cells migrate through the pores and attach to the gold electrode in the bottom side of the membrane.

2.6. Apoptosis assay

To study netrin-1 effect on apoptosis, triptolide was used as an apoptotic agent for THP-1 cells. Triptolide is a compound found in *Tripterygium wilfordii* Hook F. and has been used in traditional Chinese medicine for centuries as an immunosuppressant and anti-inflammatory substance. It has also been reported that triptolide has anti-neoplastic activity, through induction of apoptosis in cancer cells.[180,181] Park and Kim showed that triptolide induces apoptosis in PMA-differentiated THP-1 macrophages through the activation of caspases.[182] Based on Park and Kim's published work, THP-1 macrophages were treated with 6.25 – 25 μM triptolide, in the presence or absence of 100 – 300 ng/mL netrin-1. THP-1 cells were differentiated as previously described and allowed to rest in PMA-free media. If phenotypes were being assessed, the cells were stimulated with pro- and anti-inflammatory cytokines, as described in section 2.2.1, for 24 h. Triptolide was added to the culture media and kept

for further 24 h before the cells were either lysed or fixed. In the groups treated with netrin-1, this protein was added to the cells 2 h prior to triptolide in concentrations of 100 ng/mL or 300 ng/mL.

2.6.1. Cleaved caspase-3 assay

The cleaved caspase-3 antibody was used in two different experiments. In the western blot (Table 2.2), the cells were lysed, and the total amount of cleaved caspase-3 was determined. In the second experiment, the total number of cleaved caspase-3 positive cells was counted and its ratio against the total number of cells was established using immunofluorescence.

Western blot

The western blot was performed as outlined in section 2.3.2. To target cleaved caspase-3, a 12% SDS-PAGE gel was prepared (Appendix B), instead of 10%, since the targets of this antibody have a low molecular weight (17-19 kDa). The samples were separated in the gel for 90 min at 120V. Gel transfer into the Immonilon™-P transfer membrane and blocking/detection were performed as described in section 2.3.3.

Immunofluorescence microscopy

THP-1 monocytes were differentiated into macrophages in 96-well optical black/clear bottom plates at a density of 40,000 cells/well. After treatments with cytokines and triptolide, the cells were fixed in 4% PFA for 20 min. After that, the cells were permeabilised with 0.1%

Triton X-100 for 90 s. The cells were blocked with 5% BSA for 1 h and then incubated with rabbit anti-CC3 antibody (1:2000 in 1% BSA) overnight, at 4°C. The wells were then washed three times for 5 min with PBS. Alexa488 goat anti-rabbit antibody was added to the wells (1:500 in 1% BSA) for 1 h, in the dark, at room temperature. The wells were washed again three times for 5 min with PBS and mounted using Prolong™ Gold Antifade Mountant with DAPI. The samples were visualised, and the data was recorded using a Luma Scope fluorescence microscope (Etaluma). The figures were acquired using the software LumaViewPro 0.8.

2.7. Intravital Microscopy – acute effect of netrin-1 in inflammation

2.7.1. Animal model

C57BL/6-Tg(Csf1r-EGFP-NGFR/FKBP1A/TNFRSF6)2Bck/J

Common name: Macrophage Fas-Induced Apoptosis (MaFIA)

This murine model has an inducible Fas apoptotic system driven by the mouse *Csf1r* promoter. Administration of the dimerization agent AP20187 to the mice induces apoptosis in macrophages and reversible depletion of this type of immune cell. Enhanced Green Fluorescent Protein (eGFP) is expressed together with Colony-Stimulating Factor 1 (CSF1) which is mainly expressed by the monocyte/macrophage lineage.[183–185] This animal model was used in the intravital microscopy experiments due to its fluorescence characteristics in the monocyte/macrophage lineage. We did not induce apoptosis for the purpose of our experiments. This model is available on The Jackson Laboratory with strain number 005070.

2.7.2. Genotyping

MaFIA mice were bred with wild type C57BL/6J. Ear samples were collected by a Biological Service Unit (BSU) technician and the DNA was extracted using REDExtract-N-Amp™ following the manufacturer instructions. After DNA extraction, a PCR reaction was prepared in PCR microtubes by mixing 10 µL ReadyMix, 1.5 µL of each primer (Table 2.6) and 4 µL DNA sample. The microtubes were spun at maximum speed for 30 s and the PCR was set up as shown in figure 2.11.

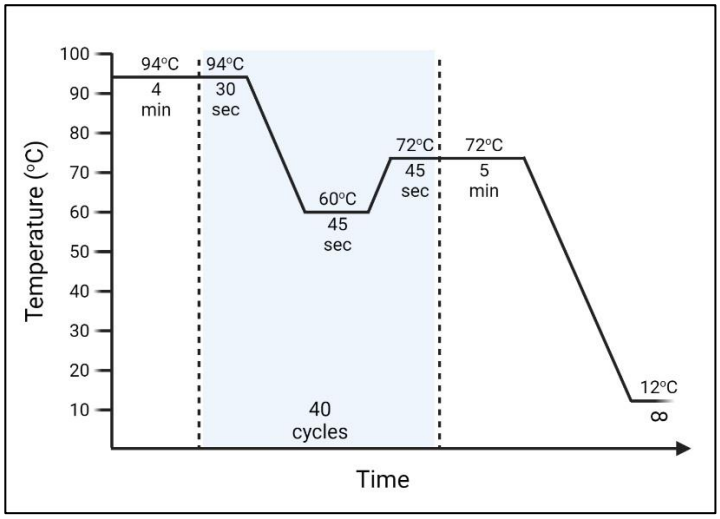

Figure 2.11 – Thermocycler program for genotyping PCR.

When the PCR was completed, 15 µL of each amplified product were loaded in a gel. For the electrophoresis, a 1.8% agarose gel was prepared in Tris-borate-EDTA buffer (TBE), containing 0.005% ethidium bromide (Appendix B). The electrophoresis ran at 200V for 25 min. After that, the gel was transferred into the G:BOX gel doc system (Syngene) to be visualised under UV light. Pictures of the gel were obtained for analysis (Figure 2.12).

Gene		Primer sequence	Notes
oIMR0872	Forward	AAGTTCATCTGCACCACCG	Transgene - GFP
oIMR1416	Reverse	TCCTTGAAGAAGATGGTGCG	Transgene - GFP
oIMR7338	Forward	CTAGGCCACAGAATTGAAAGATCT	Positive Control
oIMR7339	Reverse	GTAGGTGGAAATTCTAGCATCATCC	Positive Control

Table 2.6 – Primer sequences for genotyping. One set of primers was included as positive control and targeting the transgene. The sequences are available on the provider's website (jax.org/strain/005070) - The Jackson Laboratory.

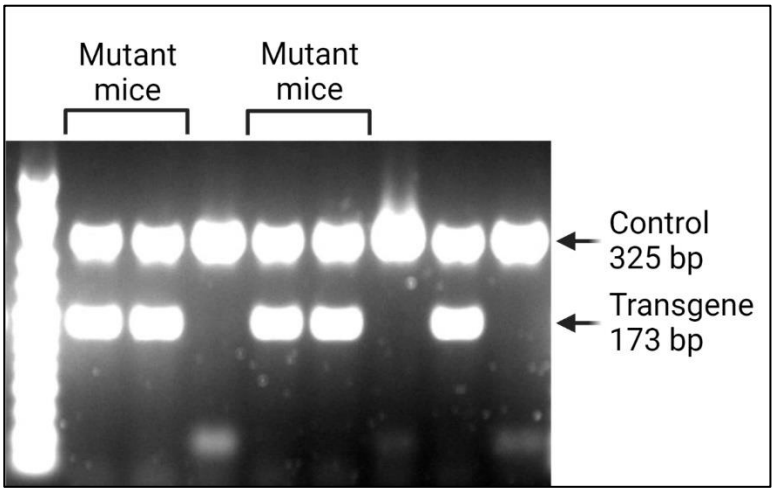

Figure 2.12 – Determination of the MaFIA colony mice genotype. Samples presenting a band for the control and transgene indicate a mouse with mutant genotype. When only the control band is observed, the offspring is wild-type.

2.7.3. ELISA

An ELISA kit for mouse netrin-1 was used to confirm whether netrin-1 injection successfully increased its levels in the mouse bloodstream. Since 100 µL of plasma were needed for the assay and not enough blood could be drawn from the mice after intravital microscopy, a preliminary study was conducted to assess the levels following injection of netrin-1 in the mice. Blood was drawn from each mouse from the *vena cava* into tubes containing heparin

and spun at 2000 x g for 15 min at 4°C. The plasma was transferred into a new tube and immediately frozen in liquid nitrogen.

All reagents, standards and samples were prepared and diluted following the manufacturer instructions. Six different standards were used to generate a standard curve for netrin-1 (Figure 2.13). Unfortunately, the absorbance values for all mice samples were below the blank value and so it was not possible to determine what the concentration of netrin-1 was in each animal's bloodstream.

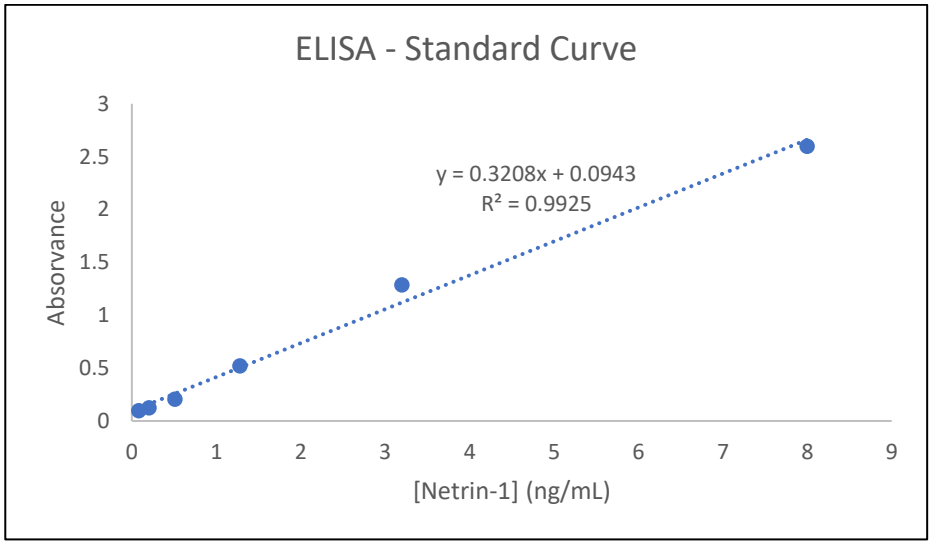

Figure 2.13- ELISA for mouse netrin-1. Standard curve obtained using the kit standards.

2.7.4. Groups and treatments

Four different groups of mice were created for this experiment. Each group contained 5 male mice. Two groups were injected with 100 µL of saline (untreated groups), sub-cutaneously, 16 h prior to terminal anaesthesia. The other two groups were injected with 500 ng recombinant mouse netrin-1 (treated groups), sub-cutaneously, at the same time point. This is the same dose of netrin-1 previously used by Ly and colleagues.[104] 4 h prior to intravital

microscopy, one untreated and one treated group were injected with either 6.25 µg LPS or saline, intra-scrotally, under light anaesthesia. All animals were also injected with 5 µg Mouse/human anti-CD11b AF488 intra-peritoneally 4 h prior to surgery, to enhance the fluorescent signal in the monocyte/macrophage lineage. The study design is detailed below in figure 2.14.

Time	Negative control group	Positive control group	Treated control group	Treated group
-16 h	Saline (S/C)	Saline (S/C)	Netrin-1 - 500 ng (S/C)	Netrin-1 - 500 ng (S/C)
-4 h	CD11b ab - 5 uL (I/P) Saline (I/Sc)	CD11b ab - 5 uL (I/P) LPS - 6.25 ug (I/Sc)	CD11b ab - 5 uL (I/P) Saline (I/Sc)	CD11b ab - 5 uL (I/P) LPS - 6.25 ug (I/Sc)
0 h	Terminal anaesthesia - Urethane			

Figure 2.14 – Study plan for intravital microscopy. 16 h prior to surgery, each group was injected sub-cutaneously (S/C) with either saline or 500 ng netrin-1. 4 h prior to surgery, all animals were injected with 5 µL CD11b antibody intraperitoneally (I/P) and either saline or 6.25 µg LPS intra-scrotally (I/Sc).

2.7.5. Surgery

The surgeries were performed in collaboration and under the supervision of Doctor Yanira Vasquez. The mice were terminally anesthetised using 2mg/kg urethane. This widely used anaesthetic has been shown to cause minimal depression of the cardiovascular system.[186,187] Severe side effects were reported using this agent and therefore it is now only used in non-recovery surgery. Figure 2.15A illustrates how the cremaster muscle was exposed for microscopy. Once the mice were under deep anaesthesia, (a) the mouse scrotum was shaved, and the skin was removed; (b) the testes were separated; (c) the cremaster muscle was identified, a small incision was made on the right ventral scrotal sac and pinned down

in a silicon plate; (d) an incision was made along the medial side of the cremaster muscle; (e) the edge of the cut was pinned; (f) the muscle was cut in a perpendicular position to the initial cut; (g) the tissue was folded over laterally and pinned to present a flat surface on the silicon surface.[188] Once the preparation was completed (Figure 2.15B), the tissue was covered with warm Tyrode's-HEPES buffer (Appendix D) and moved to the intravital microscope.

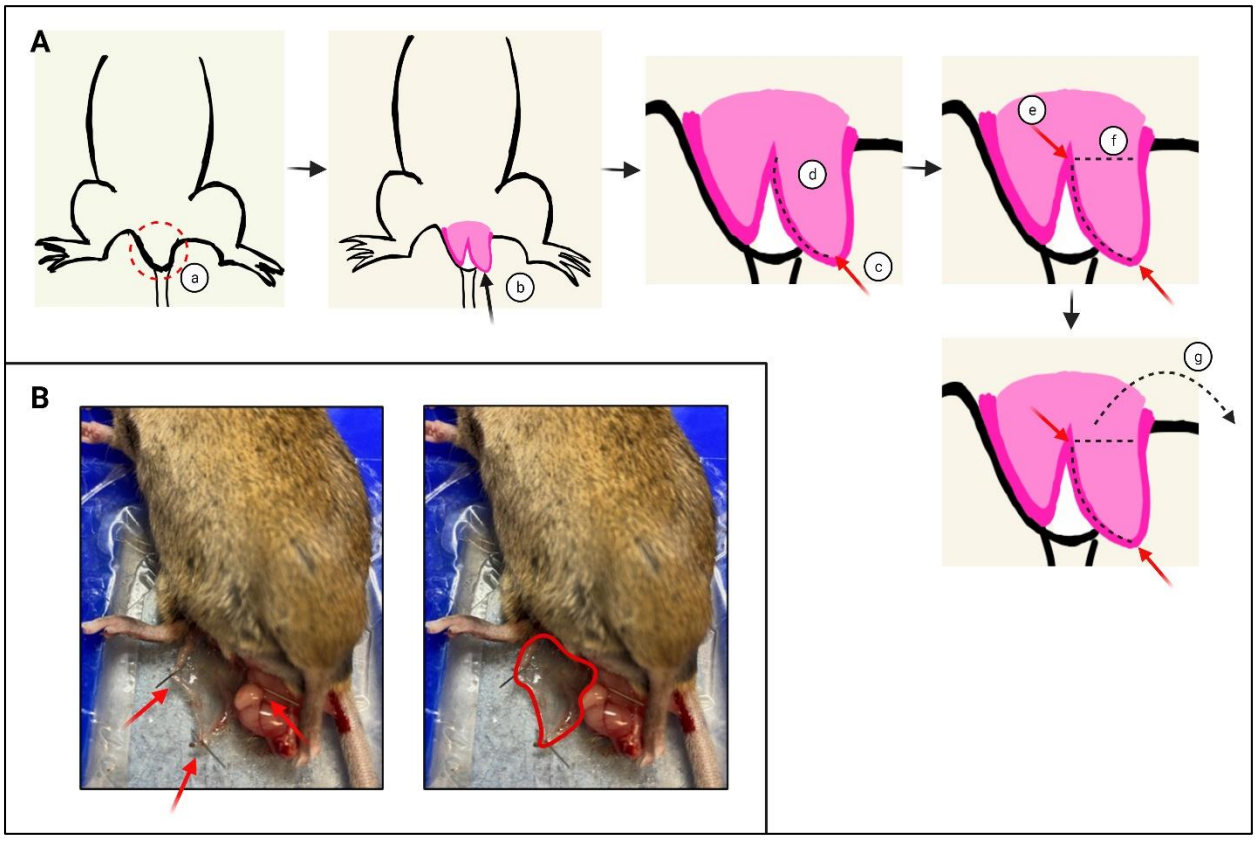

Figure 2.15 – Surgery to expose the cremaster muscle for intravital microscopy. (A) Schematic representation of the surgical procedure. (B) Cremaster muscle exposed. The arrows point to the various pins' locations. The red area shows the muscle surface exposed for microscopy.

2.7.6. Intravital microscopy

Whilst the surgery and the videos were captured, the temperature of the mice was regulated with a heated mat and by superfusion of warmed Tyrode's-HEPES buffer. The cremaster

muscle was observed under a Zeiss Axioskop 2 inverted reflective fluorescence microscope with a digital CMOS ORCA-Flash 2.8 camera (Hamamatsu) and a water immersed 40x objective lens. Under blue laser and dimmed bright field light, both monocyte/macrophage and the vessels' architecture could be clearly observed. The videos were recorded using IHC acquisition software (Hamamatsu). At least two different videos per mouse were recorded for 20 s to measure the adherence of monocytes and macrophages in the tissue. The number of fluorescent cells in the tissue were counted, as well as the number of cells rolling and arrested on the endothelium.

2.8. Chronic effect of netrin-1 in atherosclerosis

2.8.1. Animal Model

B6.129S7-Ldlr^{tm1Her}/J

Common name: Ldlr KO or *LDLR*$^{-/-}$

These are mice homozygous for the *Ldlr*^{tm1Her} mutation, which have elevated cholesterol levels in the serum, which can reach >2,000 mg/dL when fed a high fat diet. This is a model commercialised by The Jackson Laboratory, Maine, USA.

2.8.2. Groups and treatments

Four groups of five *LDLR*$^{-/-}$ mice were implanted with minipumps containing either saline or netrin-1 and maintained for 6 weeks either on normal chow or a 60% high-fat diet (HFD), figure 2.16. The mice were implanted at 12 to 16-weeks of age and placed into single cages

after surgery, to avoid any damage to the sutures. The weight of the mice was monitored weekly. Due to the high incidence of ulcerative dermatitis in this mouse model, together with the increased risk of this related to HFD feeding, a scoring system sheet was created for the monitoring of scratching and development of lesions.[189] Each mouse was scored twice per week, and if the lesion progressed beyond the treatable point, the mouse was culled, following the NVS advice. From the 20 initial mice, two from the 'treated group' and one from the 'positive control group' were euthanised before the end of the study (Table 2.7). For that reason, one mouse from the 'treated control group' was transferred into the 'treated group' on week 2.

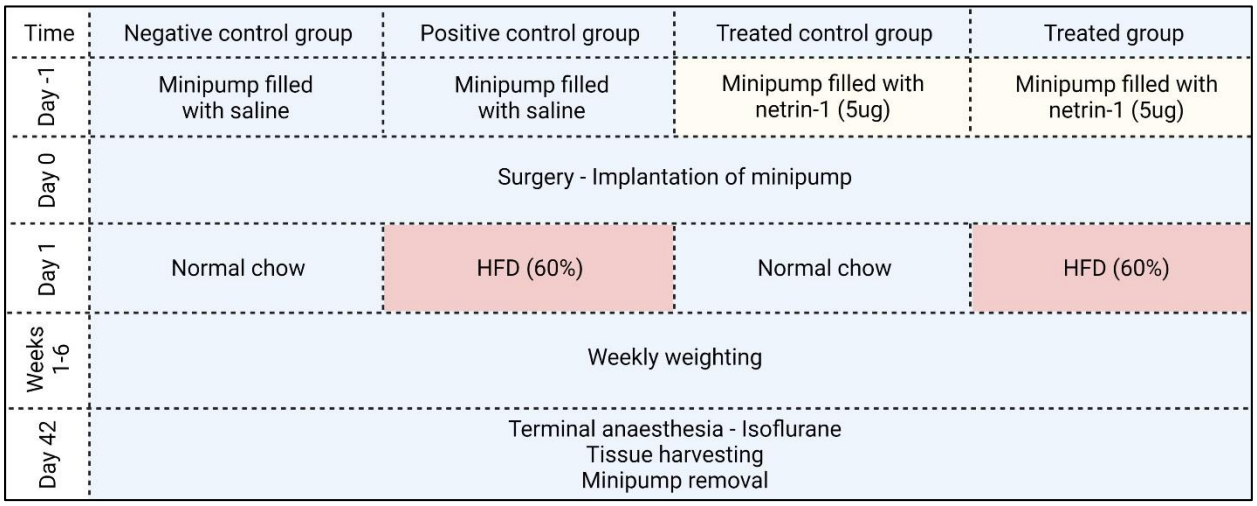

Figure 2.16 – Study plan for atherosclerosis study. Osmotic minipumps were implanted in *LDLR*$^{-/-}$ mice containing either 5 µg netrin-1 or saline. One day after surgery the diet of one of the 'treated' and one of the 'untreated' groups was changed to 60% HFD for 6 weeks.

	Negative control group	*Positive control group*	*Treated control group*	*Treated group*
Number	5	4	4	4
%Sex (M/F)	80/20	75/25	75/25	100/0
Age	12-16 weeks			
Initial Weight (g)	28.76 ± 3.63	28.45 ± 3.68	29.9 ± 3.38	26.56 ± 2.23
Final Weight (g)	29.88 ± 2.29	33.86 ± 3.01	29.58 ± 2.61	33.45 ± 2.07

Table 2.7 – Characteristics of the mice included in the atherosclerosis study. 4-5 mice were included in each group. The majority of the mice were males aged 12 to 16 weeks. Each group contained one mouse from a litter of mice that were heavier than the average, but in the Treated group this mouse was culled prior to the end of the study, and therefore its data was not included.

2.8.3. Minipump implant

Osmotic minipumps were used to continuously deliver small amounts of recombinant netrin-1 into the mice's system. This reduces the animal stress and discomfort as compared with periodic drug injections and decreases the chance of human error. The osmotic minipumps (42-days) were weighed and filled in with either 200 µL sterile saline or netrin-1 (25 µg/mL). According to the manufacturer, the minipump infusion rate is 0.15 µL/h equating to 3.75 ng/h netrin-1. The pumps were incubated in saline overnight at 37°C.

All mice were weighed prior to and after surgery. The surgical procedures for the implantation of the minipumps were conducted under aseptic technique, in collaboration and under the supervision of Doctor Fulye Argunhan. The osmotic pumps were weighed prior to implantantion. The mice were anaesthetised using isoflurane, and intraperitoneal analgesia was administered prior to surgery (0.05 mg meloxicam). Figure 2.17 shows a schematic of the surgery. (a) The fur on the upper dorsal skin was removed and the skin cleaned with iodine. (b) A small incision was made in that area and (c) blunt dissection was performed to separate the skin from the muscles of the mouse. (d) A needle-less syringe containing 1 mL saline was inserted and emptied in the incision. The saline was used to lubricate and facilitate

the sliding of the minipump towards the caudal end of the mouse (e). (f) The incision was sutured with non-absorbable sutures discontinuously. The mice were kept in a warm cabinet for 24 h, and monitored for signs of discomfort, pain or infection.[190]

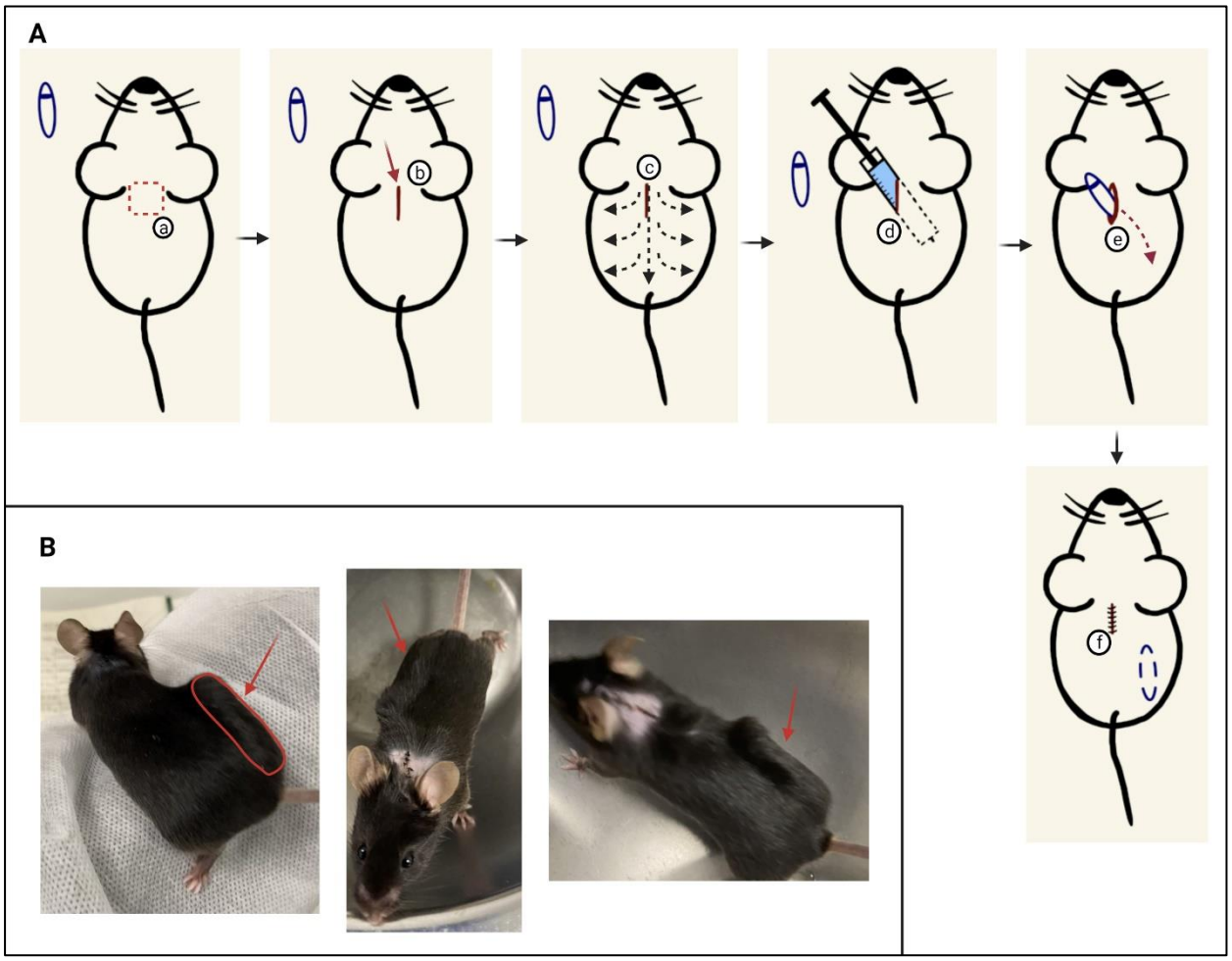

Figure 2.17 – Surgery to implant osmotic minipump in *LDLR*$^{-/-}$ mice. (A) Schematic representation of the surgical procedure. (B) Mice implanted with osmotic minipump 1-7 days after surgery. Arrows point to the minipump.

2.8.4. Organ harvesting

On day 42, the mice were terminally anesthetised using isoflurane and an incision was made along the ventral area. The organs and fat tissue were moved to the side and the *vena cava*

was exposed. A blood sample was acquired in a tube containing heparin and spun as described in section 2.7.5. The heart containing a small portion of the aortic root was harvested, as well as the aortic arch, and pinned to a cork surface and fixed in 4% PFA for 24 h, at 4°C. The osmotic pumps were also recovered and weighed. The minipump's reservoirs were opened, and a needle was inserted to verify whether there was any liquid inside.

2.8.5. ELISA

Blood samples were acquired to measure the concentration of netrin-1 in the bloodstream after the minipump disposal. Similarly to what was described in section 2.7.3, no netrin-1 was detected in the plasma of the mice using the ELISA kit.

2.8.6. Histology

The tissues were processed and embedded by technicians at the Innovation Hub, KHP Cancer Biobank, Guy's Hospital, and delivered as paraffin blocks.

The blocks were cut using a microtome (Leica), transverse section of 5 μm thickness and transferred to poly-L-lysine coated slides. The sections were left to dry overnight at room temperature. The sections were deparaffinized by submerging them into 10% xylene for 15 min followed by 100%, 90% and 70% alcohol for 5 min each to rehydrate the tissue. The slides were washed with double-distilled water for 2 min and then stained.

The sections were stained with Harris haematoxylin solution for 1 min and washed with double-distilled water until the blue colour was no longer visibly coming out of the section.

The sections were then counterstained with Eosin Y solution for 3 min and dehydrated through changes of 70%, 90% and 100% ethanol for 5 min each. The sections were then submerged in xylene, for 15 min, and allowed to dry. The slides were subsequently mounted with Dibutylphthalate Polysterene Xylene (DPX) for imaging.

Images were obtained using an Olympus Colourview III camera connected to an Olympus BX51 using CellSens Dimension viewing software. The images were analysed using FIJI ImageJ. The aortic sinus areas were measured using the tools available in the software.

2.9. Statistical Analysis

All data is presented throughout as mean±SD. Statistical analyses were carried out using one-way ANOVA (analysis of variation) plus Tukey post hoc test when the data followed a normal distribution, or Kruskal-Wallis test with Dunn's multiple comparison for non-parametric data. In chapter five, due to the small number of biological replicates, statistical analysis was performed using one-way ANOVA plus Dunnett's post hoc test for multiple comparisons. All analyses were two-tailed, and significance was taken as $P<0.05$.

Chapter Three

Netrin-1 isoform expression in different macrophage phenotypes

3.1. Introduction

Macrophages are the main type of immune cell present in atherosclerotic plaque.[191] Different macrophage phenotypes can be found in different areas of the plaque and have different roles in the inflammatory process. While vulnerable areas of the plaque, such as the 'shoulders' present mainly M1 macrophages, the fibrous cap expresses both M1 and M2 markers.[41,192] This type of leukocyte has a remarkable plasticity and can change between M1 and M2 (these constitute the extremes of a large spectrum of pro- and anti-inflammatory possible phenotypes) when the microenvironment around them changes.[26,193]

Macrophages within the plaque express netrin-1, which has been identified predominantly as a pro-atherogenic agent, leading to their accumulation, increased survivability and inhibition of their egress to the lymph nodes.[134] However, these studies were focused on the netrin-1 secreted (full-length) isoform, but the role of its truncated isoform in macrophages, within the plaque, is still unknown.

The truncated isoform of netrin-1 has been described as the products of an alternative promoter. [108] Paradisi and colleagues showed that the netrin-1 gene is a direct transcriptional target of NF-κB in colorectal tumour cells.[138] Similar results were presented in an endothelial cell model. Passacquale and colleagues showed that truncated netrin-1 is upregulated in endothelial cells in the presence of pro-inflammatory conditions, whilst the secreted isoform is downregulated. NF-κB inhibition led to downregulation in expression of the truncated isoform.[136] However, there is still no data available that shows how the two isoforms are differentially regulated in macrophages.

The human monocytic cell line THP-1, which will be one of the models used in the experiments presented in this chapter, is widely used to study monocyte and macrophage

biology. Although this cell line is not as 'natural' as cells freshly isolated from human subjects, there are some advantages in using it over PBMC-derived monocytes/macrophages. The long-term storage, low costs, fast growth, immortality and relative homogeneity are benefits that cannot be relied on when using primary cells.[194] For that reason, the majority of our data was related to this cell type, and some experiments were repeated for confirmation in primary cells.

3.2. Aims

1. To study how macrophage phenotype affects the expression of netrin-1 isoforms.
2. To determine the role of NF-κB in the regulation of netrin-1 isoforms in macrophages.

3.3. Cytokine expression & foam cell formation – confirmation of phenotype

As mentioned before, macrophages are leukocytes with a remarkable plasticity, adapting and changing phenotype depending on the microenvironment around them.[26,193] To study how the expression of netrin-1 isoforms varies depending on macrophage phenotype, specific markers were used to confirm that phenotypic transformation was successful. Primers for IL-1β and CD206 were included in each experiment (both sets of primers were included in duplicate for each sample) and the samples were only valid for further analysis if there was a clear upregulation of IL-1β in the M1 cell cultures, or upregulation of CD206 in M2 macrophage colonies.

The data presented in figure 3.1 illustrates the validating test that was performed after each experiment to confirm phenotypic changes. In THP-1 derived M1 macrophages, the expression of IL-1β increased between 4- and 8-fold after exposure to 50 ng/mL IFN-γ and 10 ng/mL LPS in comparison to non-stimulated macrophages. The expression of CD206 remained similar before and after stimulation with pro-inflammatory cytokines. In M2 macrophages, stimulated with 20 ng/mL IL-4, the expression of CD206 mRNA was upregulated between 2- and 16-fold.

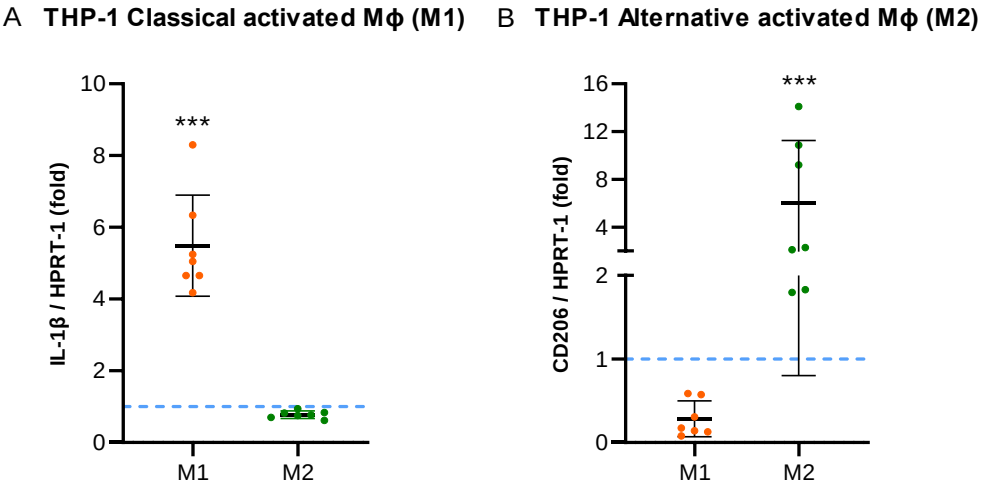

Figure 3.1 – Gene expression of pro- and anti-inflammatory markers to confirm THP-1-derived macrophage phenotypes using qPCR. (A) Gene expression changes for IL-1β in M1 and M2 macrophages. (B) Gene expression changes for CD206 in M1 and M2 macrophages. Mean±SD, n=7. ***P<0.001 between groups indicated and control group (blue line).

Similarly to what was observed in THP-1, PBMC-derived macrophages stimulated with pro-inflammatory cytokines presented an upregulation in the expression of IL-1β, but to a greater magnitude, varying between a 2- and a 150-fold increase, when compared with naïve macrophages. M2 PBMC-derived macrophages expressed 1.5- to 5-fold more CD206 than non-stimulated macrophages.

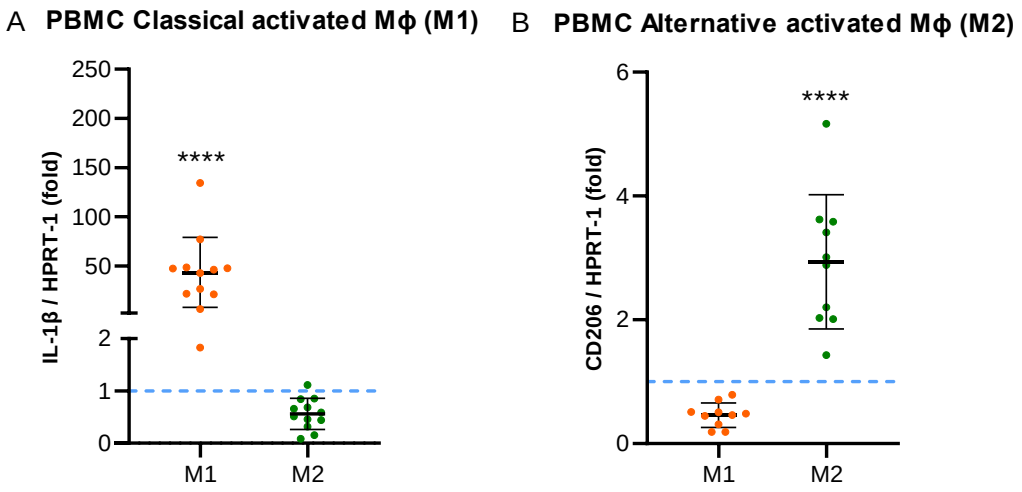

Figure 3.2 – Gene expression of pro- and anti-inflammatory markers to confirm PBMC-derived macrophage phenotypes using qPCR. (A) Gene expression changes for IL-1β in M1 and M2 macrophages. (B) Gene expression changes for CD206 in M1 and M2 macrophages. Mean±SD, n=10-12. ****P<0.0001 between groups indicated and control group (blue line).

To confirm the generation of foam cells, Oil Red O staining was used to stain internalised lipid; red staining was quantified using image analysis software. Figure 3.3 shows THP-1 macrophages (non-stimulated) after exposure to different concentrations of LDL (native or acetylated) for 48 h.

The quantification of the area stained by Oil Red O, normalised to the number of cells in the picture, is shown in figure 3.4. A significant increase in the uptake of LDL was observed when cells were treated with nLDL or acLDL. As mentioned above, treatment with acLDL led to a significantly greater increase in uptake than native LDL and a further rise was observed when the cells were treated with higher concentrations of acLDL. Interestingly, treating the cells with commercial acLDL led to significant less internalisation of acLDL when compared with treatment with the same concentration of LDL acetylated in the laboratory, from 3418.2 to 2042.9 pixels/cell.

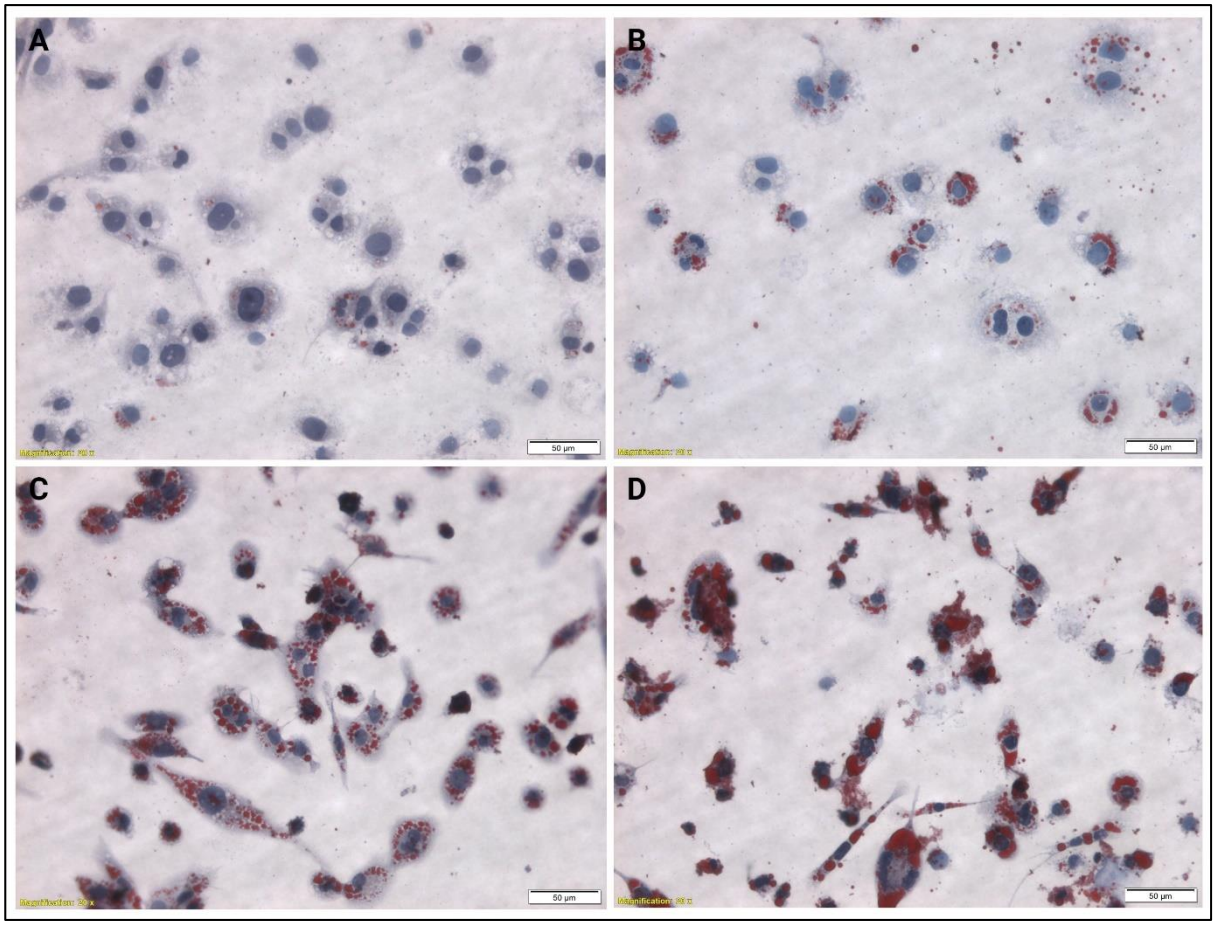

Figure 3.3 - Foam cell formation in THP-1-derived macrophages. (A) Untreated macrophages. (B) Macrophages treated with 50 µg/mL native LDL for 48 h. (C) Macrophages treated with 50 µg/mL acLDL for 48h. (D) Macrophages treated with 200 µg/mL acLDL for 48 h.

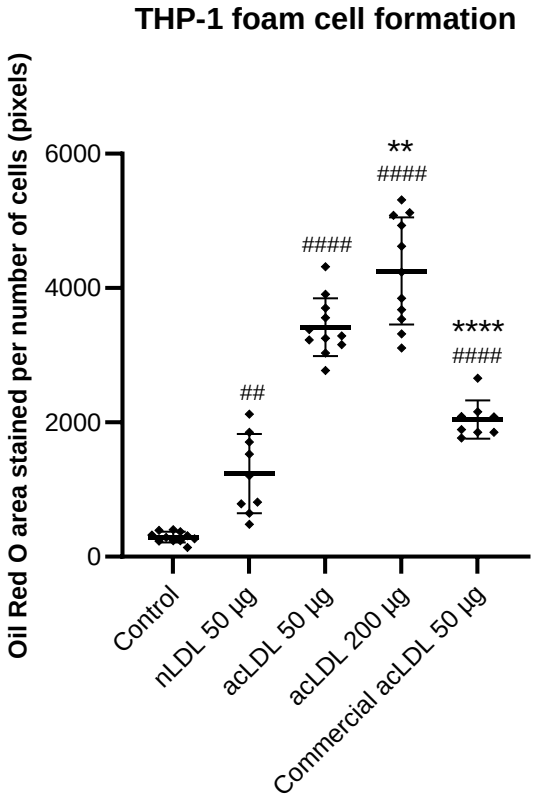

Figure 3.4 - Quantification of Oil Red O staining for different treatments with LDL. Oil Red O staining was quantified in each picture using ImageJ and normalised to the total number of cells. THP-1 macrophages presented more and larger fat vesicles in the cytoplasm after exposure to LDL acetylated in our laboratory. Mean±SD, n=8-11. ##P<0.01 and ####P<0.0001 between groups indicated and control group. **P<0.01 and ****P<0.0001 between groups indicated and acLDL 50 µg group.

3.4. Netrin-1 protein expression

We undertook several attempts to quantify netrin-1 isoforms at the protein level. However, as described below, this was a major challenge mainly because the antibodies currently available on the market do not appear to reliable recognise either isoform of netrin-1. Western blot and immunoprecipitation experiments were performed, all ultimately without success.

3.4.1. Antibodies commercially available that target netrin-1 failed to reliably detect its truncated isoform

Work published by Passacquale *et al* and Delloye-Burgeois *et al* demonstrated expression of both netrin-1 isoforms in western blots from endothelial cell extracts in HUVEC and IMR32 cells, respectively.[108,136] Unfortunately, the netrin-1 antibody used in those studies and sold by R&D Systems is no longer available and an alternative antibody was created by the company. A different antibody sold by Abcam was also extensively tested.

Human/Mouse/Rat Netrin-1 Antibody (R&D Systems)

Samples of supernatants, as well as cell lysates from different phenotypes of THP-1-derived macrophages were used to validate this product. The supernatant samples showed solid bands at roughly 200 and 52 kDa. Only full-length netrin-1 would be expected to be detected in supernatant samples, since the truncated isoform is not secreted.[108] None of the bands observed was close to predicted molecular weight for full-length netrin-1 (70 kDa).

In the cell lysates, there were several bands detected, from 75 to 35 kDa. According to the product datasheet, the strong band visible at 67 kDa should correspond to the full-length isoform of netrin-1. However, there is no band evident at the truncated isoform molecular weight. Instead, a mix of very faint bands are packed in the that area (Figure 3.5).

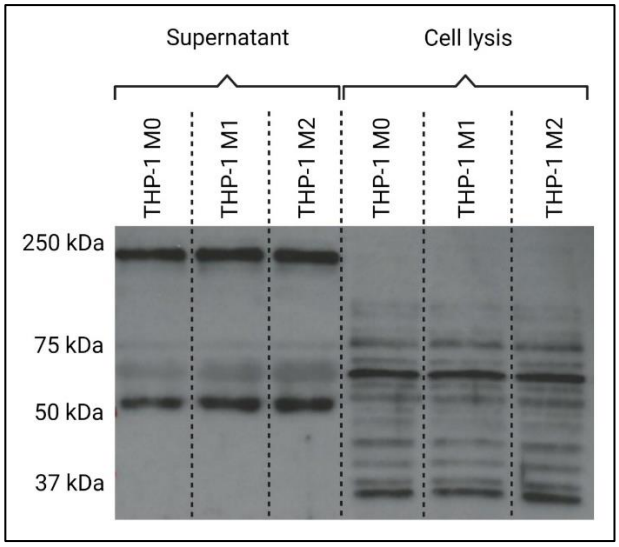

Figure 3.5 – Western blot for THP-1 derived macrophages, blotted with sheep anti-netrin-1 antibody (R&D Systems). Supernatant and cell lysates were separated by electrophoresis on a 10% SDS-PAGE gel, transferred and blottled with sheep anti-netrin-1 antibody and rabbit anti-sheep HRP antibody.

Human/Mouse Netrin-1 Antibody (Abcam)

An antibody available at the time, sold by Abcam, was also extensively tested. Figure 3.6 shows a blot of THP-1-derived macrophage samples from the NF-κB inhibitor experiment. Although the different wells presented a considerable amount of background, there are two band sizes that correspond to the predicted molecular weights of the two netrin-1 isoforms (70 kDa and 55 kDa). There are other bands visible also, with smaller molecular weights and so further experiments were conducted to confirm whether the bands that correspond to the predicted sizes were in fact netrin-1.

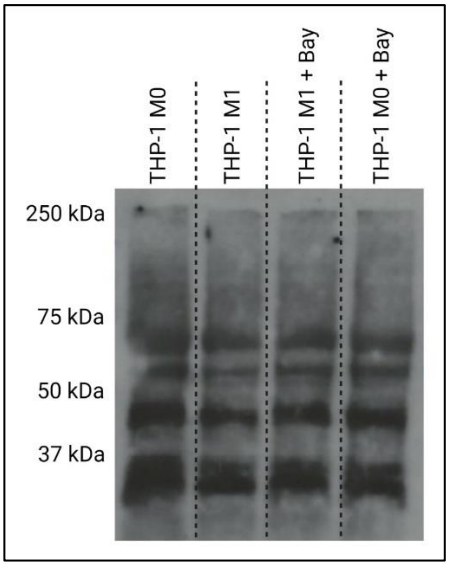

Figure 3.6 - Western blot for THP-1 derived macrophages, blotted with chicken anti-netrin-1 antibody (Abcam). Cell lysates were separated by electrophoresis on a 10% SDS-PAGE gel, transferred and blottled with chicken anti-netrin-1 antibody and bovine anti-chicken HRP antibody.

Cell lysates from a human non-small cell lung cancer cell line (H358) were kindly provided by Professor Patrick Mehlen, from University of Lyon to validate this netrin-1 antibody. Three different samples were sent by this group: where one of them was not genetically modified (WT) and the other two were transfected with small interfering RNA to silence the expression of both netrin-1 isoforms. The blot in the figure 3.7 shows one of the membranes prepared with these samples and the predicted molecular weights for both isoforms. The antibody did not specifically detect netrin-1 in the samples, in as much as the putative bands corresponding to full-length and truncated netrin-1 were not suppressed in the netrin-1 silenced samples.

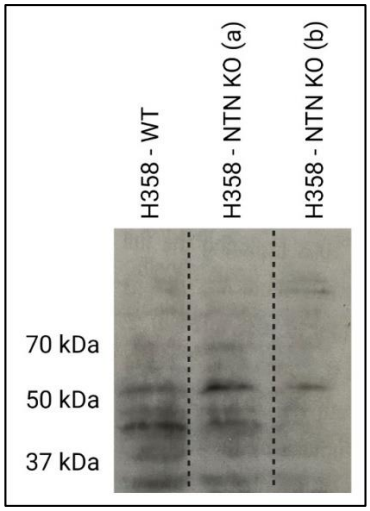

Figure 3.7 - Western blot for H358 cells, wild-type and *NTN1*-silenced cells, blotted with chicken anti-netrin-1 antibody (Abcam). Cell lysates were separated by electrophoresis on a 10% SDS-PAGE gel, transferred and blottled with chicken anti-netrin-1 antibody and bovine anti-chicken HRP antibody.

3.4.2. Validation of netrin-1 primary antibodies through immunoprecipitation did not detect truncated netrin-1

Immunoprecipitation was also used with the antibody provided by Abcam (Figure 3.8). A band at 70 kDa, corresponding to the molecular weight of full-length netrin-1 was detected, however, there were no bands present at the truncated isoform predicted molecular weight. The strong background observed in the western blot membrane, together with the presence of multiple bands that are not close to the predicted molecular weights, the presence of bands corresponding to netrin-1 in siRNA transfected samples and the absence of bands corresponding to the truncated isoform in the immunoprecipitation experiments collectively confirmed that this antibody was not suitable for netrin-1 detection or indeed quantification.

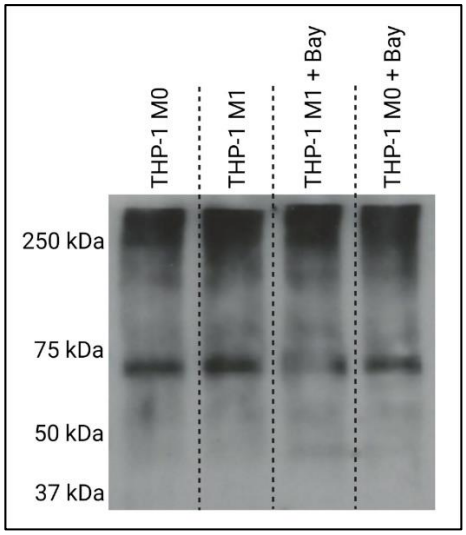

Figure 3.8 – Immunprecipitation and blotting with chicken anti-netrin-1 antibody (Abcam). Cell lysates were incubated with IP beads as previously described and separated by electrophoresis on a 10% SDS-PAGE gel, transferred and blottled with chicken anti-netrin-1 antibody and bovine anti-chicken HRP antibody.

3.5. Netrin-1 isoforms gene expression is different depending on macrophage phenotype and cytokine stimulation

To determine the gene expression of both netrin-1 isoform at the mRNA level, two different sets of primers were used, one targeting a portion of the gene that is exclusively found in the full-length isoform (blue) and another that targets a sequence that is common to both isoforms (black) targeting total netrin-1 (Figure 3.9).

The efficiencies and amplification factors of these sets of primers were calculated and the Pfaffl equation used to calculate how the mRNA expression varies under different conditions.[178] This mathematical model allows direct comparison between different sets of primers, by considering the amplification factor in its equation. By these means, the expression of truncated isoform can be calculated by subtracting the full-length isoform expression from that of total netrin-1.

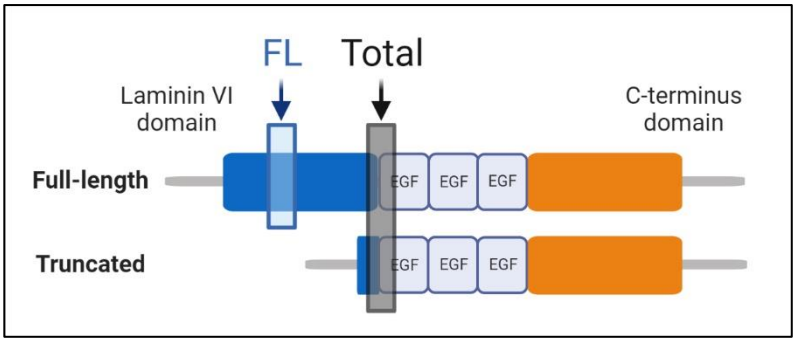

Figure 3.9 – Sets of primers targeting *NTN1* FL and *NTN1* Total. Schematic representation of the DNA segments targeted by the two sets of primers. In blue, the primers target a portion that is exclusively found in the full-length isoform (FL) and in black, the sequence targeted is common to both netrin-1 isoforms (Total).

3.5.1. Primer efficiencies

The primer efficiencies and amplification factors of both netrin-1 primer sets, and of the housekeeping gene (*HPRT-1*), were calculated using a series of dilutions of different samples. Both M0 and M1 phenotypes were included in this experiment, as well as both the cell line (THP-1) and primary cells (PBMC). A range of 50 to 60 individual values were considered for each set of primers (Figure 3.10).

As detailed in section 2.4.5, the slope of the linear regression was used to determine the amplification factor (E), using the equation $E = 10^{-1/slope}$. The primers' efficiencies were determined using the equation Efficiency (%) = $(10^{-1/slope}-1)x100$. The set of primers designed to target the total amount of netrin-1 and the housekeeping gene *HPRT-1* presented similar amplification factor values of 2.05, which represent an efficiency of 105%, with a coefficient of determination (R^2) of 0.9924 and 0.9930, respectively. The set of primers used to target exclusively full-length netrin-1 had an amplification factor of 1.98, which translates into an efficiency of 98% and a coefficient of determination value of 0.9906 (Figure 3.10; Table 3.1). The amplification factor values shown in table 3.1 were then used in the Pfaffl equation to determine relative gene expression of both netrin-1 isoforms, as detailed in section 2.4.6.

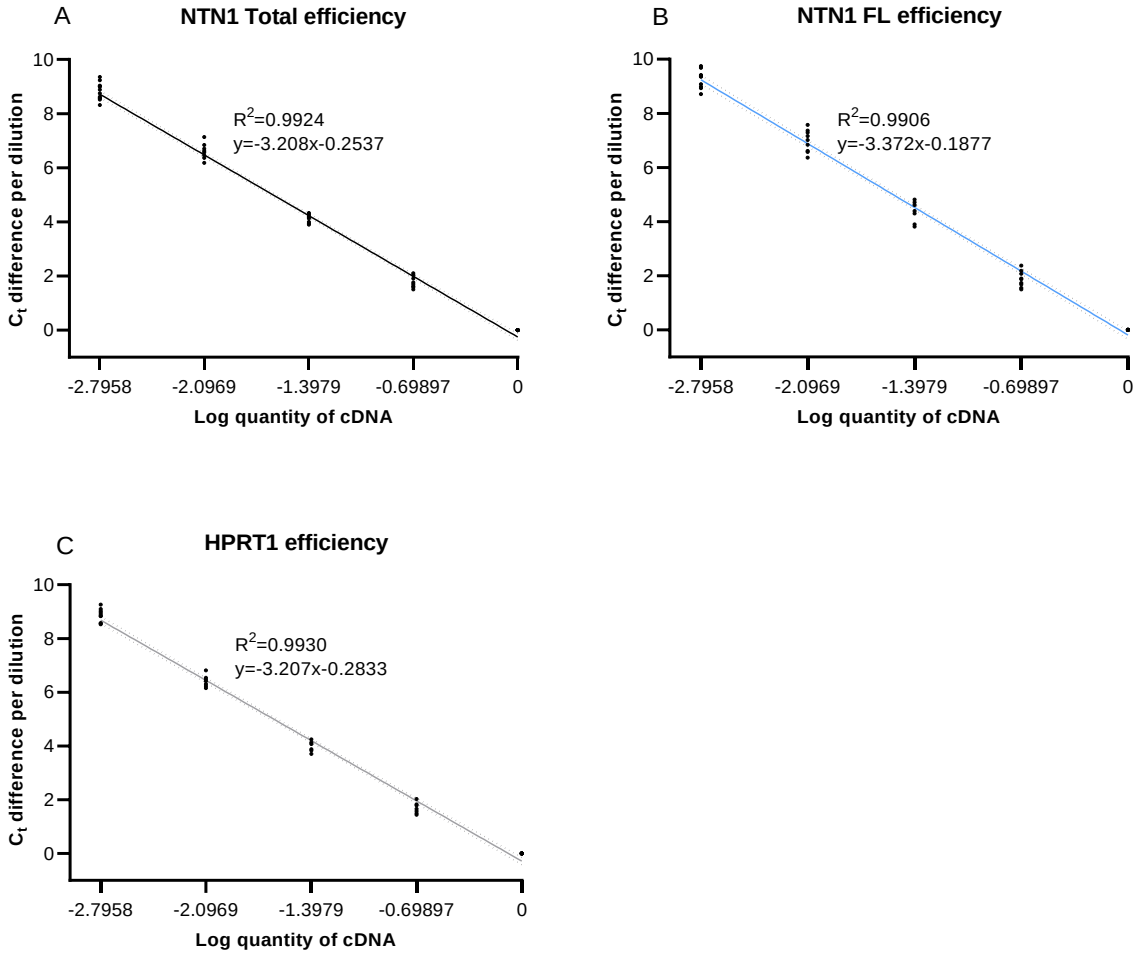

Figure 3.10 – Efficiencies for *NTN1* Tot, *NTN1* FL and *HPRT-1* sets of primers. (A) Linear regression was used to draw a standard curve using the C_t values acquired in the series of dilutions. Linear regression follows the linear equation y=mx+c, where m is the slope value. The variation of the values was determined by the coefficient of determination (R^2). n= 50-60.

Primers	*Slope*	*Amplification factor (E)*	*Efficiency (%)*
NTN1 total	-3.208	2.05	105%
NTN1 FL	-3.372	1.98	98%
HPRT-1	-3.207	2.05	105%

Table 3.1- *NTN1* Tot *NTN1* FL and *HPRT-1* amplification factors and efficiencies.

The following sets of results were obtained by quantifying changes in mRNA expression using qPCR. In this study, the Pfaffl equation was employed to calculate fold changes in the truncated isoform of netrin-1 by subtracting the full-length isoform from the total netrin-1. After the subtraction, the data from each isoform was normalised to the respective control sample.

3.5.2. Pro-inflammatory macrophages are the main contributor to the expression of netrin-1 isoforms

The expression of total and full-length netrin-1 were determined in different macrophage phenotypes, in both THP-1- and human primary PBMC-derived macrophages, isolated from fresh blood. The expression changes presented are relative to unstimulated macrophages (naïve – M0).

In the case THP-1, treatment of macrophages with pro-inflammatory cytokines (M1) led to a significant upregulation of both netrin-1 isoforms after 12 h stimulation, with a 2.9-fold increase in the full-length isoform and a 5-fold increase in the truncated isoform. However, after 24h stimulation, only the truncated isoform expression was significantly increased – 3.7-fold.

In PBMC-derived macrophages, pro-inflammatory stimulation led to a greater upregulation of both isoforms at both time points, 12 h and 24 h. Full-length netrin-1 expression increased 137.2-fold after 12 h and 232.1-fold after 24 h. The truncated isoform increased 50.0-fold after 12 h stimulation and 63.4-fold after 24 h (Figure 3.11).

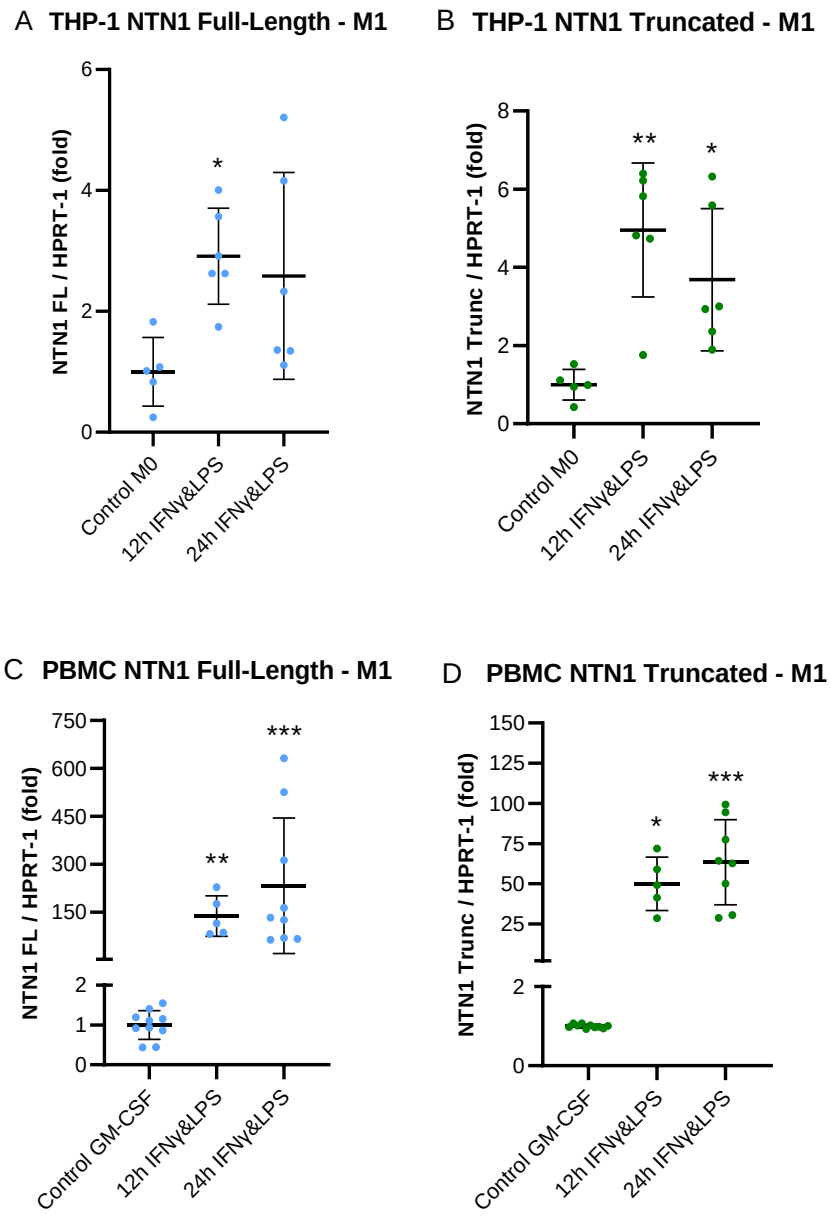

Figure 3.11 – Netrin-1 isoform expression in classical activated macrophages. (A) While netrin-1 full-length isoform is upregulated in M1 THP-1 derived macrophages only after 12 h stimulation, the truncated one is upregulated after 12 and 24 h exposure to IFN-γ and LPS (B). (C) Pro-inflammatory stimulation for 12 and 24 h led to the upregulation of full-length netrin-1, as well as the truncated isoform (D) in PBMC-derived macrophages. Mean±SD, n=5-10. *P<0.05, **P<0.01 and ***P<0.001 between groups indicated and the control group.

In alternative activated macrophages, effects on the expression of both netrin-1 isoforms were much smaller when compared with classical activated macrophages (Figure 3.12).

In THP-1-derived macrophages, the only isoform that was significantly upregulated was the truncated one, where there was a 3.7-fold increase after 12 h stimulation with IL-4. In PBMC-derived macrophages, no significant differences were observed in either isoform at any time point tested.

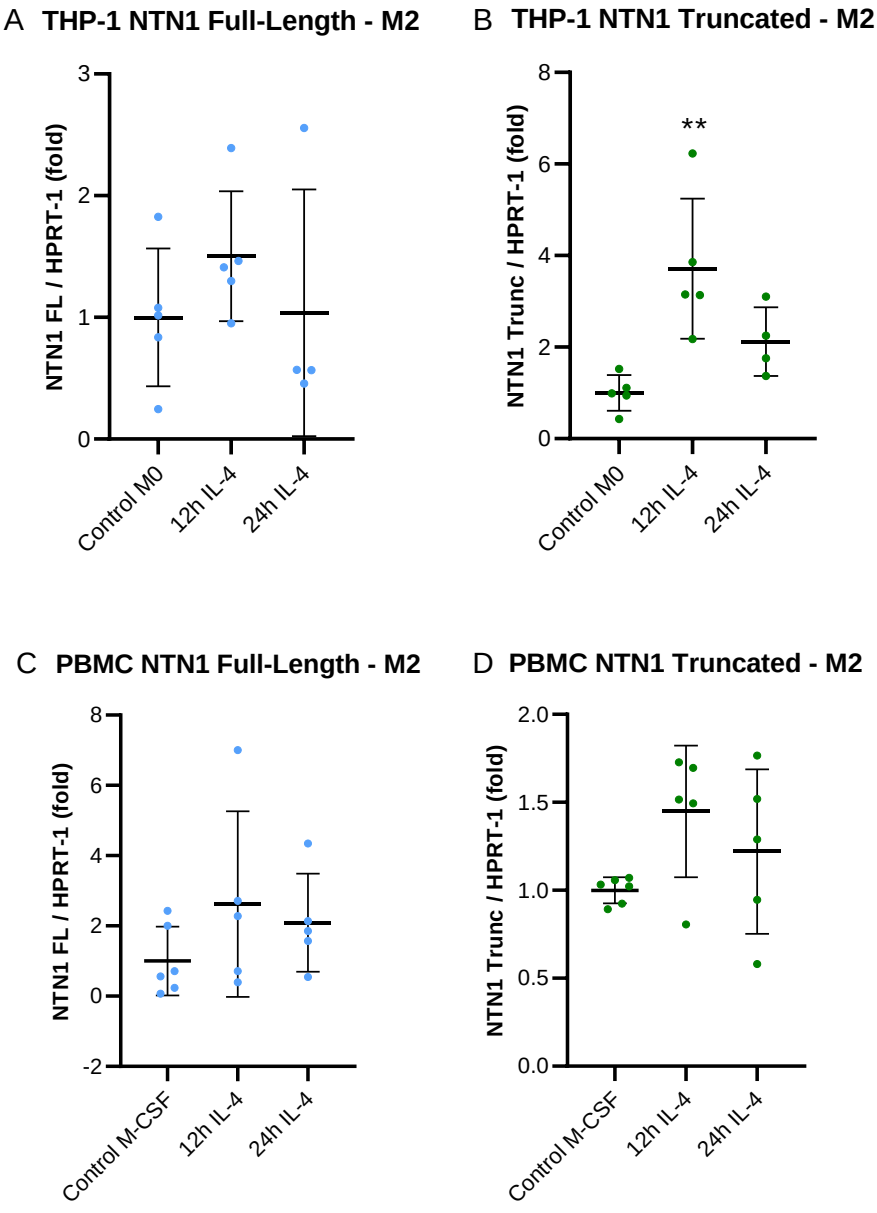

Figure 3.12 - Netrin-1 isoform expression in alternative activated macrophages. (A) Exposure to IL-4 did not affect the expression of full-length netrin-1 after either 12 or 24 h in THP-1-derived macrophages. (B) The truncated isoform was only upregulated after 12 h anti-inflammatory stimulation. In PBMC-derived M2 macrophages neither full-length (C) nor truncated (D) isoforms were affected after IL-4 stimulation, after 12 or 24 h. Mean±SD, n=4-6. **P<0.01 between groups indicated and the control group.

The isoform that is predominantly expressed in macrophages is the truncated isoform (Figure 3.13A). In THP-1-derived macrophages, the ratio of truncated to full-length netrin-1 varied between 0.59 and 0.78. Interestingly, under both pro- and anti-inflammatory conditions, the ratio of truncated to full-length isoforms increased when compared with unstimulated macrophages.

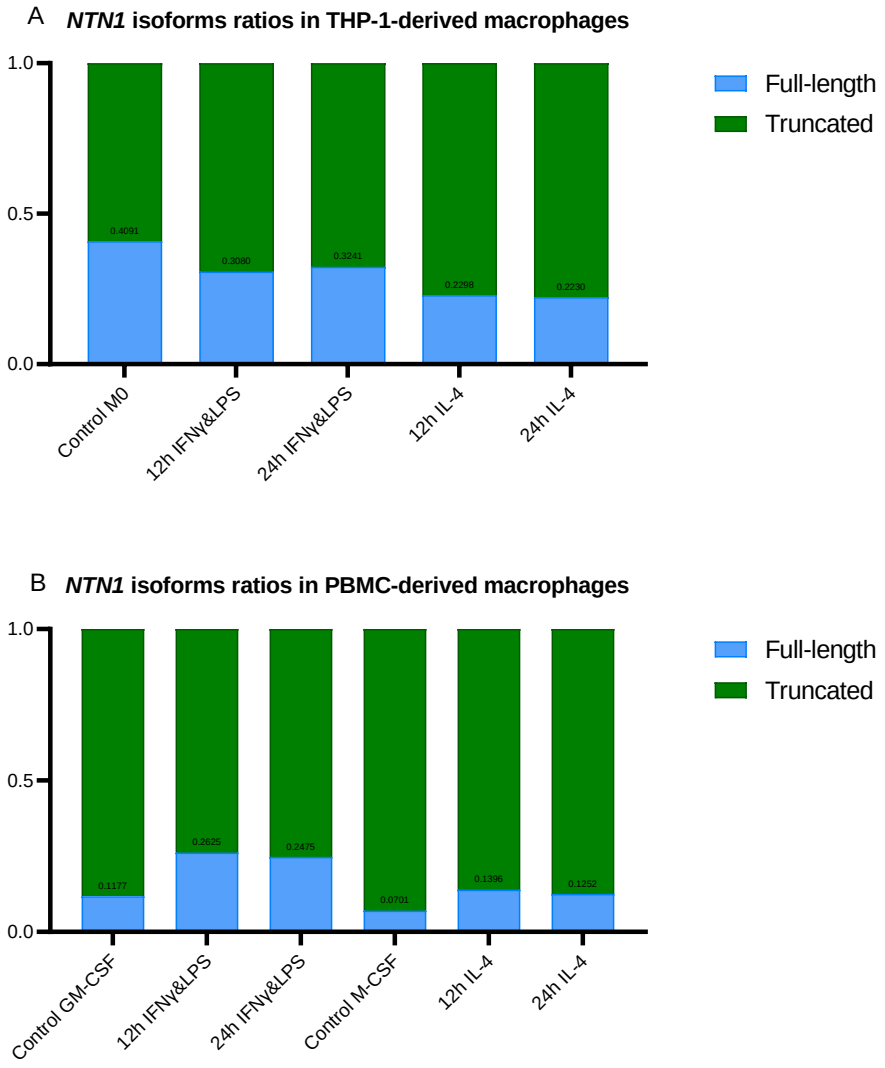

Figure 3.13 – Truncated netrin-1 is the main isoform expressed in macrophages. (A) THP-1-derived macrophages' expression ratio between full-length and truncated isoforms varies between 0.59 and 0.78. (B) PBMC-derived macrophages' expression ratio between full-length and truncated isoforms varies between 0.74 and 0.93.

This increase was more obvious in the M2 macrophages. In PBMC-derived macrophages, the truncated netrin-1 was the most expressed isoform in all phenotypes (Figure 3.13B). The ratio varied between 0.74 and 0.93 and, in contrast to what was observed in THP-1-derived macrophages, the truncated to full-length isoform ratio decreased after cytokine stimulation.

3.5.3. Generation of foam cells using acLDL did not affect the expression of netrin-1

The figures acquired when cells were treated with 200 µg/mL showed cellular features associated with stress and apoptosis such as cell shrinkage and fragmentation. The cells treated with 50 µg/mL showed clear internalisation of lipids while keeping the normal cellular features. For that reason, 50 µg/mL was chosen as the condition to generate foam cells. THP-1-derived macrophages were exposed to 50 µg/mL acLDL for 48h. The cells were treated with pro- and anti-inflammatory cytokines, as described previously, halfway through acLDL exposure (the last 24 h).

Commercial acLDL

As shown in figure 3.14, treating cells with acLDL alone did not affect the expression of either netrin-1 isoform. Pro-inflammatory stimulation led to an upregulation of both isoforms in foam cells. While full-length netrin-1 expression significantly increased 7.9-fold, truncated isoform increased 16.3-fold when compared with unstimulated foam cells. Similarly, to what was observed in non-foam cells, stimulation with IL-4 did not have a significant effect on the expression of either isoform.

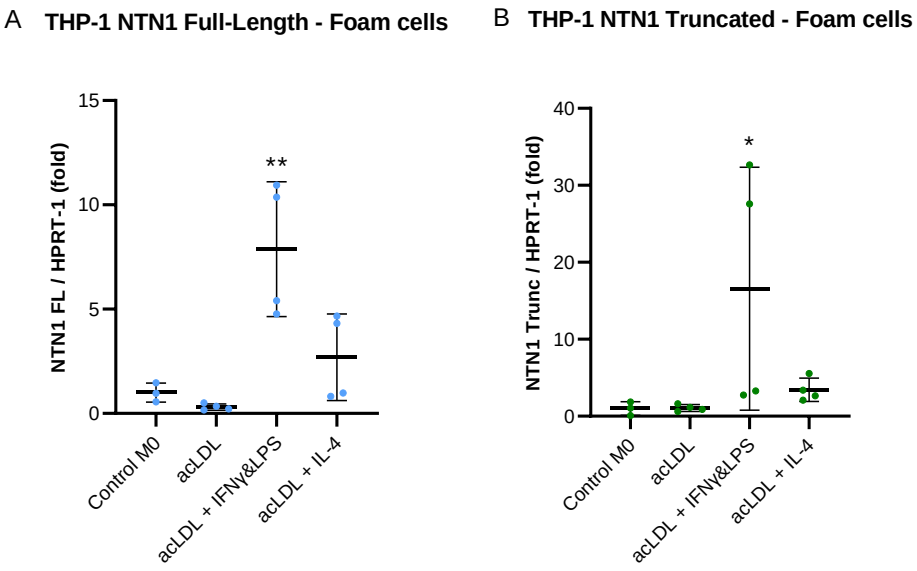

Figure 3.14 - Foam cells generated with commercial acLDL. (A) Exposure to acLDL, or combination of acLDL and IL-4 did not affect the expression of full-length netrin-1, but pro-inflammatory stimulation led to an upregulation of this isoform, in THP-1-derived macrophages (B) Netrin-1 truncated isoform was only upregulated when IFN-γ and LPS were combined with acLDL. Mean±SD, n=3-4. *P<0.05 and **P<0.01 between groups indicated and the control group.

LDL acetylated in house

Interestingly, when LDL acetylated in house was used to generate foam cells, *NTN1* gene expression presented different results from those obtained with commercial acLDL. As observed with commercial acLDL, generating foam cells did not change the expression of either isoform. Stimulating the foam cells with pro- and anti-inflammatory cytokines led to a 4.8- and 5.1-fold upregulation respectively of full-length netrin-1 when compared with unstimulated foam cells (Figure 3.15A). However, the truncated isoform expression was only affected when the foam cells were stimulated with IL-4, showing a 7.0-fold increase in its expression (Figure 3.15B).

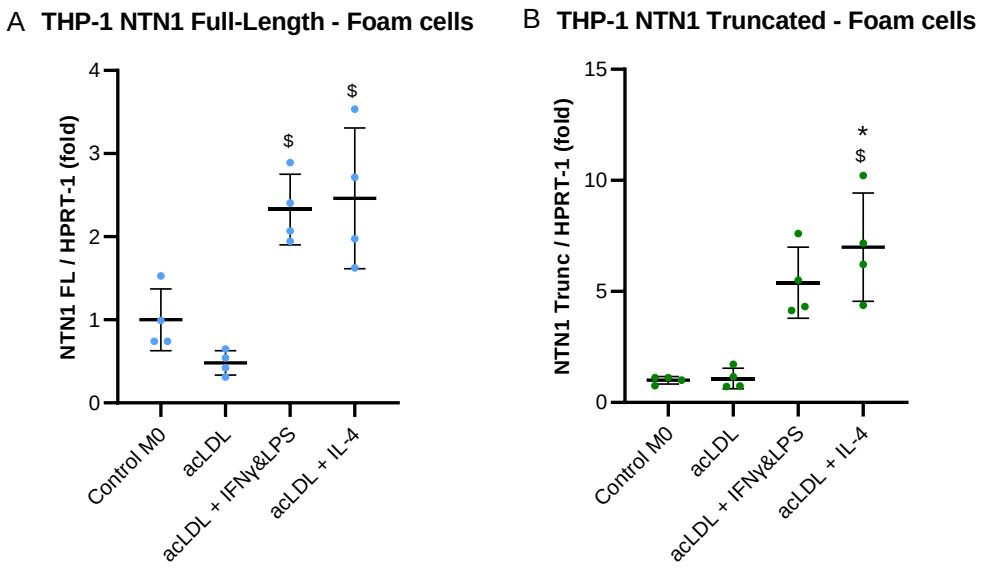

Figure 3.15 - Foam cells generated with acLDL. (A) Exposure to LDL acetylated in house did not affect the expression of full-length netrin-1, but when combined with pro- and anti-inflammatory stimulation there was an upregulation of this isoform, when compared with unstimulated foam cells. (B) Truncated netrin-1 was only upregulated when the foam cells were exposed to IL-4. Mean±SD, n=4. *P<0.05 between groups indicated and the control group; $P<0.05 between groups indicated and the acLDL group.

3.5.4. Netrin-1 isoform dependency on NF-κB

The role of NF-κB in the expression of netrin-1 isoforms was studied using two different inhibitors that target this pathway. Bay 11-7082 and JSH 23 are two inhibitors commonly used in research and target the NF-κB molecular cascade at different points, as described previously.

Bay 11-7082

IL-1β is a downstream product of NF-κB and was used to monitor whether Bay 11-7082 inhibits this nuclear factor. The upregulation found in IL-1β expression after stimulation with IFN-γ and LPS appear to be reduced when 5 μM Bay 11-7082 were used as treatment

(Figure 3.16). In the absence of pro-inflammatory cytokines, Bay 11-7082 alone had no effect on the basal expression of IL-1β mRNA.

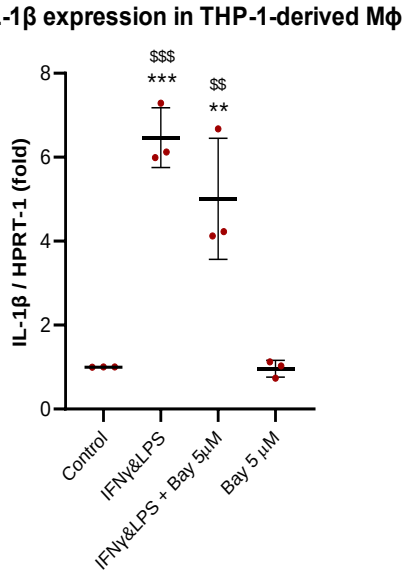

Figure 3.16 – Bay 11-7082 does not inhibit the expression of IL-1β in THP-1-derived macrophages after pro-inflammatory stimulation. IFN-γ combined with LPS upregulate the expression of IL-1β in the presence and absence of Bay 11-7082. Mean±SD, n=3. **P<0.01 and ***P<0.001 between groups indicated and the control group; $^{\$\$}$P<0.01 and $^{\$\$\$}$P<0.001 between groups indicated and the Bay 5 μM group.

Bay 11-7082 treatment alone led to an upregulation of both netrin-1 isoforms (Figure 3.17). While pro-inflammatory stimulation did not show a significant upregulation of either isoform, the combination of cytokines and 5 μM Bay 11-7082 led to an increase in the expression of both isoforms by 11.9- and 8.7-fold, respectively. Doubling the concentration of Bay11-7082 further upregulated the expression of both isoforms, to 13.8-fold for the full-length isoform and 9.4-fold for the truncated one. 5 μM Bay 11-7082 treatment alone did not show an effect on the expression of netrin-1 isoforms, but 10 μM gave rise to a significant upregulation of

both isoforms, by 12.5-fold for the full-length and 8.2-fold for the truncated isoform, when compared with untreated cells.

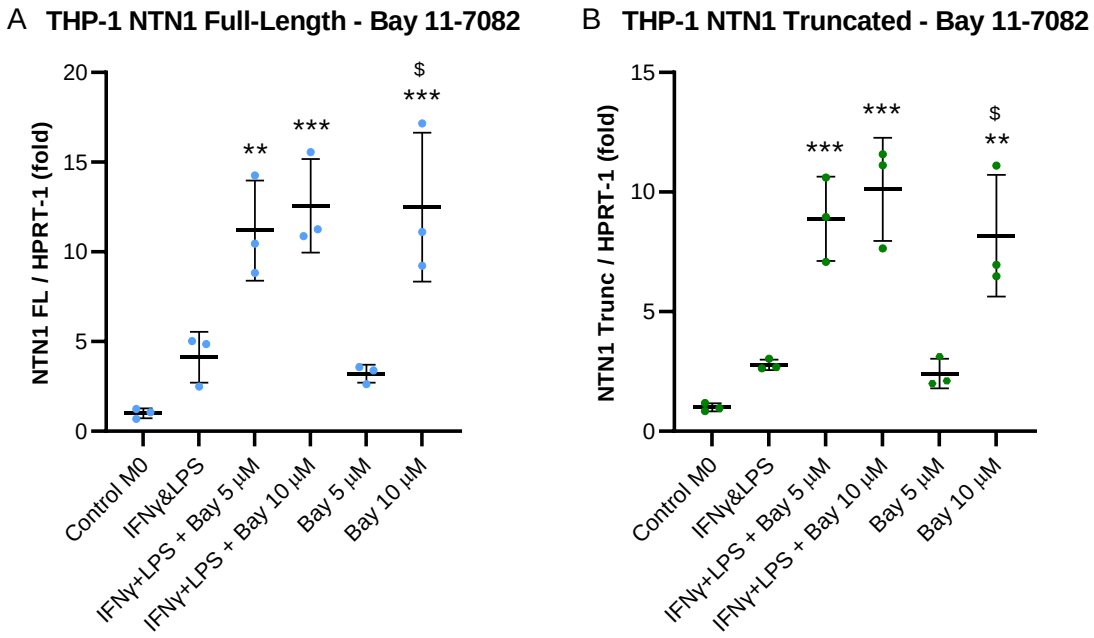

Figure 3.17 - Bay 11-7082 upregulates netrin-1 isoform's expression in the absence of inflammatory stimuli, in THP-1-derived macrophages. In the absence of pro-inflammatory stimulation, 10μM Bay 11-7082 led to an upregulation in the gene expression of both netrin-1 isoforms: full-length (A) and truncated (B). Mean±SD, n=3. *P<0.05, **P<0.01 and ***P<0.001 between groups indicated and the control group; $P<0.05 between groups indicated and the IFNγ&LPS group.

JSH 23

The second inhibitor used in this set of experiments was JSH 23, which is a nuclear translocation blocker, and acts through a different mechanism from Bay 11-7082. Similarly to the experiment using Bay 11-7082, IL-1β expression was used as a tool to monitor the degree of inhibition of NF-κB. Moreover, a set of primers for IL-6 was also included in the experiment to generate more robust evidence for the effect of JSH 23 (Figure 3.18). On its own, the inhibitor showed no effect on expression either of these pro-inflammatory cytokines in both THP-1- and PBMC-derived macrophages. In THP-1 M1 macrophages, the

expression of IL-1β and IL-6 increased 92.3- and 15,315.4-fold respectively in response to IFN-γ and LPS. Pre-treating the cells with 50 μM JSH 23 significantly reduced IL-1β upregulation to 15.1-fold and IL-6 to 2,940.8-fold. Interestingly, doubling the concentration of the inhibitor led to a similar inhibitory effect.

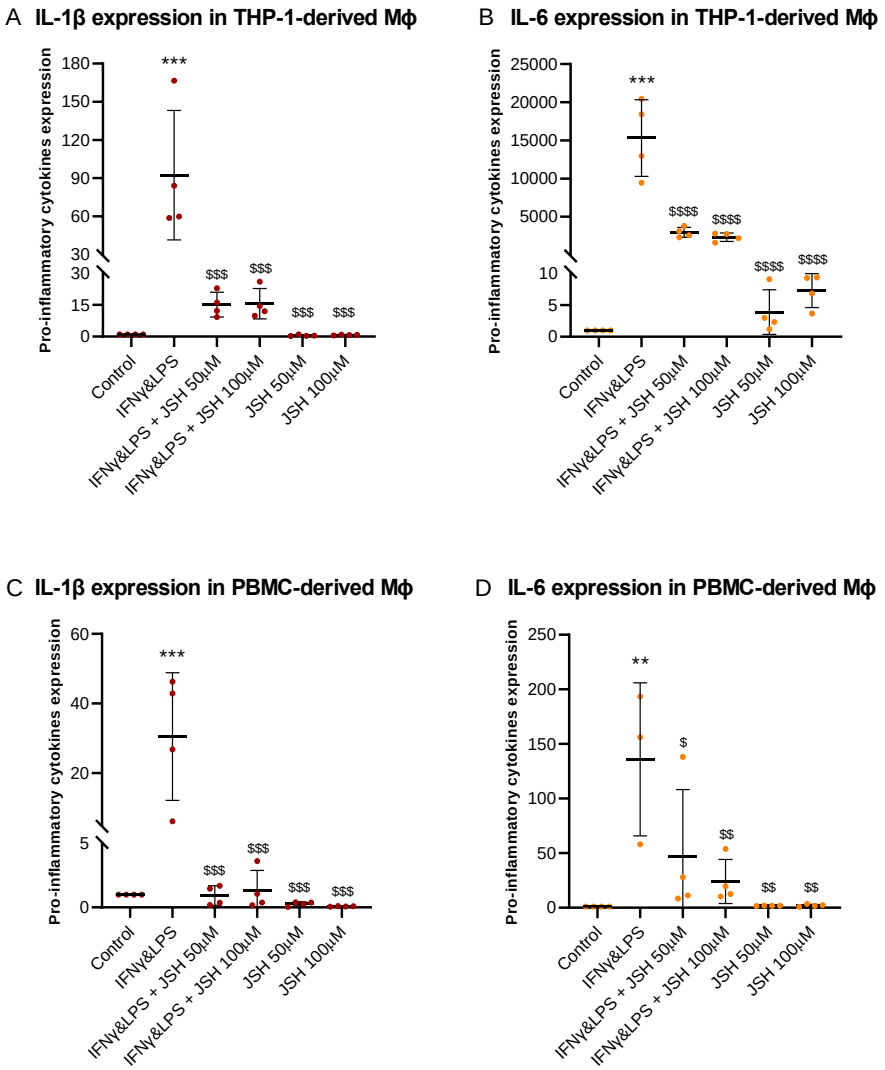

Figure 3.18 – JSH 23 inhibits the expression of IL-1β and IL-6 in classical activated THP-1- and PBMC-derived macrophages. Pre-treatment with 50 μM and 100 μM JSH 23 inhibits the upregulation of IL-1β (A) and IL-6 (B) in THP-1-derived macrophages after IFN-γ and LPS stimulation. The upregulation of IL-1β (C) and IL-6 (D) was also inhibited in PBMC-derived macrophages when the cells were treated with JSH 23. Mean±SD, n=4. **P<0.01 and ***P<0.001 between groups indicated and the control group; $P<0.05, $$P<0.01 and $$$P<0.001 between groups indicated and the IFNγ&LPS group.

In PBMC-derived macrophages, treating the cells with JSH 23 prior to stimulation with pro-inflammatory cytokines led to a complete inhibition of the upregulation of both IL-1β and IL-6 expression. The effects of pro-inflammatory stimulation on the expression of IL-1β were suppressed after treating the cultures with 50 or 100 μM JSH 23, decreasing from a 30.5-fold increase to basal levels. The expression of IL-6 mRNA also decreased when the cells were pre-treated with JSH 23. 50 μM of inhibitor reduced the upregulation of this cytokine from 135.9-fold to 46.4-fold, and 100 μM had a greater effect, bringing it down to 24.1-fold. Treating the cells with JSH 23 alone at either concentration did not affect the expression of either cytokine in PBMC.

Having confirmed that JSH 23 was an appropriate NF-κB inhibitor to use in both cell models, the expression of netrin-1 isoforms was assessed under the same conditions that were used for the pro-inflammatory cytokines (Figure 3.19). In THP-1-derived macrophages, the expression of both isoforms significantly decreased when cells were treated with 50 μM JSH 23. Netrin-1 full-length isoform expression after pro-inflammatory stimulation decreased by 60% when the cultures were pre-treated with 50 μM JSH 23. The truncated isoform expression was also non-significantly reduced by 45% when the cells were pre-treated with the inhibitor.

Interestingly, JSH 23 significantly decreased the expression of only truncated netrin-1, in PBMC-derived macrophages. When compared with the pro-inflammatory stimulated group, treatment with 50 μM and 100 μM JSH 23 led to a decreased upregulation of netrin-1 by 61% and 82% for the truncated isoform, respectively. Even though the expression of secreted netrin-1 showed a decrease of 74% and 89% when JSH 23 (50 and 100 μM, respectively) was used, those were not significant.

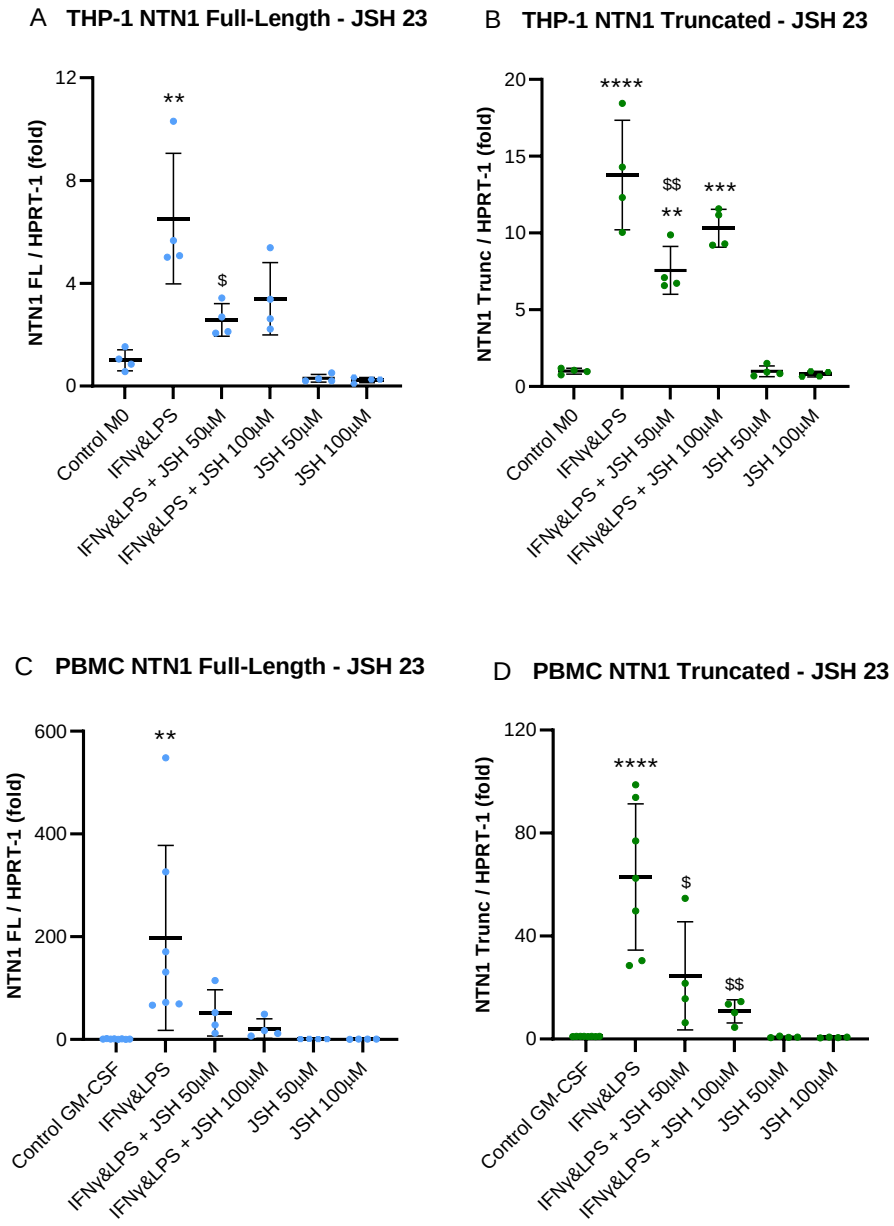

Figure 3.19 - JSH 23 inhibits the expression of both netrin-1 isoforms in THP-1- and PBMC-derived macrophages. Pre-treatment with 50 μM JSH 23 inhibits the upregulation of both full-length (A) and truncated netrin-1 isoform (B) in THP-1-derived macrophages after IFN-γ and LPS stimulation. The upregulation of IL-1β (C) and IL-6 (D) was also inhibited in PBMC-derived macrophages, when the cells were treated with JSH 23. Mean±SD, n=4-7. **P<0.01, ***P<0.001 and ****P<0.0001 between groups indicated and the control group; $P<0.05, and $$P<0.01 between groups indicated and the IFNγ&LPS group.

3.6. Discussion

3.6.1. Macrophage phenotypes

IL-1β is a marker commonly used to confirm the phenotypical change of macrophages towards a pro-inflammatory phenotype, in THP-1 and PBMC-derived macrophages.[195,196] Shiratori and colleagues performed similar experiments to the ones presented here and produced comparable results. There was a clear upregulation of IL-1β in both cell types, but that effect was greater in THP-1 than PBMC-derived M1 macrophages after 24 h stimulation.[196] Interestingly, this was the opposite response to that obtained in our experiments, where we found the upregulation of IL-1β mRNA to be nearly ten times higher in PBMC-derived macrophages. In two different studies, Tedesco *et al* and Schildberger *et al* compared the polarization of THP-1 vs PBMC-derived macrophages and found a greater effect in the expression of inflammatory markers, such as IL-1β and IL-6, from stimulated primary cells when compared with the cell line. This supports the results we found from our work.[197,198]

There was considerable variability in the expression levels of IL-1β in response to IFN-γ and LPS in PBMC-derived macrophages. These cells were acquired from blood samples from different individuals and therefore there is an expected natural variability. Individual characteristics such as age, sex, hormones, and genetic polymorphisms will have an impact in the polarization of macrophages, and cytokine expression. For example, the expression of TLR4 and pro-inflammatory cytokines is different between males and females. Peritoneal macrophages from male mice produce more pro-inflammatory cytokines after stimulation with LPS than the female counterparts. Human neutrophils from males also produce more

TLR4 and TNF-α than females. Even within the same sex, differences are often observed and can be related with multiple factors such as nutrition or menstrual cycle.[199,200]

CD206, or mannose receptor C1, is a well-known marker for alternative activated macrophages.[27,197] This cellular membrane receptor is upregulated in M2-like macrophages but not in M1, and therefore its expression was measured to confirm successful phenotypical change into alternative activated macrophages in the presented experiments. Stimulation with IL-4 led to a greater upregulation of CD206 in THP-1-derived macrophages than PBMC-derived macrophages.. The gene expression profiles reported by Tedesco and colleagues show a similar variation in the CD206 upregulation in PBMC to the ones presented in this chapter. However, while we showed that THP-1 presented a greater upregulation of CD206, they found that the increase in the expression of this marker in THP-1 was negligible after the same treatment with IL-4.[197] The data acquired in this study confirmed that stimulating THP-1 cells with IFN-γ and LPS promoted the development of a pro-inflammatory macrophage phenotype. Likewise, anti-inflammatory macrophages were successfully generated using IL-4. This was first step necessary to test the hypothesis that netrin-1 expression is affected by macrophage phenotype and cytokine stimulation.

To study the foam cells' response to pro- and anti-inflammatory stimuli, THP-1 cells were exposed to 50 μg/mL acLDL for 48h. An acetylation reaction, rather than oxidation, was used to modify the LDL due to the toxicity of the products of the oxidation reaction. Guyton and colleagues showed that copper-oxidised LDL (the most common reaction to generate oxLDL) is cytotoxic when used to treat smooth muscle cells.[201] Asmis *et al* went further and showed that oxLDL promoted cell lysis and apoptosis of human macrophages.[202] Orekhov and colleagues demonstrated that the internalisation of acLDL is not as high as oxLDL, but is still considerably higher than nLDL.[203] They also showed that the signalling pathways on

which each type of modified LDL depend are different and that might explain why the cellular cholesterol content varies. Microscopy analysis and staining quantification showed that in our experiments both 50 and 200 µg/mL acLDL concentrations successfully generated foam cells. The higher concentration of acLDL seemed to negatively affect the cells, which presented smaller cytoplasms and more cellular debris. For that reason, only 50 µg/mL acLDL was used in subsequent experiments. Interestingly, cholesterol uptake was higher when the cells were treated with acLDL modified in the lab, when compared with commercially available acLDL. This is likely to have happened because the sample modified by us was not pure nLDL and there was a mix of other cholesterol-containing lipoproteins. Jones *et al* found that treating macrophages in a pigeon model with acLDL leads to an increased uptake of other cholesterol-containing lipoproteins, through endocytosis and macropinocytosis.[204] The treatments used in our cell cultures provided an *in vitro* model that mimics the macrophage populations found in the atherosclerotic plaque. We were therefore able to create a panel of cell types that allows the determination of how the expression of netrin-1 varies in non-foam and foam pro-inflammatory and pro-resolving macrophages.

3.6.2. Primer efficiencies

Primer efficiencies were determined using series of dilutions of cDNA from M0 and M1 macrophages in both the cell line and primary cells. All the linear regressions presented a coefficient of determination higher than 0.990, which brings a good certainty to the calculated efficiencies. The amplification factors for all three sets of primers were either 1.98 or 2.05, which means that after each cycle, one strand of DNA originates 1.98 and 2.05 strands, respectively. This translates into efficiency values of 98% and 105%. These values are within the range of accepted efficiencies for qPCR (90-110%), according to the

guidelines for validation of qPCR.[205] This, together with the melting curves presented previously, provides good evidence that these are three reliable sets of primers for our experiments. We were therefore comfortable using these sets of primers to study how different netrin-1 isoform expression varied under pro- and anti-inflammatory conditions.

3.6.3. Classical activated phenotype is the main type of macrophage that expresses netrin-1 isoforms

The data acquired through qPCR shows an upregulation of both netrin-1 isoforms after pro-inflammatory stimulation. In THP-1-derived macrophages, the peak of upregulation seemed to happen earlier (after 12 h exposure) than in PBMC, which showed higher expression at the 24 h time point. The truncated isoform showed a greater increase after stimulation than the full-length isoform in THP-1-derived macrophages, but not in PBMC. PBMC-derived macrophages showed a greater increase in the expression of both isoforms when compared with the THP-1 cell line. Passacquale and colleagues showed in endothelial cells, that pro-inflammatory stimulation with TNF-α leads to a non-significant increase in the full-length isoform, but a greater and significant upregulation in total netrin-1.[136] Since the secreted netrin-1 increase was minimal, the isoform that was more expressed after stimulation was inferred to the truncated isoform. This is in line with the results obtained in our experiments in THP-1 cells, which after 24h exposure only showed significant upregulation of the truncated isoform.

Although there is no published evidence regarding netrin-1 isoform expression in PBMC-derived macrophages, Fiorelli *et al* studied patients with coronary artery disease and found that groups that presented higher levels of serum C-reactive protein, and therefore have

evidence of a generalised inflammatory process, also presented higher intracellular amounts of netrin-1 in their monocyte-derived macrophages.[161] Paradisi and colleagues also showed that treating HCT116 and HBL100 cells with TNF-α led to upregulation of total netrin-1.[138] At the time that this study was published, there was no knowledge regarding netrin-1 isoforms and therefore only the total amount was considered.

Contrary to classical activated macrophages, netrin-1 isoform upregulation was much less in response to IL-4. Interestingly, PBMC-derived macrophages showed no difference in the expression of either isoform, even though this type of cells showed a very strong response to the pro-inflammatory cytokines. Non-inflammatory conditions promote the expression of endothelial-derived netrin-1 into the circulation and provide a protective effect against inflammation.[126,127,160,206,207] However, we showed that in macrophages, pro-inflammatory stimulation upregulates the expression of netrin-1, together with other pro-inflammatory cytokines.

Exposing THP-1-derived macrophages to acLDL led to a non-significant downregulation of secreted netrin-1, but no effect on the truncated isoform, with both types of acLDL used. Van Gils *et al* showed contrasting data in an animal model, where foam cells within the plaque of *LDLR*$^{-/-}$ and *ApoE*$^{-/-}$ mice fed with high-fat diet expressed significantly more netrin-1 when compared with mice fed with normal chow. They also treated isolated peritoneal macrophages with oxLDL and the upregulation observed *in vivo* was replicated *in vitro*. This was determined at both mRNA and protein levels.[134] There are inflammatory processes happening inside the atherosclerotic plaque and this may explain the difference between our results and the *in vivo* results presented by this group. In our studies, indeed, when either type of foam cells were stimulated with pro-inflammatory cytokines, the expression of full-length netrin-1 was upregulated. This corroborates the results observed in van Gils' study.

Stimulation with IL-4 upregulated the expression of both isoforms in foam cells treated with LDL acetylated in house, but to a lower and non-significant extent in cultures treated with commercial acLDL. When the foam cell responses are compared with those of non-foam cells after pro-inflammatory stimulation, the upregulation in foam cells was greater. When non-foam and foam cells were compared, the uptake of LDL did not seem to be directly related with the expression of netrin-1. Once again, the evidence related with netrin-1 upregulation pointed towards a dependency on inflammatory stimulation. The single-cell sequencing data published by Kim *et al* and Depuydt *et al* presented foam-cells as a non-inflammatory macrophage subset which did not contribute to the inflammatory stimulation.[64,71] Our results agreed with that premise, where acLDL treatment alone did not show any differences in the expression of netrin-1.

After determining that the expression of macrophage-derived netrin-1 is closely related with inflammation, we assessed whether there is a link between NF-κB signalling and netrin-1 isoform expression in macrophages. To test this, Bay 11-7082, which is a NF-κB inhibitor, was used in THP-1-derived macrophages, prior to stimulating them with pro-inflammatory cytokines. The expression of IL-1β increased when the macrophages were stimulated with IFN-γ and LPS. When the cells were pre-treated with Bay 11-7082, the upregulation of IL-1β was inhibited and, on its own, Bay 11-7082 did not have any effect on the expression of the cytokine. However, exposing THP-1-derived macrophages to Bay 11-7082 alone led to an upregulation of both netrin-1 isoforms, and indeed 5 μM Bay 11-7082 gave rise to a similar increase in the expression of netrin-1 isoforms as did IFN-γ and LPS. When the concentration of Bay 11-7082 was doubled, the upregulation of secreted and truncated isoforms was greater still, reaching similar fold values to those attained where the inhibitor was combined

with pro-inflammatory cytokines. For this reason, Bay 11-7082 was deemed unsuitable for the purpose of our experiments.

JSH 23 was used as an alternative NF-κB inhibitor. To assess the effectiveness of this inhibitor, IL-1β expression was measured as previously mentioned, together with that of IL-6. These are two well-known products downstream of NF-κB activation.[208] The expression of IL-1β increased after stimulation with IFNγ and LPS. This difference in the upregulation of IL-1β between the experiment using Bay 11-7082 and the experiment using JSH 23, when only pro-inflammatory stimulation was used, is likely to be related to the change in the vial of THP-1 cells. A new vial of this cell line was acquired from ATCC and an earlier passage was used in this experiment. Pre-treatment with 50μM JSH 23 partially inhibited IL-1β upregulation. Doubling the amount of inhibitor had no further effect, keeping the upregulation at the same level. The expression of IL-6 was strongly upregulated after pro-inflammatory stimulation and was partially inhibited when 50 μM and 100 μM JSH 23 decreasing its expression 5 to 6 times. Treatment with JSH 23 alone did not affect the expression of these cytokines. This confirmed that JSH 23 is a suitable inhibitor to confirm whether NF-κB is involved in the expression of netrin-1 isoforms, in THP-1. JSH 23 was also trialled in PBMC-derived macrophages. IL-1β expression was completely inhibited to unstimulated levels when JSH 23 was used. IL-6 was significantly inhibited, after 50 μM treatment and its effect doubled when 100 μM of the inhibitor were used. In a study published by Shin and colleagues, 30 μM JSH 23 completely supressed the upregulation of IL-1β and IL-6 after stimulating RAW 264.7 macrophages with 1 μg/mL LPS.[173] After validating the inhibitory agent, the expression of netrin-1 isoforms was assessed in the same conditions.

In THP-1, 50 μM JSH 23 significantly decreased the upregulation of both netrin-1 isoforms. In the presence of JSH23, full-length and truncated isoforms upregulation decreased 60%

and 45% when compared with untreated cultures. 100 μM JSH 23 also showed an inhibitory effect on both isoforms, however this was not as effective as 50 μM, leading to a smaller. In PBMC-derived macrophages, only the truncated isoform expression was significantly inhibited when JSH 23 was used. The inhibitor reduced the truncated isoform upregulation in 60% and 83% after 50 μM and 100 μM treatment, respectively.

Together, the data above provides good evidence that NF-κB plays a role in the expression of both netrin-1 isoforms. Since total inhibition in the expression of the isoforms in THP-1 cells was not achieved, it is likely that NF-κB is not the only signalling mechanism involved in the expression of netrin-1 isoforms of this cell line. Paradisi *et al* showed in colorectal cancer cells that the netrin-1 gene is a direct transcriptional target of NF-κB.[138] TNF-α stimulation led to an upregulation of total netrin-1 and, using the inhibitor Bay11-7082 (5 μM), the upregulation decreased roughly 60%. Van Gils and colleagues also showed that netrin-1 expression was upregulated when NF-κB was activated through binding of oxLDL to CD36. Using a *NTN1* promoter luciferase reporter gene, they established that the promoter activity was induced by oxLDL and its induction was inhibited by Bay 11-7082.[134] Passacquale *et al* also showed in an endothelial cell model that NF-κB is involved in the expression of netrin-1.[136] The upregulation, observed mainly in the truncated isoform, was significantly reduced when the cells were treated with Bay 11-7082, which confirms the data acquired in our PBMC-derived macrophage cultures. However, this group also showed that pro-inflammatory stimulation led to a decrease in the expression of secreted netrin-1 in endothelial cells, the upregulation being associated exclusively with the truncated isoform. This data shows the opposite response to that observed in macrophages.

Our study supports the data presented by these research groups, where NF-κB is at least partially involved in the expression of netrin-1. Pro-inflammatory macrophages secrete

netrin-1 and this promotes atherogenesis.[134,161] Our data complements the work from Schlegel et al which demonstrated that silencing myeloid netrin-1 contributes to plaque regression.[166] Truncated netrin-1 has been linked not only to ribosome biogenesis but also as a potential transcription factor in cancer cells.[108,209] Its role in other cells models such as leukocytes is still unknown. We showed that macrophages do express this isoform, but its impact in inflammation and in the development of atherosclerosis still needs to be investigated.

3.7. Limitations

The principal limitation of these studies lies in the inability to acquire an antibody that recognises both netrin-1 isoforms thus limiting our ability to quantify the protein levels. In future experiments, we will use mass spectrometry to achieve this. Gene expression information through mRNA analysis, using qPCR, is useful but one has to bear it in mind that post-transcriptional regulation, post-translational modification and alternative splicing can affect the final protein levels. Looking at the expression of truncated netrin-1 indirectly, by subtracting the full-length isoform to the total netrin-1 expression may lead to less accurate data. Primers targeting the UTR portion of the truncated mRNA might improve the quality of the data related to this isoform expression.

The effect of Bay 11-7082 on the expression of netrin-1 in macrophages led us to deem it unsuitable for our studies, and the results obtained using JSH 23 will need corroboration by other means, including NF-κB silencing.

The blood used to isolate PBMCs was acquired from the Blood and Transplant service – NHS. For confidentiality reasons, no details regarding the donor's sex, age or other or any

other individual characteristics were shared. This limited our ability to assess and discuss potential individual differences that may have an impact in the results acquired.

3.8. Summary

- IL-1β and IFN-γ stimulation successfully transformed naïve macrophages into the classical activated phenotype, and IL-4 successfully generated alternative activated macrophages.
- Pro-inflammatory stimulation significantly upregulated the expression of both netrin-1 isoforms.
- The NF-κB promoter is at least partially involved in the expression of both netrin-1 isoforms, in both THP-1- and PMBC-derived macrophages.
- Classical activated is the main macrophage phenotype that contributes to the expression of netrin-1.

Chapter Four

The role of full-length netrin-1 in the apoptosis and migration of THP-1-derived macrophages

4.1. Introduction

When netrin-1 was first described, it was established that it promotes the outgrowth and guiding of axons during embryonic development.[210] The ability of netrin-1 to modulate migration was also observed in the development of branched organs, such as pancreas, mammary glands and lungs, and other types of cells, such as leukocytes.[104,109,119,120,135,207]

Another cellular process that has been associated with netrin-1 is the prevention of apoptosis. In the same decade that it was discovered, Mehlen and colleagues showed that netrin-1 may act as a survival factor through its receptor DCC. DCC is a dependency receptor and it was suggested that it induces apoptosis in the absence of its ligand.[113,154] Since then, studies in multiple cell types have supported this hypothesis. Llambi *et al* showed in an *in vivo* model that knocking out the expression of netrin-1 led to major defects in the nervous system, but also fewer neurons, due to increased cell death. They also showed that the UNC5 family of receptors is involved in this physiological process.[113] Moreover, Chen *et al* showed that netrin-1 reduces neuronal injury and neuronal apoptosis.[211] Mazelin and colleagues showed that inducing the expression of netrin-1 in mouse gastrointestinal tract promotes tumorigenesis through spontaneous formation of neoplastic and hyperplastic lesions, most likely due to promotion of cell survivability.[212] Furthermore, Ko and colleagues found that pre-treating mice with netrin-1 promotes survivability of cells in lung tissue after hypobaric oxygen exposure.[207] Similarly to what was observed above, Huang and colleagues found that netrin-1 produced an anti-apoptotic signal in B-cells from patients with acute lymphoblastic leukaemia. This group observed an upregulation in the expression of Bcl-2 (an anti-apoptotic protein) and a decrease in the expression of Bax (a death-promoting protein).[213]

So far as cell migration goes, Ly and colleagues provided the first insights that netrin-1 affects the migration of leukocytes.[104] This group showed that secreted netrin-1 inhibits the active migration of monocytes, granulocytes and lymphocytes, in response to chemokine-induced chemoattraction. Furthermore, van Gils and colleagues showed in a RAW264.7 model and primary peritoneal cells that netrin-1 inhibits macrophage migration and abrogates the CCL2, CCL19 and CCL21 chemoattractant effects.[134] Ramkhelawon *et al* also showed that adipose tissue macrophage migration towards CCL19 is reduced in the presence of netrin-1.[135]

In this chapter, the role of netrin-1 on apoptosis and migration in THP-1-derived macrophages will be analysed. To study apoptosis and the role of netrin-1 in this process, triptolide was used as a pro-apoptotic agent for THP-1 cells. Triptolide has been reported to have immunosuppressant, anti-inflammatory and anti-neoplastic activity, the latter through induction of apoptosis in cancer cells. Park and Kim showed that triptolide induces apoptosis in PMA-differentiated THP-1 macrophages through the activation of caspase-3.[182]

4.2. Aims

1. To study the effect of the secreted isoform of netrin-1 on triptolide-induced apoptosis of THP-1-derived macrophages.
2. To determine the chemoattractant/repellent effect of the secreted isoform of netrin-1 on THP-1-derived macrophages.

4.3. Macrophage apoptosis

The netrin-1 receptors DCC and UNC5b are two dependence receptors that have long been shown to be involved in cell apoptosis.[113,213] The UNC5b intracellular domain contains a death domain and a caspase-3 cleavage site, which in the absence of its ligand activates p-53-mediated apoptosis.[214] Caspase-3 is an apoptosis executioner which is produced in its inactive form (procaspase dimer) and must be cleaved to become active. It is cleaved at an aspartate residue to yield p12 and p17 subunits which form the active enzyme.[215,216] Procaspase-3 consists of a large subunit, a small subunit and a prodomain. Once activated, proteolysis adjacent to Asp175 releases the large subunit (≈19 kDa) which can be further proteolyzed, removing the short prodomain, becoming a smaller peptide (≈17 kDa).[217,218] Therefore, increased amounts of cleaved caspase-3 is a good indicator that cells are undergoing apoptosis.[219]

Triptolide has been shown to be pro-apoptotic for the THP-1 cell line, after PMA-dependent differentiation, through activation of caspase-3 and -9.[182] The main dependence-receptor for netrin-1 in THP-1 cells is UNC5b and the cleavage of its death domain is caspase-3 mediated.[113] Therefore, triptolide seem to be a good agent to study netrin-1 effect on the apoptosis of THP-1-derived macrophages. A cleaved caspase-3 antibody was used to measure the degree of apoptosis, both as number of cleaved caspase-3-positive cells on immunofluorescence microscopy and as amount of cleaved caspase-3 as determined by western blot.

4.3.1. Netrin-1 did not have any effect on the ratio of triptolide-induced apoptosis in THP-1 macrophages

The number of apoptotic cells were counted using a secondary Alexa Fluor 488 antibody that binds to cleaved caspase-3 and DAPI, which stains nuclei through binding to A-T rich regions in the DNA (Figure 4.1).

The number of cleaved caspase-3 positive cells were counted and normalised to the total number of cells (DAPI positive). Only cells showing colocalization of both cleaved caspase-3 and DAPI were analysed, so that no cell debris (stained with cleaved caspase-3 but not with DAPI) was considered. Chromatin condensation (Figure 4.1C) was observed in most of the positive cells.

The percentage of apoptotic cells increased with higher concentrations of triptolide, and netrin-1 did not show any effect on triptolide-induced apoptosis, in THP-1-derived M0, M2 and foam cell-derived macrophages (Figure 4.2). Similar results to the other phenotypes were also observed in classical activated (M1) macrophages, but in this phenotype, the combination of 12.5 nM triptolide and 100 ng/mL netrin-1 also showed an increase in the apoptotic cell percentage, in comparison to 12.5 nM triptolide alone. Even though non-significant, the apoptotic cells percentage presented an apparent increase in a concentration-dependent manner compared to untreated cells.

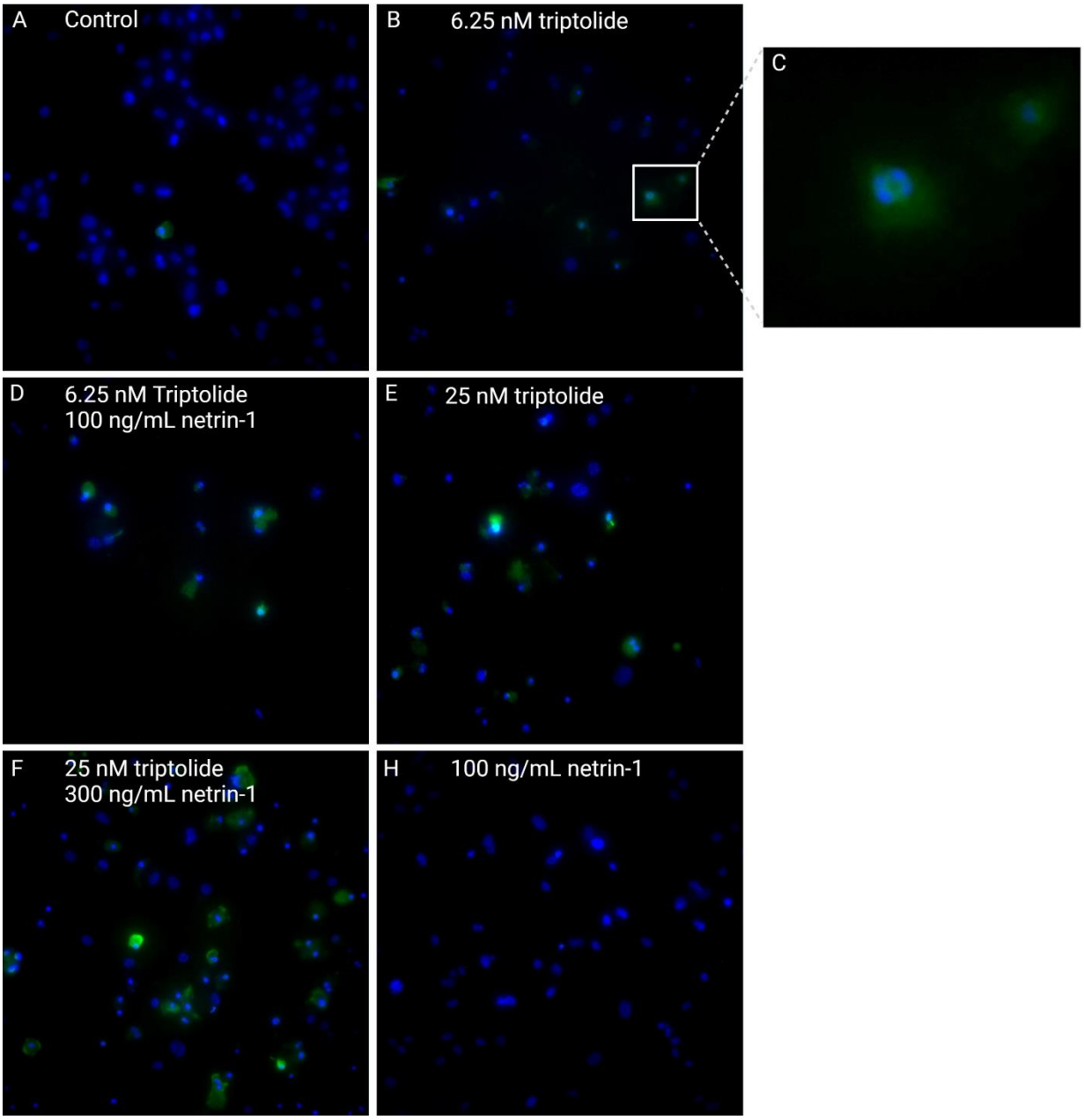

Figure 4.1 – Triptolide induced apoptosis in THP-1-derived M0 macrophages. Cleaved caspase-3 (green) indicates apoptotic cells. 200x magnification. (A) M0 macrophages control group; (B and E) cells treated solely with triptolide and amplification on apoptotic cell showing chromatin condensation (C). (D and F) triptolide and netrin-1 treated macrophages. (H) Netrin-1 treated M0 macrophages.

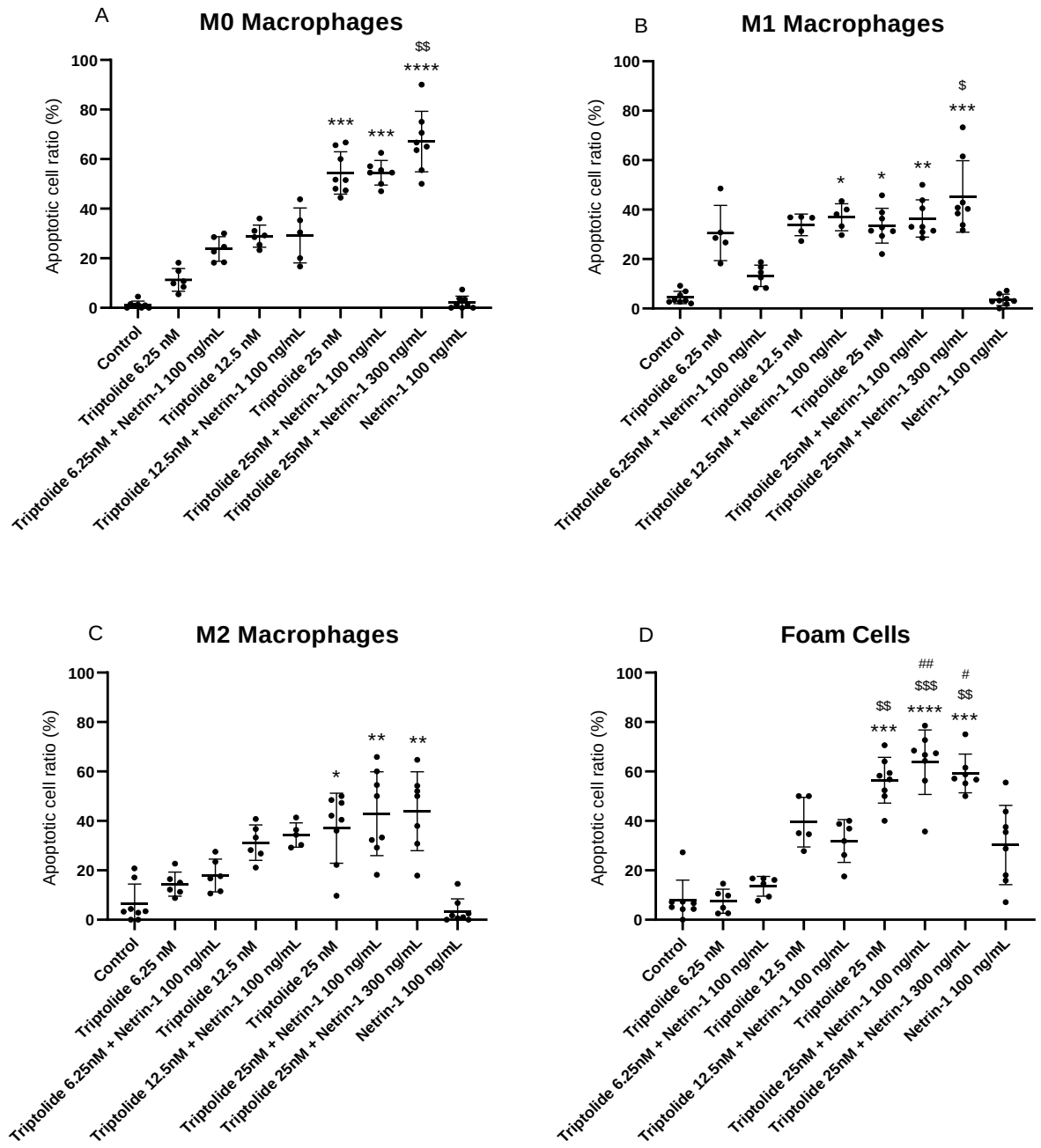

Figure 4.2 – Effects of netrin-1 on the percentage of apoptotic cells in triptolide-treated THP-1-derived macrophages. THP-1 cells treated with different concentrations of triptolide, in the presence or absence of netrin-1 at different concentrations. The number of cleaved caspase-3 (CC3) positive cells were counted and normalised to the total number of cells. (A) Unstimulated macrophages. (B) Classical activated macrophages. (C) Alternative activated macrophages. (D) Macrophage-derived foam cells. Mean±SD, n=6-8. *P<0.05, **P<0.01, ***P<0.001 and ****P<0.0001 between groups indicated and the control group; $^{\$}$P<0.05, $^{\$\$}$P<0.01 and $^{\$\$\$}$P<0.001 between groups indicated and the Triptolide 6.25 nM group; $^{\#}$P<0.05 and $^{\#\#}$P<0.01 between groups indicated and the Triptolide 6.25 nM + Netrin-1 100 ng/mL.

4.3.2. Triptolide did not show any effect on the amount of cleaved caspase-3 produced during triptolide-induced apoptosis in THP-1 macrophages

The cleaved caspase-3 antibody targets the active large subunit after the procaspase is cleaved at the Asp175 position. This subunit has a molecular weight of ≈17-19 kDa, depending on whether further proteolysis occurs.[217,218] Both bands were quantified and summed to determine the total amount of active caspase-3.

In accordance with what was determined in the apoptotic percentage experiment, netrin-1 did not affect triptolide-induced expression of cleaved caspase-3 (Figure 4.3). 12.5 nM triptolide significantly increased the expression of cleaved caspase-3 in all macrophage phenotypes studied. In unstimulated macrophages, 6.25 nM triptolide did not significantly increase the expression of cleaved caspase-3. However, the combination of the same concentration of triptolide and netrin-1 led to an increased amount of active subunit expression. In classical activated macrophages (Figure 4.3B), the increase observed with 6.25 nM triptolide did not change when cells were pre-treated with either 100 ng/mL or 300 ng/mL netrin-1. Similarly, netrin-1 did not affect the increased levels of cleaved caspase-3, when triptolide was applied to M2 macrophages (Figure 4.3C). These data together with those from the immunofluorescence experiments described above, provide clear evidence that netrin-1 did not affect the triptolide-dependent expression of cleaved caspase-3 at any concentration used, and therefore, the study was not repeated in foam cells.

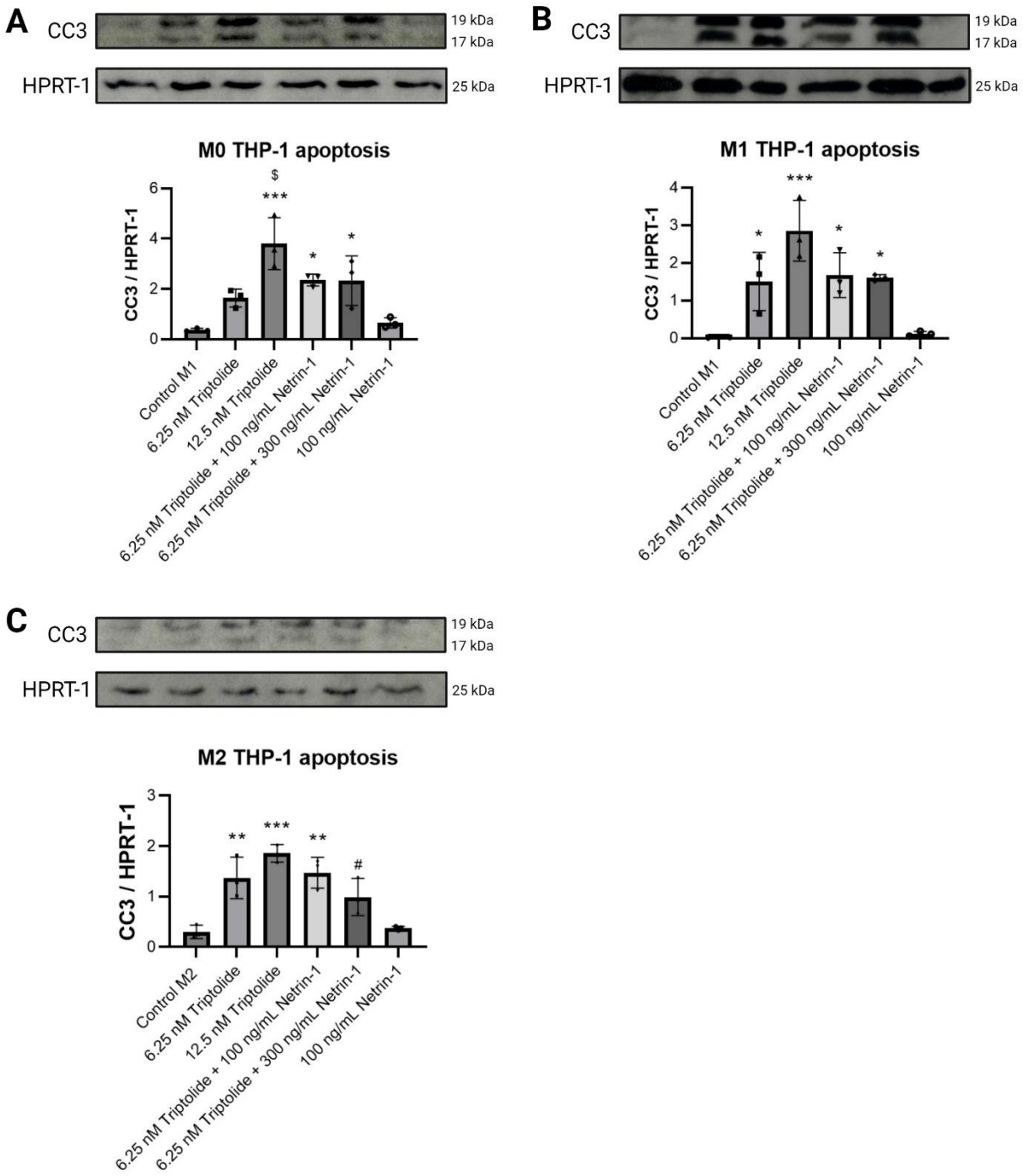

Figure 4.3 – Effect of netrin-1 on triptolide-dependent expression of cleaved caspase-3 in THP-1-derived macrophages. THP-1 cells were treated with different concentrations of triptolide, in the presence or absence of different concentrations of netrin-1. The expression levels of both cleaved caspase-3 (CC3) bands were quantified and normalised to the housekeeping protein – *HPRT-1*. (A) Unstimulated macrophages. (B) Classical activated macrophages. (C) Alternative activated macrophages. Mean±SD, n=3. *P<0.05, **P<0.01 and ***P<0.001 between groups indicated and the control group; $^{\$}$P<0.05 between groups indicated and the Triptolide 6.25 nM group; $^{\#}$P<0.05 between groups indicated and the Triptolide 12.5 nM group.

4.4. Macrophage migration - xCELLigence™

The xCELLigence™ RTCA DP system was used to measure the migration of THP-1-derived macrophages towards the chemokine CCL2, in the presence or absence netrin-1. This system is a real-time biosensor that measures cell indices (CI) with a high-density gold electrode array. The cells attached to the electrode influence the electric impedance across the array and this is recorded by the software. The greater the number of adherent cells, the greater the CI value; and in contrast, when cell adhesion decreases and cells detach, the CI decreases. CI value is 0 when there are no cells in the well.[220,221]

Two different types of plates were used in this experiment: E-plates, and CIM-plates. E-plates are usually used to measure cell adhesion and proliferation. These plates consist of wells with an electrode array in the bottom (Figure 2.10). CIM-plates have modified Boyden Chambers in each well with electrodes attached to the underside of the porous membrane. The adhesion of cells is measured through the resistance to alternating current in the electrodes (impedance) and is expressed as arbitrary units.[220,222]

4.4.1. THP-1 macrophages adherence and CI increased proportionally to the number or cells seeded

In this study, the E-plates were used to determine the optimal cell density for the THP-1 cell line to be used in the migration assay. Different cell densities were used to determine the maximum number of cells that could be used without reaching a plateau, at which point there would be no space in the electrode for the cells to adhere to.

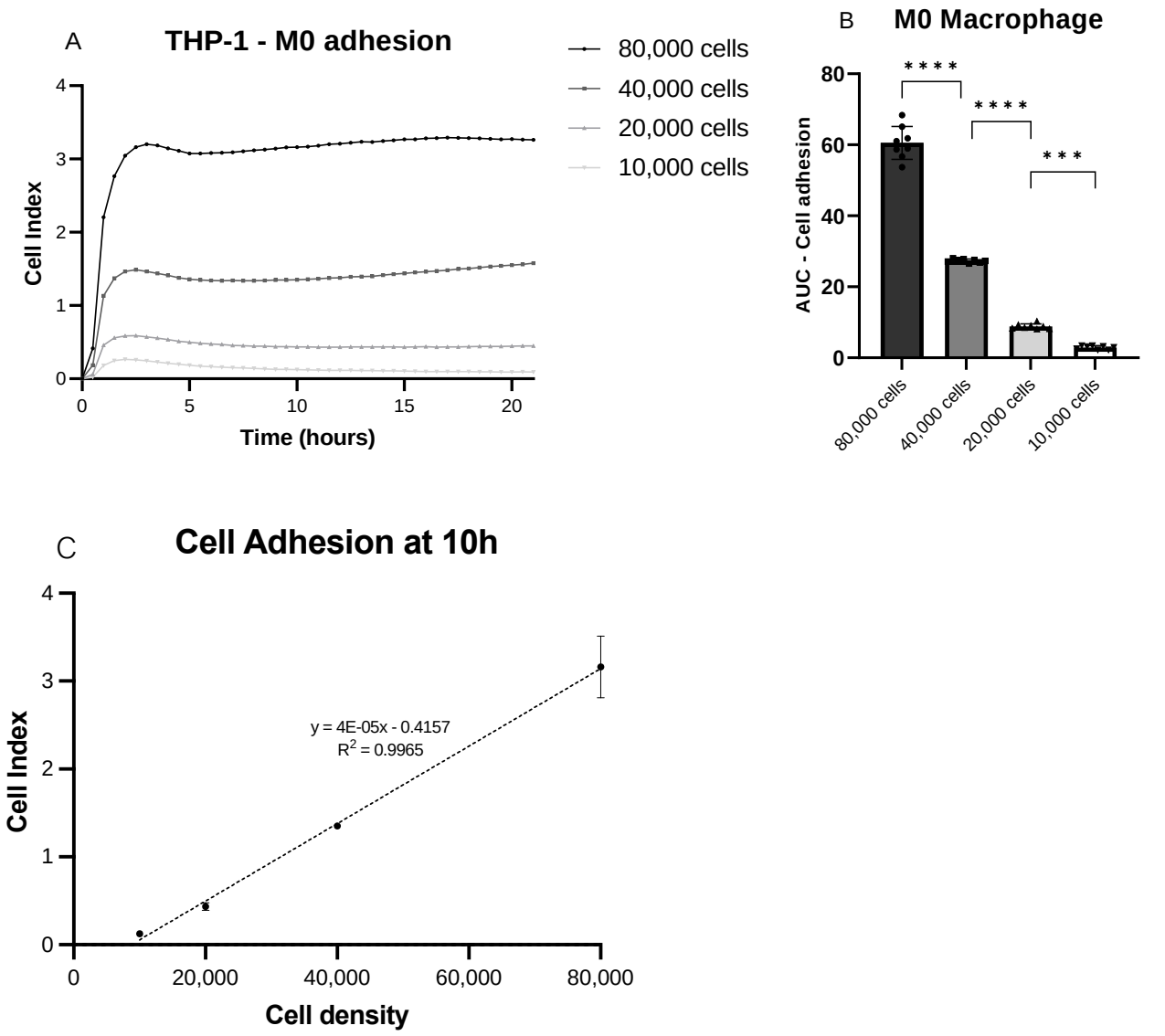

Figure 4.4 – THP-1-derived macrophage adhesion to the E-plates. Measurement of the impedance and CI of different cell densities. (A) CI for the four different cell densities over 21 h. (B) Area under the curve (AUC) for the different CI over 21 h. (C) Linear correlation between the cell density and the CI at 10 h time point . Mean±SD, n=8. ***P<0.001 and ****P<0.0001 between groups indicated.

Four different cell densities were trialled in the E-plates (10,000 – 80,000 cells). The different CI peaked after 3 h and remained constant up to 21 h. The CI value for 80,000 cells reached 3.3 and, after a slight decrease at 5 h, stayed constant between 3.1 and 3.3. The CI for 40,000 cells density increased in the first 2 h and stayed constant afterwards with CI values varying between 1.3 and 1.6. When 20,000 cells were seeded in the E-plates, the CI

increased during the first 1.5 h up to a CI value of 0.6 and varied between 0.4 and 0.6 in the following 19.5 h. The lowest cell density (10,000 cells) peaked at a CI value of 0.3 after 2 h and varied between 0.1 and 0.3 for the duration of the assay (Figure 4.4A). The area under the curve (AUC) of the CI for 10,000 cells was 2.9. There was a significant increase in the AUC for the 20,000; 40,000 and 80,000 cells densities: 8.8, 27.3 and 60.5, respectively (Figure 4.6B). Since there was no evidence that a plateau was reached with the higher density, 80,000 cells/well were used in the migration assay – CIM plates. At 10 h after the assay started there was a linear correlation between the cell density and the CI, so that the CI value increased in a cell number-dependent manner (Figure 4.5C).

4.4.2. Netrin-1 inhibited CCL2 chemoattractant effect in unstimulated THP-1 macrophages

The migration of the difference macrophage phenotypes was assessed using CIM-plates in the xCELLigence™ system. Each migration assay ran for 21 h, and the AUC for the CI of each group was acquired through the RTCA software Pro. Wells that presented an abnormal initial CI value after the quality control read were disregarded.

In M0 macrophages, all four conditions (control, CCL-2, netrin-1, CCL2 + netrin-1) showed a constant increase in the CI over time, peaking at 21 h. When no cytokines were included in the lower chamber (control), the migration happened slower than all other conditions, presenting the lowest CI values. CCL2 alone was the treatment that gave rise to the highest CI values, reflecting its chemoattractant effect on the macrophages. Similarly, netrin-1 appeared to show a lesser chemoattractant effect on this cell type, however this was not

significant. When CCL2 and netrin-1 were combined, the CI values were lower than either CCL2 or netrin-1 and approximated to control levels (Figure 4.5A).

Translating the CI values into AUC, M0 THP-1-derived macrophages presented a 1.7-fold increased migration towards the lower reservoir of the Boyden chamber in the presence of 100 ng/mL CCL2 than its absense. Interestingly, this increased response to the chemoattractant was inhibited when CCL2 and netrin-1 were combined in the same well, bringing the impedance values back to basal levels. Netrin-1, on its own, appeared to show a chemoattractant effect (1.4-fold) but this was non-significant (Figure 4.5B).

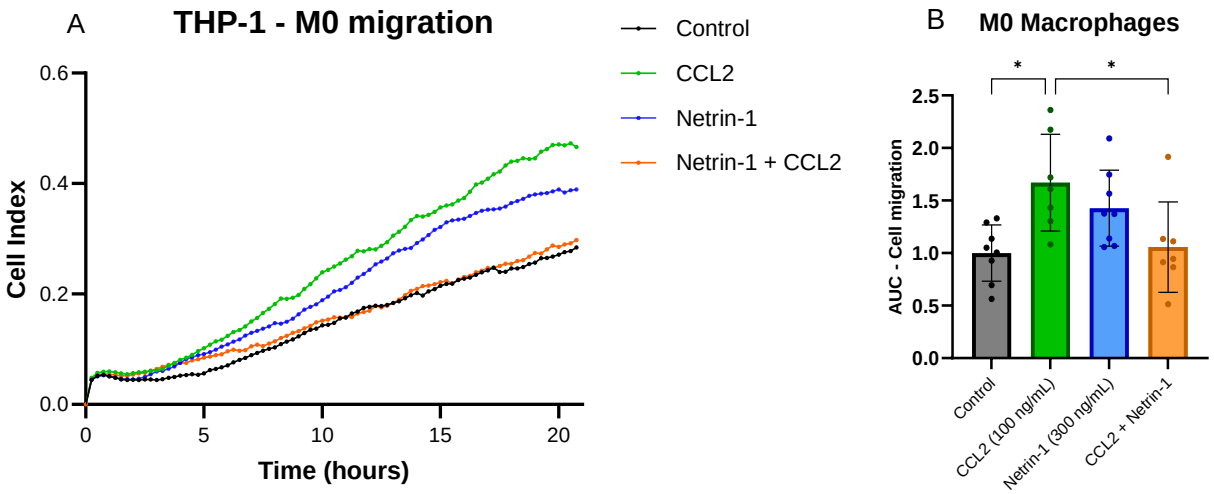

Figure 4.5 – Migration of M0 macrophages in CIM-plates. The impedance generated by cells that migrated into the bottom chamber of the CIM-plate was measured in the presence/absence of CCL2 and/or netrin-1. (A) CI for the four different conditions over 21 h. (B) Area under the curve (AUC) for the different CI over 21 h. Mean±SD, n=7-8. *P<0.05 between groups indicated.

In classical activated macrophages (M1), a peak in the CI was achieved 1 h after the cells were seeded in the CIM-plates, with a CI value of 0.054 for the control and individual treatments, and 0.042 for the combined conditions. After that, the CI kept decreasing down to negative values (Figure 4.6A). Netrin-1 was the condition that showed the highest CI

values over time in M1 macrophages, followed by CCL2. However, CCL2 CI values were similar to control in the first 6 h of the assay. As observed in M0 macrophages, combination of both CCL2 and netrin-1 showed a lower CI than the individual conditions and in this cell type, it was lower than the control wells.

Netrin-1 was the cytokine that showed the stronger chemoattractant effect, with a significant increase (1.9-fold) when compared with chemokine-free media (Figure 4.6B). As observed in M0 macrophages, this attractant effect was inhibited when CCL2 was combined with netrin-1, decreasing it four-fold to an AUC of 0.46. Moreover, the inhibition observed with the combined cytokines, was significant when compared with CCL2 alone.

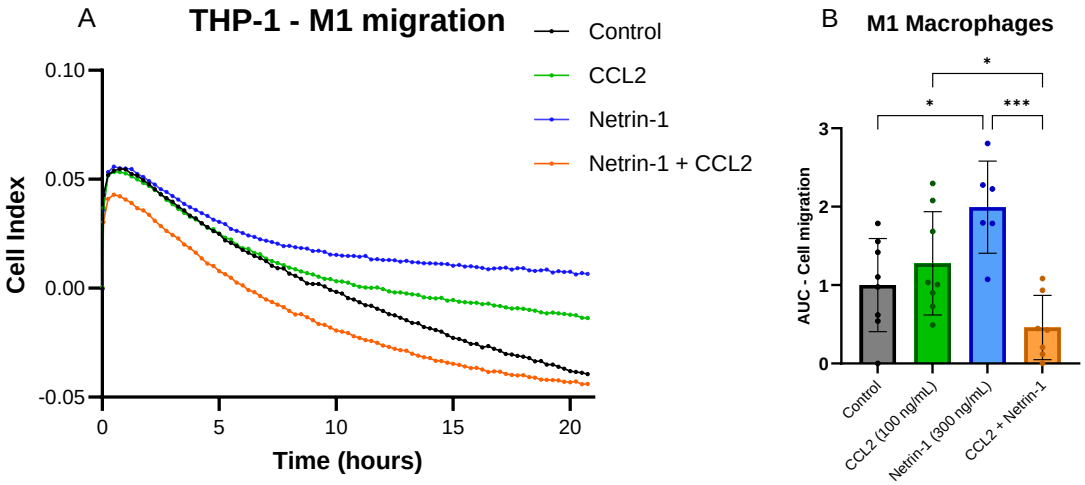

Figure 4.6 - Migration of M1 macrophages in CIM-plates. The impedance generated by cells that migrated into the bottom chamber of the CIM-plate was measured in the presence/absence of CCL2 and/or netrin-1. (A) CI for the four different conditions over 21 h. (B) Area under the curve (AUC) for the different CI over 21 h. Mean±SD, n=7-8. *P<0.05; ***P<0.001 between groups indicated.

The CI values for M2 macrophages peaked after 0.5 h, with a CI of 0.022 for the control and combined chemokines, and 0.033 for the individual treatments (Figure 4.7A). Both CCL2 and netrin-1 alone presented the highest CI values during the 21 h of migration. Combining

CCL2 with netrin-1 led to lower CI values over time, but these were higher than the control group.

The chemoattractant effects of CCL2 and netrin-1 observed in M0 and M1 macrophages were not evident in alternative activated macrophages (Figure 4.7B). Although the CI values suggest that both netrin-1 and CCL2 had a chemoattractant effect on M2 macrophages, and the combination of both nullified their effect, the AUC showed no significant difference between the different conditions.

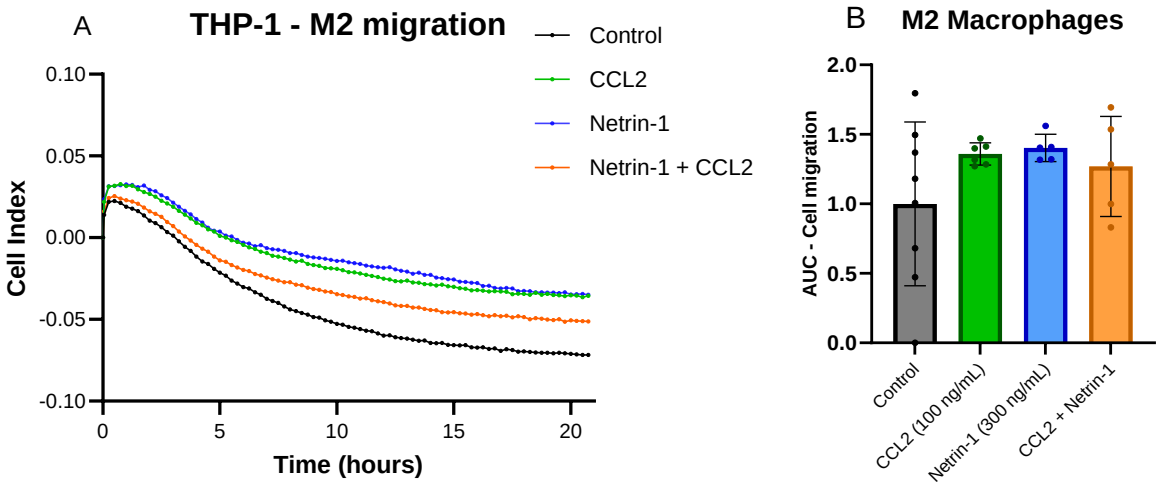

Figure 4.7 - Migration of M2 macrophages in CIM-plates. The impedance generated by cells that migrated into the bottom chamber of the CIM-plate was measured in the presence/absence of CCL2 and/or netrin-1. (A) CI for the four different conditions over 21 h. (B) Area under the curve (AUC) for the different CI over 21 h. Mean±SD, n=5-7.

Foam cell migration peaked in the first 1.5 h of the assay. The control and individual conditions CI values varied between 0.068 and 0.071, and the combined condition value was 0.083. Over time, the combined cytokines presented the highest average CI values, followed by netrin-1 and CCL2 alone (Figure 4.8A). Looking at the AUC, neither CCL2 nor netrin-1 had any effect on their migration towards the lower chamber (Figure 4.8B). When

CCL2 and netrin-1 were combined, there appeared to be a 1.5-fold increase in foam cell migration when compared with untreated wells, but this is not significant.

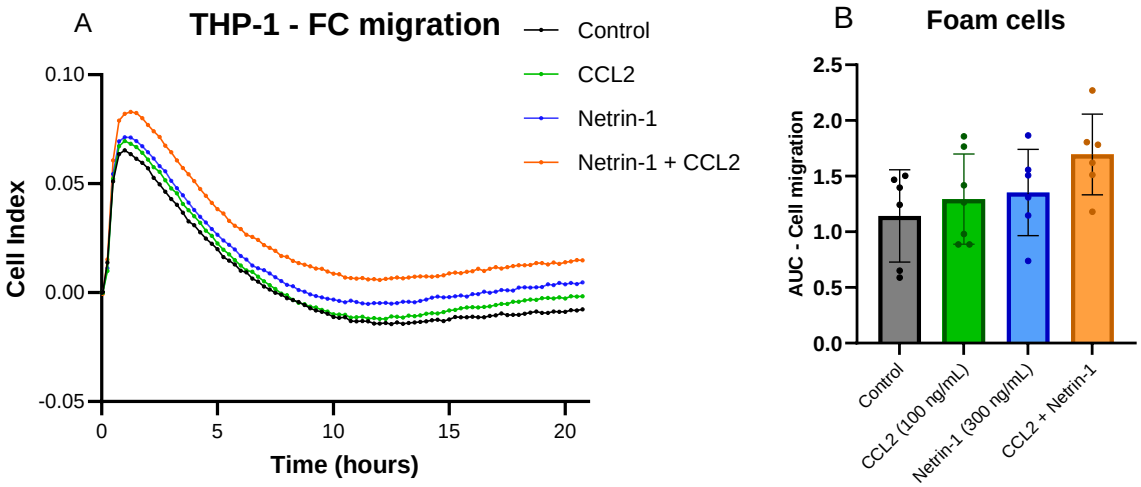

Figure 4.8 - Migration of macrophage-derived foam cells in CIM-plates. The impedance generated by cells that migrated into the bottom chamber of the CIM-plate was measured in the presence/absence of CCL2 and/or netrin-1. (A) CI for the four different conditions over 21 h. (B) Area under the curve (AUC) for the different CI over 21 h. Mean±SD, n=6-7.

4.5. Discussion

4.5.1. Netrin-1 showed no effect on triptolide-induced apoptosis

In our studies, apoptosis was confirmed in THP-1-derived macrophages as evidenced by increased levels of cleaved caspase-3. While in cell lysates, the total amount of cleaved caspase-3 was determined, in fixed cultures, the number of cells stained for cleaved caspase-3 were counted, together with membrane blebbing, chromatin condensation and fragmentation.[223,224] When a cell starts its apoptotic programme, it shrinks, and the chromatin condenses into fragments that are located at the edge of the nuclear membrane. The cell dimensions decrease and cytoplasmatic blebs form at the cell membrane.[224]

Netrin-1 had no effect in either of these sets of experiments on triptolide-induced apoptosis. When looking at the apoptotic cell percentage, the positive-apoptotic cells appear to increase in a concentration-dependent manner. Although, the concentration dependence did not reach statistical significance. This corroborates Park and colleagues findings, who showed similar data using cell death detection ELISA.[182] Neither 100 ng/mL nor 300 ng/mL netrin-1 showed any effect on triptolide-induced apoptosis in THP-1-derived macrophages. Moreover, the amount of cleaved caspase-3 produced increased when a higher concentration of triptolide was used. However, treating the cells with netrin-1 did not show any effect in the amount of cleaved caspase-3 produced. Llambi *et al* showed that netrin-1 prevents apoptosis in transfected human embryonic kidney cells and olfactory neuroblasts, where UNC5 receptors were expressed by the cells.[113] Moreover, Castets and colleagues showed that netrin-1 prevents human umbilical vein endothelial cells (HUVEC) and human umbilical artery endothelial cells (HUAEC) apoptosis when this was induced through serum starvation. This survival signal was UNC5b-dependent.[112] Work published by Mao and colleagues in an *in vivo* model also provides evidence that netrin-1 reduces apoptosis in cardiomyocytes, using isografts. Netrin-1 administration led to a lower number of TUNEL-positive cardiomyocytes 24 hours after transplantation, than the control group.[129] Netrin-1 also induced an anti-apoptotic effect in B-cell acute lymphoblastic leukaemia, playing an oncogenic role in this disease. This effect was UNC5b-dependent.[213]

There is no evidence that the effect of triptolide on THP-1-derived macrophages is UNC5b-dependent. Park and colleagues determined that triptolide treatment increased caspase-9 activity. Caspase-9 is a factor that initiates apoptosis, and this effect is likely not UNC5b-related. While both caspase-9 and UNC5b have a caspase-3 domain, only caspase-9 appears to be activated by triptolide. As a result, the anti-apoptotic impact of netrin-1 seen

in other models was not accomplished in our experiment. Therefore, it is likely that other apoptotic agents would show different results on THP-1-derived macrophages treated with netrin-1. For example, starving the cell from serum, which is the model presented by Castets and colleagues, might be a good alternative to study netrin-1 effects on the apoptosis of macrophages.[112]

4.5.2. Netrin-1 inhibits CCL2 chemoattractant effect on THP-1-derived macrophages

Using the xCELLigence RTCA DP system allowed monitoring in real time of the adhesion and migration of THP-1-derived macrophages. Initially, E-plates were used to determine the best cell density to be used in the migration assays. Only M0 macrophages were used in this type of plate. The four different densities showed a rapid increase in the CI in the first three hours of the assay and then the value remained constant throughout the remainder of the experiment. These results were expected since THP-1 cells lose proliferative activity after PMA differentiation from monocytes to macrophages and once all the cells in the well attach to the electrode, there are no further cellular process that will affect the electrical impedance.[221,225] The range of cell densities used (10,000-80,000 cells) was selected following the manufacturer's advice and general guidelines for cell numbers to be seeded in 96-well plates. Higher number of cells led to an increase in the CI in a cell number-dependent manner. This is concordant to the data presented by Chiu and colleagues, where there was an increase of CI when higher numbers of tenocytes were seeded in the E-plate, under the same conditions.[226] The CI increase observed when the cell-density was highest (80,000

cells/well) and the lack of evidence that a plateau was reached allow us to determine that that would be a good cell density to be used in the migration assays.

The migration of M0 macrophages exhibited an increase in CI over time in all conditions, which is expected for this assay.[220] The CI values for the chambers where CCL2 was used as condition showed an increased migration when compared with the control. This is expected since CCL2 (or monocyte chemoattractant protein-1) is a potent macrophage chemoattractant.[227,228] van Gils *et al* performed a similar experiment using the same technology, but with RAW264.7 cells and obtained comparable results. They also showed that the combination of CCL2 and netrin-1 decreased the chemoattractant effect observed and presented a CI value similar to the unstimulated wells. This was also demonstrated in our experiment. However, although not significant, we showed that netrin-1 appeared to exert a chemoattractant effect on THP-1-derived macrophages, but this was the opposite to what van Gils and colleagues demonstrated in RAW264.7-derived macrophages, which presented a lower CI than the control group, therefore a repulsive effect.[134] Interestingly, Mentxaka and colleagues demonstrated that netrin-1, on its own, had a chemoattractant effect on the migration of epithelial cells isolated from colorectal adenocarcinoma (Caco-2 cells).[229] We showed therefore that netrin-1, on its own, seems to have a chemoattractant effect on THP-1 derived macrophages, but when combined with CCL2 it inhibits its chemoattractant effect. These findings bring some insight for netrin-1 as a main player in the trapping of macrophages in the plaque, as it may abolish the chemoattractant effect of other chemokines. Further investigation using chemokines such as CCL19, which has been linked with the egress of cells to the lymph nodes, will clarify further whether netrin-1 can be a potential target for a therapy that reduces the atherosclerotic plaque burden.[230]

The CI graphs for the assays performed for M1 and M2 macrophages and foam cells showed a different shape from what was expected. A rapid increase in the CI was observed in the first few hours of the assay, which might be associated with the initial attachment and migration of cells to the lower chamber of the plate. However, the CI started decreasing after reaching the respective peaks and, in some cases, reached negative values. Kho *et al* showed that decreasing the adherence of endothelial cells by using sphingosine-1-phosphate led to a decrease of the CI immediately after administration.[221] Moreover, Kho *et al* and Grimsey and colleagues showed that cell death is characterised by a sustained decrease in the CI.[221,231] It is therefore possible that after migrating into the lower chamber, these THP-1-derived macrophages did not adhere strongly enough to the electrode and detached into the media or went through a cell-death program.

Even though it is possible that the classical activated macrophages detached from the electrode, the migration speed towards the bottom chamber of the CIM-plates is likely to be affected by the chemokines. In this phenotype, netrin-1 alone showed a stronger chemoattractant effect than CCL2. As observed in M0, the combination of CCL2 and netrin-1 showed a significant weaker effect than each chemokine alone. Interestingly, in foam cells, the combination of both chemokines appears to show a stronger chemoattractant effect than the individual chemokines. However, these differences were non-significant.

To generate M1-like macrophages, THP-1 macrophages were stimulated with LPS. Liu and colleagues and Zhu *et al* showed that treating THP-1 cells with LPS induces apoptosis of the cell line and that caspase-3 and caspase-7 are involved in this process.[232,233] Similarly, to what was observed in M1 macrophages, acLDL has also been showed to have pro-apoptotic effects in THP-1-derived macrophage and this is C/EBP Homologous Protein (CHOP)-

dependent. Tao *et al* and DeVries-Seimon *et al* found evidence of increased stress in the endoplasmic reticulum related with the lipid-loaded THP-1 macrophages and consequently, increased apoptosis.[234,235] A study published by Yang *et al* showed that generation of foam cells using oxLDL downregulated the expression of CCR7 in RAW 264.7 macrophages. Downregulation of CCR7 led to the inhibition of the migration by this cell type.[172] It is possible that generation of foam cells using acLDL has a similar effect on THP-1-derived macrophages.

EDTA combined with scraping was the detaching method used to remove the cells from the T75 flask. This method was selected to avoid phenotypic and functional changes in the cells.[236] However, the physical pressure related to scraping may affect cell viability and damage cell structure.[237] Moreover, data published by Lund and colleagues suggests that PMA-differentiated THP-1 macrophages lose up to 65% adherence after 5 days of differentiation.[238] These could be some of the factors that conditioned the cells used in our assay and that promoted the detachment of M1, M2 and foam cells from the electrode. The usage of cytokines to change the macrophage phenotype and the effects they have on the THP-1 cells could explain the decrease observed in CI in treated cells.

4.6. Limitations

Triptolide might induce apoptosis in THP-1-derived macrophages through a pathway that is UNC5b-independent and for that reason, netrin-1 showed no effect in this cellular process.

The treatment of macrophages with IFN-γ and LPS, IL-4 or acLDL, together with exposure to EDTA and the physical stress of scrapping might have affected their adherence

properties. Therefore, the cells did not attach strongly enough to the plate electrode, and it was impossible to determine netrin-1 effects on the migration of the different macrophage phenotypes.

4.7. Summary

- Triptolide induces apoptosis of THP-1-derived macrophages.
- Netrin-1 showed no effect on triptolide-induced apoptosis in THP-1-derived macrophages.
- Netrin-1 inhibited the chemoattractant effect of CCL2 on THP-1-derived M0 macrophages.

Chapter Five

The role of netrin-1 in atherosclerosis

5.1. Introduction

The initiation of atherosclerosis is triggered by the accumulation of LDL particles within the arterial wall. Modification of the accumulated LDL promotes a pro-inflammatory environment and its uptake by macrophages and modified VSMC, via scavenger receptors. Once established, the progression of the plaque continues through the accumulation of lipids and lipid-engorged cells. The accumulation of these products over the years, together with extracellular matrix macromolecules increase the size of the atherosclerotic plaque and decrease its stability.[239]

The monocyte/macrophage cell lineage is key in the development and exacerbation of atherosclerosis. OxLDL activates the endothelium, leading to an upregulation of adhesion molecules and chemokines, such as CCL2. This leads to the recruitment of monocytes to the plaque site, and differentiation into macrophages, increasing the cell burden and inflammation.[240,241] The recruitment of monocytes to the arterial wall is a multi-step process, initiated by the expression of P-selectin on the endothelium, which interact with the monocyte P-selectin glycoprotein ligand-1 and promotes the tethering and rolling of the circulating monocytes.[241] However, selectins alone do not bind with enough affinity to capture the leukocytes, and cooperation with other adhesion molecules such as integrins is necessary.[242]

Systemic netrin-1 was identified as an anti-inflammatory mediator that prevents the adhesion and migration of monocytes into the tissue. This effect is related to the suppression of vascular adhesion molecules and pro-inflammatory cytokines such as CCL2, IL-1β and IL-6, by the endothelial cells.[159] Bruikman and colleagues showed that systemic levels of netrin-1 and the degree of atherosclerosis are inversely correlated. This group showed that patients with no atherosclerosis express significantly higher systemic levels of netrin-1 when

compared with patients with subclinical atherosclerosis. Moreover, this group also demonstrated that netrin-1 suppressed the expression of vascular adhesion molecules, and therefore inhibited monocyte adhesion to endothelial cells.[160] Podjaski *et al* showed concordant results in human brain-derived endothelial cells. Netrin-1 led to a significant reduction of the expression of CCL2, IL-8 and IL-6.[243] Bruikman *et al* showed in a different study that a mutation in netrin-1 identified in a family led to premature development of atherosclerosis. Treating endothelial cells with this type of mutated netrin-1 resulted in increased monocyte adhesion and pro-inflammatory cytokine expression.[162]

5.2. Aims

- To confirm the short-term effect of netrin-1 on monocyte recruitment in the context of acute inflammation.
- To study the more long-term role of netrin-1 in the development and progression of atherosclerosis.

5.3. Pilot study - netrin-1 acute effect on inflammation

Intravital microscopy provides information on cellular events in their normal physiological context, surrounded by other elements, such as protein and cells, which provide a more accurate reflection of *in vivo* processes in real time. It can be used to study many physiological and cellular processes, including cell migration.[244]

The cremaster muscle was first described in the 1960s, in a rat model, as extensions of the *obliquus internus* and *transversus abdominis* muscles.[245] This muscle is commonly used to visualise the microvasculature in mice. This is a very thin tissue which contains many venules and arterioles and can be exposed for microscopy with minimally invasive procedures.[246]

An injection of LPS was administered intra-scrotally in our mice to promote leukocyte recruitment to the tissue. This model was used to mimic the inflammatory environment found in the atherosclerotic plaque region.

5.3.1. Monocyte/macrophage lineage detection on the MaFIA mouse model required signal enhancement when using intravital microscopy

The mouse model used in our study expresses eGFP in the monocyte/macrophage lineage, but this signal alone was not detected using our microscope after inflammatory stimulation (Figure 5.1A). Alexa Fluor 488 CD11b antibody was injected in the mice to enhance the monocyte/macrophage signal. Dimmed bright was used together with fluorescence to show the vessel and tissue architecture.

To confirm that the administration of the CD11b antibody alone did not lead to the detection of cells in the absence of mutation, mice from the MaFIA colony litters that did not possess the mutation were injected with intra-peritoneal CD11b antibody and intra-scrotal LPS. In these mice, no positive cells were detected after inflammatory stimulation (Figure 5.1B). Therefore, neither the mutation nor the antibody injection alone produced a signal strong enough to be detected by our equipment. Only the combination of both showed positive cells during intravital microscopy.

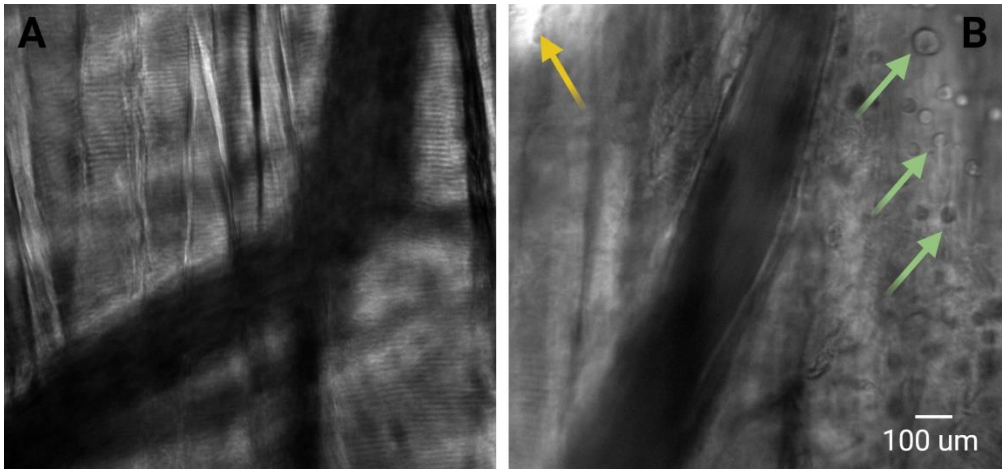

Figure 5.1- Leukocyte detection in cremaster muscle microvasculature, after intra-scrotal LPS injection, using intravital microscopy. (A) MaFIA mouse without injection of AF488 CD11b antibody. (B) Wild-type mouse injected with AF488 CD11b antibody. No cells were detected in the microcirculation in either condition. The yellow arrow indicates a fluorescent artifact within the tissue. The green arrows indicate erythrocytes in the buffer, above the tissue, due to minor bleeding.

5.3.2. Intravital microscopy of the cremaster muscle

The first group of mice (negative control group) were injected saline, both as subcutaneous treatment, 16 h prior to microscopy, and intra-scrotal stimulation. Figure 5.2 shows a picture of the intravital microscopy recording at the 10 s time point. Since no differences were observed throughout the recording, only one time point was included to illustrate this group. No cells were observed rolling, adherent or within the tissue.

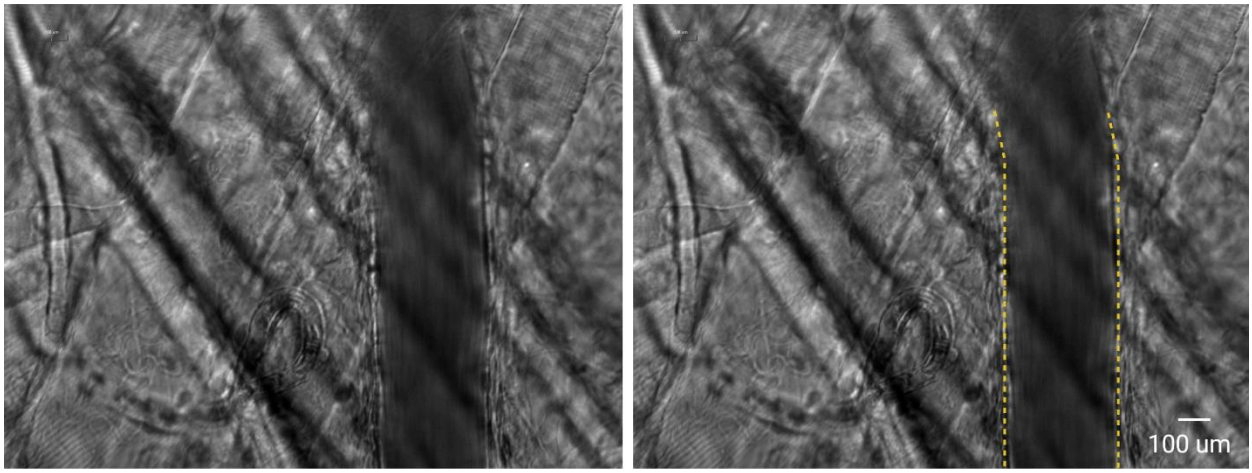

Figure 5.2 – Intravital microscopy imaging of the cremaster muscle in a mouse of the negative control group. Mirrored images of the recording at 10 s time point. On the left, picture of the recording. On the right, same image with features marked. No differences were observed at any time point, during the 20 s recording. No cells were detected in either the tissue or vasculature. Yellow dotted line defines the endothelium of the vessel.

In the positive control group, the mice were treated with intra-peritoneal saline prior to generation of local inflammation using an intra-scrotal LPS injection. Figure 5.3 represents an example recording obtained in this group of mice. Three different time point were included to show which cells remained adherent and which ones were rolling on the endothelium. The inflammatory stimulation led to recruitment of monocytes to the tissue (red dotted circles), as well as to rolling and adherence of monocytes to the endothelium (green and yellow dotted circles, respectively). The green dotted line indicates the distance that the cells rolled throughout the recording period (from 0 s until the time point indicated).

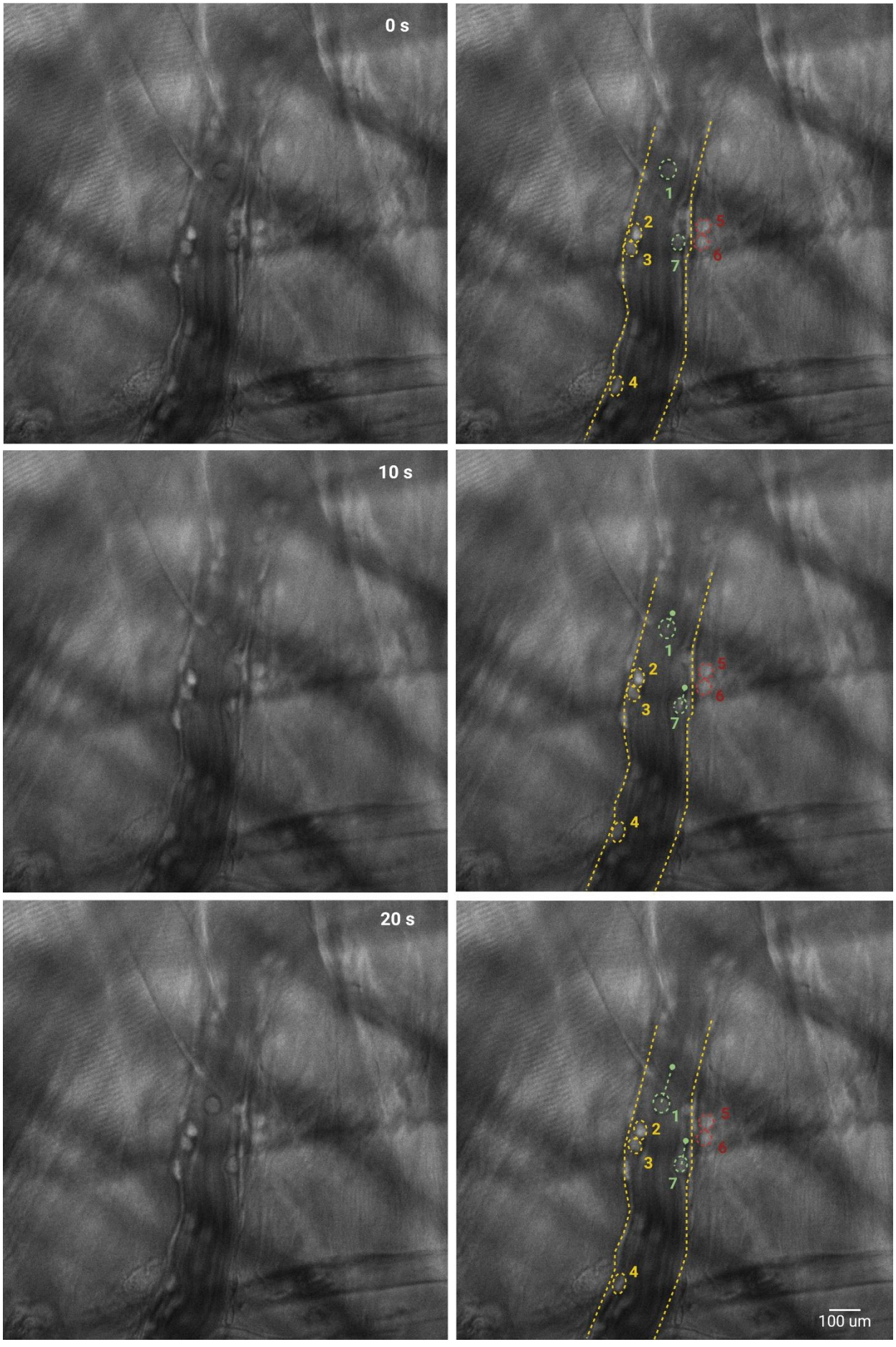
0 s
1
2
3
4
5
6
7
10 s
1
2
3
4
5
6
7
20 s
1
2
3
4
5
6
7
100 um

Figure 5.3 - Intravital microscopy imaging of the cremaster muscle in a mouse of the positive control group. Mirrored images of the recording at 0, 10 and 20 s time points. On the left, pictures of the recording. On the right, the same images with features marked. Video recorded over 20 s. Yellow dotted line defines the endothelium of the vessel. The yellow dotted circles indicate adherent cells that did not roll during the 20 s recording. The green dotted circles indicate cells that rolled and the green dotted line the trajectory of the cell. The red dotted circles indicate cells in the tissue.

Similarly to what was observed in the Negative Control group, the treated control group (treated with subcutaneous netrin-1, and administered intra-scrotal saline) did not exhibit any cells rolling or adherent at any time point. Figure 5.4 shows an example of the recording obtained in one mouse of this group. Only one time point is shown to illustrate this group results.

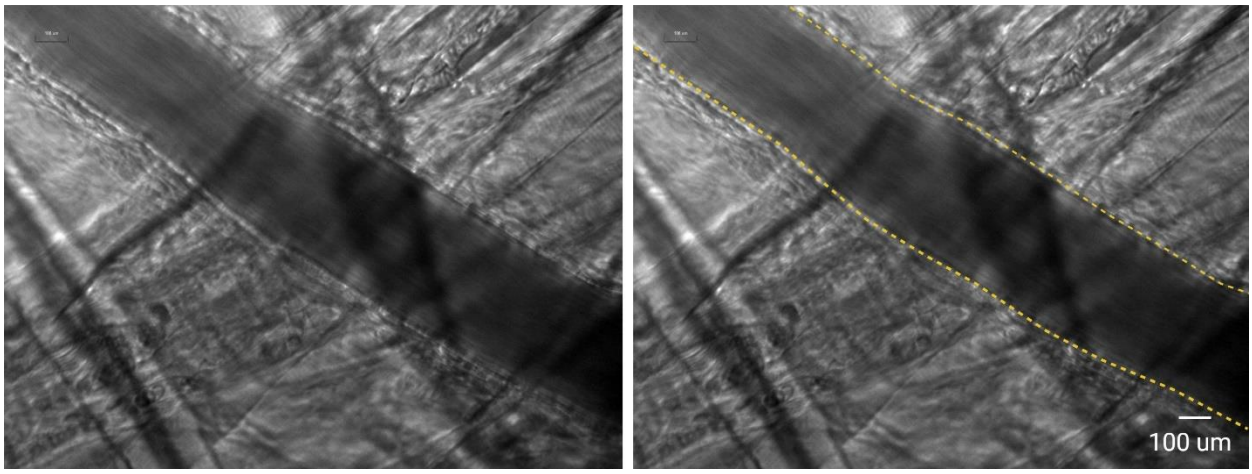

Figure 5.4 – Intravital microscopy imaging of the cremaster muscle in a mouse of the treated control group. Mirrored images of the recording at 10 s time point. On the left, picture of the recording. On the right, same image with features marked. No differences were observed at any time point, during the 20 s recording. No cells were detected in either the tissue or vasculature. Yellow dotted line defines the endothelium of the vessel.

The last group analysed using intravital microscopy was the treated group, which was treated with netrin-1 subcutaneously 12 h prior to generation of inflammation and with LPS intra-scrotally 4 h prior to surgery.

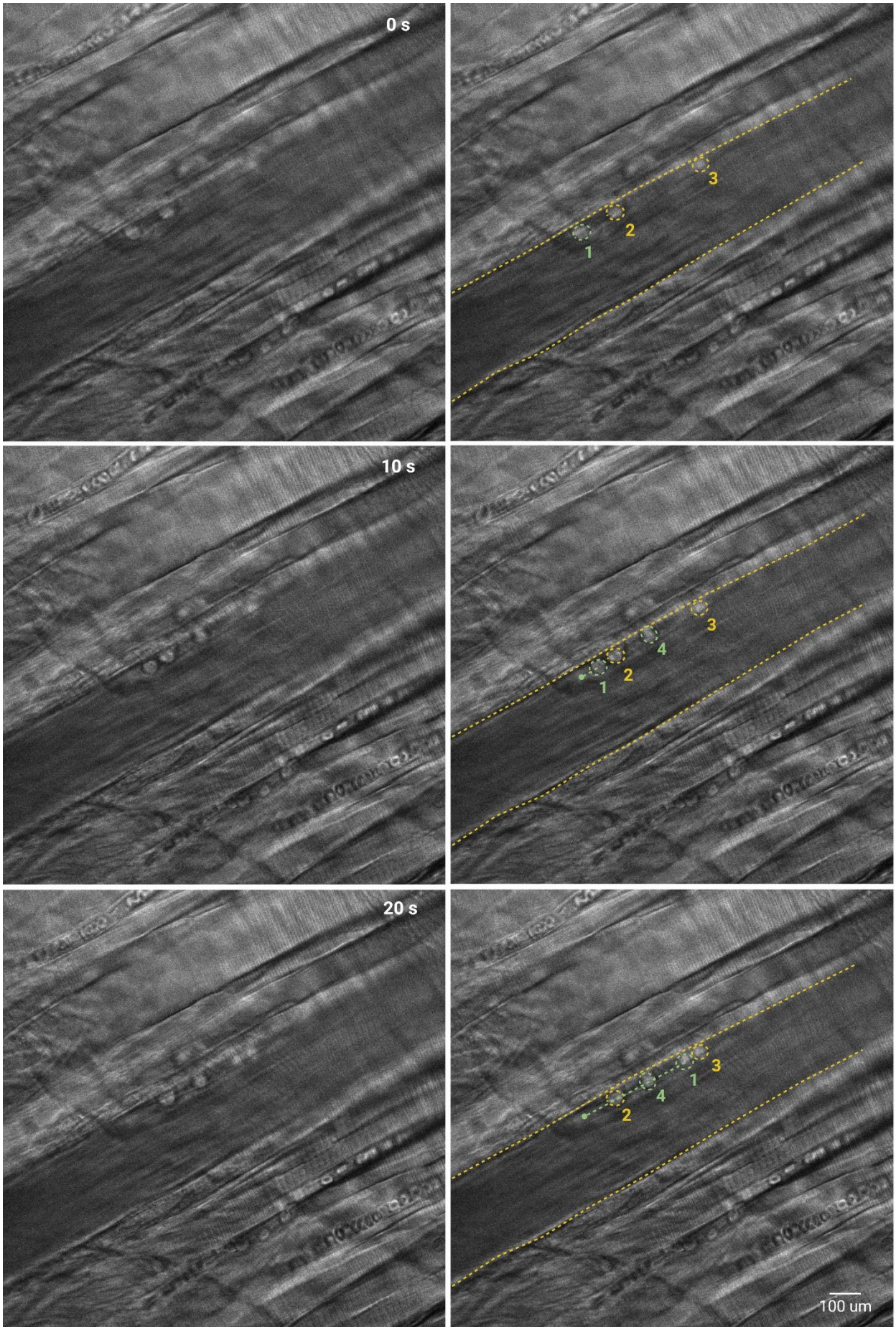
0 s
1
2
3
10 s
1
2
3
4
20 s
1
2
3
4
100 um

Figure 5.5 - Intravital microscopy imaging of the cremaster muscle in a mouse of the treated stimulated group. Mirrored images of the recording at 0, 10 and 20 s time points. On the left, pictures of the recording. On the right, the same image with features marked. Video recorded over 20 s. Yellow dotted line defines the endothelium of the vessel. The yellow dotted circles indicate adherent cells that did not roll during the 20 s recording. The green dotted circles indicate cells that rolled and the green dotted line the trajectory of the cell.

In this group, less cells were observed within the tissue. Interestingly, more cells rolled on the endothelium than in the mice that were not pre-treated with netrin-1. Even though only adherent and rolling cells are shown in figure 5.5, some recordings showed the presence of cells within the tissue. These were quantified and shown in section 5.3.3. In this figure, cell 4 rolled from the bottom of the vessel into the focused area and was only visible moments after the recording started.

5.3.3. Netrin-1 reduced the number of monocytes that migrated from the bloodstream into the tissue after inflammatory injury

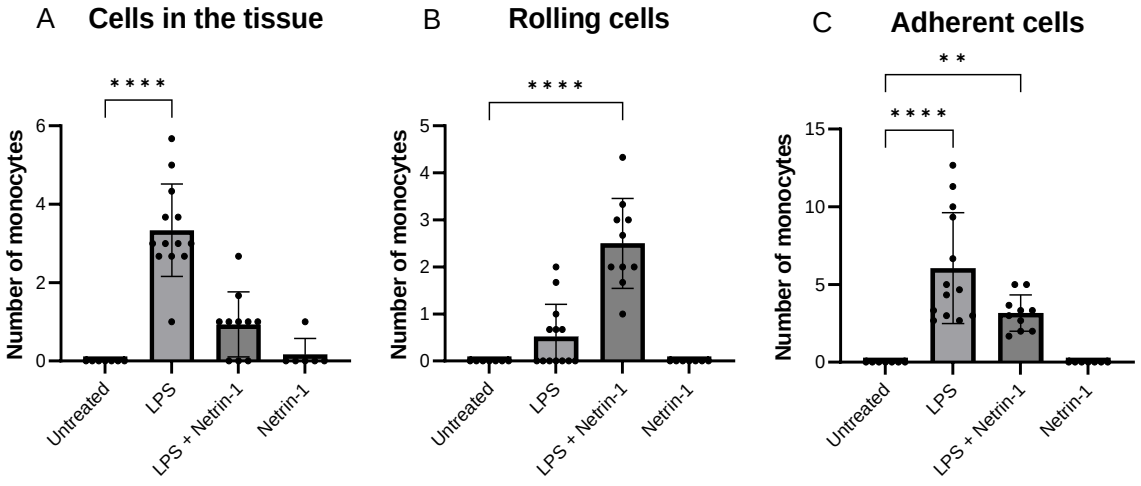

Figure 5.6 – Netrin-1 treatment led to a reduction in the number of monocytes/macrophages in the tissue after inflammatory stimulation, but an increased number of cells rolling. (A) Number of cells detected in the tissue (outside vasculature). (B) Number of cells detected rolling on the endothelium during the 20 s recording. (C) Number of detected cells adherent to the endothelium that did not move during the 20 s recording time. Mean±SD, n=7-13. **P<0.01 and ****P<0.0001.

The videos were analysed in blinded fashion by Dr Fan Yang and the number of fluorescent cells were counted, and identified as being in the tissue, rolling or adherent to the endothelium (Figure 5.6). While the inflammation generated by the LPS increased the number of cells that migrated into the cremaster muscle, pre-treating the mouse with netrin-1 led to an abrogation of this effect (Figure 5.6A).

Interestingly, the opposite response was observed in the number of rolling cells. Mice treated with netrin-1 and stimulated with LPS showed almost 5 times more cells rolling on the endothelium than the positive control group (Figure 5.6B). Only the treated stimulated group (netrin-1 + LPS) showed a significant increase in the number of rolling cells when compared with the unstimulated groups.

Both groups stimulated with LPS showed a significant upregulation of adherent cells on the endothelium, when compared with the unstimulated groups (Figure 5.6C). No significant differences were observed when netrin-1 was administered prior to inflammatory stimulation.

5.4. Pilot study - netrin-1 longer term effect on atherosclerosis

To determine whether netrin-1 can prevent the progression of atherosclerosis, osmotic minipumps filled with netrin-1 were implanted in mice before 60% HFD was given to a *LDLR*$^{-/-}$ mice for 6 weeks. Baumer and colleagues measured the formation of plaque in *LDLR*$^{-/-}$ mice and showed that the macrophage content increased dramatically in the aortic root within 4 weeks of feeding HFD to their colonies.[247] Since the largest osmotic minipumps available commercially last for 42 days, this was the period of time chosen for our study.

5.4.1. Osmotic minipumps

Mice implanted with osmotic minipumps containing netrin-1 had a 3.75 ng dose released systemically each hour. The minipumps were weighed prior to implantation and after organ harvesting. Figure 5.7 shows that the weight of the minipump decreased over the 42 days, reflecting release of netrin-1 stored in each pump as it was delivered into the mouse circulation.

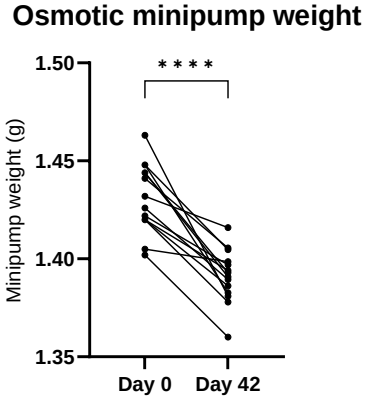

Figure 5.7 – Osmotic minipump weight prior to implantation and after organ harvesting. The weight of each minipump decreased as the liquid in the reservoir was delivered into the mouse system. Mean±SD, n=14. ****P<0.0001 between the time points indicated.

5.4.2. Mouse weight increased after feeding HFD for 6 weeks

The weight of the mice was monitored weekly (Figure 5.8). The change in weight of the mice in the vehicle/normal chow group varied between -0.9% and 7.7%, with a mean 1.9% increase after 6 weeks. Similarly, the netrin-1/normal chow group showed a mean -0.9% weight change after 6 weeks range -5.1% to 2.3%. The weight of the mice in both groups fed with 60% HFD increased significantly compared to groups fed normal chow, with a mean increase in the vehicle/HFD group of 19.8% (range 6.1%-23.3%) and in the netrin-1/HFD group of 26.2% (range 15.9%-35.3%).

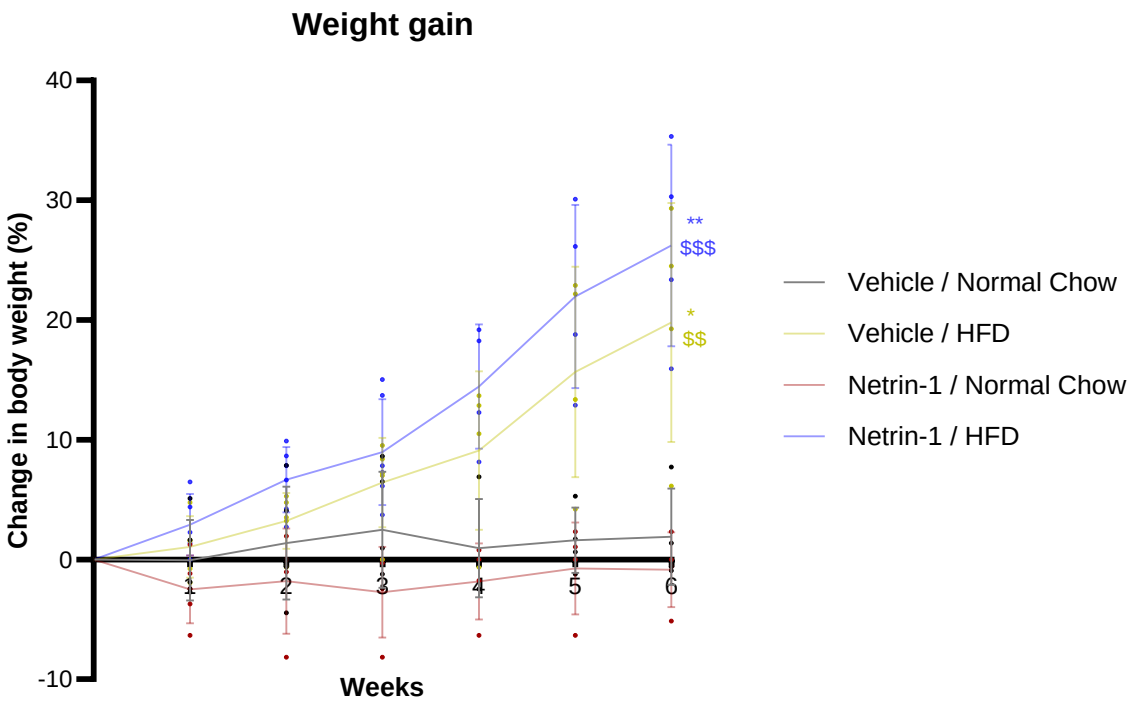

Figure 5.8 – Mice weight variation after being fed with normal chow or HFD for 6 weeks. The weight of the mice fed with 60% HFD increased after 6-weeks, in both groups, when compared with mice fed with normal chow. n=4-5. *P<0.05 and **P<0.01 between groups indicated and the vehicle/normal chow; $^{\$\$}$P<0.01 and $^{\$\$\$}$P<0.001 between groups indicated and the netrin-1/normal chow group.

5.4.3. Netrin-1 reduced the enlargement of the aortic sinus promoted by the HFD

The hearts of the mice were harvested and fixed in 4% PFA at the 42 days' time point. The tissue was processed and sectioned transversely from the bottom to the top of the heart, until the cusps of the valves in the aortic sinus were found.[248] One section per mouse from equivalent parts of the aortic root were selected for measurement of the total area of the aortic sinus, as well as areas that showed enlargement and hence development of atherosclerotic lesions (Figure 5.9). As before, the samples were blinded by Dr Fan Yang.

The three cusps (left coronary, right coronary and noncoronary) were visible in the sections. In a few cases, the cusps were fragmented as observed in figure 5.9B. The region where the

cusp leaflets connect to the vessel are particularly prone to thickening and development of plaque. All sections, regardless of group, showed some degree of enlargement.

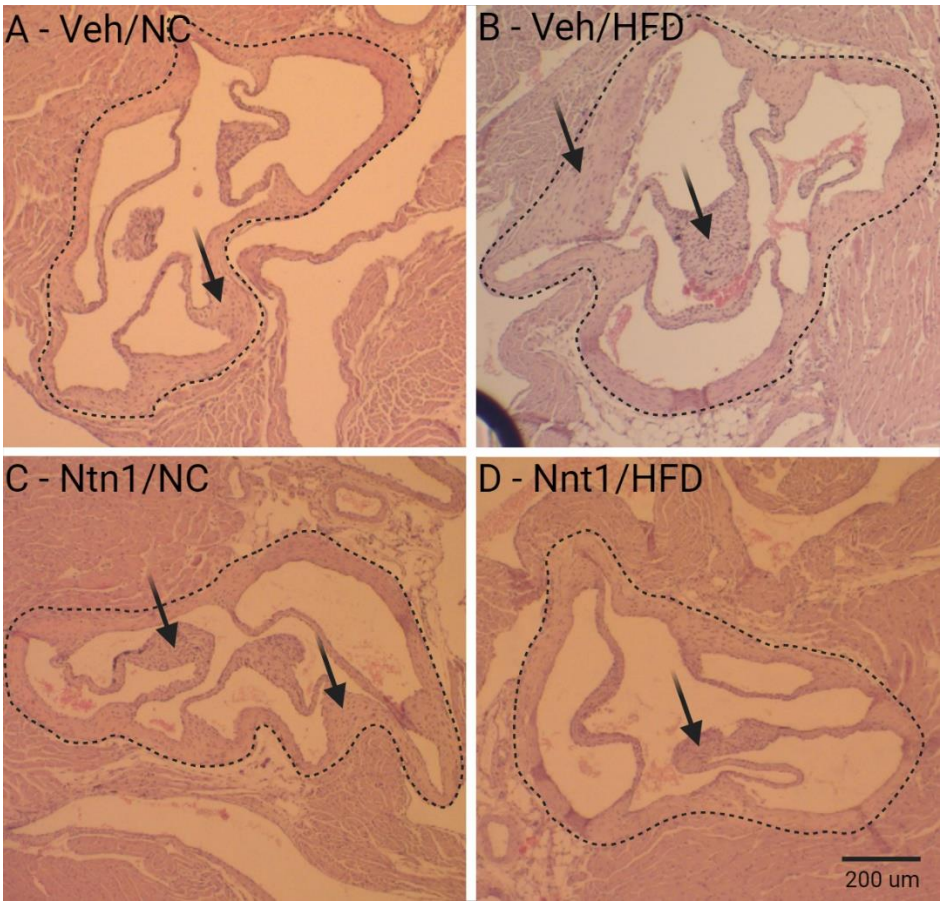

Figure 5.9 – Aortic sinus histology sections from *LDLR*$^{-/-}$ mice after being fed with normal chow or HFD and treated with vehicle or netrin-1 for 6 weeks. Dotted lines show the sinus outlines. Solid arrows point to thickened aortic cusps and possible development of plaque. (A) vehicle/normal chow, (B) vehicle/HFD, (C) netrin-1/normal chow and (D) netrin-1/HFD.

Mice fed HFD and treated with vehicle exhibited sinuses with a significant larger area than any other group (Figure 5.10A). This group sinuses had an area of 249.3±110.5 x10^3 μm^2, three times larger than the vehicle/normal chow group and five times larger than the two groups treated with netrin-1. Similarly to what was observed in the total area, the enlarged areas found in the sinus appeared to be larger in the vehicle/HFD group (85.8±64.4 x10^3

μm^2) than in any other groups (5.2±3.3 – 5.8±4.5 x10^3 μm^2). However, this difference was not significant (Figure 5.10B).

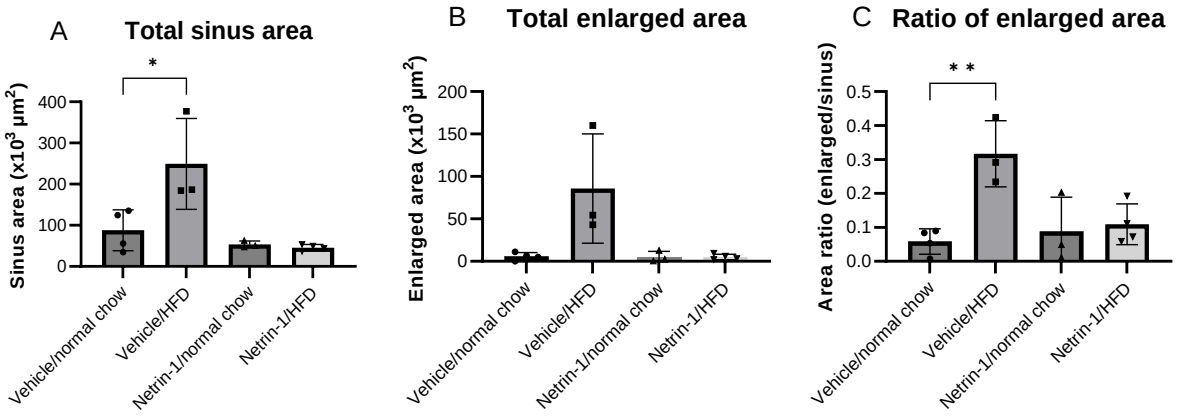

Figure 5.10 – Measurement of atherosclerotic plaque after *LDLR*$^{-/-}$ mice being fed with normal chow or HFD and treated with vehicle or netrin-1 for 6 weeks. Using ImageJ, the total area of the sinus was measured (A), as well as the areas that show arterial thickness of the arterial wall and cusps (B). (C) shows the ratio of the area of enlarged over the total sinus area. n=3-4. *P<0.05 and **P<0.01 between groups indicated.

Mice fed HFD and treated with vehicle exhibited sinuses with a significant larger area than any other group (Figure 5.10A). This group sinuses had an area of 249.3±110.5 x10^3 μm^2, three times larger than the vehicle/normal chow group and five times larger than the two groups treated with netrin-1. Similarly to what was observed in the total area, the enlarged areas found in the sinus appeared to be larger in the vehicle/HFD group (85.8±64.4 x10^3 μm^2) than in any other groups (5.2±3.3 – 5.8±4.5 x10^3 μm^2). However, this difference was not significant (Figure 5.10B).

The ratio of the enlarged to the total sinus areas (Figure 5.10C) was greater in the vehicle/HFD group (0.32±0.10) when compared with the vehicle/normal chow group (0.06±0.04). The treatment with netrin-1 in mice fed with HFD prevented this increase.

5.5. Discussion

5.5.1. Netrin-1 reduced the recruitment of monocytes to the tissue after inflammatory injury

The MaFIA mouse model was used in the intravital microscopy experiments due to its fluorescence characteristics. The monocyte/macrophage lineage expresses eGFP and emits a bright signal when a blue laser is applied. Since eGFP in the mouse model was not detected using our equipment, an Alexa Fluor 488 CD11b antibody was administered to detect monocyte/macrophages. Shaked and colleagues showed successful binding of labelled antibodies to circulating cells in mice. In their studies, the antibodies bound to the cells in the blood, when the antigens were expressed in the membrane, but not intracellularly.[249] CD11b is a marker expressed by the monocyte/macrophage lineage, as well as granulocytes and natural killer cells.[250] Since this marker is not specific to the monocyte/macrophage lineage, an initial experiment was designed to confirm that injection of the antibody on its own, did not have a signal strong enough to make cells detectable and only the combination of both the mutation and the antibody would be detected. Mice from the MaFIA colony that did not present the mutation (wild-type) were used to test the antibody, under inflammatory conditions. In the absence of the mutation, the antibody on its own did not show enough signal to be detected using intravital microscopy. We were therefore satisfied that the CD11b antibody on its own was not sufficient to be detected by the camera. This provides strong evidence that only the monocyte/macrophage lineage was detected in our intravital microscopy experiments. However, injecting an CD11b antibody in the circulation may affect the function of this integrin. This integrin is often co-expressed with CD18 and contributes to the rolling and adherence of leukocytes to the endothelium, after

inflammatory stimulation.[251] Even though we were unable provide evidence to whether the injection of the CD11b antibody affected our experiment, Yao and colleagues showed that activation of CD11b in macrophages reduced their inflammatory response to LPS, by blocking this cytokine interaction with TLR4.[252] The inflammatory injury induced by the injection of LPS seemed to still be effective in this pilot study, but a different mouse model, with stronger fluorescent properties will be selected for the following-up study to remove any undesirable molecular interferences.

In the absence of local inflammation, no cells were detected while using intravital microscopy. The blood flow is likely to be too fast to allow the detection of circulating fluorescent cells using our equipment. These cells are oftens concealed by the high number of circulating erythrocytes, unless there are interactions of the circulating cells with the endothelium which impede their flow.

LPS is a substance, found in gram-negative bacteria, well known to have a pro-inflammatory effect and promote the upregulation of adhesion molecules by endothelial cells. Dayang *et al* showed that after 2 h, LPS exposure led to the upregulation of E-selectin and VCAM-1 in HUVEC.[253] These adhesion molecules are also found in atherosclerosis, where E-selectin mediates rolling and VCAM-1 mediates adhesion of monocytes on the inflamed aortic endothelium.[254,255] Cerri *et al* also provided evidence that the expression of inflammatory cytokines, such as CCL2 and IL-1β, are increased within 4 h after the administration of LPS into mice hippocampus.[256] Furthermore, Puntambekar and colleagues showed that injection of LPS induced the expression of CCL2 and the recruitment of macrophages to the central nervous system in a murine model.[257] Our intravital microscopy experiment supports the

results obtained in the studies above where fluorescent cells were found interacting with the endothelium and in the tissue when LPS was used to generate local inflammation.

After the inflammatory injury, the monocytes follow the general paradigm of adhesion and trafficking which consists of rolling, adhesion, and transmigration from the circulation to the tissue.[254] The firm adhesion required for the transmigration across the endothelium relies on other cytokines as well, such as CCL2 and IL-8.[258] The number of positive cells outside the vasculature (within the cremaster muscle) were counted. These were cells that completed the whole trafficking process. Only the animals stimulated with LPS and treated with vehicle (positive control) showed a significant increase in this number. Pre-treatment of the mice with netrin-1 led to a significant reduction in the transmigration of monocytes to the tissue after LPS injection. This is likely to be related to weaker adhesion of the circulating monocytes to the activated endothelium. van Gils and colleagues showed in an *in vitro* model that blocking netrin-1 with an anti-netrin-1 peptide increased the adhesion of THP-1 monocytes to activated human coronary artery endothelial cells (activated with either LPS or TNF-α). Moreover, this group used intravital microscopy in the cremaster muscle of C57BL/6J mice and showed that when the animals were treated with a netrin-1 blocker peptide, the adhesion of the leukocytes to the endothelium increased approximately 2-fold.[171] Lin and colleagues showed that netrin-1 suppresses TNF-α induced expression of adhesion molecules and cytokine production by endothelial cells and this leads to a weaker binding of monocytes to the endothelium, under inflammatory conditions. They also showed that netrin-1 selectively suppresses TLR4 which has been established to recognise LPS.[159]

Interestingly, the number or adherent cells is in our study was not different when netrin-1 was administered to the mice. The injection of LPS led to an increase in the number of

adherent cells, in both the presence and absence of netrin-1. The transmigration process can take from minutes to hours and not all the monocytes that were adherent to the endothelium throughout the 20 s recording will transmigrate into the muscle, so a later time point could bring some insight on whether the cells adherent to the endothelium transmigrate or go back into the circulation.[259] Moreover, we administered netrin-1 16 h prior to surgery in order to guarantee a systemic effect. Possibly, a different concentration of netrin-1, or administration of the protein at a time point closer to the inflammatory stimulation could lead to different results on the cell adhesion properties.

The number of monocytes rolling on the endothelium was also assessed. These were the cells that either rolled on the endothelium during the 20 s recording, or that rolled and went back into the circulation. This number was increased in the netrin-1/LPS group and was significantly higher than in the mice that were only injected with LPS. As mentioned previously, the weaker adhesion to the endothelium might lead to an incomplete trafficking process and these cells may never migrate into the tissue. The reduced number of cells found in the tissue in the netrin-1/LPS groups is likely to be related with the inability of the monocytes to stop rolling into a firmly adherent state.

5.5.2. Netrin-1 reduced the enlargement of the aortic sinus promoted by feeding HFD

The minipumps were weighed for comparison before they were implanted and after the animals were culled. However, the weight of the minipumps was affected by a small amount of connective tissue that was produced around them. The pumps were cleaned after the mice were euthanized and prior to weighting, however, due to the sticky nature of the

connective tissue, it was very difficult to remove it in its totality, and this had an impact on the on its final weigh. To help confirm that its content was delivered in the animal system, the reservoirs were opened and using a needle, we attempted to remove any liquid still within. The weight of the minipumps decreased and the amount of liquid aspirated with the syringe was negligible. We were therefore confident that both vehicle and netrin-1 were successfully delivered during the duration of the study.

Even though the *LDLR*$^{-/-}$ mice had a considerable weight gain after being fed HFD for 42 days, some researchers contend that this model exhibits a delay in the development of atherosclerotic plaque when compared with *ApoE*$^{-/-}$ mice, and this time point might therefore not be optimal to acquire good insight on the effect that different treatments may have in this inflammatory process.[260] Moreover, the mice used in each group were in their majority males. This may have had an impact in the data collected since sexual dimorphism is a biological variable in atherosclerosis. Mansukhani and colleagues showed that in *LDLR*$^{-/-}$ mice, males presented lower levels of cholesterol and LDL in the blood stream after 14 weeks of HFD, when compared with females. Interestingly, after feeding HFD for 8 weeks, both males and females presented a similar degree of atherosclerosis in the aortic root. However, after 14 weeks, there was a significant difference, where females presented a more advanced lesion than the males.[261] Even though this pilot study included HFD for 6 weeks, and this would develop a similar degree of inflammation in the aortic root, the following up studies should include individuals from both sex to take into account sex differences that may happen when netrin-1 is used as treatment.

The aortic sinus is a lesion-prone area where the development of atherosclerotic plaque can be detected early.[262,263] This characteristic makes this tissue of particular usefulness to study

diet-induced atherosclerosis and it has been used in numerous such studies, since the late 1980s.[264] Considering the time points chosen for our experiment, this was considered to be the best location to assess the effect of netrin-1 on the development of plaque.

We showed that after 6 weeks, the enlarged area in the sinus accounted for 85.8±64.4 $x10^3$ μm^2. These are comparable results with Ma and colleagues which showed that after one month of feeding a 21% HFD to *LDLR*$^{-/-}$ mice, the lesions in the aortic sinus amounted to roughly 80.0 $x10^3$ μm^2.[265] However, this increase was non-significant in our study, likely due to the high variability found within the group. The same research group showed that after three months of feeding HFD, the artery arch lesion was 4% of the total lumen and aortic sinus area of the damage was roughly 320.0 $x10^3$ μm^2. They show that 6 months on HFD would be good time point to get better insight on the development of plaque in different areas, such as aortic arch or thoracic aorta. Otero-Losada and colleagues also showed a significant development of plaque in the aortic sinus after 8 weeks of feeding *ApoE*$^{-/-}$ with Coca-Cola®, reaching 23.0 $x10^3$ μm^2.[266]

The enlargements observed in our study were found mainly in the cusps' leaflets. Otero-Losada *et al* described similar findings, where the leaflets were thickened and the borders presented loose fibrotic excrescence.[266] These structures are particularly vulnerable to the development of inflammation with lipid deposition, cell infiltration, stiffening, calcification and bone formation.[267]

The ratio of enlarged areas was significantly higher when the mice were fed HFD, in the absence of netrin-1 treatment. Treating the animals with netrin-1 decreased this effect to values close to the controls fed with normal chow. However, this difference is not significant. Bruikman *et al* showed a negative correlation between netrin-1 plasma levels and the plaque

volume in humans. Higher amounts of systemic netrin-1 were found in patients with no evidence of plaque.[160] Moreover, Fiorelli and colleagues showed that the systemic levels of netrin-1 were significantly lower in patients with coronary artery disease and patients that suffered acute myocardial infarction when compared with healthy subjects.[161] Our results are consistent with the data presented above.

Further assessment is required in the histology sections to confirm that the enlargement observed is indeed atherosclerotic plaque. Different staining sets will be a useful tool to bring further information about the content of the sinus. Moreover, systemic netrin-1 has been reported to play a role in reducing the cell recruitment to the plaque. We are currently working on developing a tool to be used in the image analysis software that allows the counting of cells within the sinus. This will bring valuable information to whether netrin-1 reduced the number of cells that migrated to the aortic root under the different conditions.

5.6. Limitation

Using a CD11b antibody to increase the signal produced by monocytes and macrophages in the MaFIA mouse colony may affect their ability to adhere and transmigrate to the tissue. Even though all mice had the same amount of antibody injected and we observed differences under the different conditions, a new animal model that does not require enhancement for detection of cells will be more appropriate to determine netrin-1 effect in the recruitment of monocytes after inflammatory stimulation.

Another major drawback in this set of experiments was the inability to measure the systemic levels of netrin-1 in the mice of either experiment. The ELISA kit failed to provide any

information regarding these mice samples since all samples showed an absorbance value smaller than the blank well. Moreover, the Project Licence approved by the Home Office for the intravital microscopy experiment does not allow the use of higher doses of netrin-1, so an amendment must be submitted to possibly repeat this work using higher doses of the substance, together with different time points.

Considering that the largest osmotic minipump available is 42 days, the mice were fed the HFD only for that period. A longer study, where the minipump is replaced with a new one might be an alternative to generate later time point data as regards effects on atherosclerotic plaque. Moreover, since the heart/aortic root were embedded in paraffin, no Oil Red O staining was possible. Freezing the tissues might be more suitable for this type of analysis.

Most of the mice used for the implantation of minipumps were males. This may have an impact on the data acquired and how the conclusions translate for both sexes. An even number of females and males should be included in the follow-up experiments to minimize the effect of this biological variable.

Statistical analysis was included in the pilot studies for the purpose of discussion of results. However, these studies will be used to produce power calculations and determine what is the number of mice necessary to determine statistical significance and understand the extent of netrin-1 effect in these experiments.

5.7. Summary

- Netrin-1 inhibited the transmigration of monocytes into the cremaster muscle after LPS injection.

- LPS injection led to an increase in the number of adherent monocytes to the endothelium.
- Netrin-1 treatment gave rise to an increase in the number of cells rolling in the endothelium, likely due to a reduced expression of adhesion molecules and cytokines by the endothelial cells.
- Untreated mice on HFD showed an increase in the aortic sinus area.
- Untreated mice fed with HFD presented a higher ratio of enlarged areas in the aortic sinus when compared with mice fed with normal chow. Netrin-1 treatment decreased the HFD effect on the enlargement of the aortic sinus.

Chapter Six

General discussion

6.1. Overview

The involvement of netrin-1 in inflammation and atherosclerosis has been studied during the last two decades. Different groups have established that netrin-1 plays a prominent role in these contexts and has different effects depending on where it is produced, and which cells are targeted by it. While endothelial-derived netrin-1 secreted into the circulation gives rise to a protective effect against atherosclerosis, macrophage-derived netrin-1 within the plaque has a pro-atherogenic effect, promoting the trapping and survivability of foam cells.[102,134,160,162]

More recently, a truncated isoform of netrin-1 was found in the nuclei of different types of cancer cells.[108] This form of netrin-1 has also been studied in endothelial cells,[136] but so far no relationship between the expression of truncated netrin-1 and macrophages has been established. The link between cytokine stimulation, macrophage phenotype and netrin-1 isoforms has until now been unclear. The work described in this thesis looked at the expression and function of netrin-1 on monocytes and different macrophage phenotypes.

6.2. Summary and contextualisation of findings

The ability of macrophages to express netrin-1 was first described by van Gils in 2012 in a murine model and has been reported to play a role in the development of atherosclerosis.[134,160] Since its isoform was identified, truncated netrin-1 was studied in different types of cancer cells and endothelial cells, but not in macrophages or in the context of cardiovascular disease.[108,136] In chapter three, we investigated the gene expression of the two netrin-1 isoforms by macrophages to understand which phenotype found within the

atherosclerotic plaque is the main source of netrin-1. After determining how its expression varied depending on inflammatory status, we analysed how this variation in the expression may affect the molecular pathways involved in the atherosclerosis, including cell migration and survivability. The data currently available regarding the effect of netrin-1 on migration and apoptosis of macrophages is related to unstimulated cells. We therefore tried to bring some insight to the effects on migration and apoptosis of M1 and M2 macrophages, as well as foam cells, in chapter four. Finally, in chapter five, we examined the *in vivo* consequences of these effects, both in context of acute inflammation and of atherosclerosis development. The main findings of this thesis are presented below, in table 6.1.

Model		Results	Conclusion
Netrin-1 isoforms expression	THP-1 macrophage / PBMC macrophage – gene expression	Both netrin-1 isoforms were significantly upregulated after pro-inflammatory stimulation	Netrin-1 isoforms expression is at least partially dependent on NF-KB and since this nuclear factor is highly activated in classical activated macrophages, this becomes the macrophage phenotype that presents the highest upregulation of netrin-1 isoforms.
		NF-KB inhibition downregulated the expression of netrin-1 isoforms	
Macrophage migration (*in vitro*)	THP-1 macrophages - xCELLigence	Netrin-1 combined with CCL2 present the same CI as the control conditions	Netrin-1 inhibits CCL2 chemoattractant effect on THP-1-derived macrophages.
Monocyte rolling, adherence and transmigration (*in vivo*)	MaFIA mouse - Injection of netrin-1 12h prior intrascrotal injection of LPS	Mice treated with exogenous netrin-1 prior to inflammatory stimulus presented less macrophages in the tissue than mice treated with vehicle.	Netrin-1 inhibits the transmigration of monocytes from the bloodstream into the tissue after inflammatory injury.
Atherosclerotic plaque development (*in vivo*)	*LDLR*$^{-/-}$ mouse – HFD for 6 weeks and continuous deliver of netrin-1 via minipump	Enlargement of the aortic sinus area after HFD was significantly reduced when mice were exogenously treated with netrin-1.	Netrin-1 prevents the enlargement of the aortic sinus after HFD in *LDLR*$^{-/-}$ mice.

Table 6. 1 – Summary of the main findings presented in this thesis.

6.2.1. Role of netrin-1 in macrophage biology

Data produced by Delloye-Bourgeois *et al* and Passacquale *et al* showed that NF-KB pathway is involved in the expression of truncated netrin-1 in cancer and endothelial cells.[108,136] We looked at this hypothesis in a macrophage cell model and found that the gene expression of both netrin-1 isoforms is at least partially dependent on the NF-KB activation. It is therefore expected that the classical activated macrophages, which have an enhanced activation of NF-KB, to present increased expression of netrin-1.[208] In fact, we showed in PBMC-derived macrophages that stimulation with IFN-γ and LPS was the only condition that significantly upregulated netrin-1. Taking into consideration the single cell sequencing work published by Cochain and colleagues, inflammatory macrophages can account up to half of the total number of macrophages found in atherosclerotic plaques.[62] Depending on the inflammatory stage of the lesion, these macrophages may be a source of high amounts of netrin-1, which are secreted into the atheroma.

We also showed that netrin-1 inhibited CCL2 chemoattractant effect in THP-1-derived macrophages. van Gils *et al* showed a similar inhibitory response when CCL19 was used a as chemoattractant in a migration assa.[134] The presence of high amounts of netrin-1 in the plaque, as described before, will therefore keep the macrophages trapped, unable to egress to the lymph nodes, increasing the plaque cellular burden. Even though we were unable to get meaningful data regarding netrin-1 anti-apoptotic effect, evidence has been published that shows that netrin-1 promotes cell survivability through its dependence receptors.[126,131,211] Again, this will increase the inflammation within the atheroma and work as a positive feedback loop, advancing the inflammatory stage of the disease.

We also showed that truncated netrin-1 is highly expressed by macrophages. This isoform is not secreted and accumulates within the cell nucleolus. There it affects cellular processes such as ribosome synthesis.[108] It is still unknown how the increase that we detected in netrin-1 truncated isoform expression may affect the macrophages within the plaque. This will be discussed in the Future Work section.

6.2.2. The effect of netrin-1 in the circulation on inflammation and atherosclerosis

Studies published by van Gils *et al* and Schlegel *et al* showed that macrophage-derived netrin-1, within the plaque, promotes atherosclerosis. Silencing or reducing the expression of macrophage-derived netrin-1 led to lower degree of atherosclerosis when compared with the wild-type mice.[134,166] However, high amounts of netrin-1 in the circulation showed to play a protective role against inflammation. Bruikman and Fiorelli and colleagues showed that the amounts of netrin-1 in the circulation are inversely correlated with the grade of atherosclerosis in humans.[160,161] The protective effect that netrin-1 provides in the circulation against atherosclerosis, was absent in an individual with a mutation in the *NTN1* gene. Individuals with the mutation presented netrin-1 with a lower affinity to bind to UNC5b. This led to premature development of atherosclerosis, even though this happened in the absence of any classical risk factors.[162]

Up to now studies related with netrin-1 and its effect on atherosclerosis have been conducted mainly by genetically silencing its expression or blocking its effect with antibodies.[134,145,166] We decided to use recombinant netrin-1 as a treatment to study its effects in inflammation. Increased levels of netrin-1 in circulation provided a protective effect

against inflammation and led to a lower number of macrophages in the tissue after LPS injection in the cremaster muscle. One possible reason for this response is related with the data that we acquired using the xCELLigence system and showed that netrin-1 inhibits CCL2 chemoattractant effect. CCL2 is not only required to recruit leukocytes to the site of inflammation, but also to promote a firm adhesion before the cells transmigrate to the tissue.[258] Its ability to keep monocytes firmly adherent to the endothelium may be inhibited when netrin-1 is increased in the bloodstream. Netrin-1 protective role also relies on inhibition in the expression of adhesion molecules by the endothelial cells. Different groups have shown that netrin-1 downregulates the expression of molecules such as E-selectin and VCAM-1.[159,160,268]

We also assessed the systemic effect of netrin-1, over a longer period of time in *LDLR*$^{-/-}$ mice, using HFD as the source of inflammation. During inflammation, such as the development of atherosclerosis, the expression of endothelial-derived netrin-1 is downregulated. We designed a pilot experiment using osmotic minipumps to increase netrin-1 systemic levels while atherosclerosis was promoted using 60% HFD. Netrin-1 generated a protective effect on the enlargement of the aortic sinus, which was seen in animals fed with HFD but treated with vehicle. Similarly to what was discussed above, netrin-1 in the circulation might impede the recruitment of monocytes to the aortic sinus by reducing the expression of adhesion molecules and inhibiting the chemoattractant effects of chemokines.

Developing a mouse model where it is possible to temporally silence *Ntn1* using Cre conditional knock-out in endothelial cells could bring further insight into the importance of the circulating netrin-1 in atherosclerosis, as well as confirm that endothelial cells are in fact the main source of this protein in the bloodstream. A different approach could also include a

mouse model where overexpression of netrin-1 could be induced, as reported by Jasmin and colleagues.[115] Inducing the overexpression of netrin-1 by endothelial cells in an atherosclerosis model could bring unvaluable insights into netrin-1 as a therapeutical target against atherosclerosis and other inflammatory diseases.

6.3. Limitations and future work

6.3.1. Netrin-1 expression analysis

The first major limitation during this project was the lack of an antibody that detected truncated netrin-1 in cell lysates. The quantification of the protein levels of each isoform in the different macrophage phenotypes is an important piece of information to compare with the data acquired on the gene expression.

We will be working in the optimisation of a mass spectrometry protocol to measure the netrin-1 isoforms protein levels in the future. We will also attempt to create an antibody that recognises both netrin-1 isoforms for future work. We will also create primers targeting the UTR portion of the truncated mRNA sequence for a direct quantification of the expression of this isoform.

Moreover, selectively silencing netrin-1 isoforms will allow us to study the effect of each one in macrophages. For example, designing small interference RNA molecules that knockdown netrin-1 full-length will be a useful tool to study and understand the role of its truncated isoform in inflammation.

6.3.2. Apoptotic agent used

Another limitation to understand the role of netrin-1 in macrophage apoptosis was the agent used to promote cell death. Triptolide activates caspase-3 through caspase-9 and this process appears to be independent from the netrin-1 receptor UNC5b. In further work, we need to identify an apoptotic agent that interacts with the caspase-3 domain attached to UNC5b in order to further explore the role of netrin-1 in this process. Work performed by Castets *et al* used a FBS starving model in endothelial cells to study netrin-1 effects on apoptosis. We will trial this approach in macrophage cell cultures.

6.3.3. In vivo pilot studies

Due to the lack of data regarding using netrin-1 as a treatment in inflammatory models, we created the pilot studies included in this thesis to acquire the information necessary to generate power calculations for the follow-up studies. These studies proved to be very useful not only to acquire preliminary data, but also to optimise protocol design and improve some flaws within our methodology.

The mouse model used to study the effect of netrin-1 after acute inflammatory injury, in the cremaster muscle, was not the most appropriate, considering the equipment available in our department. Due to the inability to detect cell signal after using fluorescence light, an AF 488 CD11b antibody was used to augment the acquisition of data. However, we cannot provide evidence that this antibody is inert and did not affect monocyte behaviour in the bloodstream. In the follow-up study a mouse model that does not require signal enhancement will be selected. Reducing the number of components injected into the mouse system will be ideal, not only for the animal wellbeing, but also for more accurate data. Alternatively, seeking

collaborations with institutions with more advanced detecting equipment will be beneficial for the acquisition of more insightful data.

The way the *in vivo* experiment for the atherosclerosis model was designed led to a loss of 3 animals due to reaching of end points, related to the specific animal model used and the high percentage of dietary fat. Also, difficulties in the sectioning of the tissue led to the loss of two hearts. Together this led to a lower than ideal number of biological replicates. Refining this protocol, to include a longer period of feeding HFD at a lower percentage to avoid reaching end points will improve the outcome of the study. Also, freezing the tissues rather than paraffin staining will allow different types of analysis, such as Oil Red O staining. Including specific cell markers will allow us also to acquire important data to confirm the role of systemic netrin-1 in the recruitment of different types of cells into the atherosclerotic plaque.

Both experiments could also be improved by using Cre-LoxP technology to create a netrin-1 conditional overexpressing mouse, using Rosa26 locus, as described by Jasmin *et al*.[115] A collaboration with this group for a pilot study will be fruitful in understanding whether this model could be used to study the protective effects of systemic netrin-1 against inflammatory chronic diseases.

In summary, the findings presented in this thesis highlight the importance of netrin-1 in macrophage biology and inflammation. This is of particular importance in the context of chronic diseases such as atherosclerosis, which require urgent new therapeutic targets, due to its current prevalence in the population. By further refining the present experimental models and protocols, we hope to bring further insight into the role of netrin-1 isoforms in

atherosclerosis in future studies and whether it can indeed be targeted as a therapeutic target.

Appendices

Appendix A – Composition of cell culture medium

RPMI 1640 Medium with L-glutamine and sodium bicarbonate – Sigma-Aldrich

Component	g/L
Inorganic Salts	
$Ca(NO_3)_2•4H_2O$	0.1
$MgSO_4$ (anhyd)	0.04884
KCl	0.4
$NaHCO_3$	2.0
NaCl	6.0
Na_2HPO_4 (anhyd)	0.8
Amino Acids	
L-Arginine (free base)	0.2
L-Asparagine (anhyd)	0.05
L-Aspartic Acid	0.02
L-Cystine•2HCl	0.0652
L-Glutamic Acid	0.02
L-Glutamine	0.3
Glycine	0.01
L-Histidine (free base)	0.015
Hydroxy-L-Proline	0.02
L-Isoleucine	0.05
L-Leucine	0.05
L-Lysine•HCl	0.04
L-Methionine	0.015
L-Phenylalanine	0.015
L-Proline	0.02
L-Serine	0.03
L-Threonine	0.02
L-Tryptophan	0.005
L-Tyrosine•2Na•$2H_2O$	0.02883
L-Valine	0.02

Continues in the following page.

Vitamins	
D-Biotin	0.0002
Choline Chloride	0.003
Folic Acid	0.001
myo-Inositol	0.035
Niacinamide	0.001
p-Amino Benzoic Acid	0.001
D-Pantothenic Acid•½Ca	0.00025
Pyridoxine•HCl	0.001
Riboflavin	0.0002
Thiamine•HCl	0.001
Vitamin B-12	0.000005
Other	
D-Glucose	4.5
Glutathione (reduced)	0.001
Phenol Red•Na	0.0053
2-mercaptoethanol	0.0039
Penicillin	100 U/mL
Streptomycin	100 U/mL
Sodium pyruvate	0.11
Foetal bovine serum (FBS)	10%

Appendix B – Gels and buffers for protein and DNA analysis

Resolving Gel

Reagent	*10%*	*12%*
30% Acrylamide	10%	12%
ddH_2O		
4x Tris-SDS pH 8.8	375 mM Tris 0.1% SDS	
Ammonium persulfate (APS)	0.04%	
Tetramethylethylenediamine (TEMED)	0.08%	

Stacking Gel

Reagent	*4%*
30% Acrylamide	4%
ddH_2O	
4x Tris-SDS pH 8.8	375 mM Tris 0.1% SDS
Ammonium persulfate (APS)	0.05%
Tetramethylethylenediamine (TEMED)	0.10%

Agarose Gel

Reagent	*1.8%*
Agarose	1.44 g
1x Tris-Borate-EDTA buffer	160 mL
Ethidium bromide	0.005%

Continues in the following page.

Electrophoresis buffer

Reagent	*g/L*
Tris base (pH 8.3)	3.0
Glycine	15.6
SDS	0.01%
ddH_2O	

Transfer buffer

Reagent	*g/L*
Tris base (pH 8.3)	3.0
Glycine	14.4
Methanol	2%
ddH_2O	

TBS buffer

Reagent	*g/L*
Tris base (pH 7.6)	2.4
NaCl	8.4
ddH_2O	

Appendix C – Netrin-1 DNA and amino acid sequence

The sequence separated by rows is continuous and follows the order presented.

Exon 1	5' UTR	actcccagcgcgagtggcggcggcggcggagccttcgggggcgagcgcgcgtgtgtgtgagtgcgcgc cggccagc
Exon 2	5' UTR	gcgccttctgcggcaggcggacagatcctcggcgcggcagggccggggcaagctggacgcagcyy
	Sequence exclusive to full-length isoform	ATGCGGCCTTCGGCAAGGACGTGCGCGTGTCCAGCACCTGCGGCCGGCCC CCGGCGCGCTACTGCGTGGTGAGCGAGCGCGGCGAGGAGCGGCTGCGCT CGTGCCACCTCTGCAACGCGTCCGACCCCAAGAAGGCGCACCCGCCCGCC TTCCTCACCGACCTCAACAACCCGCACAACCTGACGTGCTGGCAGTCCGAG AACTACCTGCAGTTCCCGCACAACGTCACGCTCACACTGTCCCTCGGCAAG AAGTTCGAAGTGACCTACGTGAGCCTGCAGTTCTGCTCGCCGCGGCCCGAG TCCATGGCCATCTACAAGTCCATGGACTACGGGCGCACGTGGGTGCCCTTC CAGTTCTACTCCACGCAGTGCCGCAAG
	Sequence common to full-length and truncated isoforms	ATGTACAACCGGCCGCACCGCGCGCCCATCACCAAGCAGAACGAGCAGGA GGCCGTGTGCACCGACTCGCACACCGACATGCGCCCGCTCTCGGGCGGC CTCATCGCCTTCAGCACGCTGGACGGGCGGCCCTCGGCGCACGACTTCGA CAACTCGCCCGTGCTGCAGGACTGGGTCACGGCCACAGACATCCGCGTGG CCTTCAGCCGCCTGCACACGTTCGGCGACGAGAACGAGGACGACTCGGAG CTGGCGCGCGACTCGTACTTCTACGCGGTGTCCGACCTGCAGGTGGGCGG CCGGTGCAAGTGCAACGGCCACGCGGCCCGCTGCGTGCGCGACCGCGAC GACAGCCTGGTGTGCGACTGCAGGCACAACACGGCCGGCCCGGAGTGCG ACCGCTGCAAGCCCTTCCACTACGACCGGCCCTGGCAGCGCGCCACAGCC CGCGAAGCCAACGAGTGCGTGG
Exon 3		CCTGTAACTGCAACCTGCATGCCCGGCGCTGCCGCTTCAACATGGAGCTCT ACAAGCTTTCGGGGCGCAAGAGCGGAGGTGTCTGCCTCAACTGTCGCCACA ACACCGCCGGCCGCCACTGCCATTACTGCAAGGAGGGCTACTACCGCGAC ATGGGCAAGCCCATCACCCACCGGAAGGCCTGCAAAG
Exon 4		CCTGTGATTGCCACCCTGTGGGTGCTGCTGGCAAAACCTGCAACCAAACCA CCGGCCAGTGTCCCTGCAAGGACGGCGTGACGGGTATCACCTGCAACCGC TGCGCCAAAGGCTACCAGCAGAGCCGCTCTCCCATCGCCCCCTGCATAA
Exon 5		AGATCCCTGTAGCGCCGCCGACGACTGCAGCCAGCAGCGTGGAGGAGCCT GAAG
Exon 6		ACTGCGATTCCTACTGCAAGGCCTCCAAGGGGAAGCTGAAGATTAACATGAA AAAGTACTGCAAGAAGGACTATG

Exon 7	Sequence common to full-length and truncated isoforms	CCGTCCAGATCCACATCCTGAAGGCGGACAAGGCGGGGGACTGGTGGAAG TTCACGGTGAACATCATCTCCGTGTATAAGCAGGGCACGAGCCGCATCCGC CGCGGTGACCAGAGCCTGTGGATCCGCTCGCGGGACATCGCCTGCAAGTG TCCCAAAATCAAGCCCCTCAAGAAGTACCTGCTGCTGGGCAACGCGGAGGA CTCTCCGGACCAGAGCGGCATCGTGGCCGATAAAAGCAGCCTGGTGATCCA GTGGCGGGACACGTGGGCGCGGCGGCTGCGCAAGTTCCAGCAGCGTGAG AAGAAGGGCAAGTGCAAGAAGGCCTAGCGCCGAGGCAGCGGGCGGGCGG GCGGGCGGGCGCCAGGGCGGGGCCGAGCGAGAGCGGGCGCCTTGGCCC GGCCGCCGCGGACTTGGCCCGCGAGGGCTTTCCCAGGTGGGGGGAGGGA GGGGGCGGGGCCGCACGGCGCGGGGGGCGGGACCCTCGGCGGCCCCTC CCCCTACCCCCACCCTGCGCGCTCTGGGCGGGAGCCGCGTGCACGCGGG GCGGGGTGCGCCGCCGGCCGGGCCCTGGAGAAATGACGAGACGTAGCTA CCTCAGGGGCTCCTTCCAGAGCAGAGACGCGCTTCCCTGGGCCTGGGCGC GGCCGCCGTGGAGGGGCTGGGGGCAGCCTGCCCTGGGGCCCGGGGGCG GGCGCAGAATCGCACAACTGGGGCCCCAGGCGCGGGGCGTGGATGGCGC GGAGACGTGGACGGGAGGAGAACTGTGAATTCTCAAGCCCGTAGTGTGGG CGGGGCGCGGAGCACCCACCAAACCACCACCCGCACGCAGCCGACGGGA TCCCCCCCTTTCTCCCCGGCCCCTTCTAGCAGTTCCCCGCGGGCCACCTGG CTGTCACAGCCTGGACTCCTCCATCTGAAGGGGCCTGGCAGCATTTGGGGA GTGGACAGCTCCTGTCCAGCCAGCATGCCCCAGGCGGCCTCTGTCTCCACT GCTACCTGCTGAGTGGGTCCTACTGGGTGGGGGCTTGGGGTCGGTGAGTG GTTCACCTGTGGAGAGAGGAGAGGAAGCCCCTGCTGCTGCCTGTCTCTGCC CCTGCCCCTGCCCCTGCCCAGCGTGGGGCTGGCCCATCCGGAAGGCAGTG GGCCCAGGGACACCCCTGAGAAGCCCAAGCCGGGTGGTCACCGCCTCATG CTGGAGCTGCCTGTTGGAGGAGGCATCGCAAACGCAAAACCTCCCAGAGA GTTTCCTTTTGGAAACTTGGAACCAGCCCTTTTTATGACGTTTTCCAGGGGGA GGGGGAGGGGCACTGGCTGGGTTTACGGCAGTGACACTATTTATGTAAATG ACATCAGCTCCCGCAAGGCCCCTCAGCAATGTCAACAGCTGGAAAGGGCCT GAACGGGCTTGGAGTCTGCAGGCTGCGAAGGCACTTGGGCCTGGCTTGGG GCCGGGGGCTTGTTTGAGCTGGGATGGGGTTTGCTGGCTCAGTGAAGTACC AGAGTGCCTGAGCCATGGGTGGGCAGGGGCACAGGAATGACCAGGTTCCT GGGGGCCAAGGAGGCCATGCTGGCTTCTCCAAGGGAAGGCACAGAGGCTG CCGGCCTGCCCCCTACAGCTGTCTTGGGTCTGGCCTGGGCCACACCTTGAC CGTGCCTTTCCAGACGGTCTTTGTGGAGTCTGCCCGTGCCCTCCACTGTGC CCCAGCCCTCCTTCCAAAATCTCCTAGAGACACGGTCCTCAAGCAGGCAGC CCCTTTTGTTCTGACCTCCTCACACAGGGTCCATTCCTGTGCCCTGGGGCCT CCTGGCTCCCTGCCTTCCTGGGCTCTCTGCACTGCCCGGGCCTCTGGCCCA CATCCTCACACCCGGCGCACTGAATTAAGAGGCCTGGCTCCCCTCACAGTC AGGAAATTGGTTTCACTTTCCCGGCCAGAGTTTGGCTGCTCAAAAGGGTCAT ACCAAGTATGAAGCTCGGCCCCCGGTGGTCTGGCTTCCCTCCGCCTTCCCC ACATTTACCCGCATCACGGCTGCCATTTATTGAGCACCTGCTGTGTGCCAGG CACTTTACCCACATGCTCCCAGTGTGTACTCATGACAACCCTGTGGGACAGG GACTCATTATCACCAGCAAGGAGACTGGAGTACACGTGCCCAAGGTCATGC TGCAAATTGGTGGCAGGACTGGGGCTCAAACTCCAGAGCCCGACTTTCTGA CCAGGGGCCACGCTGGCCCTCACTGCACTCCAGCTCTGCAGCCTACCCGC CCAATCCCTGTGCAGGCTGGGAGGGTGCTCTTGGGGGAGTGGCCACCGAG CCCCTGGCCCTGGTTACTGCCTCTTGAGGACACTGGCATCTGGGCTGGAGA ACAGGAGCCCGGGGTGGGGTAGGGCATGGGGACAATCACATCTTCAGAGG AGGCAGCAAAGTGGTGCGGGATGCAGGGACGGACTTGCCAGATGGCAGCT CCAGGTTCCAGGAAGGCAGGCCTTGGATGCTCCGAAGAGGTGGTAGAAAG GTGTTTTTAGAAAGGTGTTTTGGCTGCCTCAGGGTGGTTGGAGAGACTCCAG GAGAGACTGGCAGAGGTGCCTCAGGGGCAGGGAGCAGACAGACCTGCCCT GGGAAGGGGCATTTGGCTTCCCTGAATCCAGCCCAAGGCTAGAAGACAGG GCCCCTCTCCAAGCTGTCAGCGCCCCTCGGATGCCCAGTGTGGTGTGCTG GGCGCCATCAGCATCACAAGGCACTACGCTGCTGGGGCGGTTGTCCTATTT CTGTCTATGCCAGTGTGGTTTCTTCACCCTGCCCAGAAGGGCTGTGGCAGC CCCACGATATCCCACCCTGGGTCTGGGTCTCACGGGTGTCCTGTGAGGGGC

		TTGCATTTGTGGTGGTCTCTGAGGCCACCTCAGCAACGGAGCTGGCGACAC GCCAAGCAACAAGGCATCTTGCGGAAAATTCAGCCAGTGTCCTGCCCCTCC CTTCGGCTCAGCACCCCGCAGGGCACAGGCTGTCCGCCCGGTGGTCTGGC CCTTGGGGAATGCGTCAGGGTGACCAGATCCACCATGCTAGCAGCCAGGTC ACTGTTGGGATTGCACGGTCGTCACGAGCTGCCTTTCCTATCCACACACCCA GCCAGGACCCAGCCCACCACTCCCGACTGCAGCCCCGGCCTCTGCGGTGA GCACCATCCTTGGGAAAGCACCCCTCCTCCACTCCGGTGCCCCACTCCAAG GAGCAGAGGGAAATGGGAATTGAGGTGTCCCGGTTTGTACAGTTAGGAAGG GATGTAAAACGGAACTAGATTTTGATTTTGAAGAGTGTATTAACCAGAATTGT GCTATGTAGGTGTTTGTTTGAAGAAAAACATACCAGATTAGTCTTTGTTTTTGA AACAGCTTCCCCAGTTGTCCTTTTTCTTACCAGCTGGGTGGTCTGGTGCCCC TGACAGCTGAGTGCCTGCTTTACGGACACGCAGTAATGCCGAAGATTTGCG GGGGAGGACATAGGGCTGTCCCCGGGATTCACCTGCTGGCTGTGGTCTCTG CCCACTGCTTCTGTCCTTGGAAAGCAGGGCAGGAGGCAGCATCCCCAGGG GCCTCTATGTGGGAGGGAGGGACACCTGGGGTCACAACCCAGGGAGGGAG GGTCACAGCCCAGGGAGGCTGGGAGCTGCTCCAAGGCCCTGGAACTCTGC CTCAGTCGCGGCATGCTGGAGAGGGGTACGGACTTACTTTCTTGGAGTTGTC CCAGGTTGGAATGAGACTGAACTCAAGAAGAGACCCTAAGGGACTGGGGAA TGGTTCCTGCCTTCAGGAAAGTGAAAGACGCTTAGGCTGTCAACACTTAAAG GAAGTCCCCTTGAAGCCCAGAGTGGACAGACTAGACCCATTGATGGGGCCA CTGGCCATGGTCCGTGGACAAGACATTCCTGTGGGCCATGGCACACCGGG GGGGATCAAAATGTGTACTTGTGGGGTCTCGCCCCTTGCCAAAAGCCAAAC CAGTCCCACTCCTGTCATTGGACGTTTCTTCCCATTCCCTCCTCCCAAATGC ACTTCCCCTCCTCCCTCTGCCCCCTCCTGTGTTTTGGATTTCTGTTCACTCAG AATTGTAAATGTTTAGTTGTGACCATGACGTATTGTTTGGGTCAATGTCCCTTT CCAATGCATACTAATATATTATGGTTATTATATATGAATATATTTAATGACATGG AAAAAGTTGTGGATTTTCTTTCTTTCCTTTTTTTTGGGGGGGGGTGGGGGGTT GGTTAGAGTTGTAATGGACCCAGATGGAACTTGTAATGTGGGCCCCACATGA TAGAACTAAATTCAGATATCATTAAATAAACTCTTGTACACTA

10	20	30	40	50	60
MMRAVWEALA	ALAAVACLVG	AVRGGPGLSM	FAGQAAQPDP	CSDENGHPRR	CIPDFVNAAF
70	80	90	100	110	120
GKDVRVSSTC	GRPPARYCVV	SERGEERLRS	CHLCNASDPK	KAHPPAFLTD	LNNPHNLTCW
130	140	150	160	170	180
QSENYLQFPH	NVTLTLSLGK	KFEVTYVSLQ	FCSPRPESMA	IYKSMDYGRT	WVPFQFYSTQ
190	200	210	220	230	240
CRKMYNRPHR	APITKQNEQE	AVCTDSHTDM	RPLSGGLIAF	STLDGRPSAH	DFDNSPVLQD
250	260	270	280	290	300
WVTATDIRVA	FSRLHTFGDE	NEDDSELARD	SYFYAVSDLQ	VGGRCKCNGH	AARCVRDRDD
310	320	330	340	350	360
SLVCDCRHNT	AGPECDRCKP	FHYDRPWQRA	TAREANECVA	CNCNLHARRC	RFNMELYKLS
370	380	390	400	410	420
GRKSGGVCLN	CRHNTAGRHC	HYCKEGYYRD	MGKPITHRKA	CKACDCHPVG	AAGKTCNQTT
430	440	450	460	470	480
GQCPCKDGVT	GITCNRCAKG	YQQSRSPIAP	CIKIPVAPPT	TAASSVEEPE	DCDSYCKASK
490	500	510	520	530	540
GKLKINMKKY	CKKDYAVQIH	ILKADKAGDW	WKFTVNIISV	YKQGTSRIRR	GDQSLWIRSR
550	560	570	580	590	600
DIACKCPKIK	PLKKYLLLGN	AEDSPDQSGI	VADKSSLVIQ	WRDTWARRLR	KFQQREKKGK
604					
CKKA					

Domains	Positions
Laminin N-terminal	47-284
Laminin EGF-like motif 1	285-340
Laminin EGF-like motif 2	341-403
Laminin EGF-like motif 3	404-453
C-terminal	472-601

Appendix D – Tyrode's-HEPES buffer (pH 7.4)

Reagent	*g/L*
NaCl	8.0
KCl	0.2
$CaCl_2 \cdot 2H_2O$	0.24
$MgCl_2 \cdot 6H_2O$	0.1
Glucose	1.0
HEPES	5.95

References

1. *Eurostat - Health Statistics*.; 2021.

2. *British Heart Foundation - UK Factsheet*.; 2022.

3. Rafieian-Kopaei M, Setorki M, Doudi M, et al. Atherosclerosis: Process, indicators, risk factors and new hopes. *Int J Prev Med*. 2014;5(8):927-946.

4. Lee J, Cooke JP. The role of nicotine in the pathogenesis of atherosclerosis. *Atherosclerosis*. 2011;215(2):281-283.

5. Ambrose JA, Barua RS. The pathophysiology of cigarette smoking and cardiovascular disease: An update. *J Am Coll Cardiol*. 2004;43(10):1731-1737.

6. Lovren F, Teoh H, Verma S. Obesity and Atherosclerosis: Mechanistic Insights. *Can J Cardiol*. 2015;31(2):177-183.

7. Ross R. Atherosclerosis - An inflammatory disease. *N Engl J Med*. 1999;340(2):115-126.

8. Krauss RM. Lipoprotein subfractions and cardiovascular disease risk. *Curr Opin Lipidol*. 2010;21(4):305-311.

9. Zhong S, Li L, Shen X, et al. An update on lipid oxidation and inflammation in cardiovascular diseases. *Free Radic Biol Med*. 2019;144:266-278.

10. J Boren, K Olin, I Lee, et al. Identification of the principal proteoglycan-binding site in LDL. A single-point mutation in apo-B100 severely affects proteoglycan interaction without affecting LDL receptor binding. *J Clin Invest*. 1998;101(12):2658-2664.

11. Yin H, Xu L, Porter NA. Free radical lipid peroxidation: Mechanisms and analysis. *Chem Rev*. 2011;111(10):5944-5972.

12. Binder CJ, Papac-Milicevic JLW. Innate sensing of oxidation-specific epitopes in health and disease. *Nat Rev Immunol*. 2016;16:485-497.

13. Brown MS, Ho YK, Goldstein JL. The cholesteryl ester cycle in macrophage foam cells. *J Biol Chem*. 1980;255(19):9344-9352.

14. Griffin EE, Ullery JC, Cox BE, Jerome WG. Aggregated LDL and lipid dispersions induce lysosomal cholesteryl ester accumulation in macrophage foam cells. *J Lipid Res*. 2005;46(10):2052-2060.

15. Shih PT, Elices MJ, Fang ZT, et al. Minimally modified low-density lipoprotein induces monocyte adhesion to endothelial connecting segment-1 by activating β1 integrin. *J Clin Invest*. 1999;103(5):613-625.

16. Vora DK, Fang ZT, Liva SM, et al. Induction of P-selectin by oxidized lipoproteins. Separate effects on synthesis and surface expression. *Circ Res*. 1997;80(6):810-818.

17. McEver RP, Cummings RD. Role of PSGL-1 binding to selectins in leukocyte recruitment. *J Clin Invest*. 1997;100(11):S97-103.

18. Dever GJ, Benson R, Wainwright CL, Kennedy S SC. Phospholipid chlorohydrin induces leukocyte adhesion to ApoE-/- mouse arteries via upregulation of P-selectin. *Free Radic Biol Med*. 2008;44(3):452-463.

19. Furnkranz A, Schober A, Bochkov V, et al. Oxidized phospholipids trigger atherogenic inflammation in murine arteries. *Atheroscler Thromb Vasc Biol*. 2005;25(3):633-638.

20. Bochkov VN, Oskolkova OV, Birukov KG, et al. Generation and biological activities of oxidized phospholipids. *Antioxidants Redox Signal*. 2010;12(8):1009-1059.

21. Berliner JA, Territo MC, Sevanian A, et al. Minimally modified low density lipoprotein

stimulates monocyte endothelial interactions. *J Clin Invest*. 1990;85(4):1260-1266.

22. Hansson GK, Hermansson A. The immune system in atherosclerosis. *Nat Immunol*. 2011;12:204-212.

23. Moore KJ, Tabas I. Macrophages in the pathogenesis of atherosclerosis. *Cell*. 2011;145(3):341-355.

24. Yu L, Zhang Y, Liu C, et al. Heterogeneity of macrophages in atherosclerosis revealed by single-cell RNA sequencing. *FASEB J*. 2023;37(3):1-13.

25. Zernecke A, Erhard F, Weinberger T, et al. Integrated single-cell analysis-based classification of vascular mononuclear phagocytes in mouse and human atherosclerosis. *Cardiovasc Res*. 2023;119(8):1676-1689.

26. Sica A, Mantovani A. Macrophage plasticity and polarization: In vivo veritas. *J Clin Invest*. 2012;122(3):787-795.

27. Bisgaard LS, Mogensen CK, Rosendahl A, et al. Bone marrow-derived and peritoneal macrophages have different inflammatory response to oxLDL and M1/M2 marker expression - Implications for atherosclerosis research. *Sci Rep*. 2016;6:1-10.

28. Murray PJ, Allen JE, Biswas SK, et al. Macrophage Activation and Polarization: Nomenclature and Experimental Guidelines. *Immunity*. 2014;41(1):14-20.

29. Murray PJ, Wynn TA. Protective and pathogenic functions of macrophage subsets. *Nat Rev Immunol*. 2011;11:723-737.

30. Rajamäki K, Lappalainen J, Öörni K, et al. Cholesterol crystals activate the NLRP3 inflammasome in human macrophages: A novel link between cholesterol metabolism and inflammation. *PLoS One*. 2010;5(7):e11765.

31. Karasawa T, Takahashi M. The crystal-induced activation of NLRP3 inflammasomes in atherosclerosis. *Inflamm Regen*. 2017;37(18):1-7.

32. Cho KY, Miyoshi H, Kuroda S, et al. The phenotype of infiltrating macrophages influences arteriosclerotic plaque vulnerability in the carotid artery. *J Stroke Cerebrovasc Dis*. 2013;22(7):910-918.

33. Stöger JL, Gijbels MJJ, van der Velden S, et al. Distribution of macrophage polarization markers in human atherosclerosis. *Atherosclerosis*. 2012;225:461-468.

34. Mantovani A, Garlanda C, Locati M. Macrophage diversity and polarization in atherosclerosis: A question of balance. *Arterioscler Thromb Vasc Biol*. 2009;29(10):1419-1423.

35. Shioi A, Ikari Y. Plaque calcification during atherosclerosis progression and regression. *J Atheroscler Thromb*. 2018;25(4):294-303.

36. Gong M, Zhuo X, Ma A. STAT6 upregulation promotes M2 macrophage polarization to suppress atherosclerosis. *Med Sci Monit Basic Res*. 2017;23:240-249.

37. Rahman K, Vengrenyuk Y, Ramsey SA, et al. Inflammatory Ly6Chi monocytes and their conversion to M2 macrophages drive atherosclerosis regression. *J Clin Invest*. 2017;127(8):2904-2915.

38. Baitsch D, Bock HH, Engel T, et al. Apolipoprotein E induces antiinflammatory phenotype in macrophages. *Arterioscler Thromb Vasc Biol*. 2011;31(5):1160-1168.

39. Bäck M, Yurdagul A, Tabas I, et al. Inflammation and its resolution in atherosclerosis: mediators and therapeutic opportunities. *Nat Rev Cardiol*. 2019;16(7):389-406.

40. Barrett TJ. Macrophages in Atherosclerosis Regression. *Arterioscler Thromb Vasc*

Biol. 2020;40(1):20-33.

41. Stöger JL, Gijbels MJJ, van der Velden S, et al. Distribution of macrophage polarization markers in human atherosclerosis. *Atherosclerosis*. 2012;225(2):461-468.

42. Cardilo-Reis L, Gruber S, Schreier SM, et al. Interleukin-13 protects from atherosclerosis and modulates plaque composition by skewing the macrophage phenotype. *EMBO Mol Med*. 2012;4(10):1072-1086.

43. Calkin AC, Forbes JM, Smith CM, et al. Rosiglitazone attenuates atherosclerosis in a model of insulin insufficiency independent of its metabolic effects. *Arterioscler Thromb Vasc Biol*. 2005;25(9):1903-1909.

44. Babaev VR, Hebron KE, Wiese CB, et al. Macrophage deficiency of Akt2 reduces atherosclerosis in Ldlr null mice. *J Lipid Res*. 2014;55(11):2296-2308.

45. Kadl A, Meher AK, Sharma PR, et al. Identification of a novel macrophage phenotype that develops in response to atherogenic phospholipids via Nrf2. *Circ Res*. 2010;107(6):737-746.

46. Gleissner CA, Shaked I, Little KM, Ley K. CXC chemokine ligand 4 induces a unique transcriptome in monocyte-derived macrophages. *J Immunol*. 2010;184(9):4810-4818.

47. Allahverdian S, Chehroudi AC, McManus BM, et al. Contribution of intimal smooth muscle cells to cholesterol accumulation and macrophage-like cells in human atherosclerosis. *Circulation*. 2014;129(15):1551-1559.

48. Oram JF. HDL apolipoproteins and ABCA1 - Partners in the removal of excess cellular

cholesterol. *Arterioscler Thromb Vasc Biol*. 2003;23(5):720-727.

49. Lao KH, Zeng L, Xu Q. Endothelial and smooth muscle cell transformation in atherosclerosis. *Curr Opin Lipidol*. 2015;26(5):449-456.

50. Anzinger JJ, Chang J, Xu Q, et al. Native low-density lipoprotein uptake by macrophage colony-stimulating factor-differentiated human macrophages is mediated by macropinocytosis and micropinocytosis. *Arterioscler Thromb Vasc Biol*. 2010;30(10):2022-2031.

51. Bohdanowicz M, Grinstein S. Role of phospholipids in endocytosis, phagocytosis, and macropinocytosis. *Physiol Rev*. 2013;93(1):69-106.

52. Csányi G, Feck DM, Ghoshal P, et al. CD47 and Nox1 mediate dynamic fluid-phase macropinocytosis of native LDL. *Antioxidants Redox Signal*. 2017;26(16):886-901.

53. Brown DI, Griendling KK. Nox proteins in signal transduction. *Free Radic Biol Med*. 2009;47(9):1239-1253.

54. Csányi G, Yao M, Rodríguez AI, et al. Thrombospondin-1 regulates blood flow via CD47 receptor-mediated activation of NADPH oxidase 1. *Arterioscler Thromb Vasc Biol*. 2012;32(12):2966-2973.

55. Miller YI, Chang MK, Binder CJ, et al. Oxidized low density lipoprotein and innate immune receptors. *Curr Opin Lipidol*. 2003;14(5):437-445.

56. Choi SH, Harkewicz R, Lee JH, et al. Lipoprotein accumulation in macrophages via toll-like receptor-4-dependent fluid phase uptake. *Circ Res*. 2009;104(12):1355-1363.

57. Kunjathoor VV., Febbraio M, Podrez EA, et al. Scavenger receptors class A-I/II and

CD36 are the principal receptors responsible for the uptake of modified low density lipoprotein leading to lipid loading in macrophages. *J Biol Chem*. 2002;277(51):49982-49988.

58. Febbraio M, Podrez EA, Smith JD, et al. Targeted disruption of the class B, scavenger receptor CD36 protects against atherosclerotic lesion development in mice. *J Clin Invest*. 2000;105(8):1049-1056.

59. Janabi M, Yamashita S, Hirano KI, et al. Oxidized LDL-induced NF-κB activation and subsequent expression of proinflammatory genes are defective in monocyte-derived macrophages from CD36-deficient patients. *Arterioscler Thromb Vasc Biol*. 2000;20(8):1953-1960.

60. Sheedy FJ, Grebe A, Rayner KJ, et al. CD36 coordinates NLRP3 inflammasome activation by facilitating intracellular nucleation of soluble ligands into particulate ligands in sterile inflammation. *Nat Immunol*. 2013;14(8):812-820.

61. Swanson KV., Deng M, Ting JPY. The NLRP3 inflammasome: molecular activation and regulation to therapeutics. *Nat Rev Immunol*. 2019;19(8):477-489.

62. Cochain C, Vafadarnejad E, Arampatzi P, et al. Single-cell RNA-seq reveals the transcriptional landscape and heterogeneity of aortic macrophages in murine atherosclerosis. *Circ Res*. 2018;122(12):1661-1674.

63. Albrecht C, Preusch MR, Hofmann G, et al. Egr-1 deficiency in bone marrow-derived cells reduces atherosclerotic lesion formation in a hyperlipidaemic mouse model. *Cardiovasc Res*. 2010;86(2):321-329.

64. Kim K, Shim D, Lee JS, et al. Transcriptome analysis reveals nonfoamy rather than

foamy plaque macrophages are proinflammatory in atherosclerotic murine models. *Circ Res*. 2018;123(10):1127-1142.

65. Wang Y, Wang Q, Xu D. New insights into macrophage subsets in atherosclerosis. *J Mol Med*. 2022;100(9):1239-1251.

66. Fernandez DM, Mundo-Sagardía JA, Figueroa Y, et al. Single-cell immune landscape of human atherosclerotic plaques. *Nat Med*. 2019;27(3):1576-1588.

67. Lin JD, Nishi H, Poles J, et al. Single-cell analysis of fate-mapped macrophages reveals heterogeneity, including stem-like properties, during atherosclerosis progression and regression. *JCI insight*. 2019;4(4):1-15.

68. Zernecke A, Winkels H, Cochain C, et al. Meta-analysis of leukocyte diversity in atherosclerotic mouse aortas. *Circ Res*. 2020;127(3):402-426.

69. Endo-Umeda K, Kim E, Thomas DG, et al. Myeloid LXR (Liver X Receptor) deficiency induces inflammatory gene expression in foamy macrophages and accelerates atherosclerosis. *Arterioscler Thromb Vasc Biol*. 2022;42(6):719-731.

70. Park I, Goddard ME, Cole JE, et al. C-type lectin receptor CLEC4A2 promotes tissue adaptation of macrophages and protects against atherosclerosis. *Nat Commun*. 2022;13(1):1-17.

71. Depuydt MAC, Prange KHM, Slenders L, et al. Microanatomy of the human atherosclerotic plaque by single-cell transcriptomics. *Circ Res*. 2020;127(11):1437-1455.

72. Fidler TP, Xue C, Yalcinkaya M, et al. The AIM2 inflammasome exacerbates atherosclerosis in clonal haematopoiesis. *Nature*. 2021;592(7853):296-301.

73. Van Kuijk K, Demandt JAF, Perales-Patón J, et al. Deficiency of myeloid PHD proteins aggravates atherogenesis via macrophage apoptosis and paracrine fibrotic signalling. *Cardiovasc Res*. 2022;118(5):1232-1246.

74. Tacke F, Alvarez D, Kaplan TJ, et al. Monocyte subsets differentially employ CCR2, CCR5, and CX3CR1 to accumulate within atherosclerotic plaques. *J Clin Invest*. 2007;117(1):185-194.

75. Li S, Gao Y, Ma K, et al. Lipid-related protein NECTIN2 is an important marker in the progression of carotid atherosclerosis: An intersection of clinical and basic studies. *J Transl Intern Med*. 2021;9(4):294-306.

76. Do TH, Ma F, Andrade PR, et al. TREM2 macrophages induced by human lipids drive inflammation in acne lesions. *Sci Immunol*. 2022;7(73):1-16.

77. Owens GK. Regulation of differentiation of vascular smooth muscle cells. *Physiol Rev*. 1995;75(3):487-517.

78. Gomez D, Shankman LS, Nguyen AT, Owens GK. Detection of histone modifications at specific gene loci in single cells in histological sections. *Nat Methods*. 2013;10(2):171-177.

79. Jacobsen K, Lund MB, Shim J, et al. Diverse cellular architecture of atherosclerotic plaque derives from clonal expansion of a few medial SMCs. *JCI Insight*. 2021;19(2):1-13.

80. Businaro R, Tagliani A, Buttari B, et al. Cellular and molecular players in the atherosclerotic plaque progression. *Ann N Y Acad Sci*. 2012;1262:134-141.

81. Katsuda S, Kaji T. Atherosclerosis and extracellular matrix. *J Atheroscler Thromb*.

2003;10(5):267-274.

82. Harman JL, Jørgensen HF. The role of smooth muscle cells in plaque stability: Therapeutic targeting potential. *Br J Pharmacol*. 2019;176(19):3741-3753.

83. Adiguzel E, Ahmad PJ, Franco C, Bendeck MP. Collagens in the progression and complications of atherosclerosis. *Vasc Med*. 2009;14(1):73-89.

84. Wilson HM. The intracellular signaling pathways governing macrophage activation and function in human atherosclerosis. *Biochem Soc Trans*. 2022;50(6):1673-1682.

85. Checkouri E, Blanchard V, Meilhac O. Macrophages in atherosclerosis, first or second row players? *Biomedicines*. 2021;9(9):1-31.

86. Chappell J, Harman JL, Narasimhan VM, et al. Extensive proliferation of a subset of differentiated, yet plastic, medial vascular smooth muscle cells contributes to neointimal formation in mouse injury and atherosclerosis models. *Circ Res*. 2016;119(12):1313-1323.

87. Kurihara O, Takano M, Miyauchi Y, et al. Vulnerable atherosclerotic plaque features: Findings from coronary imaging. *J Geriatr Cardiol*. 2021;18(7):577-584.

88. Kataoka Y, Puri R, Hammadah M, et al. Spotty calcification and plaque vulnerability in vivo: frequency- domain optical coherence tomography analysis. *Cardiovasc Diagn Ther*. 2014;4(6):460-469.

89. Shi X, Gao J, Lv Q, et al. Calcification in atherosclerotic plaque vulnerability: Friend or Foe ? *Front Physiol*. 2020;11(56):1-12.

90. Akers EJ, Nicholls SJ, Bartolo BA. Plaque Calcification - Do lipoproteins have a role ? *Arterioscler , Thromb , Vasc Biol*. 2019;39:1902-1910.

91. Karlöf E, Seime T, Dias N, et al. Correlation of computed tomography with carotid plaque transcriptomes associates calcification with lesion-stabilization. *Atherosclerosis*. 2019;288:175-185.

92. Jin HY, Weir-McCall JR, Leipsic JA, et al. The relationship between coronary calcification and the natural history of coronary artery disease. *JACC Cardiovasc Imaging*. 2021;14(1):233-242.

93. Murray AM, Mostofsky E. Physical, psychological and chemical triggers of acute cardiovascular events: Preventive strategies. *Circulation*. 2012;124(3):346-354.

94. Bentzon JF, Otsuka F, Virmani R, Falk E. Mechanisms of plaque formation and rupture. *Circ Res*. 2014;114(12):1852-1866.

95. Burke A, Farb A, Malcom GT, et al. Coronary risk factors and plaque morphology in men with coronary disease who died suddenly. *N Engl J Med*. 1997;1:1276-1282.

96. Yurchenco PD, Wadsworth WG. Assembly and tissue functions of early embryonic laminins and netrins. *Curr Opin Cell Biol*. 2004;16(5):572-579.

97. Kappler J, Franken S, Junghans U, et al. Glycosaminoglycan-binding properties and secondary structure of the C-terminus of netrin-1. *Biochem Biophys Res Commun*. 2000;271(2):287-291.

98. Yamagishi S, Yamada K, Sawada M, et al. Netrin-5 is highly expressed in neurogenic regions of the adult brain. *Front Cell Neurosci*. 2015;9(146):1-9.

99. Wang H, Copeland NG, Gilbert DJ, et al. Netrin-3, a mouse homolog of human NTN2L, is highly expressed in sensory ganglia and shows differential binding to netrin receptors. *J Neurosci*. 1999;19(12):4938-4947.

100. Yin Y, Sanes JR, Miner JH. Identification and expression of mouse netrin-4. *Mech Dev*. 2000;96(1):115-119.

101. Kennedy TE. Cellular mechanisms of netrin function: Long-range and short-range actions. *Biochem Cell Biol*. 2000;78(5):569-575.

102. Claro V, Ferro A. Netrin-1: Focus on its role in cardiovascular physiology and atherosclerosis. *JRSM Cardiovasc Dis*. 2020;9:1-10.

103. Bruikman CS, Zhang H, Kemper AM, et al. Netrin Family: Role for protein isoforms in cancer. *J Nucleic Acids*. 2019;3647123:1-9.

104. Ly NP, Komatsuzaki K, Fraser IP, et al. Netrin-1 inhibits leukocyte migration in vitro and in vivo. *Proc Natl Acad Sci*. 2005;102(41):14729-14734.

105. Xu K, Wu Z, Renier N, et al. Structures of netrin-1 bound to two receptors provide insight into its axon guidance mechanism. *Science*. 2014:1-8.

106. Kennedy TE, Serafini T, de la Torre JR, Tessier-Lavigne M. Netrins are diffusible chemotropic factors for commissural axons in the embryonic spinal cord. *Cell*. 1994;78:425-435.

107. Kye WP, Grouse D, Lee M, et al. The axonal attractant netrin-1 is an angiogenic factor. *Proc Natl Acad Sci U S A*. 2004;101(46):16210-16215.

108. Delloye-Bourgeois C, Goldschneider D, Paradisi A, et al. Nucleolar localization of a netrin-1 isoform enhances tumor cell proliferation. *Sci Signal*. 2012;5(236):1-14.

109. Srinivasan K, Strickland P, Valdes A,et al. Netrin-1/neogenin interaction stabilizes multipotent progenitor cap cells during mammary gland morphogenesis. *Dev Cell*. 2003;4:371-382.

110. Shimizu A, Nakayama H, Wang P, et al. Netrin-1 promotes glioblastoma cell invasiveness and angiogenesis by multiple pathways including activation of RhoA, cathepsin B, and cAMP-response element-binding protein. *J Biol Chem*. 2013;288(4):2210-2222.

111. Akino T, Han X, Nakayama H, et al. Netrin-1 promotes medulloblastoma cell invasiveness and angiogenesis, and demonstrates elevated expression in tumor tissue and urine of patients with pediatric medulloblastoma. *Cancer Res*. 2014;74(14):3716-3726.

112. Castets M, Coissieux MM, Delloye-Bourgeois C, et al. Inhibition of endothelial cell apoptosis by netrin-1 during angiogenesis. *Dev Cell*. 2009;16(4):614-620.

113. Llambi F, Causeret F, Bloch-Gallego E, Mehlen P. Netrin-1 acts as a survival factor via its receptors UNC5H and DCC. *EMBO J*. 2001;20(11):2715-2722.

114. Ahn EH, Kang SS, Ye K. Netrin-1/receptors regulate the pathogenesis in Parkinson's diseases. *Precis Futur Med*. 2021;5(2):50-61.

115. Jasmin M, Ahn EH, Voutilainen MH, et al. Netrin-1 and its receptor DCC modulate survival and death of dopamine neurons and Parkinson's disease features. *EMBO J*. 2021;40(3):1-16.

116. Li Y, Xiao M, Guo F. The role of Sox6 and Netrin-1 in ovarian cancer cell growth, invasiveness, and angiogenesis. *Tumor Biol*. 2017;39(5):1-9.

117. Li B, Shen K, Zhang J, et al. Serum netrin-1 as a biomarker for colorectal cancer detection. *Cancer Biomarkers*. 2020;28(3):391-396.

118. Frees S, Zhou B, Han KS, et al. The role of netrin-1 in metastatic renal cell carcinoma

treated with sunitinib. *Oncotarget*. 2018;9(32):22631-22641.

119. Dalvin S, Anselmo MA, Prodhan P, et al. Expression of netrin-1 and its two receptors DCC and UNC5H2 in the developing mouse lung. *Gene Expr Patterns*. 2003;3(3):279-283.

120. De Breuck S, Lardon J, Rooman I, Bouwens L. Netrin-1 expression in fetal and regenerating rat pancreas and its effect on the migration of human pancreatic duct and porcine islet precursor cells. *Diabetologia*. 2003;46(7):926-933.

121. Opitz R, Hitz MP, Vandernoot I, et al. Functional zebrafish studies based on human genotyping point to netrin-1 as a link between aberrant cardiovascular development and thyroid dysgenesis. *Endocrinology*. 2015;156(1):377-388.

122. Mirakaj V, Thix CA, Laucher S, et al. Netrin-1 dampens pulmonary inflammation during acute lung injury. *Am J Respir Crit Care Med*. 2010;181(8):815-824.

123. Mirakaj V, Gatidou D, Potzsch C, et al. Netrin-1 signaling dampens inflammatory peritonitis. *J Immunol*. 2010:549-555.

124. Chen Z, Chen Y, Zhou J, et al. Netrin-1 reduces lung ischemia-reperfusion injury by increasing the proportion of regulatory T cells. *J Int Med Res*. 2020;48(5):1-12.

125. Grenz A, Dalton JH, Bauerle JD, et al. Partial netrin-1 deficiency aggravates acute kidney injury. *PLoS One*. 2011;6(5):1-10.

126. Wang W, Reeves WB, Pays L, et al. Netrin-1 overexpression protects kidney from ischemia reperfusion injury by suppressing apoptosis. *Am J Pathol*. 2009;175(3):1010-1018.

127. Ranganathan PV, Jayakumar C, Ramesh G. Netrin-1-treated macrophages protect

the kidney against ischemia-reperfusion injury and suppress inflammation by inducing M2 polarization. *Am J Physiol - Ren Physiol*. 2013;304(7):F948-F957.

128. Bouhidel J, Wang P, Li Q, Cai H. Pharmacological postconditioning treatment of myocardial infarction with netrin-1. *Front Biosci (Landmark ed)*. 2014;3(19):566-570.

129. Mao X, Xing H, Mao A, et al. Netrin-1 attenuates cardiac ischemia reperfusion injury and generates alternatively activated macrophages. *Inflammation*. 2014;37(2):573-580.

130. Zhang J, Cai H. Netrin-1 prevents ischemia/reperfusion-induced myocardial infarction via a DCC/ERK1/2/eNOSs1177/NO/DCC feed-forward mechanism. *J Mol Cell Cardiol*. 2010;48(6):1060-1070.

131. Aherne CM, Collins CB, Eltzschig HK. Netrin-1 guides inflammatory cell migration to control mucosal immune responses during intestinal inflammation. *Tissue Barriers*. 2013;1(2):e24957.

132. Aherne CM, Collins CB, Masterson JC, et al. Neuronal guidance molecule netrin-1 attenuates inflammatory cell trafficking during acute experimental colitis. *Gut*. 2012;61(5):695-705.

133. Mediero A, Ramkhelawon B, Wilder T, et al. Netrin-1 is highly expressed and required in inflammatory infiltrates in wear particle-induced osteolysis. *Ann Rheum Dis*. 2016;75(9):1706-1713.

134. Van Gils JM, Derby MC, Fernandes LR, et al. The neuroimmune guidance cue netrin-1 promotes atherosclerosis by inhibiting the emigration of macrophages from plaques. *Nat Immunol*. 2012;13(2):136-143.

135. Ramkhelawon B, Hennessy EJ, Ménager M, et al. Netrin-1 promotes adipose tissue macrophage retention and insulin resistance in obesity. *Nat Med*. 2014;20(4):377-384.

136. Passacquale G, Phinikaridou A, Warboys C, et al. Aspirin-induced histone acetylation in endothelial cells enhances synthesis of the secreted isoform of netrin-1 thus inhibiting monocyte vascular infiltration. *Br J Pharmacol*. 2015;172:3548-3564.

137. Harter PN, Zinke J, Scholz A, et al. Netrin-1 expression is an independent prognostic factor for poor patient survival in brain metastases. *PLoS One*. 2014;9(3):1-10.

138. Paradisi A, Maisse C, Bernet A, et al. NF-κB regulates netrin-1 expression and affects the conditional tumor suppressive activity of the netrin-1 receptors. *Gastroenterology*. 2008;135(4):1248-1257.

139. Boyer NP, Gupton SL. Revisiting netrin-1: one who guides (Axons). *Front Cell Neurosci*. 2018;12(221):1-18.

140. Cirulli V, Yebra M. Netrins: Beyond the brain. *Nat Rev Mol Cell Biol*. 2007;8(4):296-306.

141. Hong K, Hinck L, Nishiyama M, et al. A ligand-gated association between cytoplasmic domains of UNC5 and DCC family receptors converts netrin-induced growth cone attraction to repulsion. *Cell*. 1999;97:927-941.

142. Wang R, Wei Z, Jin H, et al. Autoinhibition of UNC5b revealed by the cytoplasmic domain structure of the receptor. *Mol Cell*. 2009;33(6):692-703.

143. Kruger RP, Lee J, Li W, Guan KL. Mapping netrin receptor binding reveals domains of Unc5 regulating its tyrosine phosphorylation. *J Neurosci*. 2004;24(48):10826-10834.

144. Llambi F, Causeret F, Bloch-Gallego E, Mehlen P. Netrin-1 acts as a survival factor via its receptors UNC5H and DCC. *EMBO J*. 2001;20:2715-2722.

145. Tadagavadi RK, Wang W, Ramesh G. Netrin-1 Regulates Th1/Th2/Th17 cytokine production and inflammation through UNC5B receptor and protects kidney against ischemia–reperfusion injury. *J Immunol*. 2010;185(6):3750-3758.

146. Wilson NH, Key B. Neogenin: One receptor, many functions. *Int J Biochem Cell Biol*. 2007;39(5):874-878.

147. Chen Q, Sun X, Zhou X hong, et al. N-terminal horseshoe conformation of DCC is functionally required for axon guidance and might be shared by other neural receptors. *J Cell Sci*. 2013;126(1):186-195.

148. Kolodziej PA, Timpe LC, Mitchell KJ, et al. frazzled encodes a drosophila member of the DCC immunoglobulin subfamily and is required for CNS and motor axon guidance. *Cell*. 1996;87(2):197-204.

149. Finci LI, Krüger N, Sun X, et al. The crystal structure of netrin-1 in complex with DCC reveals the bifunctionality of netrin-1 as a guidance cue. *Neuron*. 2014;83(4):839-849.

150. Fearon ER, Cho KR, Nigro JM, et al. Identification of a chromosome 18q gene that is altered in colorectal cancers. *Science*. 1990;247:49-56.

151. Reyes-Mugica M, Rieger-Christ K, Ohgaki H, et al. Loss of DCC expression and glioma progression. *Cancer Res*. 1997;57:382-386.

152. Koren R, Dekel Y, Sherman E, et al. The expression of DCC protein in female breast cancer. *Breast Cancer Res Treat*. 2003;80:215-220.

153. Boneschansker L, Nakayama H, Eisenga M, et al. Netrin-1 augments chemokinesis in

CD4+ T cells in vitro and elicits a proinflammatory response in vivo. *J Immunol*. 2016;197:1389-1398.

154. Mehlen P, Rabizadeh S, Snipas SJ, et al. The DCC gene product induces apoptosis by a mechanism requiring receptor proteolysis. *Nature*. 1998;395(6704):801-804.

155. Leroyer AS, Blin MG, Bachelier R, et al. CD146 (Cluster of Differentiation 146). *Arterioscler Thromb Vasc Biol*. 2019;39:1026-1033.

156. Jiang RC, Zheng XY, Yang SL, et al. CD146 mediates the anti-apoptotic role of netrin-1 in endothelial progenitor cells under hypoxic conditions. *Mol Med Rep*. 2022;25(1):1-9.

157. Rosenberger P, Schwab JM, Mirakaj V, et al. Hypoxia-inducible factor-dependent induction of netrin-1 dampens inflammation caused by hypoxia. *Nat Immunol*. 2009;10(2):195-202.

158. Ly A, Nikolaev A, Suresh G, et al. DSCAM is a netrin receptor that collaborates with DCC in mediating turning responses to netrin-1. *Cell*. 2008;133(7):1241-1254.

159. Lin Z, Jin J, Bai W, Li J, Shan X. Netrin-1 prevents the attachment of monocytes to endothelial cells via an anti-inflammatory effect. *Mol Immunol*. 2018;103:166-172.

160. Bruikman CS, Vreeken D, Hoogeveen RM, et al. Netrin-1 and the grade of atherosclerosis are inversely correlated in humans. *Arterioscler Thromb Vasc Biol*. 2020;40(2):462-472.

161. Fiorelli S, Cosentino N, Porro B, et al. Netrin-1 in atherosclerosis: Relationship between human macrophage intracellular levels and in vivo plaque morphology. *Biomedicines*. 2021;9(2):1-11.

162. Bruikman CS, Vreeken D, Zhang H, et al. The identification and function of a netrin-1 mutation in a pedigree with premature atherosclerosis. *Atherosclerosis*. 2020;301:84-92.

163. Taylor L, Brodermann MH, McCaffary D, et al. Netrin-1 reduces monocyte and macrophage chemotaxis towards the complement component C5a. *PLoS One*. 2016;11(8):e0160685.

164. Daynes RA, Jones DC. Emerging roles of PPARs in inflammation and immunity. *Nat Rev Immunol*. 2002;2(10):748-759.

165. Ranganathan PV, Jayakumar C, Mohamed R, et al. Netrin-1 regulates the inflammatory response of neutrophils and macrophages, and suppresses ischemic acute kidney injury by inhibiting COX-2-mediated PGE2 production. *Kidney Int*. 2013;83(6):1087-1098.

166. Schlegel M, Sharma M, Brown EJ, et al. Silencing myeloid netrin-1 induces inflammation resolution and plaque regression. *Circ Res*. 2021;129(5):530-546.

167. Serafini T, Colamarino SA, Leonardo ED, et al. Netrin-1 is required for commissural axon guidance in the developing vertebrate nervous system. *Cell*. 1996;87:1001-1014.

168. Bin JM, Han D, Lai K, et al. Complete loss of netrin-1 results in embryonic lethality and severe axon guidance defects without increased neural cell death. *Cell Rep*. 2015;12(7):1099-1106.

169. Grenz A, Dalton JH, Bauerle JD, et al. Partial netrin-1 deficiency aggravates acute kidney injury. *PLoS One*. 2011;6(5):e14812.

170. Ramkhelawon B, Yang Y, Van Gils JM, et al. Hypoxia induces netrin-1 and Unc5b in atherosclerotic plaques:Mechanism for macrophage retention and survival. *Arterioscler Thromb Vasc Biol*. 2013;33(6):1180-1188.

171. Van Gils JM, Ramkhelawon B, Fernandes L, et al. Endothelial expression of guidance cues in vessel wall homeostasis dysregulation under proatherosclerotic conditions. *Arterioscler Thromb Vasc Biol*. 2013;33(5):911-919.

172. Yang X, Zhang J, Chen L, et al. The role of UNC5b in ox-LDL inhibiting migration of RAW264.7 macrophages and the involvement of CCR7. *Biochem Biophys Res Commun*. 2018;505(3):637-643.

173. Shin HM, Kim MH, Kim BH, et al. Inhibitory action of novel aromatic diamine compound on lipopolysaccharide-induced nuclear translocation of NF-κB without affecting IκB degradation. *FEBS Lett*. 2004;571(1):50-54.

174. Huang L, Li F, Deng P, Hu C. MicroRNA-223 promotes tumor progression in lung cancer A549 cells via activation of the NF-κB signaling pathway. *Oncol Res*. 2016;24(6):405-413.

175. Ramachandran S, Sennoune SR, Sharma M, et al. Expression and function of SLC38A5, an amino acid-coupled Na+/H+ exchanger, in triple-negative breast cancer and its relevance to macropinocytosis. *Biochem J*. 2021;478(21):3957-3976.

176. Bouhlel MA, Derudas B, Rigamonti E, et al. PPARγ activation primes human monocytes into alternative M2 macrophages with anti-inflammatory properties. *Cell Metab*. 2007;6:137-143.

177. Chanput W, Mes J, Vreeburg RAM, et al. Transcription profiles of LPS-stimulated THP-

1 monocytes and macrophages: A tool to study inflammation modulating effects of food-derived compounds. *Food Funct*. 2010;1(3):254-261.

178. Pfaffl MW. A new mathematical model for relative quantification in real-time RT-PCR. *Nucleic Acids Res*. 2001;29(9):e45.

179. Livak KJ, Schmittgen TD. Analysis of relative gene expression data using real-time quantitative PCR and the $2^{-\Delta\Delta CT}$ method. *Methods*. 2001;25(4):402-408.

180. Chen BJ. Triptolide, a novel immunosuppressive and anti-inflammatory agent purified from a Chinese herb Tripterygium Wilfordii Hook F. *Leuk Lymphoma*. 2001;42(3):253-265.

181. Lee KY, Chang WT, Qiu D, et al. PG490 (triptolide) cooperates with tumor necrosis factor-α to induce apoptosis in tumor cells. *J Biol Chem*. 1999;274(19):13451-13455.

182. Park SW, Kim Y Il. Triptolide induces apoptosis of PMA-treated THP-1 cells through activation of caspases, inhibition of NF-κB and activation of MAPKs. *Int J Oncol*. 2013;43(4):1169-1175.

183. Burnett SH, Kershen EJ, Zhang J, et al. Conditional macrophage ablation in transgenic mice expressing a Fas-based suicide gene. *J Leukoc Biol*. 2004;75(4):612-623.

184. Stanley ER, Chitu V. CSF-1 receptor signaling in myeloid cells. *Cold Spring Harb Perspect Biol*. 2014;6(6):a021857.

185. Tang J, Frey JM, Wilson CL, et al. Neutrophil and macrophage cell surface colony-stimulating factor 1 shed by ADAM17 drives mouse macrophage proliferation in acute and chronic inflammation. *Mol Cell Biol*. 2018;38(17):1-19.

186. Maggi CA, Meli A. Suitability of urethane anesthesia for physiopharmacological

investigations. Part 3: Other systems and conclusions. *Experientia*. 1986;42(5):531-537.

187. Hara K, Harris RA. The anesthetic mechanism of urethane: The effects on neurotransmitter-gated ion channels. *Anesth Analg*. 2002;94(2):313-318.

188. Shah SA, Kanabar V, Riffo-Vasquez Y, et al. Platelets independently recruit into asthmatic lungs and models of allergic inflammation via CCR3. *Am J Respir Cell Mol Biol*. 2021;64(5):557-568.

189. Hampton AL, Hish GA, Aslam MN, et al. Progression of ulcerative dermatitis lesions in C57BL/6Crl mice and the development of a scoring system for dermatitis lesions. *J Am Assoc Lab Anim Sci*. 2012;51(5):586-593.

190. Argunhan F, Thapa D, Aubdool AA, et al. Calcitonin gene-related peptide protects against cardiovascular dysfunction independently of nitric oxide in vivo. *Hypertension*. 2021;77(4):1178-1190.

191. Libby P, Hansson GK. Inflammation and immunity in diseases of the arterial tree: Players and layers. *Circ Res*. 2015;116(2):307-311.

192. Eligini S, Gianazza E, Mallia A, et al. Macrophage phenotyping in atherosclerosis by proteomics. *Int J Mol Sci*. 2023;24(3):1-20.

193. Leitinger N, Schulman IG. Phenotypic polarization of macrophages in atherosclerosis. *Arterioscler Thromb Vasc Biol*. 2013;33(6):1120-1126.

194. Chanput W, Mes JJ, Wichers HJ. THP-1 cell line: An in vitro cell model for immune modulation approach. *Int Immunopharmacol*. 2014;23(1):37-45.

195. Mohd ZN, Mohd FN, Hoe CH, Yvonne-Tee GB. Macrophage polarization in THP-1 cell

line and primary monocytes: A systematic review. *Differentiation*. 2022;128:67-82.

196. Shiratori H, Feinweber C, Luckhardt S, et al. THP-1 and human peripheral blood mononuclear cell-derived macrophages differ in their capacity to polarize in vitro. *Mol Immunol*. 2017;88:58-68.

197. Tedesco S, De Majo F, Kim J, et al. Convenience versus biological significance: Are PMA-differentiated THP-1 cells a reliable substitute for blood-derived macrophages when studying in vitro polarization? *Front Pharmacol*. 2018;9:1-13.

198. Schildberger A, Rossmanith E, Eichhorn T, Strassl K, Weber V. Monocytes, peripheral blood mononuclear cells, and THP-1 cells exhibit different cytokine expression patterns following stimulation with lipopolysaccharide. *Mediators Inflamm*. 2013;2013:697972.

199. Buscher K, Ehinger E, Gupta P, et al. Natural variation of macrophage activation as disease-relevant phenotype predictive of inflammation and cancer survival. *Nat Commun*. 2017;8:1-10.

200. Klein SL, Flanagan KL. Sex differences in immune responses. *Nat Rev Immunol*. 2016;16(10):626-638.

201. Guyton JR, Lenz ML, Mathews B, et al. Toxicity of oxidized low density lipoproteins for vascular smooth muscle cells and partial protection by antioxidants. *Atherosclerosis*. 1995;118(2):237-249.

202. Asmis R, Begley JG. Oxidized LDL promotes peroxide-mediated mitochondrial. *Circ Res*. 2003;92(1):1-10.

203. Orekhov AN, Sukhorukov VN, Nikiforov NG, et al. Signaling pathways potentially

responsible for foam cell formation: Cholesterol accumulation or inflammatory response—what is first? *Int J Mol Sci*. 2020;21(8):1-17.

204. Jones NL, Reagan JW, Willingham MC. The pathogenesis of foam cell formation: Modified LDL stimulates uptake of co-incubated LDL via macropinocytosis. *Arterioscler Thromb Vasc Biol*. 2000;20(3):773-781.

205. Broeders S, Huber I, Grohmann L, et al. Guidelines for validation of qualitative real-time PCR methods. *Trends Food Sci Technol*. 2014;37(2):115-126.

206. Li J, Conrad C, Mills TW, et al. PMN-derived netrin-1 attenuates cardiac ischemia-reperfusion injury via myeloid ADORA2B signaling. *J Exp Med*. 2021;218(6):1-18.

207. Ko CL, Lin JA, Chen KY, et al. Netrin-1 dampens hypobaric hypoxia-induced lung injury in mice. *High Alt Med Biol*. 2019;20(3):293-302.

208. Liu T, Zhang L, Joo D, Sun SC. NF-κB signaling in inflammation. *Signal Transduct Target Ther*. 2017;2:e17023.

209. Harter PN, Zinke J, Scholz A, et al. Netrin-1 expression is an independent prognostic factor for poor patient survival in brain metastases. *PLoS One*. 2014;9(3):e92311.

210. Serafini T, Kennedy TE, Gaiko MJ, et al. The netrins define a family of axon outgrowth-promoting proteins homologous to C. elegans UNC-6. *Cell*. 1994;78:409-424.

211. Chen J, Du H, Zhang Y, et al. Netrin-1 prevents rat primary cortical neurons from apoptosis via the DCC/ERK pathway. *Front Cell Neurosci*. 2017;11:1-10.

212. Mazelin L, Bernet A, Bonod-Bidaud C, et al. Netrin-1 controls colorectal tumorigenesis by regulating apoptosis. *Nature*. 2004;431(7004):80-84.

213. Huang L, An X, Zhu Y, et al. Netrin-1 induces the anti-apoptotic and pro-survival effects of B-ALL cells through the Unc5b-MAPK axis. *Cell Commun Signal*. 2022;20(122):1-14.

214. Huang Y, Zhang Z, Miao M, Kong C. The intracellular domain of UNC5B facilities proliferation and metastasis of bladder cancer cells. *J Cell Mol Med*. 2021;25(4):2121-2135.

215. Porter AG, Jänicke RU. Emerging roles of caspase-3 in apoptosis. *Cell Death Differ*. 1999;6(2):99-104.

216. O'Donovan N, Crown J, Stunell H, et al. Caspase 3 in breast cancer. *Clin Cancer Res*. 2003;9(2):738-742.

217. Lavrik IN, Golks A, Krammer PH. Caspase: Pharmacological manipulation of cell death. *J Clin Invest*. 2005;115(10):2665-2672.

218. Boudreau MW, Peh J, Hergenrother PJ. Procaspase-3 overexpression in cancer: A paradoxical observation with therapeutic potential. *ACS Chem Biol*. 2019;14(11):2335-2348.

219. McIlwain DR, Berger T, Mak TW. Caspase functions in cell death and disease. *Cold Spring Harb Perspect Biol*. 2015;7(4):1-28.

220. Bird C, Kirstein S. Real-time, label-free monitoring of cellular invasion and migration with the xCELLigence system. *Nat Methods*. 2009;6(8):v-vi.

221. Kho D, MacDonald C, Johnson R, et al. Application of xCELLigence RTCA biosensor technology for revealing the profile and window of drug responsiveness in real time. *Biosensors*. 2015;5:199-222.

222. Hamidi H, Lilja J, Ivaska J. Using xCELLigence RTCA instrument to measure cell adhesion. *Bio-Protocol*. 2017;7(24):1-16.

223. Oberhammer FA, Hochegger K, Fröschl G, et al. Chromatin condensation during apoptosis is accompanied by degradation of lamin A+B, without enhanced activation of cdc2 kinase. *J Cell Biol*. 1994;126(4):827-837.

224. Best PJM, Hasdai D, Sangiorgi G, et al. Apoptosis basic concepts and implications in coronary artery disease. *Atheroscler Thromb Vasc Biol*. 1999;19(1):14-22.

225. Auwerx J. The human leukemia cell line, THP-1: A multifacetted model for the study of monocyte-macrophage differentiation. *Experientia*. 1991;47(1):22-31.

226. Chiu C, Lei KF, Yeh W, et al. Comparison between xCELLigence biosensor technology and conventional cell culture system for real-time monitoring human tenocytes proliferation and drugs cytotoxicity screening. *J Orthpaedic Surg Res*. 2017;12(149):1-13.

227. Satish LD, Sergey SA and BES. Monocyte Chemoattractant Protein-1 (MCP-1): An Overview. *J Interf CYTOKINE Res*. 2009;29(6):313-326.

228. Vogel DYS, Heijnen PDAM, Breur M, et al. Macrophages migrate in an activation-dependent manner to chemokines involved in neuroinflammation. *J Neuroinflammation*. 2014;11(23):1-11.

229. Mentxaka A, Javier G, Neira G, et al. Increased expression levels of netrin-1 in visceral adipose tissue during obesity favour colon cancer cell migration. *Cancers (Basel)*. 2023;15:1-14.

230. Förster R, Davalos-Misslitz AC, Rot A. CCR7 and its ligands: Balancing immunity and

tolerance. *Nat Rev Immunol*. 2008;8(5):362-371.

231. Grimsey NL, Graham ES, Dragunow M, Glass M. Cannabinoid receptor 1 trafficking and the role of the intracellular pool: Implications for therapeutics. *Biochem Pharmacol*. 2010;80(7):1050-1062.

232. Liu B, Sun R, Luo H, et al. Both intrinsic and extrinsic apoptotic pathways are involved in Toll-like receptor 4 (TLR4)-induced cell death in monocytic THP-1 cells. *Immunobiology*. 2017;222(2):198-205.

233. Zhu C, Zhou J, Li T, et al. Urocortin participates in LPS-induced apoptosis of THP-1 macrophages via S1P-cPLA2 signaling pathway. *Eur J Pharmacol*. 2020;887:173559.

234. Jian-ling T, Xiong-zhong R, Hang L, et al. Endoplasmic reticulum stress is involved in acetylated low-density lipoprotein induced apoptosis in THP-1 differentiated macrophages. *Chin Med J (Engl)*. 2009;122(15):1794-1799.

235. Devries-seimon T, Li Y, Yao PM, et al. Cholesterol-induced macrophage apoptosis requires ER stress pathways and engagement of the type A scavenger receptor. *J Cell Biol*. 2005;171(1):61-73.

236. Chen S, So EC, Strome SE, Zhang X. Impact of detachment methods on M2 macrophage phenotype and function. *J Immunol Methods*. 2015;426:56-61.

237. Veldhoven PP Van, Bell RM. Effect of harvesting methods, growth conditions and growth phase on diacylglycerol levels in cultured human adherent cells. *Biochim Biophys Acta*. 1988;959:185-196.

238. Lund ME, To J, Brien BAO, Donnelly S. The choice of phorbol 12-myristate 13-acetate differentiation protocol influences the response of THP-1 macrophages to a pro-

inflammatory stimulus. *J Immunol Methods*. 2016;430:64-70.

239. Libby P, Buring JE, Badimon L, et al. Atherosclerosis. *Nat Rev Dis Prim*. 2019;5(1):1-18.

240. Hilgendorf I, Swirski FK, Robbins CS. Monocyte fate in atherosclerosis. *Arterioscler Thromb Vasc Biol*. 2015;35(2):272-279.

241. Mestas J, Ley K. Monocyte-endothelial cell interactions in the development of atherosclerosis. *Trends Cardiovasc Med*. 2008;18(6):228-232.

242. Ma YQ, Plow EF, Geng JG. P-selectin binding to P-selectin glycoprotein ligand-1 induces an intermediate state of αMβ2 activation and acts cooperatively with extracellular stimuli to support maximal adhesion of human neutrophils. *Blood*. 2004;104(8):2549-2556.

243. Podjaski C, Alvarez JI, Bourbonniere L, et al. Netrin 1 regulates blood-brain barrier function and neuroinflammation. *Brain*. 2015;138(6):1598-1612.

244. Vaghela R, Arkudas A, Horch RE, Hessenauer M. Actually seeing what is going on – Intravital microscopy in tissue engineering. *Front Bioeng Biotechnol*. 2021;9:1-18.

245. Grant RT. The effects of denervation on skeletal muscle blood vessels (rat cremaster). *J Anat*. 1966;100(2):305-316.

246. Merrill-Skoloff G, Dubois C, Atkinson B, et al. *Real Time in Vivo Imaging of Platelets during Thrombus Formation*. Third Edit. Elsevier Inc.; 2013.

247. Baumer Y, McCurdy S, Jin X, et al. Ultramorphological analysis of plaque advancement and cholesterol crystal formation in Ldlr knockout mouse atherosclerosis. *Atherosclerosis*. 2019;287:100-111.

248. Venegas-Pino DE, Banko N, Khan MI, et al. Quantitative analysis and characterization of atherosclerotic lesions in the murine aortic sinus. *J Vis Exp*. 2013;82:50933.

249. Shaked I, Hanna RN, Shaked H, et al. Transcription factor Nr4a1 couples sympathetic and inflammatory cues in CNS-recruited macrophages to limit neuroinflammation. *Nat Immunol*. 2015;16(12):1228-1234.

250. Rhein P, Mitlohner R, Basso G, et al. CD11b is a therapy resistance- and minimal residual disease-specific marker in precursor B-cell acute lymphoblastic leukemia. *Blood*. 2010;115(18):3763-3771.

251. Ley K, Laudanna C, Cybulsky MI, Nourshargh S. Getting to the site of inflammation: The leukocyte adhesion cascade updated. *Nat Rev Immunol*. 2007;7(9):678-689.

252. Yao X, Dong G, Zhu Y, et al. Leukadherin-1-Mediated activation of CD11b Inhibits LPS-Induced pro-inflammatory response in macrophages and protects mice against endotoxic shock by blocking LPS-TLR4 interaction. *Front Immunol*. 2019;10:1-14.

253. Dayang EZ, Plantinga J, Ter Ellen B, et al. Identification of LPS-activated endothelial subpopulations with distinct inflammatory phenotypes and regulatory signaling mechanisms. *Front Immunol*. 2019;10:1-12.

254. Shi C, Pamer EG. Monocyte recruitment during infection and inflammation. *Nat Rev Immunol*. 2011;11:762-774.

255. Gerhardt T, Ley K. Monocyte trafficking across the vessel wall. *Cardiovasc Res*. 2015;107(3):321-330.

256. Cerri C, Genovesi S, Allegra M, et al. The chemokine CCL2 mediates the seizure-enhancing effects of systemic inflammation. *J Neurosci*. 2016;36(13):3777-3788.

257. Puntambekar SS, Davis DS, Hawel L, et al. LPS-induced CCL2 expression and macrophage influx into the murine central nervous system is polyamine-dependent. *Brain Behav Immun*. 2011;25(4):629-639.

258. Gerszten RE, Garcia-Zepeda EA, Lim YC, et al. MCP-1 and IL-8 trigger firm adhesion of monocytes to vascular endothelium under flow conditions. *Nature*. 1999;398(6729):718-725.

259. Carman C V., Springer TA. A transmigratory cup in leukocyte diapedesis both through individual vascular endothelial cells and between them. *J Cell Biol*. 2004;167(2):377-388.

260. Mushenkova N V, Summerhill VI, Silaeva YY, et al. Modelling of atherosclerosis in genetically modified animals. *Am J Transl Res*. 2019;11(8):4614-4633.

261. Mansukhani NA, Wang Z, Shively VP, et al. Sex differences in the LDL receptor knockout mouse model of atherosclerosis. *Artery Res*. 2017;20(1):8-11.

262. Tangirala RK, Rubin EM, Palinski W. Quantitation of atherosclerosis in murine models: Correlation between lesions in the aortic origin and in the entire aorta, and differences in the extent of lesions between sexes in LDL receptor-deficient and apolipoprotein E-deficient mice. *J Lipid Res*. 1995;36(11):2320-2328.

263. Nakashima Y, Plump AS, Raines EW, et al. ApoE-deficient mice develop lesions of all phases of atherosclerosis throughout the arterial tree. *Arterioscler Thromb*. 1994;14(1):133-140.

264. Paigen B, Morrow A, Holmes PA, et al. Quantitative assessment of atherosclerotic lesions in renal arteries. *Atherosclerosis*. 1987;42(3):231-240.

265. Ma Y, Wang W, Zhang J, et al. Hyperlipidemia and atherosclerotic lesion development in Ldlr-deficient mice on a long-term high-fat diet. *PLoS One*. 2012;7(4):1-8.

266. Otero-Losada ME, Loughlin SM, Rodríguez-Granillo G, et al. Metabolic disturbances and worsening of atherosclerotic lesions in ApoE-/- mice after cola beverages drinking. *Cardiovasc Diabetol*. 2013;12(1):1-7.

267. Helske S, Kupari M, Lindstedt KA, Kovanen PT. Aortic valve stenosis: An active atheroinflammatory process. *Curr Opin Lipidol*. 2007;18(5):483-491.

268. Khan JA, Cao M, Kang BY, et al. Systemic human netrin-1 gene delivery by adeno-associated virus type 8 alters leukocyte accumulation and atherogenesis in vivo. *Gene Ther*. 2011;18(5):437-444.